Improving Spatial Reuse and MAC Efficiency for Future WLANs

Ioannis Selinis

Submitted for the Degree of
Doctor of Philosophy
from the
University of Surrey

Institute for Communication Systems (ICS), home of Innovation Centre (5GIC)
Faculty of Engineering and Physical Sciences
University of Surrey
Guildford, Surrey GU2 7XH, U.K.

November 2019

To my family

Leaving is easy with

eyes closed

Summary

One of the ways to provide greater coverage and capacity for future wireless networks is through network densification. This is also one of the drivers for future IEEE 802.11 deployments, aiming not only to improve throughput per link, but the overall network performance in dense deployments. That said, the IEEE 802.11ax amendment is currently focusing on addressing the challenges and improving the spectrum efficiency in dense deployments with hundreds of Access Points (APs) and Stations (STAs). This work strives to shed some light in the area of spectrum efficiency by trying to understand (i) the operation and the impact of the newly introduced Spatial Reuse feature of the IEEE 802.11ax amendment and (ii) if it is possible to realise multicast/broadcast transmissions over Wi-Fi while preserving reliability.

Although the IEEE 802.11ax Spatial Reuse feature, namely BSS Color, offers several advantages and good potential for improving spectrum efficiency, it also imposes several challenges. Towards filling the aforementioned gaps and address challenges, particular contributions were made in this thesis. First, this work presents a performance evaluation of the BSS Color scheme in various scenarios, where its shortcomings are identified. Second, this work proposes a generic framework to obtain throughput for dense cellular-like (small-cell) deployments, based on a mathematical model. Third, this work introduces COST, a novel Spatial Reuse technique for improving BSS Color performance by exploiting the information provided by this scheme and providing throughput gain of up to 57% while preserving fairness between BSSs. Fourth, this thesis proposes the design of a rate control algorithm that leverages the BSS Color and COST, providing up to 113% throughput gain in dense deployments when compared to the traditional off-the-shelf MinstrelHT. Finally, this thesis elaborates a network coding approach to enable multicast/broadcast transmissions over Wi-Fi, that could enhance throughput performance by 20% when compared with the legacy MAC feedback mechanism. The main goal for this contribution is to provide a means for realising reliable multicast/broadcast communications by reducing the use of the Wi-Fi feedback mechanism.

The above contributions were evaluated through system-level simulations, emulating real-world deployments. This work showed that advanced techniques, that exploit all available information by monitoring the inter-BSS and intra-BSS frames, are required to support the IEEE 802.11ax Spatial Reuse feature operation and provide throughput gain while preserve fairness among users. Furthermore, it was shown that the network coding should carefully be designed and enabled only when it is required, otherwise throughput loss could be observed due to the transmitted overhead. The scenario and application's requirements should also be taken into account (e.g. latency).

Key words: IEEE 802.11ax, Spatial Reuse, BSS Color, Rate Control Algorithms, Network Coding, Next-Generation WLANs, High-Density WLANs.

Email: ioannis.selinis@surrey.ac.uk
WWW: http://www.eps.surrey.ac.uk/5gic

Acknowledgements

First, I would like to express my gratitude to my supervisors Prof. Rahim Tafazolli and Dr. Seiamak Vahid, for giving me the opportunity to join their team. It was back in 2013 when I first joined ICS (known as CCSR) as an intern during the MSc, and met with Dr. Seiamak Vahid without whom I would not really have started the PhD. His continuous support, patience, and the fruitful discussions thoughout the PhD have been very valuable to me.

I would also like to show my sincere appreciation to all the academics, researchers, and fellow PhD students in 5G-ICS for the discussions, the feedback, and for giving me opportunity to present my work in technical workshops and internal meetings. Special thanks to the former researcher; Dr Konstantinos Katsaros for the useful feedback and collaboration we had had for the past few years and former PhD students; Dr Niklas Palaghias, Dr Nikolaos Loumis, and Dr Nikolaos Papachristou for their valuable feedback, support, and happy memories made. Thanks to Dr Marcin Filo for his valuable help and support, to Chris for the countless laughs we shared since we first started and to Alexios Thanos for the fruitful discussions, stories, and laughs we shared (during the breaks) for the past one year.

Thanks to Dr Chuan Heng Foh for his valuable feedback and help, especially during the past few months, to Dr. Boris Bellalta and his team; Sergio Barrachina-Muñoz and Francesc Wilhelmi, for the fruitful discussions, collaboration, and for giving me the opportunity to present my work. I would like to thank Prof. Ning Wang and the former colleague Dr. Chang Ge for being supportive, and Dr. Victor Sucasas and Ricardo Bassoli for their valuable help.

My sincere gratitude to Dr Marion Allayioti for her continuous support and understanding during these years. Thank you for helping me and standing by me through all those tough times.

Last but not least, I would like to thank my family; my parents Nikos and Kyriaki and my brothers Kostas and Aggelos for their unconditional support, understanding, motivation, and love during these years. Although, you may never come across this thesis, I know I would never have made it without you. Finally, I offer my sincere gratitude to those who have stood by me and have given me the strength to carry on, although being apart; my family, my friends, and especially my beloved aunt Haroula.

Contents

List of Figures

List of Tables

Nomenclature

Symbols

$alpha$	A constant variable
b_t	The stochastic process representing the backoff time counter for a given station
$beta$	A factor that is applied to calculate the $Margin$
C	Speed of light (299792458 m/s)
$ceta$	A variable that acts as a guard for the $Margin$
c	Positive constant
d	Distance
d_{BP}	The breakpoint distance (for PL models)
δ	Propagation Delay
$delta$	Failure probability of a decoding process
$E[P]$	The average payload information transmitted in a time slot
f_c	The frequency (in GHz)
Ga	Antenna Gain [dBi]
H	The packet header (including PHY and MAC headers)
K	Incoming symbols in the encoder
λ	Wavelength
l	The number of asynchronous transmission that will extend the busy duration for an exposed node that is currently locked on an ongoing transmission
Lc	Cable Loss [dB]
m	Maximum backoff stage

k	The total number of asynchronous transmissions that can occur in the deployment
mcs_{best}	The MCS rate with the highest throughput based on teh statistics collected
N_A	The number of apartment per floor and N_L
N_F	The number of floors
N_L	The number of apartment rows per floor
N	Outgoing symbols from the encoder
N_W	The number of walls per floor
p	Collision Probability
PL	The path loss (in dB)
P_s	Probability of a successful tranmission in a time slot
P_{tr}	The transmission probability
q	Busy Probability
q'	Busy probability to account for asynchronous transmissions
R	The ripple size (RSD)
S	Throughput
τ	Transmission Probability
T_b	The time required for a node to drop a frame due to the color mismatched
T_s	The average time the channel is sensed busy because of a successful transmission
T_c	the average time the channel is sensed busy during a packet collision
$TxPwr$	Transmit Power [dBm]
$TxPwr_r^{n,i}$	Received Power from the transmitter n to the node i
$TxPwr_{step}$	The step for tuning the transmit power level
u	Transition probability of recapturing the channel for a given node
W	Minimum Contention Window
x	Relation of DIFS over slot
y	Relation of DIFS over a data transmission

Z	The overhead required (encoded information) to recover the original information

Acronyms

$3GPP$	Third Generation Partnership Project
$4G$	Fourth Generation
$5G$	Fifth Generation
$5G\text{-}PPP$	5G - Infrastructure Public Private Partnership
$5GAA$	5G Automotive Association
$A\text{-}BFT$	Association Beamforming Training
$A\text{-}BFT$	Beam-Refinement phase
$A\text{-}MPDU$	Aggregate MAC Protocol Data Unit
$A\text{-}MSDU$	Aggregate MAC Service Data Unit
A/D	Analog-to-Digital
$AARF$	Adaptive ARF
ABS	Almost Blank Subframe
AC	Access Class
AC_BE	AC Best Effort
AC_BK	AC Background
AC_VI	AC Video
AC_VO	AC Voice
ACB	Access Class Barring
ACK	Acknowledgment
AGC	Automatic Gain Control
AID	Association ID
$AIFS$	Arbitration Interframe Spacing
AP	Access Point
API	Application Programming Interface
$APSD$	Automatic Power Save Delivery
AR	Augmented Reality

ARF	Auto Rate Fallback
ARQ	Automatic Repeat Request
ATI	Announcement Transmission Interval
BATS	BATched Sparse Code
BB	Base-Band
BCC	Binary Convolutional Code
BCCH	Broadcast Control Channel
BCH	Broadcast Channel
BCU	Basic Channel Unit
BEB	Binary Exponential Back-off
BER	Bit Error Rate
BF	Beamforming
BHI	Beacon Header Interval
BI	Beacon Interval
BS	Base Station
BSR	Buffer Status Report
BSS	Basic Service Set
BTI	Beacon Transmission Interval
C-Plane	Control (signaling) Plane
CA	Carrier Aggregation
CAQ	Channel Availability Query
CARA	Collision-Aware Rate Adaptation
CBAP	Contention-Based Access Period
CC	Component Carrier
CCA	Clear Channel Assessment
CCCH	Common Control Channel
CDMA	Code Division Multiple Access
CEF	Channel Estimation Field
CFO	Carrier Frequency Offset

$CMOS$	Complementary Metal-Oxide-Semiconductor
$CoMP$	Coordinated Multipoint
$COST$	Control OBSS/PD Sensitivity Threshold
CP	Circular Polarization
CP	Cyclic Prefix
CRC	Cyclic Redundancy Check
CRS	Common Reference Signal
CS	Carrier Sensing
$CSAT$	Carrier Sensing Adaptive Transmission
CSI	Channel State Information
CSM	Channel Scheduling Management
$CSMA/CA$	Carrier-Sense-Multiple-Access with Collision-Avoidance
$CTMC$	Continuous Time Markov Chain
CVS	Contact Verification Signal
CW	Contention Window
D/A	Digital-to-Analog
$D2D$	Device-to-Device
$DCCH$	Dedicated Control Channel
DCF	Distributed Coordination Function
$DELBA$	Delete Block ACK Session
DFS	Dynamic Frequency Selection
$DIFS$	DCF Interframe Spacing
DL	Downlink
$DL\text{-}SCH$	DL-Shared Channel
DMG	Directional Multi-Gigabit
$DMRS$	Demodulation Reference Signal
DQS	Disjoint Queue Scheduler
DRX	Discontinuous Reception
DSC	Dynamic Sensitivity Control

$DTCH$	Dedicated Traffic Channel
DTI	Data Transfer Interval
$DTIM$	Delivery TIM
$DTMC$	Discrete Time Markov Chain
DTX	Discontinuous Transmission
$DwPTS$	DL Pilot Time Slot
EAB	Extended Access Barring
ED	Energy Detection (CCA)
$EDCA$	Enhanced Distribute Channel Access
$eDMG$	Enhanced DMG
EDT	Early Data Transmission
$EIFS$	Extended Interframe Spacing
$eIMTA$	Enhanced Interference Mitigation and Traffic Adaptation
$EIRP$	Effective Isotropic Radiator Power
EMA	Exponential Moving Average
$eMBB$	enhanced Mobile Broadband
EPC	Evolved Packet Core
ER	Extended Range
$ESPAR$	Electronically Steerable Passive Array Radiator
$ETSI$	European Telecommunications Standards Institute
$EWMA$	Exponential Weighted Moving Average
FCC	Federal Communications Commision
FDD	Frequency Division Duplex
$FDMA$	Frequency Division Multiple Access
FEC	Forward Error Correction
FFR	Fractional Frequency Reuse
FFT	Fast Fourier Transform
FSS	Frequency Selective Scheduling
FST	Fast Session Transfer

Gbps	Gigabits per Second
GDB	Geolocation Database
GDD	Geolocation Database Dependent Entities
GI	Guard Interval
GNSS	Global Navigation Satellite System
GP	Guard Period
GPRS	General Packet Radio Service
GPS	Global Positioning System
GSM	Global System for Mobile communications
HARQ	Hybrid-ARQ
HCCA	HCF Controlled Channel Access
HCF	Hybrid Coordination Function
HDMI	High-Definition Multimedia Interface
HE	High-Efficiency
HPLMN	Home Public Land Mobile Network
HSPA	High-Speed Packet Access
HSS	Home Subscriber Server
HT	High-Throughput
HTC	Human Type Communications
ICD	Inter-Cell Distance
ICI	Inter-Carrier Interference
ICIC	Inter-Cell Interference Coordination
IE	Information Element
IEEE	Institute of Electrical and Electronic Engineers
IETF	Internet Engineering Task Force
IoT	Internet of Things
IP	Internet Protocol
ISI	Inter-Symbol Interference
ITU	International Telecommunication Union

JFI	Jain's Fairness Index
JQS	Joint Queue Scheduler
$L\text{-}SIG$	Legacy Signal Field
LAA	Licensed Assisted Access
LBT	Listen-Before-Talk
$LDPC$	Low-Density-Parity-Check
$LHCP$	Left-Hand CP
$LMDS$	Local Multipoint Distribution Service
LNC	Linear Network Codes
$LoRa$	Long-Range
$LoRaWAN$	LoRa Wide Area Network
LOS	Line-of-Sight
LP	Linear Polarization
$LPSC\text{-}OFDM$	Low-Power SC-OFDM
$LPWAN$	Low-Power Wide Area Network
LT	Luby Transform
LTE	Long Term Evolution
LTF	Long Training Field
$M2M$	Machine-to-Machine
MAC	Medium Access Control
$Max\text{-}C/I$	Max-Carrier-to-Interference
$MBMS$	Multimedia Broadcast Multicast Services
$MBSFN$	Multicast/Broadcast Single-Frequency Network
$MCCH$	Multicast Control Channel
MCH	Multicast Channel
MCS	Modulation and Coding Scheme
MEC	Mobile Edge Computing
$MEMS$	Micro-Electro-Mechanical System
$MIMO$	Multiple-Input-Multiple-Output

MME	Mobility Management Entity
$MMSE$	Minimum Mean Squared Error
$mMTC$	massive Machine Type Communications
$mmWave$	Millimeter Wave
$MR-FSK$	Multi-Rate Frequency Shift Keying
$MR-O-QPSK$	MR- Offset Quadrature Phase Shift Keying
MTC	Machine-Type Communication
$MTC-IWF$	MTC-Inter-Working Function
$MTCH$	Multicast Traffic Channel
MU	Multi User
$NACK$	Negative-ACK
$NAICS$	Network Assisted Interference Cancellation and Suppression
NAV	Network Allocation Vector
NB	NarrowBand
NDP	Null Data Packet
NFV	Network Function Virtualization
$NLOS$	Non-Line-of-Sight
$NOMA$	Non-Orthogonal Multiple Access
NR	New Radio
$OBSS$	Overlapping BSS
$OFDM$	Orthogonal Frequency Division Multiplexing
$OFDMA$	Orthogonal Frequency Division Multiple Access
$P\text{-}GW$	Packet-Data-Network Gateway
$PAID$	Partial AID
$PARP$	Peak-to-Average-Power ratio
$PBCH$	Physical Broadcast Channel
$PCCH$	Paging Control Channel
$PCDCH$	Physical Control DL Channel
$PCell$	Primary Cell

PCF	Point Coordination Function
$PCFICH$	Physical Control Format Indicator Channel
PCH	Paging Channel
PCP	Personal-Basic-Service-Set Control Point
PCS	Physical Carrier Sensing
$PDCP$	Packet Data Convergence Protocol
PDG	Reverse Direction Grant
PDR	Packet Delivery Ratio
$PDSCH$	Physical Data Shared Channel
PDU	Protocol Data Unit
PER	Packet Error Rate
$PHICH$	Physical Hybrid-ARQ Indicator Channel
PHY	Physical
PLC	Physical Layer Capture
$PLCP$	Physical Layer Convergence Procedure
$PMCH$	Physical Multicast Channel
$PPDU$	PLCP Protocol Data Unit
PRA	Prioritized Random Access
$PRACH$	Physical Random-Access Channel
$ProSec$	Proximity Services
$PS-Poll$	Power Save Poll Frame
$PSBCH$	Physical Sidelink Broadcast Channel
PSD	Power Save Mode
PSD	Power Spectral Density
$PSDCH$	Physical Sidelink Discovery Channel
$PSDU$	PLCP Service Data Unit
PSM	Power-Saving Mode
$PSMP$	Power Save Multi-Poll
$PSSCH$	Physical Sidelink Shared Channel

PUCCH	Physical UL Control Channel
PUSCH	Physical UL Shared Channel
QoE	Quality of Experience
QoS	Quality of Service
RACH	Random-Access Channel
RAT	Radio Access Technology
RAW	Restricted Access Window
RB	Resource Block
RDP	Reverse Direction Protocol
RE	Resource Element
RF	Radio-Frequency
RHCP	Right-Hand CP
RID	Response Indication Deferral
RLC	Radio-Link Control
RLNC	Random LNC
RLQP	Registered Location Query Protocol
RLSS	Registered Location Secure Server
ROM	receive-only mode
RRC	Radio Resource Control
RRM	Radio Resource Management
RSD	Robust Soliton Distribution
RSIN	Rate Selection for Industrial Networks
RSSI	Received Signal Strength Indicator
RTS/CTS	Request-to-Send and Clear-to-Send
RU	Resource Unit
S-GW	Serving Gateway
S-RLNC	Systematic RLNC
SA	System Architecture (Working Group)
SC-FDMA	Single-Carrier FDMA

SC-OFDM	Single-Carrier OFDM
SC-PTM	Single-Carrier Point-to-Multipoint
SCC	Serially Concatenated Code
SCell	Secondary Cell
SCS	Service Capability Server
SDM	Spatial-Division Multiplexing
SDN	Software Defined Network
SIFS	Short Interframe Spacing
SINR	Signal-to-Interference-plus-Noise ratio
SISO	Single-Input-Single-Output
SLS	Sector-Level-Sweep
SLSS	Sidelink Synchronization Signal
SNR	Signal-to-Noise rate
SON	Self-Organizing Network
SP	Service Period
SPS	Semi-Persistent Scheduling
SR	Spatial Reuse
SRG	Spatial Reuse Group
SS	Spatial Stream
SST	Slice/Service Type
SST	Subchannel Selective Transmission
SSW	Sector Sweep
STA	Station
STBC	Space-Time Block Coding
STF	Short Training Field
TAU	Tracking Area Updates
TCP	Transmission Control Protocol
TDD	Time Division Duplex
TDMA	Time Division Multiple Access

TETRA	Terrestrial Trunked Radio
TG	Task Group
TID	Traffic Indication Map
TPC	Transmit Power Control
TRN	Training
TTI	Transmission Time Interval
TVWS	Television/TV White Spaces
TWT	Target Wake Time
TxOP	Transmission Opportunity
U-Plane	User (data) Plane
UDP	User Datagram Protocol
UE	User Equipment
UHD	Ultra-High-Definition
UL	Uplink
UL-SCH	UL-Shared Channel
UMTS	Universal Mobile Telecommunications System
UpPTS	UL Pilot Time Slot
uRLLC	ultra-high Reliable and Low Latency
USB	Universal Serial Bus
V2I	Vehicle-to-Infrastructure
V2P	Vehicle-to-Pedestrian
V2V	Vehicle-to-Vehicle
V2X	Vehicle-to-Everything
VANETs	Vehicular Ad-hoc Networks
VCS	Virtual Carrier Sensing
VGA	Variable Gain Amplifiers
VHT	Very-High-Throughput
VNF	Virtual Network Function
VR	Virtual Reality

$WCDMA$	Wideband Code Division Multiple Access
WEP	Wired Equivalent Privacy
$Wi-SUN$	Wi- Smart Utility Networks
$WLAN$	Wireless Local Area Network
$WRAN$	Wireless Regional Area Network
WSD	White Space Device
WSM	White Space Map

Chapter 1

Introduction

1.1 Overview and Motivation

Emerging services and applications/use-cases, such as autonomous vehicles, remote health care, smart city etc, along with the proliferation of smartphones have led to the evolution of the existing (wireless) networks towards more sophisticated systems to firstly support, and also satisfy users' needs and requirements. The upcoming wireless networks aim at improving the Quality of Experience (QoE) of the users in dense heterogeneous networks. The need for greater capacity, lower latency, spectrum efficiency, energy efficiency, reliability and connectivity for a massive number of devices are some of the requirements that are under the microscope for the operators and vendors. To address these demands and challenges for the wireless networks, both the Institute of Electrical and Electronic Engineers (IEEE) and the Third Generation Partnership Project (3GPP) camps should be and are walking hand in hand towards the realization of the future networks.

To this extend, new IEEE 802.11 Task Groups (TGs) have been introduced the last decade to support various use-cases, such as the support for the Internet of Things (IoT) with the introduction of the IEEE 802.11ah amendment or the need for high data rates by exploiting the millimeter wave bands with the IEEE 802.11ad/ay for short-range communications. Of a particular interest is the IEEE 802.11ax amendment that is introduced to address the challenges in the already congested 2.4/5 GHz bands and

to provide connectivity to users in dense deployments. In contrast to its predecessors, this amendment aims at not only providing higher data rates per user but also utilise the spectrum resources by incorporating advanced and sophisticated features.

One of the main advantages that WLANs offer is the uncotrolled and unmanaged deployment of the Access Points (APs), making them a cost-efficient solution that offers access to the internet, which is also the main reason for their success. At the same time, these advantages pose some challenges for the smooth operation of the WLANs. The most significant perhaps, inherent challenge is the high and uncontrolled interference level introduced in Overlapping Basic Service Sets (OBSSs) that lies on the way that IEEE 802.11 networks access the channel. Although, there are a lot of approaches available in the literature for controlling the interference level and the channel access, it was not until the IEEE 802.11ax that introduced a mechanism, known as BSS Color, to cope with the interference level and Wi-Fi's inherent limitation of not utilising the spectrum due to the exposed node problem. Although, most of the works were used to refer to the well known hidden node problem in WLANs and propose solutions for it, limited work was presented for the exposed node problem. The main reason for this is due to the nature of the IEEE 802.11 networks, where they had been designed for small indoor environments.

Wi-Fi's importance in the 5G era has been acknowledged given that by 2022, the traffic over Wi-Fi will account for more than 50% of the total IP traffic [1]. Wi-Fi also serves stationary or nomadic users at a much lower cost than the cellular systems. Of course, the cellular technologies are necessary for serving high mobile users and providing wide coverage. Wi-Fi will complement the cellular technology and will support different use cases (e.g. indoor use cases) [2].

Moreover, Wi-Fi will act as a complementary technology to the cellular in outdoor scenarios too, by forming ultra dense small networks/ hot-spots for traffic offloading. In scenarios like these, where the users density is high and multiple BSS are overlapping, the exposed node problem is even more profound and could lead to poor spectrum utilisation by most of the WLANs refrain from transmissions, when they should not.

The motivation for this research is to study and understand the potential for the IEEE

802.11ax BSS Color and to develop novel algorithms that build upon this feature for the future wireless networks. Algorithms that provide throughput gain whilst preserving fairness for the users is quite challenging in dense networks. This thesis focuses on filling the gaps that may have not been addressed in this amendment, since many aspects for the implementation of BSS Color are left to the discrepancy of the manufacturers. The impact of the rate control algorithms is also exploited in order to take advantage of the Medium Access Control (MAC) features that have a significant impact on the performance. The algorithms in this study are designed in such a way that can be realised in practice without requiring any additional information to be exchanged between the users. Further, this thesis looks into the reliability aspect and the reduction of the control frames exchanged in an IEEE 802.11 network. Reliability is considered as one of the main drivers for the future networks (ultra-Reliable Low Latency Communications (uRLLC)), where guaranteed services are required, such as in the healthcare, entertainment, transport industries etc. [3]. Although, only 5G-3GPP is addressing International Telecommunication Union - International Mobile Telecommunications - 2020 (ITU-IMT-2020) standards, Wi-Fi is working towards this direction, with the low-latency and high-reliability requirements to be amongst those that need to be further enhanced for Wi-Fi [4], [5].

1.2 Research Questions

The main objectives of this work are summarised below, in the form of a series of research questions:

- What are the potentials of the IEEE 802.11ax BSS Color feature and its drawbacks in various scenarios?
- Is it possible to improve its performance in terms of throughput while preserving fairness for the users, especially the cell-edge users, without introducing any additional overhead?
- Is it possible to design a rate control algorithm built on top of the IEEE 802.11ax

BSS Color that exploits any useful information from the MAC layer and enhances the network performance in dense deployments?

- Is it possible to provide reliable communications by incorporating Network Coding in the upper MAC layer for the IEEE 802.11 technology and at the same time reduce the use of the control frames (i.e. acknowledgments) to enable broadcast/multicast communications?

1.3 Key Contributions from this PhD Work

The main contributions of this work can be summarised as follows:

- Development and evaluation of the Spatial Reuse techniques that were initially proposed as possible candidates for the upcoming IEEE 802.11ax.
- Development of the capture model according to the IEEE 802.11ax guidelines to emulate the reception in the off-the-shelf devices. The capture effect has significant impact on the performance since packets may survive a collision that is caused by hidden nodes or concurrent transmissions.
- Development of an analytical model that captures the behaviour of multiple OBSSs operating on the same channel and provides accurate results (in terms of throughput) when compared with off-the-shelf simulators.
- Development of a novel algorithm that is specifically designed to exploit the IEEE 802.11ax BSS Color and improve its performance without any additional overhead exchanged between the nodes.
- Design and development of a rate control algorithm that builds on top of the IEEE 802.11 BSS Color, aiming to exploit any information that can be obtained from the MAC layer without any additional overhead (transmitted frames) and improve the performance of well known off-the-shelf algorithms.
- Design, development, and evaluation of a Network Coding scheme for IEEE 802.11 nodes, operating on a shim layer between MAC and Network layers that offers

reliable communications and reduces the use of acknowledgments. This new shim layer including the Network Coding scheme is part of the IEEE 802.11ax upper MAC layer.

1.4 Publications

The publications made for this work, against the main contributions of this PhD thesis are as follows:

- State of the Art and initial development of the Spatial Reuse techniques for the IEEE 802.11ax amendment:
  - ⋆ I. Selinis, M. Filo, S. Vahid,J. Rodriquez, and R. Tafazolli, "Evaluation of the DSC Algorithm and the BSS Color Scheme in Dense Cellular-like IEEE 802.11ax Deployments," 2016 IEEE 27th Annual International Symposium on Personal, Indoor, and Mobile Radio Communications (PIMRC '16), pp. 1-7, 2016.
  - ⋆ I. Selinis, K. Katsaros, M. Allayioti, S. Vahid, and R. Tafazolli, "The Race to 5G Era; LTE and Wi-Fi," IEEE Access, vol. 6, pp. 56598-56636, 2018.
  - ⋆ F. Wilhelmi, S. B.-Muñoz, C. Cano, I. Selinis, and B. Bellalta, "Spatial Reuse in IEEE 802.11ax WLANs," *Submitted in Journal of Network and Computer Applications (JNCA)*
- Development of the capture model and its impact on the IEEE 802.11ax Spatial Reuse mechanism:
  - ⋆ I. Selinis, K. Katsaros, S. Vahid, and R. Tafazolli, "Exploiting the Capture Effect on DSC and BSS Color in Dense IEEE 802.11Ax Deployments," Proceedings of the Workshop on ns-3 (WNS3 '17), pp. 47-54, 2017.
- Development of an analytical model that captures the behaviour of the IEEE 802.11ax Spatial Reuse, BSS Color:

  - ⋆ S. B.-Muñoz, F. Wilhelmi, I. Selinis, and B. Bellalta, "Komondor: a Wireless Network Simulator for Next-Generation High-Density WLANs," 2019 IEEE Wireless Days (WD '19), pp. 1-8, 2019.
  - ⋆ I. Selinis, C.-H. Foh, S. Vahid, and R. Tafazolli, "An Analytical Model for the IEEE 802.11ax BSS Color," *To be submitted in IEEE Wireless Communications Letters*

- Development of a novel algorithm that exploits the IEEE 802.11ax BSS Color and improves its performance:
  - ⋆ I. Selinis, K. Katsaros, S. Vahid, and R. Tafazolli, "Control OBSS/PD Sensitivity Threshold for IEEE 802.11ax BSS Color," 2018 IEEE 29th Annual International Symposium on Personal, Indoor and Mobile Radio Communications (PIMRC '18), pp. 1-7, 2018.

- Design and development of a rate control algorithm to further enhance throughput performance in dense deployments, by leveraging the IEEE 802.11ax BSS Color:
  - ⋆ I. Selinis, K. Katsaros, S. Vahid, and R. Tafazolli, "Damysus; A Practical IEEE 802.11ax BSS Color Aware Rate Control Algorithm," International Journal of Wireless Information Networks (Springer), pp. 1-23, 2019.

- Design, development, and evaluation of a Network Coding scheme for IEEE 802.11 nodes:
  - ⋆ I. Selinis, K. Katsaros, S. Vahid, and R. Tafazolli, "Eliminating the Use of IEEE 802.11 Acknowledgements; A Network Coding Approach," 2019 IEEE Wireless Communications and Networking Conference (WCNC '19), pp. 1-7, 2019.
  - ⋆ V. Sucasas, O. Kebkal, I. Selinis, V. Seiamak, S. Mumtaz, and J. Rodriguez, "Performance of RLNC for Underwater Broadcasting," 2020 IEEE Networking Letters, vol. -, no. -, pp. 1-1.

- Benefits of enabling schedulers by exploiting the IEEE 802.11ax BSS Color (Research Directions):

⋆ I. Selinis, K. Katsaros, S. Vahid, R. Tafazolli, "An IEEE 802.11ax Interference -Aware MAC Queue," *To be submitted*

1.5 Thesis Outline Organisation

The remainder of this thesis is organised as follows. Chapter 2 surveys the existing literature in Radio Access Network (RAN) for both cellular and IEEE 802.11 systems. It provides an insight on the technology enablers for the future networks and highlights the challenges and the potentials for these networks. Chapter 3 shows the potentials for the Spatial Reuse (SR) techniques as they were proposed (early stage) for the upcoming IEEE 802.11ax. Chapter 4 presents the design of the capture model used in this study and its impact on the SR features in a small indoor scenario. Chapter 5 presents an analysis of the behaviour for the IEEE 802.11 cellular-like deployments consisting of multiple OBSSs, based on Markov chain, whilst showing the potentials of the BSS Color. It also serves as a driver for designing an algorithm to improve the performance of the IEEE 802.11ax BSS Color, which is presented in Chapter 6. This novel algorithm is the first one designed and proposed for improving the IEEE 802.11ax BSS Color that can be applied in both the stations (STAs) and APs. Chapter 7 proposes a rate control algorithm that further extends the operation of the mechanism presented in Chapter 6 and leverages the available information that a node holds. Chapter 8 presents a Network Coding scheme that shows high decoding success rate in order to provide reliable communications in fading channels. It also functions in the absence of acknowledgments, that add additional delay and overhead in the system. Finally, Chapter 9 concludes this study and provides future directions regarding this research.

References

[1] Cisco, "White Paper: Cisco Visual Networking Index: Forecast and Methodology, 2017-2022," Cisco, Tech. Rep., 2018. [Online]. Available: `https://www.cisco.com/c/en/us/solutions/collateral/service-provider/visual-networking-index-vni/white-paper-c11-741490.html`.

[2] ——, (2020). 5 Things to Know About Wi-Fi 6 and 5G, [Online]. Available: https://www.cisco.com/c/m/en_us/solutions/enterprise-networks/802-11ax-solution/nb-06-5-things-WiFi6-5G-infograph-cte-en.html (visited on 2020).

[3] 5G Americas, "White Paper: New Services & Applications with 5G Ultra-Reliable Low Latency Communications," 5G Americas, Tech. Rep., 2018. [Online]. Available: https://www.5gamericas.org/new-services-applications-with-5g-ultra-reliable-low-latency-communications/.

[4] W. B. Alliance, "White Paper: The Role of Wi-Fi and Unlicensed Technologies," Wireless Broadband Alliance, Tech. Rep., 2017. [Online]. Available: https://www.wballiance.com/wp-content/uploads/2017/09/5G-Networks-Role-of-Wi-Fi-and-Unlicensed-Technologies-V2.pdf.

[5] A. Myles, "Document (IEEE802.11-15/1279): Should IEEE 802.11 be Proposed as an IMT-2020 Technology?" IEEE, Tech. Rep., 2016. [Online]. Available: https://mentor.ieee.org/802.11/dcn/16/11-16-0092-01-00ay-multi-beamforming-in-polarized-channels-for-11ay.pptx.

Chapter 2

Literature Review

The fifth generation (5G) systems will be the first realization in this new digital era where various networks will be interconnected forming a unified system. With support for higher capacity as well as low-delay and machine-type communication (MTC) services, the 5G networks will significantly improve performance over the current fourth generation (4G) systems and will also offer seamless connectivity to numerous devices by integrating different technologies, intelligence, and flexibility. In addition to ongoing 5G standardization activities and technologies under consideration in the Third Generation Partnership Project (3GPP), the Institute of Electrical and Electronic Engineers (IEEE) based technologies operating on unlicensed bands, will also be an integral part of a 5G eco-system. Along with the 3GPP-based cellular technology, IEEE standards and technologies are also evolving to keep pace with the user demands and new 5G services.

This chapter provides an overview of the evolution of the cellular and Wi-Fi standards, two complementary technologies, over the last decade with a particular focus on Medium Access Control (MAC) and Physical (PHY) layers, and highlights the ongoing activities in both camps driven by the 5G requirements and use-cases. It initially classifies the work that has been conducted into three main categories, namely, millimeter wave (mmWave) mobile communications, operating at above 6 GHz bands, conventional systems operating in below the 6 GHz frequency bands, and advancements in both Long Term Evolution (LTE) and IEEE 802.11 for the support of MTC. Each one of these

categories is further organized into LTE and Wireless Local Area Network (WLAN) systems. Finally, it argues about the current shortcomings in literature with regard to the upcoming IEEE 802.11 amendments, which will be tackled in this research.

2.1 Introduction

The forecasts for the number of devices connected to internet and the expected traffic load by 2021 do vary but it is generally agreed that many billions of devices and 49 exabytes of traffic per month, will need to be supported, with most of the traffic expected to be delivered over wireless networks [1]. To support such massive connectivity and traffic demands, both the cellular systems and WLANs are evolving [6], [7].

Emerging services, such as remote health care or learning, connected vehicles exchanging safety-critical information and ultra-high resolution video streaming will require higher data rates and lower latency than is available today. To support the stringent requirements of the next generation services will be enormously challenging in terms of capacity and coverage for the next generation networks, a.k.a. 5G. The vision for 5G is to provide a perception of an unlimited bandwidth to every user, everywhere, anytime.

The time for 5G networks has arrived, considering that approximately every decade, a new generation is deployed; 1G in 1980s', 2G in 1990s', 3G in early 2000's, and 4G in 2010s'. Different technologies have been deployed for each generation, to accommodate specific/primary use cases. For example, analog Frequency Division Multiple Access (FDMA) was deployed in 1G systems when voice was the targeting use case, Time Division Multiple Access (TDMA)/FDMA for voice and text in 2G networks, Code Division Multiple Access (CDMA) in 3G systems when mobile internet access was supported, and Orthogonal Frequency Division Multiple Access (OFDMA) is currently applied in 4G when high data rates and video over internet were the targeting use cases. However, 5G systems may comprise various waveforms; new or mature access scheme technologies, to meet requirements in different scenarios.

Some of the 5G requirements described in ITU report [8], back in early 2017, include 20 Gigabits per Second (Gbps) and 10 Gbps peak rates for downlink (DL) and uplink

(UL), respectively, while DL spectral efficiency of 30 bit/s/Hz and 15 bit/s/Hz for UL are targeted. Moreover, lower latency requirements, very high density of devices e.g. 1 million devices per km^2, and support of various classes of mobility at speeds of up to 500 km/h are also defined in that draft. According to ITU and 5G - Infrastructure Public Private Partnership (5G-PPP) [9], 5G network services are classified into three principal dimensions (also referred to as "use case families"); enhanced Mobile Broadband (eMBB), massive Machine Type Communications (mMTC), and ultra-high Reliable and Low Latency Communications (uRLLC). To meet these requirements and address the challenges of diverse use cases and vertical industries, heterogeneous ultra-dense networks operating in various frequency bands will be deployed as part of 5G network [10]. Thus, 5G can indeed be regarded as "a network of networks".

High frequency spectrum above the 6 GHz band, is likely to be allocated for 5G cellular to deliver very high data rate services [11]–[15]. Many vendors have already released the next wave of chipsets with well known names e.g. Intel, Samsung, Qualcomm amongst them, supporting enormous bandwidths at millimeter wave (mmWave) frequencies [16]. Significant studies and measurement campaigns have also been conducted to provide better understanding of propagation characteristics and validate the channel models at mmWave frequencies [17]–[19]. This in turn, will result in identifying the challenges and technologies that can be used to overcome them.

On the other hand, Sub-1 GHz frequency bands have already been exploited by both the cellular and more recent WLAN amendments, for applications that require lower data rates and wider coverage range [20], [21]. However, additional spectrum is incorporated as it becomes available, e.g. the spectrum at 700 MHz, allocated for long-range communication of low-power devices [22]. The unused broadband frequencies, known as White Spaces, also enable long range communications suitable for applications such as smart grid or smart cities. The small bandwidths also enable low power consumption, which is crucial for sensors deployed in areas that are not easily accessible e.g. forests.

Energy efficiency is also one of the requirements defined for future networks [23]–[25]. Green communication networks is not a new concept, however, it is even more critical now, with the massive number of devices connected to wireless networks [26], [27].

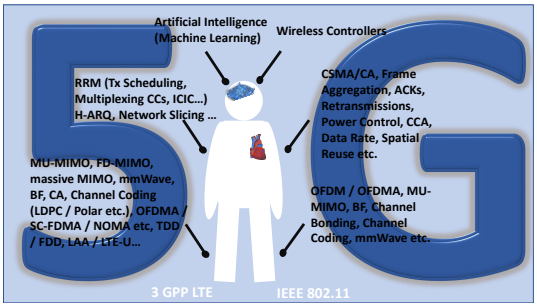

(a)

	3GPP LTE	IEEE 802.11
Technology	Synchronous – Controlled by BS	Asynchronous – (DCF is mainly used)
First Released	LTE – Release 8 (4G), 2008	Late 1990s'
Channel Access	UEs are allocated with resources after a successful preamble contention. Different channels are used, depending on the traffic and link type.	Access to the medium follows CSMA/CA procedure. Transmissions occupy the whole channel and occur over the same channel.
Operating Frequency	700 MHz – 6 GHz	TVWS / Sub-1, 2.4, 5, and 60 GHz
BS/AP Coordination	Yes	No
Dual Connectivity	Yes	No
Deployment	Controlled/Managed (Outdoor)	Uncontrolled/Unmanaged
Coverage Range	Multiple km	A few hundred meters
Channel Access Scheme	OFDMA / SC-FDMA	OFDM
Max. Transmit Power	48 / 24 dBm [macro cell BS / UEs]	20 dBm
Inter-Cell Interference	Controlled	Uncontrolled
MIMO // MU-MIMO	8x8 DL and 4x4 UL // DL/UL	8x8 DL/UL (IEEE 802.11ac) // DL
Channel BW // CA	1.4 MHz – 20 MHz // up to 32 CCs	20 MHz // up to 160 MHz
Peak Data Rate	3 Gbps (DL) & 1.5 Gbps (UL)	6.77 Gbps (DL/UL)

(b)

Figure 2.1: LTE versus IEEE 802.11: a) key technologies and b) high-level comparison.

Energy harvesting is also an approach that researchers are looking to for Internet of Things (IoT) applications [28], [29].

The introduction of new frequency spectrum for wireless communications, does not mean that the conventional 2.4/5 GHz licensed/unlicensed bands are not considered for 5G networks. Advancements have also been proposed in both the cellular systems and the WLANs by the 3GPP and the IEEE standards respectively, to keep pace with the explosive growth in mobile data traffic, use cases, and user requirements. The unlicensed technologies will play a significant role on forming the future wireless networks (i.e. 5G) and meeting the requirements, since several technologies were initially used in IEEE 802.11 networks before adopted by 3GPP (e.g. Multiple-Input-Multiple-Output (MIMO), channel bonding etc.) [30].

Figure 2.1a depicts the current key and planned features (MAC and PHY layers) in LTE and IEEE 802.11 technologies. Although, most of the functionalities and operations in IEEE 802.11 devices are handled locally by the MAC layer, nevertheless, enterprise-level access controllers that are used to manage networks consisting of multiple APs, can add intelligence to the system. Figure 2.1b illustrates the similarities and differences of these technologies at a high level [1].

[1] Throughout this thesis, the transmit power refers to the output power of the transmitter [dBm] (note that $EIRP = Pt - Lc + Ga$ where Lc is the Cable Loss [dB] and Ga the Antenna Gain [dBi].))

2.2 Technologies Designed to Operate at Above 6 GHz Bands

This section is classified into three parts. The first one presents the potentials, challenges and the enabling technologies at PHY and MAC layers, for systems operating in mmWave bands. The 5G New Radio (NR) technology is explained in the second subsection as part of the 3GPP cellular systems, while the last subsection describes the IEEE 802.11 amendments that have already hit the market or are under active development.

2.2.1 Opportunities, Challenges, and Candidate Technologies

Exploiting the mmWave bands [2] can potentially offer many advantages but at the same time impose several challenges. Wider bandwidths can offer not only higher data rates but also lower relative power consumption, provided that the channel is not severely attenuated [31]. Although, mmWave-based communication systems already exist, e.g. Local Multipoint Distribution Service (LMDS) [32], operating at 23-32 GHz bands with range over 1 km, they are not used for mobile communications. The main obstacles for using those technologies in portable devices, include the size, cost, high losses, and power consumption of the electronic components (e.g. power amplifiers, mixers, antennas) [33].

The signal in mmWave frequencies can be severely attenuated by absorption due to atmospheric gases, foliage, and rainfall. However, recent measurements in New York City [34]–[36], show that cell sizes of 200m radius can provide the required coverage for mmWave systems; the results of investigations indicate that the signal does not significantly attenuate at this distance, even in Non-Line-of-Sight (NLOS) environments. Path loss however, can be further reduced by enabling highly directional antennas, resulting in similar or even reduced path loss than the current cellular systems experience.

However, highly directional antennas (e.g. horn, patch, and antenna arrays that employ directive radiating elements) suffer from limited coverage, due to their very narrow

[2]The 30-300 GHz band is referred to as mmWave (wavelength 1cm to 1mm approx.). Since radio waves above the 6 GHz band share similar propagation characteristics with those at 30-300 GHz band, industry currently considers mmWave as the 6-300 GHz frequency band.

beams. The coverage can be improved however, by employing beamforming (BF) or using beam steerable, sectorized or switched beam array antennas at the Base Stations (BSs) and/or portable devices [37], [38]. This allows the beam to be directed in the desired direction.Beamforming appropriately weights the amplitude and phase of individual antenna signals to create narrowly focused radiation. This makes it possible to provide better coverage in an indoor environment and at the edge of a cell. Beamforming concentrates energy into smaller areas, and by concentrating the signal, it helps operators achieve the goal of improving coverage while minimizing interference. BF can also be used to avoid unwanted interference, since the envisaged beams are typically very narrow and are directed only towards specific users.

That is, by combining multiple signals from an antenna array, a directional beam is formed towards a user. Directivity is a function of the number of elements and their spacing [39]. It improves with the number of elements or spacing. However, the number and level of side lobes increase with the number of elements, thus reducing antenna's gain and directivity [40]. Moreover, when the element spacing increases, the amplitude of grating lobes increases. This can in turn lead to high interference to or from close-by-users. Apart from the number of elements and their spacing, unequal power and/or phase distribution (to the elements) can be applied to alter direction, side lobe level, and directivity.

Switched beam antenna arrays and beam steerable antennas require multiple Radio-Frequency (RF) chains, leading to excessive cost and power consumption. At large BS sites, where size is not a constraint, beam switchable antennas can be deployed. However, since for portable devices size is an important constraint, switchable antennas are not a viable option. A beamformer in a directional antenna can give the perception (to a user) of "full" coverage, by tracking the user and steering the beam toward it.

2.2.2 3GPP LTE Technology - Directions for mmWave Bands

To efficiently support larger bandwidths, deal with the challenges at mmWave bands and the new use cases, 3GPP has been working on a new Radio Access Technology (RAT)

and addressing physical and higher layer protocol requirements. Although, the new 5G RAT is being designed for operation at frequencies from Sub-1 GHz to 100 GHz, this subsection describes some of its features relating to the mmWave band operations. This new RAT is not required to be backward compatible with LTE, but forward compatible in the sense that future evolution is ensured [41].

5G NR is the name of the wireless standard for air interface of the next generation of mobile networks [42], [43]. BF, Massive MIMO, Orthogonal Frequency Division Multiplexing (OFDM) scalability, slot flexibility, energy efficiency, and advanced channel coding are the main case studies that have been considered for the 5G NR. The mmMAGIC project [44] that is developed by the European 5G-PPP during Phase 1, has proposed solutions to coding schemes for providing robustness and higher throughput, lower complexity for MIMO, and flexible Frequency Division Duplex / Time Division Duplex (FDD/TDD) frame structure. Multiple contributions have also been submitted to 3GPP and ITU in regards to channel measurements and modelling at frequency bands over 6 GHz. The BF and Massive MIMO that are strongly related with the mmWave bands are described in the following subsection.

2.2.2.1 PHY Layer Enhancements

2.2.2.1.1 Beamforming Techniques

BF is a technique that can be applied to reconfigure antenna's beam in terms of main beam direction and amplitude. Depending on BF architecture, BF schemes can be classified into three main categories; Analogue or RF, Digital, and Hybrid, as depicted in Figure 2.2.

The Analogue BF comprises one RF chain even when substantial number of antenna arrays is used. It enables low complexity, low power consumption, and operation at reduced costs if small number of phase shifters is used. The entire phased antenna array is driven by a single base-band (BB) processing module. It uses Variable Gain Amplifiers (VGAs), which enable the amplitude of the applied signals to be varied, along with phase shifters that enable adjustment of the phase of the applied signals.

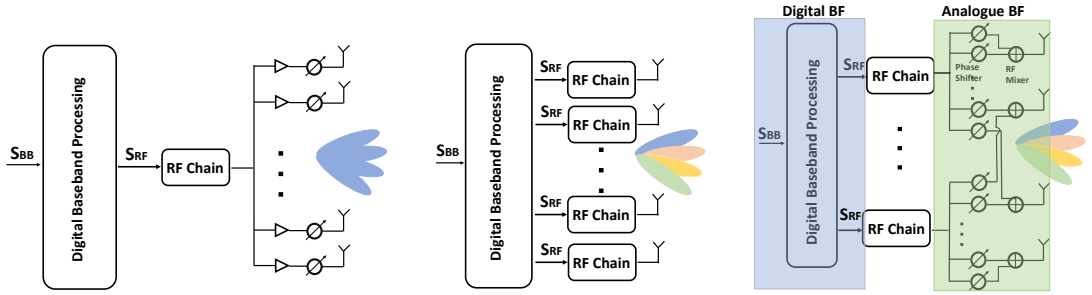

(a) (b) (c)

Figure 2.2: Beamforming Techniques: a) Analogue/RF, b) Digital/Precoding, and c) Hybrid.

It is therefore, possible to control both amplitude and phase of the signals applied to antenna's elements. Analogue BF is simpler than Digital BF, since it only requires one RF chain per antenna array, which also reduces power consumption (transmit and processing power) and overcomes the RF hardware limitations [45], [46]. Analogue BF provides an effective method of generating high BF gains from substantial number of antennas. It is cheaper to implement and operate than Digital BF. However, Analogue beamformers do not provide multiplexing gains, since transmissions on multiple parallel streams is not supported, resulting in poorer performance than Digital BF.

Digital BF, on the other hand, is achieved using digital precoding, which involves multiplying a particular coefficient to the modulated BB signal per RF chain. This means that multiple beams can be supported simultaneously, theoretically as many as the number of antenna elements, which allows more users to be served at the same time [47]. It offers the ability of sending data in parallel streams, exploiting spatial diversity and multiplexing. It also provides continuous steering and can be used to enhance performance of MIMO systems at the cost of high complexity, especially when using massive MIMO; since one RF chain per antenna would then be required. In conventional (operating below 6 GHz) systems, precoding is usually done in BB, in order to have better control over the entries of the precoding matrix [48]. However, the excessive cost, power consumption of mixed signal components, and complexity (due to Analog-to-Digital converters) make full digital BB precoding prohibitive for millimeter wave frequencies, with the currently available semiconductor technologies. The design of the precoding

matrices in Digital BF usually relies on having complete Channel State Information (CSI); an overhead that increases with the number of antennas [48] and is difficult to obtain for substantial number of antennas (e.g. mmWave Systems) [49]. Furthermore, another reason that CSI is difficult to acquire, is the small Signal-to-Noise ratio (SNR) associated with the signals before BF is applied [48]. Digital BF provides higher degree of freedom in comparison to Analogue BF that can be used by MIMO systems to improve system's performance.

There are however, a number of open issues with this technology, including calibration, complexity, and cost [50]. The implementation of a dedicated RF chain per antenna element, makes it unsuitable for cost-limited or small portable power-limited devices [51]. To combine the advantages of both Analogue and Digital techniques, Hybrid BF has therefore been proposed, reducing both the complexity/power consumption and feedback overheads [48], [52], [53].

Hybrid BF offers a trade-off between performance/ flexibility and simplicity/cost [47]. In Hybrid BF, a directive beam is formed through Analogue BF with the aid of phase shifters and VGAs [53], whereas Digital BF is used to provide the flexibility required for advanced multi-antenna techniques, such as multi-beam MIMO [54]. Hybrid BF can overcome the hardware constraints of Analogue-only BF, whilst providing the performance advantages associated with Digital BF, e.g. transmission of multiple parallel streams. On the other hand, it suffers from certain disadvantages. For example, it requires multiple RF chains along with a complicated architecture [50] and the requirement to obtain CSI for large number of antennas is still another obstacle for Hybrid BF.

2.2.2.1.2 Beam-Steering Techniques

Beam-steering can be considered to be a variant of Analogue BF technique, which is applied to reconfigure the directionality of the main antenna's beam. It mostly offers only discrete steering and not continuous [55]. It is relatively simple and low-cost technique, and is considered to be suitable for small power-limited devices, depending on the structure of the antenna.

Continuous beam-steering is essential for maintaining the communication link between two devices, since it can easily be disrupted in high frequencies. For example, narrow beams are highly affected by wind, which could lead to beam misalignment. However, robustness can be preserved by the antenna array's geometric shape; circular antenna arrays are more robust against small vibrations or angle variations due to axial symmetry [56]. Continuous beam-steering can be achieved either with phased arrays or with Electronically Steerable Passive Array Radiator (ESPAR) antennas.

The phase of each element in phased arrays, is controlled through phase shifters [57], e.g. CMOS, MEMS etc. However, the use of phase shifters imposes some challenges, such as relatively high-cost, complexity, and high insertion losses in high frequencies. Nevertheless, such losses can be mitigated, using phase shifters based on MEMS materials at a price of increased system's cost. Moreover they are inherently narrowband (NB) [58].

On the other hand, ESPARs steer the beam through varactors and have lower power consumption, since only one element of the array is fed by signal power (driven element). However, they suffer from limited steering range and high parasitic losses of the reactive loads in high frequencies. It is also challenging to calibrate all the reactive loads for obtaining the desired steering angle while keeping the antenna acceptably matched [59]. The analysis of these techniques is out of the scope of this study, and the reader can refer to [60]–[64], for more information.

2.2.2.1.3 Massive MIMO

Massive MIMO is another key technology capable of handling the huge growth in data traffic and coping with the high path loss of mmWave frequencies (enhanced coverage) [65]. Massive MIMO relies on considerable number of antennas to serve multiple users simultaneously. The short free-space wavelength (λ) at high frequencies, enables small sized antennas, thus enabling incorporation of larger number of antenna elements in a given area, compared to centimeter-wave frequencies [66]. However, the shorter coherence time due to higher Doppler spread in mmWave bands, reduces its spatial multiplexing gains.

Moreover, the use of substantial number of antennas provides robustness to transmissions (i.e. better bit error rate for the same SNR level, use of lower Modulation and Coding Scheme (MCS) with lower SNR requirements whereas targeted data rate is achieved (spatial multiplexing)), and to failures in one or more antenna units. It also, averages out noise, small-scale fading, and any hardware imperfections [67]. Hence, it can be assumed that all OFDM sub-carriers for example, will experience the same gain. This in turn, will affect the resource allocation algorithms, since users could use (be allocated) the whole bandwidth or any resource block independently of channel conditions.

Reduction in transmit power for single-antenna users can also be achieved when combined with a Massive MIMO receiver. Users can scale-down their transmit power proportional to the number of antennas at the BSs with perfect CSI or to square root with imperfect CSI [68]. On the other hand, computational complexity of precoder increases with the number of antennas, thus, low complexity precoding methods are required.

Another barrier to fully exploit Massive MIMO, is the pilot contamination issue [69]. The limited number of orthogonal pilots, confines the number of users that can simultaneously be served. Pilot reuse, the usage of non-orthogonal pilots, and blind-techniques for channel estimation are some of the approaches that can be followed to address pilot contamination.

Furthermore, data processing is also challenging due to the huge-amounts of data sources that Massive MIMO enables, which will cause high processing complexity at BSs. A potential solution to deal with the high processing complexity at BSs, is to offload data processing to a centralized data center (cloud computing) [70]. However, cloud computing may increase traffic load on the backhaul and latency due to communication link between BSs and cloud servers, which make it more suitable for applications that are not delay-sensitive. For applications that require instantaneous response and where the data volume to be processed is small (e.g. IoT sensors for smart traffic lights), processing can be realized at the edge of a network, close to the source devices (edge computing).

Massive MIMO can work in both Line-of-Sight (LOS) and NLOS environments, but the

main challenge is if it can be used in FDD systems [71]. TDD based Massive MIMO can support more users due to a lower overhead and provide cell throughput gain of up to 200% against FDD [72], whereas in FDD systems, channel estimation is required in both DL and UL bands as they operate in different frequency. Moreover, the channel coherence (time/bandwidth) that depends on the propagation environment, operating frequency, and user mobility, severely affect the amount of overhead. Therefore, Massive MIMO is more suitable for supporting low-mobility nodes operating in low-frequency spectrum in FDD systems.

2.2.2.1.4 Additional Methods for Enhanced Coverage

In addition to steering and Massive MIMO techniques, two other approaches can be followed to improve coverage in mmWave bands; Distributed Antenna Arrays and Relaying (i.e. Amplify and Forward, Compress and Forward, Detect and Forward, Decode and Forward) [73]. By employing multiple antenna arrays in predefined locations, coverage, cell-edge performance, and energy consumption could be improved (if there is a LOS communication link, a lower transmit power could be used) [74], [75]. However, synchronization of distributed antennas is challenging; Carrier Frequency Offset (CFO) caused by the mismatch of transceiver oscillators due to Doppler effect [76], phase noise due to imperfect hardware; oscillators' instabilities, especially for mmWave frequencies [77], and time synchronization between transceivers' clocks are the main reasons for Inter-Symbol Interference (ISI) and degrade system performance [78], [79]. The use of Separate (independent) or Common Local oscillators also affect phase noise [80]. The former oscillators are mainly applied when the distance between the antennas is large [81], e.g. Distributed Antenna Arrays. There are several algorithms proposed in the literature to address the synchronization of distributed antennas [82]–[84]. On the other hand, Relaying can be used to prevent blockage for low-velocity users.

2.2.2.2 MAC Layer Enhancements

Summarizing the benefits of exploiting mmWave spectrum, it can be stated the following: mmWave bands i) provide wider bandwidths enabling high throughput communi-

cations in the order of Gbps, ii) enable deployment of large number of antennas (packed into a small area), and iii) inherently support Spatial Reuse (SR) enhancements due to the propagation characteristics in high frequencies. SR can be further improved by using directional antennas, lowering down antenna's height (at BSs), and/or down-tilting the beam.

The use of directional antennas in mmWave spectrum, poses some challenges at the MAC layer [85]. Current cellular or Wi-Fi technologies rely on omni-directional communications and contention-based channel access (mainly), thus, alterations are required to some Layer 2 functionalities to support the innovative antenna technologies.

First, the use of directional antennas during the initial access is challenging. With omni-directional antennas acquiring frequency/time synchronization (signals' detection) is relatively easy. However, if narrow-beams are used during the scanning and/or synchronization procedures, additional delays may arise. BSs and users need to transmit and search in various angles/directions until synchronization is achieved.

An overview and comparison of the techniques proposed for the initial access in mmWave systems (e.g. exhaustive, iterative, and Context-Information search algorithms), is presented in [86]. Under the exhaustive search category, both users and BSs use a predefined sectorized antenna, consisting of multiple narrow beams to provide a 360°coverage. The second category, iterative schemes, comprises algorithms that follow a two-step procedure for the initial access. In the first stage, BSs use a sectorized antenna with wide beams. Once, a pair of sectors is established, then BSs initiate the second phase, where they search for a narrower beam within this wide beam sector, to optimize performance. The Context-Information search techniques, follow a three-step procedure. First, the macro BSs broadcast the Global Positioning System (GPS) coordinates of all micro BSs that operate at mmWave frequencies. Secondly, users also get their own GPS coordinates, while in the last step, users select their closest micro BS to connect to. The exhaustive search approach is more suitable for cell-edge users, since it provides better coverage (high gain beams) than the iterative search, which comes at the cost of high discovery delay. On the other hand, iterative search algorithms can be used for users that are close to a BS, exploiting their good channel conditions and the low-delay chan-

nel discovery. Context-Information techniques can also be applied in LOS scenarios, providing low-delay channel discovery but increasing energy consumption due to the three-stage procedure.

A two-step synchronization method is proposed in [87], aiming at reducing overhead. In the first stage, users obtain information that is required for switching to the correct mmWave frequency. This is achieved from the synchronization signals that macrocell BSs broadcast in the control channel, using low frequencies and omni-directional antennas. Once, users have switched to the mmWave band for the data frame communication, they extract any additional information from the pilot signals that are periodically sent, using their multiple antennas.

Secondly, during the random-access phase, users either contend for preamble (contention -based) or are assigned a specific one (contention-free, e.g. handover) to reduce overhead and delay. During the contention-based period, a user randomly selects a preamble from a pool and transmits it to the BS. If the user does not receive an acknowledgement, then it assumes that either a collision occurred or the signal was too weak to be detected by the BS. In both cases, the user retransmits the preamble after a random back-off with higher power. However, if transmitter's and receiver's antennas are misaligned, then none of the above mechanisms seem to resolve the failed transmission (deafness problem). A mechanism to distinguish the type of failed transmission; misalignment or preamble collision is presented in [88]. For example, a hard-decision energy detector may be used to identify if there was a preamble collision (high received energy level) or that deafness, blockage etc., was the main reason for the failed transmission. Once the type of failed transmission has been identified, BSs send a MAC frame to inform users about the collision occurred. The absence of the signal or an acknowledgement corresponds to deafness or blockage cases, thus, the user scans other angles instead of performing an unnecessary back-off.

Thirdly, frequent handovers in dense small deployments, is another challenging task for MAC in mmWave. To achieve smooth seamless handover, a user may enable multiple simultaneous connections to different BSs, which requires their cooperation or maintaining a link to a macrocell (operating in low frequencies) for control frames along

with data plane links to small cells operating at mmWave frequencies [89].

Lastly, the distribution of Resource Units (RUs) to users is very essential. Due to BF and Massive MIMO, each antenna may simultaneously serve multiple users within a cell. If each group consists of different number of users with diverse Quality-of-Service (QoS) requirements, then fairness issues may arise. Hence, sophisticated scheduling algorithms are required to adjust resources per group, based on the users' needs. Moreover, it might not be possible to employ Inter-Cell Interference Coordination (ICIC) mechanisms to the same extent as in current cellular systems, due to high signal attenuation in mmWave frequencies.

2.2.3 IEEE 802.11 Technologies Operating in mmWave Bands

Most of the challenges and solutions described in Section 2.2.1 are also applicable to IEEE 802.11 systems operating in mmWave frequencies. However, the limited capabilities and the size of Access Points (APs) to mainly serve indoor users impose certain constraints. For example, due to application scenarios, AP's limited size and low cost/complexity etc., only a limited number of antennas can be deployed. This section overviews the IEEE 802.11 amendments related to IEEE 802.11ad and IEEE 802.11ay standards, that have been introduced or are currently under development, for operation at mmWave bands.

2.2.3.1 IEEE 802.11ad

Although IEEE 802.11ad [90] (a.k.a. WiGig) was introduced in 2012, initial real-world deployments started in early 2018 with the first WiGig devices hitting the market. WiGig capable portable devices are also known as Directional Multi-Gigabit Stations (DMG-STAs). Operating at 60 GHz band, it enables a plethora of new applications, such as sync-n-go (file transfer), wireless display, etc., replacing High-Definition Multimedia Interface (HDMI) cables and Universal Serial Bus (USB) flash drivers [91]. Taking advantage of the wide bandwidth (2.16 GHz wide channels), IEEE 802.11ad offers up to 7 Gbps peak rate over short distances (approx. 10m), although by embedding the radar functionality and modifying the preamble part, the serving range may

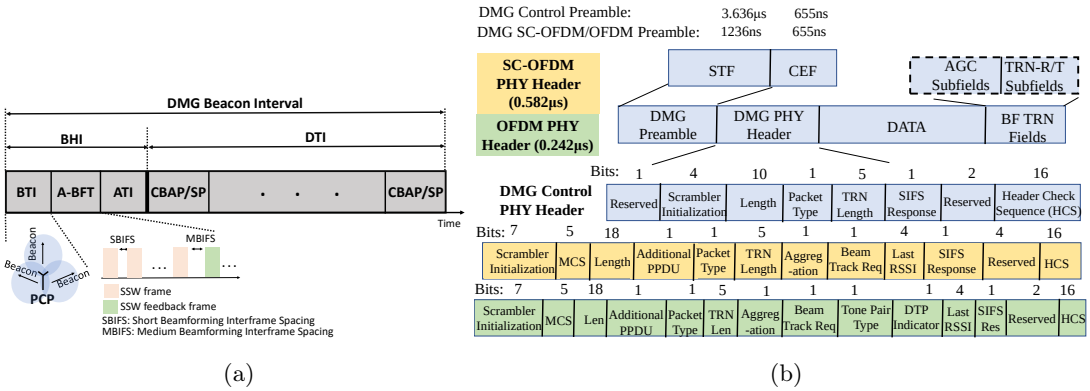

(a) (b)

Figure 2.3: IEEE 802.11ad a) Beacon Interval and b) PHY frame structure.

increase up to 200m [92]. Moreover, it supports Fast Session Transfer (FST) between the 60 and 2.4/5 GHz frequency bands.

IEEE 802.11ad takes advantage of beamforming in azimuth to cope with the high signal attenuation that 60 GHz frequency bands experience. It uses the concept of antenna sectors (sectorized antennas); each sector focuses antenna gain to a specific-predefined direction.

2.2.3.1.1 Access Scheme

In IEEE 802.11ad, prior to data transfer, beamforming training procedure takes place following an iterative search approach, where a pair of nodes agree on the optimal sectors that they are going to use. It is a two-stage procedure, where the nodes initially identify the optimal pair of predefined sectors that optimize performance, known as Sector-Level-Sweep (SLS) phase. This is achieved by transmitting and receiving training symbols as they sweep their sectors. Second stage includes the optimization of their link, by applying antenna weights, known as Association Beamforming Training (A-BFT) [93].

Alterations have been applied to Beacon Interval (BI) to support directional communications, as depicted in Figure 2.3a. BI duration is advertised in the beacon and can be changed during operation. It comprises two intervals, namely, Beacon Header Interval (BHI) and Data Transfer Interval (DTI). BHI starts with Beacon Transmission Interval (BTI), where the network coordinator, called Personal-Basic-Service-Set Control Point

(PCP), transmits multiple beacon frames in various directions. In that way, devices that use directional antennas can detect the presence of PCP. During this period, the first phase of beamforming training (i.e. SLS), occurs. The second period included in BHI, is the optional Beam-Refinement phase (A-BFT), where antenna weights are applied to further optimize a pair of sectors. This is accomplished through Sector Sweep (SSW) frames and SSW feedback frames. The optional Announcement Transmission Interval (ATI) comes last in BHI. During the ATI period, management frames (if required) are exchanged among a PCP and the associated WiGig devices.

The end of BHI period triggers the start of DTI, which comprises Contention-Based Access Periods (CBAPs) and Scheduled Service Periods (SPs). During CBAPs, DMG-STAs contend to grant access to the medium following the IEEE 802.11 Enhanced Distribute Channel Access (EDCA). On the other hand, SPs are assigned to specific pair of nodes for data transfer. Furthermore, beamforming training is also allowed during DTI, either by a DMG-STA that has captured the medium through Carrier-Sense-Multiple-Access with Collision-Avoidance (CSMA/CA) and may begin SLS, or by a PCP transmitting training parameters.

2.2.3.1.2 PHY Layer

Four different PHY layer formats are defined in IEEE 802.11ad [94]; Control PHY, Single-Carrier OFDM (SC-OFDM), Low-Power SC-OFDM (LPSC-OFDM), and OFDM. The first one is used prior to beamforming (BTI and A-BFT periods) for signal detection and pair discovery, hence, the lowest MCS level is used (i.e. MCS0). The second structure is mainly used by power-limited DMG-STAs, while the third one is introduced to further decrease power consumption and complexity. Therefore, Low-Density-Parity-Check (LDPC) has been replaced with Reed-Solomon. OFDM format is used from the devices that require high performance, thus, higher MCSs than MCS0 are used. The PHY structure is depicted in Figure 2.3b and comprises Physical Layer Convergence Procedure (PLCP) preamble, PLCP header, MAC header, payload, and beamforming training.

Preamble includes the Short Training Field (STF) and Channel Estimation Field (CEF),

which are used for packet detection, Automatic Gain Control (AGC), frequency offset estimation, synchronization, modulation indication, and channel estimation. PHY header carries information about the transmitted packet (e.g. MCS, length etc.) while the MAC header contains information required by that layer, such as source/destination addresses, type of the frame (e.g. management) etc. Note that MAC layer is responsible for packets' reordering due to aggregation/fragmentation, generating and transmitting acknowledgements, Request-to-Send and Clear-to-Send (RTS/CTS) frames etc. Following the MAC header, the data payload is appended and thus the PHY layer payload comprises PHY header, MAC header, and Data payload. Cyclic Redundancy Check (CRC) is the last mandatory field that is applied to the whole PHY payload for error-correction (detecting the errors), while the optional AGC and Training (TRN) fields might be appended to PHY payload for beamforming reconfiguration after the initial beamforming training. These two fields are used to improve beamforming training in DTI (beamtracking in DTI) through AGC gain calculation and channel estimation. Other DMG PHY characteristics are listed in Appendix A (Table A.1).

2.2.3.1.3 MAC Layer

The IEEE 802.11ad MAC layer supports CBAPs and TDMA schemes for SPs periods to utilize the whole bandwidth. CBAPs rely either on the Distributed Coordination Function (DCF) that is based on the CSMA/CA scheme or the Hybrid Coordination Function (HCF), which is used for scheduled transmission opportunities. On the other hand, SPs are applicable only to DMG-STAs (not to PCPs) and enable scheduled or dynamic allocation services. With dynamic allocation, a PCP polls a DMG-STA and allocates slots based on its needs. The allocated slots might be within the same or following BI.

Similar to its predecessors, i.e. IEEE 802.11n/ac, in IEEE 802.11ad frame aggregation at the high or low MAC layer is supported. These are known as Aggregate MAC Service Data Unit (A-MSDU) and Aggregate MAC Protocol Data Unit (A-MPDU), respectively. The maximum size of transmitted frame is 262143 bytes, while transmission duration must not exceed 2 ms (PLCP Protocol Data Unit (PPDU) time $\leq$ 2 ms).

2.2.3.2 IEEE 802.11ay

To keep pace with user demands and new applications that require capacities of over 10 Gbps (e.g. cellular offload, HDMI, Augmented Reality (AR), Virtual Reality (VR)), a new IEEE 802.11 Task Group (TG), started its activity in 2015, namely IEEE 802.11ay [95]. The TG is aiming to develop enhancements to the IEEE 802.11ad standard to enable operation in license-exempt bands above 45 GHz [96]. Even though, there is still a lot of work to be done until IEEE 802.11ay reaches a stable release, this subsection overviews some of the basic enhancements proposed so far.

IEEE 802.11ay shares a lot of similarities with IEEE 802.11ad, however, a number of new features have been proposed and are currently under consideration in this amendment [97], including: i) Channel Bonding and Carrier Aggregation (CA), ii) MIMO Beamforming, Multi User - MIMO (MU-MIMO) Beamforming, iii) antenna polarization, iv) TDD, and v) Network Coding.

2.2.3.2.1 PHY Layer Enhancements

IEEE 802.11ay uses 6 different channel bandwidth combinations via channel bonding; the mandatory 2.16 GHz and 4.32 GHz, and the optional support of contiguous 6.48, 8.64 GHz and non-contiguous 2.16 + 2.16, and 4.32 + 4.32 GHz. Note that there is a difference between Channel Bonding and CA, i.e. in the former case a single waveform occupies the whole contiguous bandwidth, whereas in the latter, each channel might use different waveform [98].

Hybrid or even Digital beamforming architecture might be used in Enhanced DMG (eDMG) amendment whilst enhancements in TRN design to increase efficiency are also planned to be introduced. MIMO Beamforming or MU-MIMO Beamforming, comprises two phases, namely Single-Input-Single-Output (SISO) phase and MIMO phase. During the first phase that is further divided into three sub-phases, eDMG STAs identify the potential sectors that will be used during the MIMO phase. The second phase, comprises four sub-phases and enables the training of the sectors selected during SISO phase.

Antenna polarization is another topic that is being studied in IEEE 802.11ay [99]–

[101]. The most popular polarization mechanisms used are linear (LP) and circular (CP) polarizations. LP is considered to be the simplest due to the fact that it requires a simple feed network and no external polarizer. There are two forms of LP; horizontal, where the electric field is parallel to Earth's surface, and vertical, where the electric field is perpendicular to Earth's surface. CP is more complicated than LP since a CP antenna usually requires an external polarizer [102]. It is however more resilient to multipath and fading and it does not require perfect alignment between the transmitter and the receiver [103]. These characteristics make CP essential for applications which involve satellite communications (i.e. portable devices with GPS capability) [104], [105]. LP on the other hand is suitable for applications that have a guaranteed LOS and for applications that require high gain antennas. However, perfect alignment between the transmitter and the receiver is essential which limits their practical use. Practically an antenna is always elliptically polarized since perfect LP or perfect CP are very hard to be achieved. Depending on the level of elliptical polarization applied, an antenna can be distinguished as either LP or CP. Polarization reconfigurable antennas are also very important, as they provide polarization diversity and flexibility [106], [107], meaning that they can be used in various applications. They can be reconfiguring between LP and CP or between Right-Hand CP (RHCP) and Left-Hand (LHCP) modes.

To mitigate interference level and address the blocking effect, where the desired packet is blocked from being detected (a node is locked onto an early packet), the support of TDD is also being studied in IEEE 802.11ay [108]. TDD may simplify the channel sounding and improve time fairness between TX and RX periods. However, challenges as the coordination of the time periods for a network, may arise in TDD systems.

2.2.3.2.2 MAC Layer Enhancements

The IEEE 802.11ay MAC layer follows the IEEE 802.11ad and IEEE 802.11ac standards, however, modifications have been introduced to support the new features, e.g. TDD. Relaxation of the Clear Channel Assessment (CCA) thresholds (i.e. aggressive CCA values) could improve the throughput and be more suitable for directional communications. Delayed Block-ACK to a following SP and enhancements in the beacon frames to

ensure co-existence with other mmWave-based technologies (e.g. IEEE 802.11ad, IEEE 802.11ay focused on different use cases) are also under consideration in TGay.

2.2.3.2.3 Relaying Advancements; A Network Coding Approach

To improve multi-hop transmission, relaying will be supported in IEEE 802.11ay amendment (similar to IEEE 802.11ad), based on a network coding technology [109]. The main objective for network coding is to enable combining of information from separate flows within an intermediate node (relay), thus increasing the network capacity [110], [111]. The receiver can, after collecting sufficient information from both links (direct and relaying), successfully decode the message.

The simplest way to perform network coding is by applying XOR operation to the input-packet streams [112], [113]. One approach to mixing information makes use of Linear Network Codes (LNC), where coefficients are selected over a finite field, known as Galois Field. For example, operations in a finite field of 2^8 (e.g. numbers ≤ 255) are performed over bytes, while XOR is performed over the bits. The computational cost increases with the size of Galois Field. Random LNC (RLNC) [114] is another class of LNC, where coefficients are randomly selected. In that way, the probability that a node will receive coded packets, which are linearly independent, remains high. The main benefit of RLNC is that it can be performed in every hop, protecting the initial message, by adding redundant information. However, this comes at the cost of high overhead due to coefficients that need to be transmitted along with the initial message, otherwise the recipient will not be able to decode the packets. Although, RLNC has been designed to operate on equal size packets, many application produce frames in a variable bitrate, hence resulting in unequal packet sizes. The work in [115] proposes a new way of arranging the raw packets based on coding macro-symbols (fixed-sized part of a packet) in order to reduce the padding information required for the RLNC.

Two approaches have been widely followed to reduce RLNC overhead, complexity, and to improve performance; a Systematic approach (S-RLNC) and a concatenation of an erasure code with RLNC to combine the advantages of both schemes. In S-RLNC [116], the original packets are transmitted along with the encoded ones. Therefore, if insuffi-

cient number of packets is received, RLNC decoder is skipped, while the recipient is still able to retrieve a part or even whole information from the uncoded packets. A two-fold gain in encoding/decoding throughput is reported in [116] as well as lower overheads (especially for good-quality links) and lower computational cost (smaller finite field can be used instead).

There has also been considerable research on concatenation schemes in the literature [117]–[120]. Concatenated codes mimic the systematic approach, however, the transmitted systematic packets are encoded, instead. They consist of an outer and an inner code. The outer code is usually a powerful fountain rateless code (e.g. Luby Transform (LT) codes), whereas the inner code is RLNC or S-RLNC, used to allow re-encoding in intermediate nodes. Hence, in case of insufficient number of received symbols, the inner code is skipped and the outer code tries to decode the message. BATched Sparse code (BATS) [117], is an example of a concatenated coding scheme that is under consideration in this task group [109]. The outer code in BATS, operates at the transmitter, whereas the inner code may reside in any intermediate node, which linearly combines only packets belonging in the same batch and flow. However, by applying both outer and inner codes on the same node, a higher performance in terms of decoding success rate can be observed [118].

The main question that needs to be answered here is, what is the best layer to apply coding? The application layer is the most convenient layer to apply a network coding scheme, as there would be no need for the Layer 3/routing and MAC protocols to be modified. However, this comes at the cost of reduced throughput and robustness gains (channel conditions are not known to that layer) [121]. By applying a network coding scheme in Transmission Control Protocol / Internet Protocol (TCP/IP) layer or above it, there is always the risk of overflowing TCP buffer(s) with encoded packets. Moreover, delay may increase, since a node must wait until a sufficient number of encoded packets is received before proceeding to decode. If network coding is performed at the lower layers (i.e. RAN), higher gains could be achieved. However, if network coding is applied at PHY layer then additional delays may arise, since information that is carried in MAC header is now encoded. This means that nodes need to collect a sufficient number of packets before attempting to decode them and accessing this information,

e.g. destination address. Moreover, complexity also increases when operating in larger frames due to headers or frame aggregation schemes, especially if the final recipient is not the node that has decoded these packets. Another issue for applying it at PHY layer in an IEEE 802.11 system, is the limited processing time that nodes have, once they grant access to the medium, e.g. dequeuing a packet from MAC queue and applying fragmentation or aggregation.

2.3 Technologies Designed to Operate at Below 6 GHz Bands

This section describes the cellular and Wi-Fi technologies operating at frequency bands below 6 GHz.

2.3.1 3GPP LTE Technology Evolution

The core network of LTE is the Evolved Packet Core (EPC), introduced in 3GPP Release-8 (Rel-8), replacing the architecture used in Global System for Mobile Communications (GSM), known as 2G system, and High-Speed Packet Access (HSPA) / Wideband Code Division Multiple Access (WCDMA) [122]. It is part of the Evolved Packet System (EPS) and it was designed to enable flat architecture, cost efficiency, and enhanced performance. EPC comprises the Serving Gateway (S-GW), the Packet-Data-Network Gateway (P-GW), the Mobility Management Entity (MME), and the Home Subscriber Server (HSS). Moreover, it separates the user data (U-Plane) and signaling control (C-Plane), providing more flexibility to vendors and network operators.

2.3.1.1 LTE Channel Architecture & Initial Access

LTE is the access scheme of EPS, which was designed to provide high spectral efficiency, low delay and overheads, and high peak data rates. LTE Rel-8, was finalized in December 2008 and the first commercial deployments were available in late 2009. It comprises four layers; the Packet Data Convergence Protocol (PDCP), the Radio-Link Control

(RLC), MAC, and finally, the PHY. A user may have multiple radio bearers, but only one PDCP and RLC per bearer. On the other hand, one MAC is supported per user, but multiple PHYs; one per Component Carrier (CC) when CA is used (from Rel-10).

Those layers are connected through channels; logical channels that connect RLC and MAC layers, transport channels between MAC and PHY, and physical channels. The logical channels are split into control and traffic channels. The control channels include, Paging Control Channel (PCCH), Broadcast Control Channel (BCCH), Common Control Channel (CCCH) for random access or to set-up a connection, Dedicated Control Channel (DCCH) for handover or power-control, and Multicast Control Channel (MCCH). Dedicated Traffic Channel (DTCH), and Multicast Traffic Channel (MTCH) are also logical channels and defined as traffic channels. The transport channels include the channels for DL and UL transmissions. The former comprises Broadcast Channel (BCH), DL-Shared Channel (DL-SCH), Paging Channel (PCH), and Multicast Channel (MCH). The latter category includes UL-Shared Channel (UL-SCH) and Random-Access Channel (RACH). Finally, transport channels link to the physical ones. The PHY channels for DL include Physical Broadcast Channel (PBCH), Physical Data Shared Channel (PDSCH), Physical Control DL Channel (PCDCH), Physical Control Format Indicator Channel (PCFICH), Physical Hybrid-ARQ Indicator Channel (PHICH), and Physical Multicast Channel (PMCH). PCFICH identifies the number of OFDM symbols used for PDCCH that carries information about DL resource scheduling or UL transmit-power level restrictions. PHICH is used for transmitting a positive or negative acknowledgement for UL data frames. On the other hand, three channels are dedicated for UL transmissions, namely, Physical UL Control Channel (PUCCH), Physical UL Shared Channel (PUSCH), and Physical Random-Access Channel (PRACH).

PRACH has bandwidth of 1.08 MHz and is used to carry random-access preambles during the random-access procedure. It is used by users (a.k.a. User Equipment - UE) to initiate data transfer. A UE randomly chooses a preamble sequence out of a pool containing 64 preamble sequences and transmits it on PRACH. If a UE does not receive a Random-Access Response in PDSCH, it will increase the transmission power and will re-send the preamble. The next step is the transmission of Device Identification Frame in PUSCH by an UE. The last step includes the transmission of

the Contention-Resolution Frame in PDCCH by a BS (a.k.a. eNodeB), which resolves preamble collisions due to multiple UEs choosing the same preamble. When a preamble collision has been detected, a UE restarts the procedure after a random back-off.

2.3.1.2 LTE Link Layer Design

PDCP is responsible for sequence numbering (delivering in order and removing duplicate data), header compression (only for data frames), ciphering protection against eavesdropping, and integrity protection for C-Plane. It also plays a significant role during handovers.

The role of RLC is to correct any residual errors passed in that layer and missing frames (gap in sequence) with the Automatic Repeat Request (ARQ) and frames' segmentation or concatenation. Frame's size affects the selection of data rate and overhead. Large frames reduce the probability of using low-data rates while small frames result in high overhead due to the headers. ARQ completely discards a packet with an error and requests for retransmission, whilst maintaining low overheads due to its size and its infrequent transmission, but it comes at the cost of low reliability [123].

Three types of ARQ are supported. Stop-and-wait, where the reception of a 1-bit Acknowledgment/ Negative-Acknowledgment (ACK/NACK) indicates if a frame is correctly or not received. The second type is go-back-N, where all packets with sequence number larger or equal to the one indicating as not-being received, are retransmitted. The last type is the selective-repeat, which is similar to the go-back-N technique, but only the missing packets or these that have been dropped due to an error, are being retransmitted. Three different modes are supported by RLC: i) the Transparent Mode that does not add any overhead (RLC header) and does not allow any type of retransmissions, ii) the Unacknowledged Mode that supports all functionalities of RLC, but retransmissions, and iii) the Acknowledged Mode, which supports all features of RLC.

Following RLC, is the MAC layer, which is responsible for random-access, multiplexing logical channels and mapping them to transport channels, and link adaptation where the transmission parameters are set based on channel conditions [124]. Hybrid-ARQ (HARQ) is also part of the MAC layer, a combination of ARQ and Forward Error

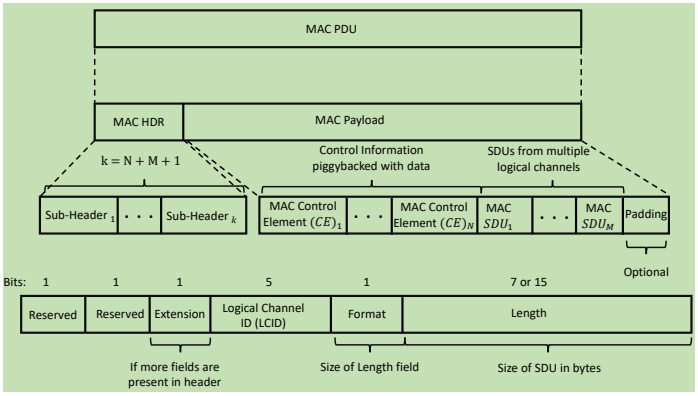

Figure 2.4: LTE MAC frame structure.

Correction (FEC), that enables fast retransmissions (frequently transmitted), high reliability, and handles with most of the errors. Three diverse types are defined for HARQ; Type-I, Type-II, and Type-III. The former is similar to RLC ARQ scheme, while Type-II retransmits parity bits that are combined with the buffered received packets. In Type-III, every packet is self-decodable, which means that even if one packet is missing, the decoding procedure does not halt. However, this tremendous advantage of Type-III comes at the cost of high overheads.

In contrast to ARQ that operates per logical channel, HARQ might retransmit data from multiple logical channels. Retransmissions in HARQ can occur either on a specific time after the end of the previous transmission (synchronous) or at any time (asynchronous). HARQ can also be transmitted in a different format and/or frequency resources if the adaptive HARQ is supported. The asynchronous adaptive HARQ is supported in DL, while the synchronous non-adaptive in UL (e.g. retransmissions occur 8 subframes after the initial transmission).

MAC also, takes care of UL and DL scheduling (requests for resources) or multiplexing of multiple CCs when CA is used. A structure of a MAC frame is depicted in Figure 2.4. Packet scheduling is responsible for allocating resources to UEs in an efficient way to maximize spectral efficiency [125].

Different scheduling approaches can be followed by vendors and network operators, based on the users' needs. However, there is a tradeoff between maximizing fairness and throughput capacity, when scheduling resources to the UEs. There are three

main scheduling approaches that can be followed: i) Round-Robin, ii) Max-Carrier-to-Interference (Max-C/I), and iii) Proportional-Fair. Round-Robin distributes the same amount of resources to UEs, without considering the channel conditions. Therefore, this scheduling method preserves fairness in terms of resources, but not in terms of QoS. The second strategy assigns resources to UEs with good channel quality (support of high-data rates (high SNR)). Although this mechanism maximizes throughput capacity, it degrades fairness between UEs with high SNR and those with poor channel conditions (e.g. cell-edge UEs) [126]. To address these fairness issues, Proportional-Fair allocates resources to UEs based on the average SNR over a period (in a long term), improving fairness as long as the average Signal-to-Interference-plus-Noise ratios (SINRs) are uniformly distributed [127].

LTE PHY layer supports both FDD and TDD schemes. TDD has lower cost than FDD, since it does not require a diplexer to separate/combine the different frequency bands used for DL and UL transmissions [128]. It is also, preferred by vendors when the available spectrum is limited and due to the low overheads when it comes to CSI reports. TDD also, efficiently deals with asymmetric traffic, since the resources in UL and DL can dynamically be allocated (DL/UL ratio) based on the user needs [129]. On the other hand, cross slot interference may occur in TDD, hence, larger guard periods (GPs) than in FDD are used, which affect throughput capacity. In FDD, the GP used to separate UL and DL in frequency bands, does not have any impact on capacity (i.e. non-contiguous bands).

Two different frame types are supported; Type-1 for FDD and Type-2 for TDD, illustrated in Figures 2.5a and 2.5b. For both types, the frame duration is 10ms and comprises 10 subframes (1 ms each subframe). Each subframe consists of 2 slots with duration of 0.5ms each one. Now, the smallest unit allocated to a user is the Resource Block (RB) that consists of 12 subcarriers in the frequency domain ($12 * (15kHz) = 180kHz$) and one 0.5ms slot in the time domain. However, the smallest physical unit in LTE is the Resource Element (RE), comprises one subcarrier during one OFDM symbol. A 0.5ms slot can accommodate either 7 OFDM symbols when the normal Cyclic Prefix (CP) is used or 6 when the extended CP is applied. The useful symbol duration is 66.7μs ($1/15kHz$), while the normal and extended CP are 4.7μs and 16.67μs, respec-

tively. When normal CP is used, the CP in the $1st$ OFDM symbol is longer than 4.7μs to fill the entire 0.5μs slot. The RBs are defined over one slot and not per subframe due to distributed DL transmission and UL frequency hopping [123]. Further, the number of RBs per carrier, ranges from 6 to 110, corresponding to the channel bandwidth (varies from 1.4 MHz to 20 MHz).

For Type-2; a TDD frame structure, the frame might be divided into two half-frames of 5ms duration each, prior the subframes. There are 7 different frame configurations for different DL/UL ratios; from 1/3 to 8/1. There are some common rules for all configurations, such as the $1st$ subframe is always a DL one carrying information about the structure that is to be followed, while the $3rd$ is an UL subframe. A special subframe is always used when switching from DL to UL subframe that consists of: i) DL Pilot Time Slot (DwPTS) that carries control information and reference signals, ii) GP to control switching from DL to UL, and iii) UL Pilot Time Slot (UpPTS) that is used for channel sounding and random access.

LTE is based on OFDM, due to the inherent advantages that this technology offers; resilience to interference, ISI, selective fading etc. It is based on a parallel data transmission and divides the available bandwidth into smaller channels, namely subcarriers (different frequency per subcarrier), using different modulation scheme for each one. Thus, based on channel conditions, high order of MCS can be used per subcarrier, achieving higher data rate. The long OFDM symbol duration along with the use of CP at the beginning of each symbol, make OFDM resilient to multipath delays and spread. ISI can be reduced by extending the length of CP, such that the maximum delay spread is less than the duration of CP. However, a very long CP reduces the data throughput, while a small one may cause strong ISI. CP is also used for synchronization by identifying the start and end points of a symbol [130].

Further, OFDM improves spectrum efficiency by tightly placing the subcarriers (subcarriers are not separated but ovelapped), that do not interfere to each other due to their orthogonality. If orthogonality is missed (inadequate CP) due to frequency mismatch in the transmitter and receiver oscillators, Inter-Carrier Interference (ICI) may occur. This mismatch may occur due to lost synchronization or the Doppler effect.

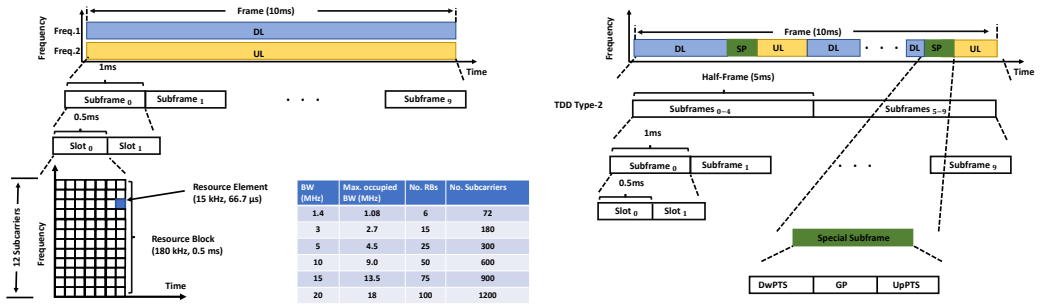

(a) (b)

Figure 2.5: LTE a) FDD structure and b) TDD structure.

To mitigate ICI, several techniques have been proposed (e.g. Minimum Mean Squared Error (MMSE)), but they are out of the scope of this research. OFDM also suffers from high Peak-to-Average-Power ratio (PARP) that occurs because several subcarriers are transmitted with extremely higher power than the average power level used throughout the subcarriers. This requires Analog-to-Digital (A/D) and Digital-to-Analog (D/A) converters capable of handling this range, which may degrade transmitter's power amplifier efficiency. Traditional methods dealing with the high PARP, include clipping and filtering, which suffer from the high Bit Error Rate (BER) due to the distortion they cause in the transmitted signals [131].

An alternative access scheme to OFDMA, used in DL, is realized for UL traffic, due to the power-limited mobile devices (power consumption). Therefore, Single-Carrier FDMA (SC-FDMA) is the scheme used in UL, because of the low PARP compared to OFDMA, since the signal is transmitted over a single carrier. On the other hand, SC-FDMA has certain disadvantages against OFDMA that prevent its usage for DL transmissions (e.g. higher computation cost at the receiver, lower spectral efficiency especially for high SNRs, channel estimation using pilots is harder due to the lack of orthogonal data on each frequency bin etc.).

2.3.1.3 LTE Evolution; An Overview through Releases

In this section, we overview the main techniques and advanced technologies introduced throughout 3GPP LTE Releases. We start from the first LTE Releases; Rel-8/9 through

to the current Rel-14. We describe the potential directions and advanced technologies that 3GPP LTE community is looking at in Rel-15, which is under active development. The evolution of LTE through releases is also depicted in Figure 2.6.

2.3.1.3.1 A walk through Releases 8-12

Even from the first releases (Rel-8/9), a lot of attention has been given paid to ICIC mechanisms, where messages are exchanged among eNodeBs through the X2 interface, aiming to improve not only the average cell capacity but cell edge users' performance. MIMO and MU-MIMO in both UL and DL directions were among the features introduced in the first release, supporting 4x4 MIMO in DL and one-layer transmission in UL to maintain low complexity, initially. Power control in the UL direction and soft/hard Fractional Frequency Reuse (FFR) are also supported to mitigate interference [132]. Soft FFR refers to the case where eNodeBs do not transmit on specific resources, whereas hard FFR to the case where eNodeBs use lower transmit powers on certain resources. Soft FFR improves spectral efficiency, since the UEs close to eNodeBs that experience high SINR can be allocated to those power-limited resources. Two diverse types of relaying schemes, e.g. Amplify-and-Forward in Layer 1, where the signal is amplified along with the noise and Decode-and-Forward in Layer 2, where noise is not forwarded but higher latency to the system might be introduced, are also supported in the very first releases [133]. The support of broadcasting/multicasting of the same content over multiple co-channel cells with Multicast/Broadcast Single-Frequency Network (MBSFN) is also initially proposed in Rel-8/9. MBSFN is an advancement on the Multimedia Broadcast Multicast Services (MBMS), a feature that was initially introduced in 2004 in Universal Mobile Telecommunications System (UMTS) Rel-6, that requires a tight frequency and time synchronization among the cells that participate in those transmissions. With MBSFN, multiple cells transmit at the same time and frequency (synchronised transmissions), using the same waveform. These multiple concurrent transmissions are perceived as a single transmission by the UEs and giving rise to constructive interference when tight synchronization among the cells is achieved (if signals are received within the CP period). Discontinuous Reception (DRX) and Discontinuous Transmission (DTX) functionalities for reducing power consumption in

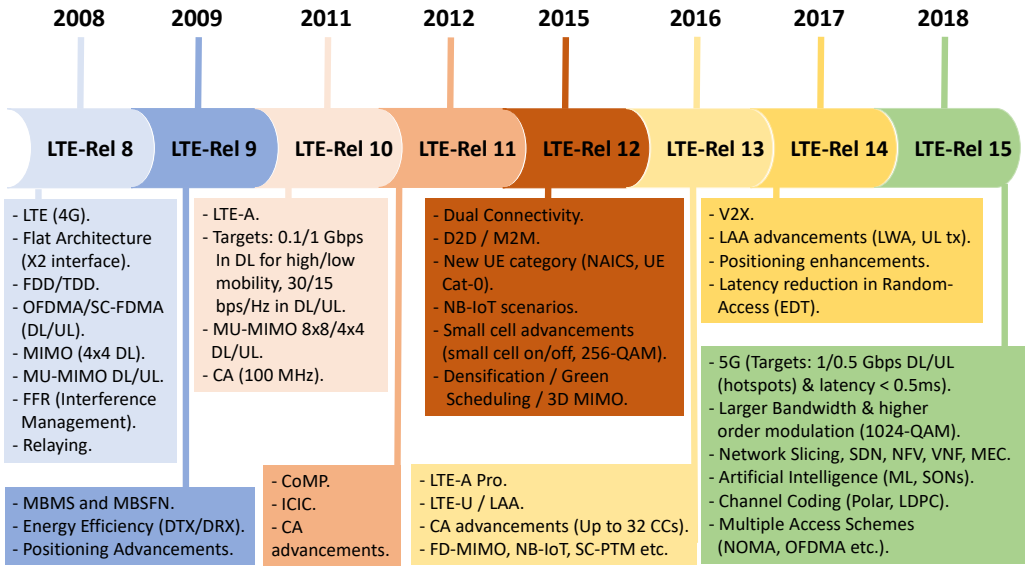

Figure 2.6: An overview of 3GPP LTE evolution.

mobile devices and advancements in positioning (i.e. position estimation by monitoring the relative time of arrival of some special signals from multiple cells) are among other features incorporated into Rel-8/9 specifications.

To meet the targets for 4G networks, 3GPP released LTE-Advanced (a.k.a Rel-10) specifications in 2011. The support of higher order MU-MIMO configurations in both directions, CA [134], and heterogeneous networks, can help to boost the peak data rates to 3 and 1.5 Gbps in DL and UL, respectively, in LTE Rel-10 [135]. At the same time a two-fold higher spectral efficiency than Rel-8 was realized. To preserve backward compatibility, the transparent relaying mode was introduced for in-band or out-band relays [136].

CA in Rel-10, allowed up to 5 CCs using the same duplex scheme, forming channel bandwidths up to 100 MHz, while the number of CCs in UL should be less than or equal to that in DL. The Primary Cell (PCell) is used for radio monitoring, re-establishing Radio Resource Control (RRC) connection, maintaining continuous communications due to mobility etc, whereas the rest of the CCs (Secondary Cells (SCells)) are used to provide additional resources. Moreover, each SCell has its own HARQ, implying that most HARQs are transmitted over the same SCell as the original data, while an ARQ (at RLC level) may be sent over different SCell, since CA is invisible above MAC.

Three diverse types of CA, namely, intra-band contiguous, intra-band non-contiguous, and inter-band were also specified. The use of different MCS and/or transmit power per CC or non-contiguous CA, especially inter-band CA, and the flexibility of scheduling PDCCH on different CCs (cross-carrier scheduling) can improve system's coverage and reduce inter-cell interference. Two different queuing structures can be used for CA; Joint Queue Scheduler (JQS), where one queue per UE for all CCs is realized or Disjoint Queue Scheduler (DQS), with one queue per CC per UE [137]. It is shown in [138] that JQS outperforms DQS in terms of spectral efficiency as packets can use all RBs in all CCs and not only the one that a queue belongs to. The scheduling of CCs is a new functionality of Radio Resource Management (RRM) in Rel-10 and is based on channel characteristics, QoS requirements, and traffic conditions (e.g. Random, Circular, and Least Selection techniques). On the other hand, implementation complexity and power consumption increase as the number of supported CCs increases [139]. Among the three CA configurations, the non-contiguous has the highest complexity, as the RRM and the RF implementation complexities in the terminal have to take into account the different Doppler shift and path loss that different frequencies experience [140].

The two main foci in Rel-11, were techniques for improving energy efficiency by reducing RAT's capabilities while other RATs providing support [141], and reducing inter-cell interference. Inter-cell interference remains the main obstacle to achieving data rates close to the theoretical bounds. Common Reference Signals (CRS) cancellation [142] and Coordinated Multipoint (CoMP) for constructive interference are among the features introduced in Rel-11, in support of higher capacity.

CoMP allows either a single transmission/reception through multiple eNodeBs with one eNodeB enabled each time, or a joint transmission/reception from multiple eNodeBs. A joint transmission could be of two types; non-coherent where each eNodeB individually and independently from the rest eNodeBs calculates the precoding matrix for a transmission and coherent where multiple eNodeBs act like a single virtual eNodeB. The latter, requires the sharing of data and messages between eNodeBs through the X2 interface. One message defined for DL ICIC, namely Relative Narrowband Transmit Power (RNTP), provides information for specific RBs. RNTP is indeed, a proactive tool that tries to prevent transmissions scheduled in RBs with low SINR. On the other

hand, two types of messages are defined for UL transmissions; High-Interference Indicator (HII) and Overload Indicator (OI). The former, works in a similar way to RNTP, while OI indicates the interference levels for different RBs, such that a neighboring eNodeB to re-schedule UEs in order to mitigate interference. Requirements on low-latency, high-capacity backhaul and the tight synchronization in time and frequency domain of eNodeB are the main challenges associated with the CoMP technology [143].

In early 2015, almost two years after the introduction of Rel-11, the Rel-12 was launched. It was the era that made operators and researchers to take into consideration and tackle the emerging issue of energy emissions by the mobile networks due to the support of massive number of portable devices, and seek solutions for improving energy efficiency [144]–[146]. For example, higher MCS might be more efficient than a lower one, considering the energy consumed by the RF components (i.e. power amplifier, circuit, feed losses etc.). The main goals for Rel-12, apart from energy efficiency, were to provide higher Quality of Experience (QoE) and support diverse types of traffic and services [147].

The support of higher order modulation (256-QAM), small cell On/Off based on the traffic demand, and dual connectivity for non-ideal backhaul links were the major features introduced in Rel-12 to enhance per user throughput, reduce signaling load and power consumption, and improve mobility robustness in heterogeneous networks [148]. Although, small cell On/Off technique reduces network's energy consumption and signaling load, there is always the risk of reduced coverage or increased scanning/discovery delay for the UEs, thus, its use was restricted to SCells only. Enhanced Interference Mitigation and Traffic Adaptation (eIMTA) feature was introduced in this release, aiming to dynamically adjust resources for DL and UL (Dynamic TDD), utilizing resources per link. Dual connectivity was introduced for non-ideal backhaul, operating on the same or not frequency band, aiming at improving mobility support whilst reducing signaling overheads during handovers.

CA between TDD and FDD was also supported in Rel-12, whereas enhancements for MBMS when an interface fails and MBMS operation on demand were also proposed for enabling seamless MBSS connectivity. Advanced (higher order) MIMO schemes were also introduced, while the study for 3D MIMO was also started. Furthermore, a new

category of UE receivers, capable of Network Assisted Interference Cancellation and Suppression (NAICS), new Device-to-Device (D2D) and Machine-to-Machine (M2M) scenarios were also part of Rel-12.

The motivation of enabling D2D Proximity Services (ProSec) communications was to support Public Safety (i.e. police, fire, and ambulance) communications [149]. Up to that time, Public Safety communications were using the Terrestrial Trunked Radio (TETRA) system, developed back in 90s' with limited capabilities. Although, Public Safety applications can use Wi-Fi or Bluetooth technologies in an ad-hoc manner, these technologies are characterized by limited range, inability to provide an adequate level of security and integrity, and independent operation from the cellular systems. Therefore, in Rel-12, 3GPP identified three main scenarios for D2D; the in-coverage, where eNodeBs control the resources, the out-of-coverage, where UEs use predefined resources, and the partial-coverage [149]. The last scenario refers to the case where one UE is in-coverage while the second device is out-of-coverage. The communication link between the devices (PC5 interface) is known as sidelink used in UL subframes by both TDD and FDD modes. Two operational phases have been introduced, namely Discovery and Communication. The former is used for broadcasting short messages and discovering devices in close proximity [150], [151]. For example, a device may transmit a message declaring its presence or requesting what devices are within its range. The latter discovery phase, uses the Physical Sidelink Discovery Channel (PSDCH) and was initially supported only for the in-coverage scenario. Prior the discovery phase, synchronization between the devices is required. Synchronization uses the Physical Sidelink Broadcast Channel (PSBCH) and can be achieved either through eNodeBs or the transmission of Sidelink Synchronization Signals (SLSSs) for the out-of-coverage scenario. Communication mode, on the other hand, uses the Physical Sidelink Shared Channel (PSSCH) and was initially supported only for the out-of-coverage case.

2.3.1.3.2 3GPP LTE-Advanced Pro - Release-13

3GPP Rel-13, also known as LTE-Advanced Pro, continued the study and work on D2D, M2M, and Narrow-Band IoT scenarios, CA enhancements (up to 32 CCs), and more

importantly the new features such as densification (LTE in unlicensed spectrum and dual connectivity enhancements), and advanced MIMO (Full-Dimension MIMO) [152]–[154]. From a system point of view, two are the main objects to highlight here; the study of core network virtualization [155], which is a mature technology that could be incorporated by 3GPP and the study of critical communications [156].

The first step for enabling substantial number of antennas in a 2D antenna array (FD-MIMO), thus, enabling beamforming in both azimuth and elevation, was the study of new 3D channel models and then an evaluation of FD-MIMO's potential benefits [157]. The substantial number of antennas (massive MIMO) could save at least an order of magnitude in transmit power, average out the effects of small-scale fading and thermal noise. On the other hand, complexity, energy consumption, and control overhead (pilot contamination) increase with the number of antennas [49]. To address pilot contamination, usage of MIMO in TDD along with lean communications were proposed [158], [159]. A four-fold gain for both cell-average and 5th percentile user throughputs were observed in [160], when both elevation and azimuth are exploited (FD-MIMO). Moreover, higher order of MU-MIMO can be realized with FD-MIMO, while maintaining the same SINR level per UE if the number of antennas increases at the same rate as the number of co-scheduled UEs [161]. In addition, MIMO is more susceptible to CFO due to multiple simultaneous data streams transmitted, thus, data-aided or blind estimation (e.g. Gardner's non-data-aided) methods are used. However, the first approach is shown to provide better performance at the cost of higher overheads.

To meet the projected traffic demands, 3GPP Rel-13 also studied the case of using unlicensed spectrum in DL along with other technologies (i.e. Wi-Fi). Two different approaches were proposed by the vendors; either a vendor deploys a Wi-Fi infrastructure and a communication link inter-operates between LTE and Wi-Fi or makes use of the unlicensed spectrum through a single network. The second approach reduces operational cost and provides better QoE, since LTE deals with the communications in the unlicensed spectrum.

The main benefits of using unlicensed spectrum are: i) increased capacity, ii) higher number of users served, and iii) enhanced system coverage [162]. On the other hand,

the main challenges arising from the coexistence of a synchronous and an asynchronous technology relate to: i) the access control, ii) traffic scheduling, iii) interference mitigation, and iv) fairness issues. Operation of LTE in the unlicensed band is based on CA, with PCells operate always in licensed spectrum, while SCells in both licensed and unlicensed bands. This is because in unlicensed spectrum, QoS is not guaranteed and interference cannot easily be controlled due to the unmanaged/ unplanned deployment of APs. SCells in unlicensed band are usually used to support low-mobility UEs, forming small-cell deployments. Thus, before enabling CA in the unlicensed spectrum, traffic load and channel information must be considered [163]. The two main techniques used in LTE to access the unlicensed spectrum are: Carrier Sensing Adaptive Transmission (CSAT) and Listen-Before-Talk (LBT).

CSAT is used in countries where there are no LBT requirements (LTE-U), e.g. USA, South Korea, and China. It is based on the Dynamic Frequency Selection (DFS), where the devices search for low-loaded channels. They also, continuously sense the medium in order to identify the channel status (BUSY or IDLE). In case that a channel is used by a higher priority technology (e.g. radar), then UEs vacate this channel within a certain period, but are able to use it after a specific time. With CSAT, eNodeBs identify and access channels based on a duty cycle that is adjustable, based on channel's activity.

On the other hand, LBT mechanism (Licensed Assisted Access - LAA) uses CCA to access the medium. Based on CCA, an LAA device monitors the channel for a period of at least 20μs and applies the Energy Detection (CCA/ED) threshold (i.e. -72 dBm) to identify channel's status. If within that period, energy level exceeds CCA/ED, then the channel is considered BUSY and the transmission is postponed. In that case, the Almost Blank Subframe (ABS) technique may be applied, where LTE transmits subframes carrying vital information (e.g. control, synchronization signals but no user-plane traffic). If the channel is sensed IDLE, devices proceed to a transmission. However, the maximum channel occupancy time is up to 10ms. In case that a transmission exceeds the maximum channel occupancy duration, DTX is performed. This, however, comes at a price of affecting frequency/time synchronization, CSI measurements, and AGC.

Since, CSAT is not CCA-based, collision overheads and latency (channel sensing dura-

tion of up to 200ms) is higher than in LBT. Moreover, it is usually, more aggressive and less fair than LBT because of the different approach followed, compared to Wi-Fi [164]. However, by utilizing CSAT On/Off periods based on traffic load, Wi-Fi performance and fairness can be preserved.

Enhancements to MBMS (eMBMS) are also introduced in this release. Single-Carrier Point-to-Multipoint (SC-PTM) uses the same system architecture as MBMS, supporting broadcast/multicast services, multiplexed over a single cell through PDSCH, instead of PMCH. It reduces the latency of MBSFN and improves radio efficiency by dynamically assigning resources to a group of UEs, based on real-time traffic load. Indoor positioning was also one of the priorities for 3GPP Rel-13, aiming at improving position accuracy [165], [166]. The requirements for indoor positioning were issued by Federal Communications Commission (FCC) to gradually improve accuracy for public and safety services/calls within a period of 6 years. In particular, until 2021, an accuracy of 50 meters for at least 80% of the calls is required to be achieved [167].

2.3.1.3.3 3GPP LTE-Advanced-Pro - Release-14

The recent 3GPP release, Rel-14, is generally considered as the last release before entering the era of 5G. This release mainly focused on enhancing LAA to support dual connectivity in UL (eLAA), and enhanced LTE-WLAN Aggregation (eLWA) in UL, FD-MIMO, M2M, and MBMS. At the same time, reduced latency and support of critical Video/Data and Vehicle-to-Everything (V2X) services were also among the items studied in Rel-14 [168].

Extending LAA to UL transmissions is challenging due to the scheduling requests, processing delay, and overhead. UEs transmit the scheduling requests in PUCCH, while eNodeBs respond to PDCCH after performed CCA (in case of LBT). When access is granted, UEs will again perform CCA to ensure that the channel is still available. This delay results in unused subframes between DL and UL transmissions. To cope with the high delay and overhead, CCA time reduction or unscheduled access in UL; similar to Wi-Fi access scheme, could be applied [169].

Limitations of FD-MIMO in 3GPP Rel-13, such as limited number of antenna ports

and no support for providing robustness for high-speed UEs, were studied and addressed in 3GPP Rel-14. The number of antenna ports increased from 16 to 32, while enhancements were also proposed on CSI reports to improve efficiency of MU spatial multiplexing [170]. Moreover, features for better CSI accuracy and robustness due to inter-cell interference and high speed, are also included in that release. A possible enhancement for FD-MIMO in the next release, could be the distributed FD-MIMO (D-FD-MIMO) [171]. Further study on MIMO performance requirements for UEs was also performed [172]. As new operating bands are continuously added to 3GPP specification, the implementation of a common radio supporting simultaneous transmission and reception of multiple bands, is a feature under consideration [173]. Benefits of applying this feature at eNodeBs include dynamic power sharing among different bands and reduced installation complexity and insertion losses for multi-band antenna sharing since a single eNodeB will be capable of supporting multiple bands with no combiner required.

Another area studied in 3GPP Rel-14, was the latency reduction [174]. Random-Access and Scheduling Request procedures, the fixed duration of Transmission Time Interval (TTI), the data processing delay, and the high handover latency (approximately 47 ms for 3GPP Rel-8/9) are the main obstacles for improving performance of applications such as gaming, real-time (e.g. VoLTE, video conference), and augmented reality which have stringent low-delay requirements. Viable solutions for reducing latency include: i) increasing the frequency of Semi-Persistent Scheduling (SPS), ii) dynamically skipping of UL Grants by eNodeBs, iii) reducing RACH procedure delay during handover in a synchronized network, and iv) reducing transmission and processing delay. The latter can be achieved by reducing TTI, however, control and reference signal overheads may increase.

Advancements in MBMS were also considered, to support the reception of non-collocated multi-carrier MBMSs to deal with the high demands of diverse types of TV services and mobile video streaming [175]. In particular, advancements in radio interface include high spectrum efficiency for larger Inter-Cell Distance (ICD) by applying a larger CP, the support of new subframe type to reducing overheads, and shared eMBMS broadcast where operators can share content, avoiding broadcasting the same content over

different networks. Free-to-air services, receive-only mode (ROM), upgraded codecs for supporting Ultra-High-Definition (UHD) television require a new Application Programming Interface (API) to simplifying eMBMS procedures, and a new transparent delivery mode so that TV formats can be of a wide range are some of the enhancements introduced for eMBMS, in 3GPP System Architecture Working Group (SA). A study was also performed and provided recommendations on the mission critical video/ data services that require high availability, low latency, security etc. (e.g. new protocol additions and security functionality). On the other hand, the use of larger CP poses a restriction for supporting high data capacity for UEs with high velocity (i.e. higher than 100 km/h). The lack of feedback in eMBMS, prohibits the use of Closed-Loop MIMO with SC-PTM and MBSFN. Due to the static resource allocation, adaptation to traffic load when QoS characteristic variations are limited, service continuity (e.g. during handover) is achieved through the unicast channel or by overlapping MBSFN areas.

LTE's rival standard for supporting Vehicle-to-Vehicle (V2V) communications i.e. Vehicular Ad-hoc Networks (VANETs), was introduced in 2010, namely IEEE 802.11p [176]. Similar to most of the IEEE standards, IEEE 802.11p is a low-cost solution that is easily deployed. However, it suffers from scalability issues, limited range, low data rates, and most importantly, QoS is not guaranteed [177]. Considering all the latest advancements in LTE and the challenges that V2X communications face, LTE enhancements for vehicular communications were also proposed in Rel-14. Twenty-seven use cases and three distinct types of V2X services; V2V, Vehicle-to-Infrastructure (V2I), and Vehicle-to-Pedestrian (V2P) were considered initially.

LTE cellular V2X is based on D2D communications for supporting vehicle communications when they are in-coverage or out-of-coverage. Moreover, D2D communications (for V2V services based on sidelink PC5) can enable fast transmissions among vehicles when they are in the proximity of each other [178]. To maintain low PARP, SC-FDMA with normal CP is used in PHY layer, while the number of Demodulation Reference Signals (DMRSs) increased from 2 to 4 in a subframe to cope with the high-speed and Doppler effects. To deal with synchronization issues in D2D links, the Global Navigation Satellite System (GNSS) is used, instead of eNodeBs [179].

2.3.1.3.4 3GPP LTE in 5G era - Release-15

Rel-15 is the first release to introduce the 5th Generation of wireless communications. The main requirements on performance targets and capabilities for 5G were approved on March 2016 [180]. Performance targets vary, depending on the environment and application. For example, per user data rates of at least 1 Gbps and 500 Mbps in DL and UL for indoor hotspot environments and 20 Gbps in DL and 10 Gbps in UL for eMBB, whilst latency less than 4ms and 1ms for eMBB and URLLC, respectively, are required. Larger bandwidths and higher-order modulation are used to achieve high data rates in small cells. Enhancements to the legacy 4G protocol stack for reducing processing delays have also been introduced, given that the lion's share of latency is contributed by PDCP operations (i.e. de-ciphering, robust header compression etc.) [181].

Moreover, the new network will be characterized by: i) optimizing signaling, ii) reducing energy consumption, iii) network flexibility (optimized service provision based on slicing and flow re-routing concepts in core network), iv) traffic steering through different RATs, and v) enhancing data rate, position accuracy, and further reductions in latency. To meet the requirements of the new use cases, new features and enhancements in both the access and the core network segments have been introduced in Rel-15 and the follow-up releases.

In the first phase, enhancements in LAA and LWA due to their inherent good potentials [182], involve service pricing by making the core network able to identify the route of packets (licensed/unlicensed) and the support of 3.5 GHz band. Moreover, there is a focus on V2X services and studies of new scenarios, such as remote driving and vehicle platooning [183]. According to the 5G Automotive Association (5GAA) future V2X services will need to provide support for: i) Safety, ii) Convenience, iii) Advanced Driving Assistance, and iv) Vulnerable Road Users. The safety related use cases aim to reduce the frequency and the severity of accidents by warning drivers of accidents and collision risk through an intersection [184]. Software updates fall into the second use case group, whereas those use cases focusing on improving traffic congestion, high definition maps, road conditions, weather alerts etc., fall within the scope of the third group. The last category comprises those use cases that support communication between vehicles and

non-vehicle road users, aiming at detecting and warning drivers about their presence. The support of up to 5 CCs is also under consideration for V2X services in Releases 15/16 [185]. The 5G-PPP Phase 2 Project, 5GCAR [186] works on optimizing V2X connectivity in terms of latency and reliability, whereas improvements in positioning accuracy for both road users and vehicles are also considered. Furthermore, Future Railway Mobile Communication Systems (FRMCS) is currently being studied for future releases [187], [188]; probably after Rel-15 [189], to support seamless connectivity, low latency, and high data rates for the railway users and the safety-related applications (real-time train tracking).

Further advancements to eMBMS for supporting TV services are also expected to be introduced in 5G releases, probably in Rel-16. The 5G-XCAST [190], a 5G-PPP Phase 2 Project, works on addressing the limitations of the current eMBMS systems and developing broadcast and multicast point to multipoint capabilities for 5G networks (e.g. for scenarios such as IoT, Public Warning Systems, etc.). Seamlessly and dynamically switching between different transmission modes (i.e. unicast, multicast, broadcast) or using them in parallel are among the main priorities of 5G-XCAST.

The study of mission critical services continues in Rel-15, where one of the enhancements includes the ability of distributing mission-critical information to a group of users. Further enhancements in D2D and relays for IoT or wearable devices to support diverse types of traffic and services with reduced power consumption and complexity, are also under the microscope [191].

2.3.1.3.4.1 PHY Layer Enhancements

As part of 5G NR, subcarrier scaling has been included in the standards [192], [193], due to the particularly detrimental impact of white noise on mmWave based communications, resulting in requirement for smaller symbol durations. Different subcarrier spacing values are also supported, based on the scenario, operating frequency, etc, resulting in alterations in CP length with various sizes to be supported. Multiple access schemes are also supported by the 5G NR, subject to application type and requirements. The main challenge is how to ensure the inter-operability of the existing mature

technology (i.e. OFDMA, SC-FDMA) with Non-Orthogonal Multiple Access (NOMA) schemes [194] that are deemed more suitable for M2M communications. Therefore, one of the first tasks for Rel-15 was the study of dual connectivity of the current LTE-A Pro as PCell and 5G NR as SCell, with up to 4 CCs in DL for LTE-A Pro (4-DL/1-UL and 1 NR) and two MAC entities per UE [195]. Frequency localization to reduce in-band and out-of-band emissions, lower power consumption by utilizing SC-FDMA for UL transmissions, and slot flexibility to support multiple services with different requirements on the same frequency are also part of the 5G NR [196]. The ONE5G [197], a 5G-PPP Phase 2 Project, has already started working on the next release (a.k.a. 5G advanced (pro)) by identifying and addressing the challenges that 5G NR will face for supporting various vertical use-cases in multiple scenarios. The objectives for ONE5G include: i) further studies and enhancements on massive MIMO, access schemes, and provisioning of wireless services to improve user experience.

Channel coding is one of the fundamental areas that is being studied for the 5G NR. There has been a lot of discussions about replacing the mature coding schemes used in the previous generations e.g. Turbo codes, with LDPC or Polar codes [198]–[202]. The recently proposed, Polar codes [203], has been approved by 3GPP as the coding scheme to be used for 5G NR DL/UL control plane for eMBB, and LDPC coding for the data channel. The main reasons for replacing Turbo codes are the higher complexity and inferior performance in scenarios where high throughputs are expected. However, it is shown in [204] that by redesigning Turbo codes at software and hardware level, 5G requirements can be met, whilst maintaining backward compatibility.

2.3.1.3.4.2 MAC Layer Enhancements

CA, dual connectivity, and CoMP are three technologies that could be used for supporting connection on different/same carrier frequencies from various RATs, also known as inter/intra frequency multi-connectivity schemes [205], [206]. Utilization of CA to reduce delay, UL data compression and signaling reduction (e.g. due to paging and handover), tight interworking to support efficient and high-performance mobility between NR and LTE, and continuing the studies to address the challenges to support aerial UEs (e.g. mobility and DL/UL interference) are amongst the work items for RAN 2 [207]–

[210]. A challenging task in supporting multi-RAT operations is the identification of the radio protocol layer where the aggregation of the different technologies should occur. Aggregation at RRC and PDCP layers seems to be the most convenient place, since these layers do not need to be time-synchronized with the lower protocol layers [211]. However, since these layers do not participate in real-time radio resources utilization or medium access, inter-RATs' coordination is limited. On the other hand, RLC and MAC layers are not fully time-synchronized with PHY layer, resulting in packet and call drops when synchronization is lost [9]. Moreover, since information splits in MAC layer for CA, tight synchronization among CCs is required. However, if tight synchronization is achieved between MAC and PHY layers, then inter-RATs' coordination and resource allocation utilization becomes possible. Aggregation of multi-RAT technologies at the PHY layer might achieve higher gains in terms of aggregated throughput and reduced latency [212], but the requirements and delays associated with different air interface technologies may prove very challenging to implement. Moreover, coordination among multiple Layer 2 entities (i.e. multiple RLC entities) is essential, i.e. for retransmissions due to different HARQ configurations based on the service requirements.

A three-layer RAT switching envisioned in [213], for supporting various RAT technologies (i.e. mmWave RAT with a microwave one). The lower layer (MAC-Low) will be responsible for transmission mode switching, while the 2nd one (RRM/MAC) will be handling control information for several air interfaces. The higher one (Network), will be enabling the slice or interface switching in the Internet Protocol (IP) layer. A three-layer protocol stack to support multi-RAT 5G scenarios is also presented in [214], developed by the European 5G-PPP during Phase 1, SPEED-5G project [215]. MAC-Low is responsible for real-time operation (i.e. multiplexing/demultiplexing), whereas High-MAC deals only with the control plane and those functions that real-time execution is not required. Multi-Path TCP is also used in the 3rd layer to realize the support of multi-RAT, where traffic is redirected through multiple RATs. Clustering of multiple eNodeBs or APs, is another enabling technology that can be applied along with Machine Learning (ML) techniques, to improve networks' efficiency, such as energy efficiency [216], transmission time reduction [217], load balancing [218], and increased reliability [219], which is one of the main targets for high-velocity scenarios.

2.3.1.3.4.3 Core Network Concepts

Other complementary technologies that will be incorporated in future releases, capable of providing networks with flexibility, control, and reconfigurability are described in the following paragraphs. Although, they might not directly be related to the RAN segment (for the time being) nevertheless, modifications (or even adoption of similar concepts e.g. slicing in RAN [220]) in the lower layers will be required for supporting them.

Network Slicing will also provide networks with flexibility and scalability [221], by sharing resources; spectrum sharing [222] and processing power or storage [223]. The slices, also known as Slice/Service Type (SST), are classified based on the features and services supported into three (standardized) categories; eMBB, URLLC, and mMTC [224]. The first one aims at supporting high data rates and high capacity for fast large file transfers, high quality video streaming etc. from multiple users. The second one, URLLC, is mostly for industrial automation and remote-control systems, while the last one for supporting massive number of IoT devices. Users will be able to simultaneously connect to multiple SSTs. However, it will also be challenging to support handovers for high-speed users or manage the various levels of QoS, security, and integrity between the services [225]. Multiple MAC/RLC/PDCP entities might be needed to handle and support the diverse SSTs where inter-coordination among them might be inevitable. The control and management of vertical slices in real-world deployments is the main focus for the SLICENET Project [226] from 5G-PPP Phase 2.

Five other technologies/concepts ([227]–[231]) that will be incorporated in future releases, include: i) Software Defined Networks (SDNs), ii) Network Function Virtualization (NFV), iii) Virtual Network Function (VNF), iv) Mobile Edge Computing (MEC), and v) enhancing CoMP using the Self-Organizing Networks (SONs) technology. The former refers to the case where network objects (e.g. routers) are deployed in an automated manner, while the second technology enables SDN functions to be hardware platform-independent (e.g. load balancing in a cloud), enabling reduced energy consumption and complexity at the eNodeBs. VNF is deployed on top of NFV, while MEC is built on the concept of enabling cloud computing at the edge of cellular network (e.g. eNodeBs), which is considered an important technology especially for V2X ser-

vices where the huge volume of data needs to be processed and delivered to the vehicles in real-time [184], [232]. The 5G-PPP Phase 2 Project, 5G ESSENCE [233] continues the work of the 5G-PPP Phase 1 Projects focusing on SDN/SON (i.e. SELFNET [234], CHARISMA [235]) and envisions a multi-RAT infrastructure where MEC is enabled at a cluster of small cells that are being managed by a centralized controller.

SONs are also studied as the technology that will allow a self-based CoMP management and operation on the fly, based on user and network traffic conditions [236], [237]. The concept of SONs is not new and is based on self-awareness, self-configuration and optimization [238], characteristics that require systems with advanced intelligence for proactive decisions regarding the efficient management of spectrum [239] or the utilization of the new technologies (e.g. Massive MIMO) [240]. SON concept is also to be applied for enhancing Network Slicing operation and management by (re-)configuring, optimizing, and healing a Network Slicing Instance. The ability of identifying the failures and applying corrective actions on the fly is essential for maintaining a stable desired state for the network.

A new group was recently formed by ITU, focusing on ML for future networks, including 5G [241]. ML techniques can be used for predictions and dealing with many issues that wireless systems face. ML is, thus, a proactive tool that enables smart radio devices by adding artificial intelligence mainly in the core network [242]–[244]. For example, ML can be applied to Massive MIMO for channel estimation, finding the optimal handover solution or clustering, which is very challenging in 5G networks due to the diverse cell sizes, technologies, etc. They are categorized into three classes; supervised (labeled samples), unsupervised (unlabeled), and deep learning.

2.3.2 IEEE 802.11 Technology

Similar to the 3GPP cellular technology, new amendments are being developed by the IEEE 802.11 standards working groups to address the demands for high data rate and wide coverage in the unlicensed 2.4/5 GHz spectrum (and mmWave and Sub-1 GHz bands). The introduction of IEEE 802.11n [245], in late 00's, was revolutionary. It was a huge milestone for IEEE 802.11 family of standards and it incorporated advanced

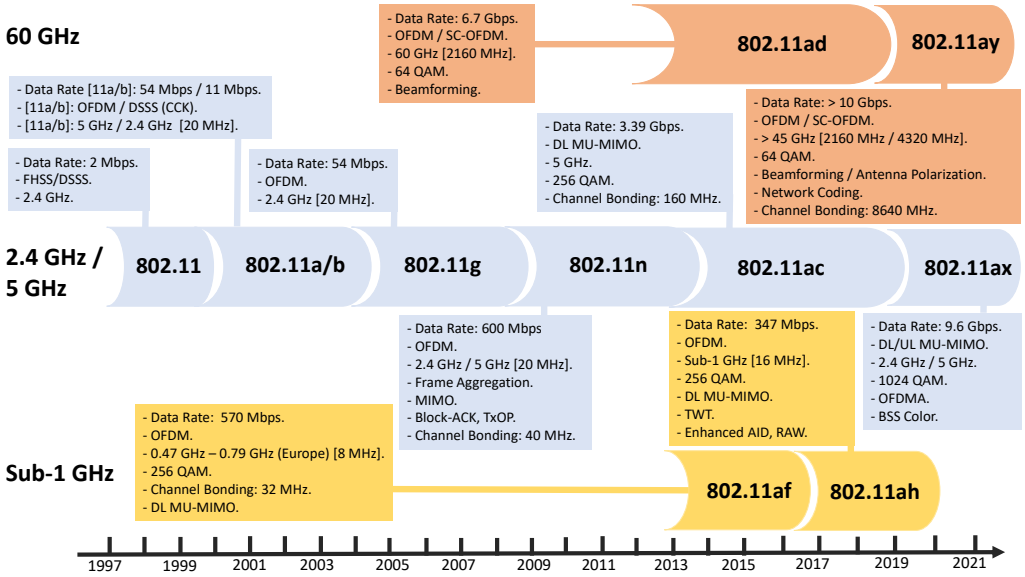

Figure 2.7: An overview of IEEE 802.11 evolution (PHY/MAC amendments).

mechanisms at the PHY and MAC layers. The IEEE 802.11n supports data rates of hundreds Mbps, MIMO, channel bonding, frame aggregation, wider coverage, and dual band support. Following the success of IEEE 802.11n, a new amendment was launched in late 2013, namely IEEE 802.11ac. In contrast to IEEE 802.11n, this new amendment operates only at 5 GHz frequency band, exploiting the benefits of wider bandwidth channels (channel bonding support to channel bandwidths of up to 160 MHz) in the 5 GHz band. By further enhancing channel bonding, MIMO, and the support of 256-QAM along with MU-MIMO in DL, IEEE 802.11ac can boost the peak link-rates to over 6 Gbps.

Although, IEEE 802.11ac can offer high data rates, it has one major drawback; it is designed, as its all predecessors, for small indoor network deployments. Therefore, Task Group IEEE 802.11ax (TGax) was formed in 2014 with the first Wi-Fi 6 capable devices just recently hitting the market. In contrast to preceding IEEE 802.11 standards aiming at enhancing link throughput, the IEEE 802.11ax amendment focuses on improving spectrum efficiency and area throughput in dense WLAN scenarios, while further reducing power consumption of mobile devices. Moreover, IEEE 802.11ax compliant APs/STAs will operate in 2.4 and 5 GHz frequency bands initially, but they could also operate in the bands between 1 and 7 GHz as they become available. Fur-

thermore, backward compatibility is one of the main requirements in IEEE 802.11ax, since heterogeneous devices are expected to be operating in the same frequencies.

This subsection initially provides a description of IEEE 802.11 access schemes and the most important enhancements that various amendments applied to the MAC and PHY layers, over the last 12 years. It continues with a detailed overview of the (under active development) IEEE 802.11ax amendment by introducing its new features with a particular focus on the SR techniques. Finally, it concludes with the overview of the IEEE 802.11af [246], an amendment that operates in Television/TV White Spaces (TVWS) bands and was introduced to provide seamless wireless connectivity in rural environments. The evolution of the IEEE 802.11 amendments at the MAC and PHY layers, is illustrated in Figure 2.7.

2.3.2.1 Basic Access Scheme

In contrast to the 3GPP LTE standard, the IEEE 802.11 is an asynchronous technology/standard, in the sense that it relies on random-access methods for granting access and transmissions over the shared medium. It also differentiates from LTE in the way that there are no dedicated channels for data, control, and DL/UL frames; all transmissions can be over the same channel. Moreover, preambles precede the transmission of data/control or management frames.

Prior to data transmissions, STAs have to establish a connection with an AP. This procedure comprises three stages: i) detection, ii) authentication, and iii) association, as illustrated in Figure 2.8a. STAs can passively or actively scan the available channels to detect any APs. When passive scanning is used, STAs monitor a channel for a certain period of time, waiting for beacon frames, before they try another channel. Beacon frames are regularly sent by APs, and carry information about their capabilities e.g. supported MCSs, traffic load, and settings for MAC layer. If active scanning is enabled, STAs transmit a probe request frame to trigger an AP, which responds with the probe response frame. During the authentication stage, STAs establish their identity with an AP. The latter decides if STAs can or cannot access the network. Four different types of authentication exist: i) Open System Authentication, ii) Shared

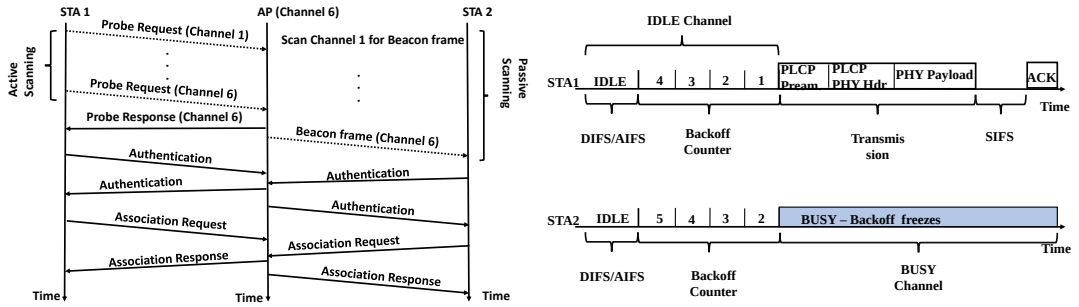

Figure 2.8: IEEE 802.11 a) connection establishment among STAs and an AP and b) data transmission after association setup.

Key Authentication (i.e. Wired Equivalent Privacy (WEP)), iii) Fast Basic Service Set (BSS) Transition of Fast Roaming Authentication, and iv) Simultaneous Authentication of Equals. The last stage is the association of a STA with an AP (typically based on Received Signal Strength Indicator (RSSI))), where their capabilities are exchanged along with the Association ID (AID). AID is assigned to every STA and represents the 16-bit ID of a STA. Re-association is invoked during a handover or when association attributes need to change.

When association between a STA and an AP is established, data frames can be exchanged. In IEEE 802.11, access to the medium relies on DCF or Point Coordination Function (PCF). DCF refers to the case where unscheduled transmissions occur, while PCF is used for scheduled transmissions between beacon frames. For example, PCF comprises two periods: the Contention-Free-Period and the Contention-Period. In DCF mode, every node senses the channel if it is BUSY or IDLE, before initiating a transmission. In the remainder of this section we mainly focus on the DCF, since is the mechanism most commonly used in Wi-Fi networks.

The channel state is determined by two factors; the energy level detected in the channel and the Network Allocation Vector (NAV). In the former case, the CCA threshold is used, which determines a channel as BUSY when the energy level is above a threshold, IDLE otherwise. CCA comprises both Carrier Sensing (CCA/CS) and CCA/ED mechanisms. CCA/CS indicates a channel as BUSY with probability greater than 90%

within 4μs for any Wi-Fi signal detected equal or larger than the minimum MCS receiver sensitivity (i.e. MCS-0), which is -82 dBm for 20 MHz channel bandwidth, according to the standard. However, most products exceed this specification by 5-10 dBs [247], [248]. When the preamble is missed (i.e. nodes not being able to successfully decode all fields), the CCA/ED kicks in and the channel is considered BUSY if energy level detected in the channel is at least 20 dB above the minimum MCS receiver sensitivity (i.e. -62 dBm for 20 MHz channel bandwidth). In some cases, where spectrum-sharing takes place, CCA/ED is applied. CCA/ED sets channel's status based on the energy level of any signal (i.e. at -72 dBm is specified for 20 MHz channel bandwidth). Note that there is always the possibility of a false alarm, even if those conservative standardized values are used. For example, false alarm rate increases with the reduction of CCA/ED (more sensitive CCA/ED). On the other hand, NAV is updated based on the value in the Duration field of any frame received. In that way, a channel is considered IDLE when the NAV timer is expired.

Once the channel is determined to be IDLE for a certain period of time, denoted as DCF Interframe Spacing (DIFS, DIFS = SIFS + 2 * Slot) or Arbitration Interframe Spacing (AIFS) for QoS nodes [249], the Binary Exponential Back-off (BEB) counter is enabled to prevent collisions, as depicted in Figure 2.8b. It decrements by one for every IDLE slot, freezes when a BUSY slot has been detected, and then resumes from that value after the channel being declared IDLE for DIFS/AIFS period. Transmissions occur when this counter expires. After a successful transmission, the back-off counter is reset and a node randomly chooses a new back-off counter within a Contention Window (CW) (i.e. CWmin) for the next transmission. If an ACK for a transmission is not received, then the node assumes that a collision has occurred, it doubles the CW size and retransmits the frame. Note that the maximum size that CW can have is $2^m * CWmin$ (i.e 1024), where m is the retransmission state.

At the other end of the link, the nodes that have detected a frame with RSSI above CCA/CS lock onto it and reception procedure starts. The first part of a frame, legacy preamble, includes the STF that is used for AGC, frequency correction, and time acquisition, the Long Training Field (LTF) for fine timing/frequency correction and channel estimation, and lastly, the Legacy Signal Field (L-SIG) carrying the length and rate in-

formation. The legacy preamble ensures inter-operability between different IEEE 802.11 technologies. However, this comes at a price of lower throughput, especially when an IEEE 802.11b preamble format is used as we explain in the following paragraph. The non-legacy part, called High-Throughput (HT), Very-High-Throughput (VHT) or High-Efficiency (HE) in IEEE 802.11n/ac/ax amendments, respectively, follows a legacy preamble and carries any additional information needed for the correct reception of a packet (i.e. channel width). Note that the fields that follow STF/LTF, and precede MAC header, form the PLCP header. When the reception of an MPDU finishes, then the recipient of this frame will transmit an ACK after SIFS. Two different SIFS timings are used for IEEE 802.11 technologies, based on the operational frequency; 10μs and 16μs in 2.4 and 5 GHz, respectively. In the case that reception was not successful, then a node defers its transmission not by DIFS, but by the Extended Interframe Spacing (EIFS). EIFS is longer than DIFS and is used to protect any ACK transmission (EIFS = SIFS + DIFS + ACK).

2.3.2.2 IEEE 802.11 Mechanisms for Legacy Inter-operability

There are four protection mechanisms to address coexistence of various IEEE 802.11 technologies, operating at the same frequency bands. The first one, is the preamble format, as already described. The IEEE 802.11b standard comprises two different formats; Long preamble with duration of 192μs and Short preamble of 96μs. A ten-fold and five-fold increase in preamble duration can be observed when the IEEE 802.11b preamble is applied, compared to the IEEE 802.11a/g preamble (duration of 20μs). The IEEE 802.11n employs three different preamble formats; Non-HT format, HT-Mixed format, and HT-Greenfield format (rarely used). The former is used to allow coexistence with IEEE 802.11b devices, the second format is used in the absence of IEEE 802.11b devices, while the latter is used only when IEEE 802.11n devices exist in the network. On the other hand, IEEE 802.11ac employs only one format, namely VHT format, which ensures coexistence with IEEE 802.11a/n devices. A second mechanism for preserving inter-operability with IEEE 802.11b devices, is the RTS/CTS scheme. The RTS/CTS control frame is transmitted at the lowest data rate i.e. 1 Mbps, used by IEEE 802.11b devices. Lastly, CTS-to-Self can also be employed by a non- IEEE 802.11b device, oper-

ating at 2.4 GHz i.e. IEEE 802.11g/n, for protecting its transmissions. This CTS frame contains identical addresses in the source and destination fields, while setting the value in Duration field, equal to the duration of data and ACK frames exchange. A fourth mechanism that is used by the IEEE 802.11n devices, is the L-SIG Transmission Opportunity (TxOP) protection. It allows for the protection of frames transmitted during a TxOP period by setting the length of the Duration field equal to the duration of the total transmission. In particular, once an IEEE 802.11n has granted a TxOP by using one of the first three mechanisms, it uses the HT-Mixed format to transmit the frames under TxOP. However, all the aforementioned mechanisms increase the overheads and severely affect network's performance. Note that coexistence in the 5 GHz band does not require the use of RTS/CTS or CTS-to-Self to ensure inter-operability, due to the absence of IEEE 802.11b devices. However, RTS/CTS may be applied to address other common issues in the wireless medium, as described in the following section.

2.3.2.3 IEEE 802.11 Hidden/Exposed Node Problem

The main shortcoming of IEEE 802.11 technology is that frame collisions may occur due to hidden nodes, while transmission opportunities are reduced due to exposed nodes. Hidden nodes are the nodes that are out-of-CS range of other nodes and their transmissions may interfere with another ongoing transmission. In other words, hidden nodes may sense the channel as IDLE, whilst there is another transmission taking place. Although, the strongest signal may survive a collision, resulting in a phenomenon known as capture effect [250], [251], transmissions by hidden nodes can severely affect network performance under moderate or heavy traffic conditions [252]. On the other hand, exposed nodes lead to poor spectrum efficiency [253], by refraining from transmissions (channel erroneously declared as BUSY), even though, their recipients may well be located sufficiently far away so no interference would have been caused, had the transmission taken place. The exposed node problem is more pronounced in scenarios where multiple co-channel Overlapping Basic Service Sets (OBSSs) coexist in an area. The CCA/CS and Transmit Power Control (TPC) are two mechanisms that are used to address the hidden/exposed node problems. However, it is almost impossible to eliminate both hidden and exposed nodes at the same time within a network, but there is a trade-

off that can be reached between them that maximizes throughput performance [254].

Another IEEE standardized (though optional) feature that was proposed to ameliorate hidden/exposed node problem is the four-way RTS/CTS handshake. It was initially introduced to tackle this issue, but can also be applied to ensure inter-operability among the different IEEE 802.11 technologies, as described earlier. However, RTS/CTS not only does not solve the hidden/exposed node problem [255], since a node updates NAV on the reception of at least one of those frames (RTS or CTS), but also adds significant overhead [256], especially when small-sized packets are transmitted. Both factors, severely degrade network throughput in high density deployments [257].

2.3.2.4 IEEE 802.11e - The QoS Amendment

Enhancements in support of QoS and specification of the original coordination functions were introduced in IEEE 802.11e-2005 amendment [249]. A new coordination function (HCF) was proposed, aiming at prioritizing traffic at the MAC layer. HCF comprises the HCF Controlled Channel Access (HCCA) and is used for scheduled transmissions, similar to PCF, and EDCA for supporting QoS when operating in DCF mechanism. Although, HCCA may provide better performance, EDCA is the mechanism that has gained wider acceptance. Both methods define 8 different classes for the traffic with different priority each one. These traffic ids (TIDs) are categorized into 4 Access Classes (ACs), namely Background (AC_BK), Best Effort (AC_BE), Video (AC_VI), and Voice (AC_VO).

Each AC is characterized by different AIFS (AIFS replaces DIFS for QoS nodes) and CW values, which define the priority of each AC. For example, AC_VO and AC_BK has the highest and lowest priority, respectively. Based on their type, packets are tagged with the AC they belong, and placed in the correct MAC queue. If two or more packets with different TID are simultaneously dequeued, then only the packet with the highest priority is transmitted. This procedure is known as internal collision and applies only for QoS nodes. TxOP is another feature introduced in IEEE 802.11e, allowing data transmission in burst mode. TxOP defines the maximum duration that frames belonging in the same AC can be exchanged in burst mode. AC_VO and

AC_VI use a TxOP value of 1.504ms and 3.008ms, respectively, while the other ACs use a value of 0. When TxOP is 0, then only one MSDU can be transmitted at a time. To further reduce control overhead, Block-Ack was also introduced in this amendment, as an optional feature. Instead of acknowledging every single MPDU, a Block-ACK frame can acknowledge up to 64 MPDUs.

2.3.2.5 IEEE 802.11n - High Throughput Amendment

Enhancements in Block-ACK scheme and new technologies, such as frame aggregation, are introduced in IEEE 802.11n. This amendment supports operation in both 2.4 and 5 GHz frequency bands. On top of the IEEE 802.11e Block-ACK, known as normal Block-ACK, IEEE 802.11n proposed the use of Compressed Block-ACK when fragmented MSDUs are not transmitted, and the Multi-TID Block-ACK for acknowledging MPDUs belonging on different TIDs. Moreover, two polices were defined for Block-ACKs; immediate Block-ACK, and delayed Block-ACK. Transmissions under the Block-ACK scheme comprise three phases: the set-up, data frame exchange, and tear-down phases. During the first phase, capability information, such as buffer size, policy etc., are being exchanged between a pair of nodes. Once Block-ACK agreement is established, then data frames are transmitted along with Block-ACKs. The last phase is initiated with the transmission of a DELBA frame by the originator, used to terminate the Block-ACK agreement between the nodes.

Frame aggregation was also first introduced in this amendment, where multiple frames belonging in the same TID can be aggregated into a single one [258]. Two types of frame aggregation have been defined in the standard; A-MSDU and A-MPDU. A-MSDU aggregation takes place on the upper MAC layer and allows MSDUs frames that contain the same source and destination addresses to form a single MPDU, thus, one MAC header per A-MSDU is used. The maximum A-MSDU length is defined to 7935 bytes when the A-MPDU aggregation is disabled, 3839 bytes otherwise. A-MPDU aggregation takes place in the lower MAC and supports the combining of up to 64 MPDU frames, each one with its own MAC header. The maximum A-MPDU size is limited by the number of frames (64) or length ($\sim$ 65 KB). The A-MPDU aggregation outperforms

A-MSDU aggregation due to the larger allowable size, especially for high data rates, while it is resilient in lossy channels due to the MAC header per MPDU [259]. Note however that a missed A-MSDU results in the retransmission of all aggregated frames, whereas in A-MPDU only the frame that has been lost, is retransmitted. The maximum PPDU time is limited to 5.484ms and 10ms for the HT-Mixed and HT-Greenfield formats, respectively. This means that with low data rates, A-MPDU is more likely to be restricted due to the maximum PPDU duration rather the maximum number of frames (64) or size ($\sim$ 65 KB). A Two-Level aggregation mechanism is also supported in the amendment, where A-MSDU and A-MPDU schemes are both applied. Two-Level aggregation is more beneficial for small MSDUs sizes [260].

The optional Reverse Direction Protocol (RDP), an advancement to TxOP, is also defined in the IEEE 802.11n. RDP allows two nodes to exchange data frames within the same TxOP. In particular, a node that grants TxOP access by setting the Reverse Direction Grant (RDG)/ More PPDU subfield of the HT Control field in MAC header to 1, thus granting permission to the recipient for responding to the transmission with data frames. However, the first PPDU of the recipient must contain a Block-ACK and the transmission duration must not exceed the remaining TxOP. In that way, overheads are reduced as devices do not have to contend to grant access to the medium.

Furthermore, two different Guard Intervals are defined; 400ns and 800ns. Channel bonding, where up to 2 channels can be concatenated, forming a channel bandwidth of up to 40 MHz, is also supported by the IEEE 802.11n devices. Even though, channel bonding was initially proposed for the 5 GHz frequency band, it is now also supported in the 2.4 GHz too. With channel bonding, the legacy fields along with the HT Signal fields (HT-SIG1/2) in the PLCP preamble and header, are duplicated over the channels; primary channel and secondary. The rest of the fields and MPDU frame are sent across the entire bandwidth channel. Although, channel bonding can potentially double the throughput, it comes at a price of reducing coverage range. This is because larger power amplifier is needed to maintain the same output power, which is costly and power consuming [247]. A good rule of thumb is that CCA/CS threshold should increase by 3 dB when the bandwidth doubles. Two FEC codes are also supported; the mandatory Binary Convolutional Code (BCC) and the LDPC as an optional feature.

One of the most impactful techniques to improve throughput and coverage, is the MIMO technology. IEEE 802.11n supports two MIMO modes, namely Space-Time Block Coding (STBC) and Spatial-Division Multiplexing (SDM). STBC enables the transmission of multiple copies of single data stream across multiple antennas, hence, enhancing range and link robustness. The most common STBC scheme, the Alamouti scheme, is the one used in this standard. For example, two data streams are combined and sent from two antennas over two-time slots. On the other hand, with SDM, independent data streams are transmitted over different antennas. The maximum data rate increases with the number of independent data streams, which is based on the number of Tx and Rx antennas. In other words, data rate increases by $min(Tx\_ant, Rx\_ant, data\_streams)$. Up to 4 antennas are supported in IEEE 802.11n, boosting the peak data rate to 600 Mbps, assuming that channel bonding and short Guard Interval are enabled.

2.3.2.6 IEEE 802.11ac - Very High Throughput Amendment

The support of higher order modulation (256-QAM), number of spatial streams (up to 8), and wider channel bandwidths (up to 160 MHz) has pushed the peak data rate close to 7 Gbps in IEEE 802.11ac [261]. Five configurations for channel bonding are supported in IEEE 802.11ac, including also non-contiguous frequency channels to form a wider channel bandwidth (e.g. 80 + 80 MHz). The 80 MHz channel bandwidth is formed by two 40 MHz channels and is a mandatory feature for the IEEE 802.11ac devices. This can provide a two-fold increase in data rate compared to IEEE 802.11n, by keeping a single spatial stream [262].

Although, beamforming is also supported in the IEEE 802.11n amendment, most vendors did not include this capability in their products. The main reason was that many beamforming techniques were included in the standard, which could increase implementation complexity (as both communicating nodes must agree on the same method to use). Thus, to avoid this, the IEEE 802.11ac standard mandates only one method, called Null Data Packet (NDP) sounding, supporting only one feedback format i.e. non-compressed immediate feedback. Moreover, MU-MIMO only supported in the DL was included in this amendment. DL MU-MIMO is based on SDM, where an AP with mul-

tiple antennas, simultaneously transmits independent data streams to multiple users. Those transmissions are overlapped in the time-frequency domain. A thorough study of MIMO and MU-MIMO is presented in [263], [264].

At the MAC layer, the maximum A-MSDU and A-MPDU sizes are further increased to 11406 bytes and 1048575 bytes, respectively, due to the support of higher data rates. Furthermore, Partial AID (PAID), a power-saving feature was also included in this amendment. It is built upon IEEE 802.11n AID feature, but its value is not unique for every STA. Moreover, the relevant Information Element (IE) is carried in the PLCP header, allowing a STA to quickly identify and abandon reception when packets are not intended for it. In that way, a STA may switch to sleep or doze state for the duration of that transmission. Along with the reduction in power consumption, throughput gain can also be observed due to the EIFS impact.

2.3.2.7 IEEE 802.11ax - High Efficiency Amendment

The rapid growth of portable devices and the plethora of new applications and scenarios [265], [266], was the motivation for IEEE 802.11ax [267]. Even though, WLANs were originally developed for small indoor environments, nowadays they can be found everywhere; from apartments, offices to outdoor venues e.g. public transport, stadiums, outdoor hotspots etc. To meet the demand for high data rates in those deployments, IEEE 802.11ax defines 5 scenarios for the assessment of the new technologies; a residential, an enterprise, and indoor small (19 BSSs with 17.32m ICD), a large outdoor (19 BSSs with 130m ICD), and a combination of a residential with an outdoor deployment. Along with the new scenarios, advanced features are also introduced in both MAC and PHY layers, allowing peak data rates close to 10 Gbps.

2.3.2.7.1 PHY Layer Enhancements

Following the paradigm of LTE i.e. OFDMA and channel sharing among multiple users, the IEEE 802.11ax amendment adopts this same technology for both DL and UL transmissions. It is a mandatory feature for the IEEE 802.11ax devices that requires their tight synchronization in frequency and time domain, especially in UL direction.

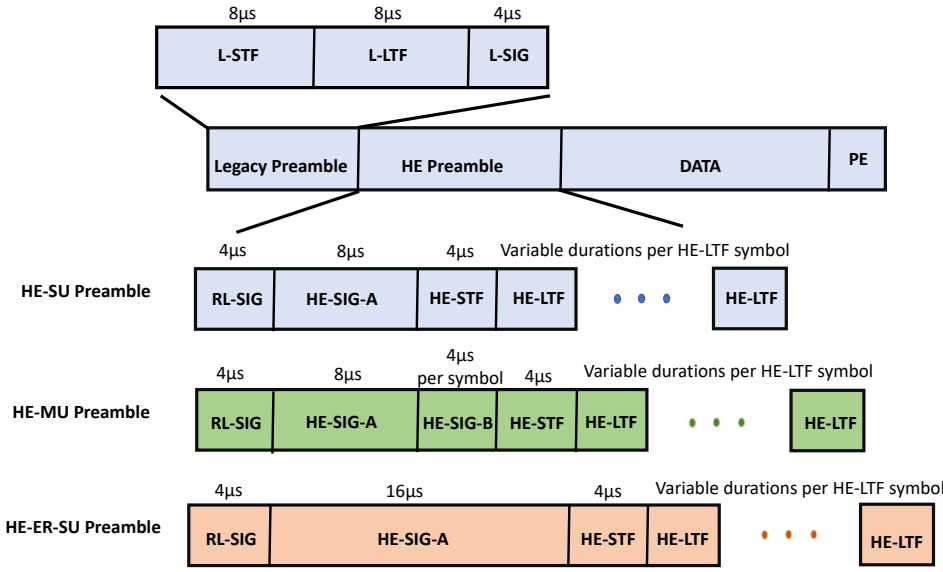

Figure 2.9: HE-Preamble structure for the IEEE 802.11ax.

Therefore, transmission resources and users participating in UL-OFDMA are announced through the Trigger frame, sent by APs. It is also used for UL MU-MIMO or to reduce power consumption when Target Wake Time (TWT) operation is used. The minimum RU is defined as 26 subcarriers that are distributed among the users, accommodating up to 9 users per 20 MHz channel bandwidth. IEEE 802.11ax also supports a higher order of modulation, i.e. 1024 QAM, as an optional feature, intended for indoor environments.

To improve robustness and performance in fading environments, larger Fast Fourier Transform (FFT) is used. This results in longer symbol duration T_s and a smaller subcarrier frequency spacing. Various T_s are supported for the HE-LTF symbols, whilst only one T_s for the data field. For example, $T_s = FFT/ChannelWidth = 256/(20MHz) = 12.8\mu$s, while the subcarrier frequency spacing is $1/(12.8\mu\text{s}) = 78.125$ kHz. Two other techniques for improving robustness in large outdoor deployments, include: i) Extended Range (ER) support and ii) Frequency Selective Scheduling (FSS). With ER, fields in HE preamble are repeated, which along with a 3 dB power boosting of some training fields, may result to 5-6 dB better preamble performance [268]. Some of the frame structures supported by IEEE 802.11ax, are illustrated in Figure 2.9. FSS technique has been extensively studied in TGax, aiming at improving OFDMA performance by selecting specific RUs for a user, based on CSI reports [269]–[271]. Furthermore, both

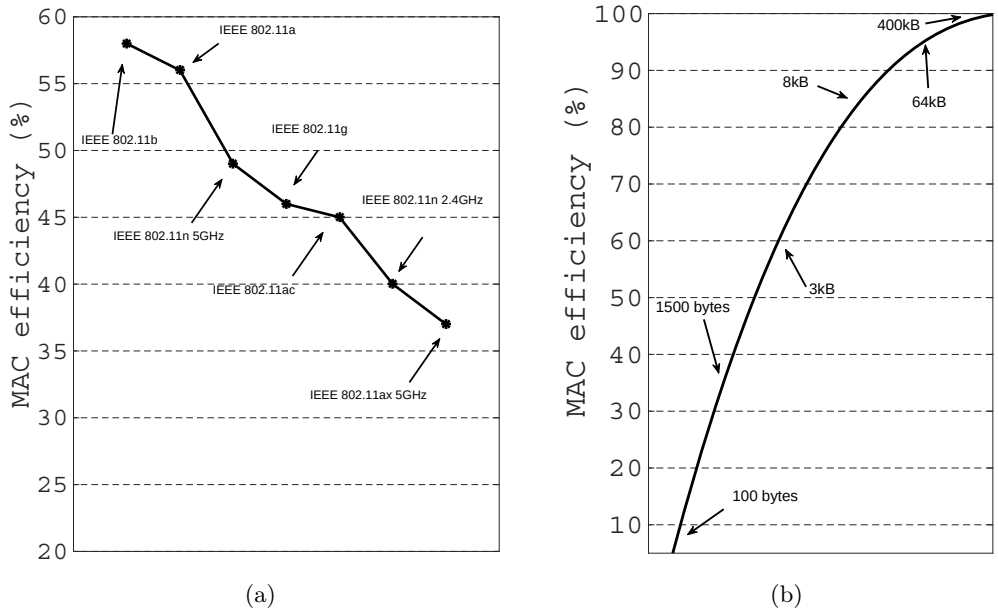

(a) (b)

Figure 2.10: MAC efficiency a) per amendment (highest data rate for 20 MHz bandwidth, 1 spatial stream, and 1500 bytes size) and b) with respect to the transmitted packet size (20 MHz, 1 spatial stream, and HE-MCS 11).

BCC and LDPC FEC codes are supported by IEEE 802.11ax devices. However, BCC is used for spatial streams less than or equal to 4, MCS less than 10, and is mandatory for RU sizes less than 484-tone. On the other hand, LDPC is mandatory for MCS-10/11, RU sizes greater than 242-tone, and channel bandwidths larger than 20 MHz.

UL MU-MIMO is also introduced in IEEE 802.11ax, to exploit the advantages of MU-MIMO in UL direction. In that way, nodes with limited number of antennas; 1 or 2, supporting low data rates, do not degrade performance by occupying the channel for long periods. As in OFDMA, a Trigger frame is used to coordinate users.

2.3.2.7.2 MAC Layer Enhancements

MAC performance decays as higher data rates per STA are used, as seen in Figure 2.10a, for constant frame sizes. Overheads, such as legacy preamble, IFS etc, make the application-level throughput to significantly vary from the theoretical one. Thus, many enhancements have been proposed to improve MAC efficiency, whilst others are

intended to enhance the performance of existing features.

MU-EDCA is used by an AP to adapt to changes in traffic load. Two sets of EDCA parameters are employed; one for all STAs and one for improving efficiency of UL MU capable STAs. These new parameters are carried in selected beacon frames and in all Probe/Association/Re-association responses. However, the APs are not expected to change these values/settings very often. A Multi-STAs Block-Ack control frame is also defined to enable concurrent acknowledgement to multiple STAs after UL MU operation, thus reducing the transmission delay of multiple Block-ACKs. MU-RTS/CTS is also proposed to protect MU-PPDUs, where STAs can simultaneously respond (CTS) to an MU-RTS from their AP.

The maximum PLCP Service Data Unit (PSDU) size is also extended to 6500631 bytes, compared to that in the IEEE 802.11ac, to further improve efficiency when advanced technologies are used (e.g. Channel Bonding, MIMO). The impact of transmitted frame's size and for different IEEE 802.11 amendments is depicted in Figure 2.10. Multi-TID A-MPDU is introduced to aggregate frames with different TID values to the same user, utilizing the scheduled RUs. MU-AMPDU is also under consideration, where frames destined to multiple recipients are aggregated into a single frame [272]. This feature further reduces MAC overhead, especially for short-length frames. MU-AMPDU applies to users that experience similar channel conditions (i.e. similar MCS) only if aggregation rules allow it (i.e. length, duration). Moreover, ACKs or Trigger frames can also be concatenated with data frames. However, Trigger frames aggregation with data frames is mandatory.

Two types of frame fragmentation are also introduced; the legacy or static fragmentation and the dynamic one. The latter is proposed to improve efficiency in UL MU operation by filling the empty space with data bytes, instead with padding (static fragmentation). Fragments may have different length, while the first one must be equal or greater than the minimum fragment size threshold. To further improve efficiency for UL MU transmissions, a new frame namely NDP short feedback is introduced - not to be confused with the NDP for channel sounding. It allows APs to collect feedback from a large number of STAs in an efficient way. That feedback frame is sent without

data payload. Further to NDP short feedback, STAs transmit the Buffer Status Report (BSR) frames to APs to allocate the right amount of resources in each STA.

Even though, dual beacon was introduced in IEEE 802.11n (STBC beacon) to extend BSS range, it was not implemented by no one. It is shown in [273] that longer CP is needed for robustness, which legacy non-HT PPDUs are not able to provide. Therefore, dual beacon was replaced with the ER beacon mechanism, since ER exploits OFDMA (i.e. longer CP) [274]. To protect STA-to-STA communications, STAs request from an HE-AP to schedule quite periods to allow STAs communicate directly. Furthermore, a tighter management for association or roaming procedures is also under consideration. It is network's responsibility to inform STAs what is the best AP to associate or when roaming should happen. This is beneficial, especially for cell-edge users, which listen multiple APs at similar RSSI levels.

2.3.2.7.3 Power-Saving Advancements

Power management has been part of IEEE 802.11 standard since its first release. The power-save techniques have been evolving the past years to reduce power consumption in portable devices. Power Save Mode (PSD) was the first technique to be introduced in IEEE 802.11. Nodes sleep for a specific period of time and wake up every X beacons to listen if there are packets buffered in the AP for them. If there are packets, then STAs send a Power Save Poll Frame (PS-Poll) to the AP, requesting for the buffered packets. Automatic Power Save Delivery (APSD) was later introduced to support TxOP and an extension of it, namely Power Save Multi-Poll (PSMP), was proposed in IEEE 802.11n amendment. TWT is proposed for IEEE 802.11ax that was adopted from IEEE 802.11ah [275]. With TWT, STAs wake at specific times to exchange frames with other STAs or an AP. This time or times are agreed in advance between a STA and an AP. TWT also allows STAs not to listen to beacons, which further reduces power consumption.

2.3.2.7.4 Spatial Reuse Techniques

A completely new mechanism has also been added in the IEEE 802.11ax amendment, namely the introduction of Spatial Reuse (SR) techniques. The main objective is to increase the number of concurrent transmissions within a given area, thus, enhancing both area throughput/capacity and spectrum efficiency. Dynamic Sensitivity Control (DSC) [276], a technique used for tuning CCA thresholds, has been proposed for IEEE 802.11ax devices, where STAs tune CCA thresholds based on beacons' RSSI (received from the associated AP), using a moving average scheme. DSC does not require any additional overhead to be exchanged and it aims at increasing probability of successful transmissions for cell-edge users. The cell-edge users can thus use low CCA thresholds, expanding their carrier range, to reduce the number of hidden nodes. However, an extremely conservative value may lead to spectrum inefficiency due to the exposed node problem and higher probability of a false alarm. The main drawbacks of DSC are that transmission opportunity for cell-edge users further decays due to the extended carrier sensing range and the increased probability of a false alarm. DSC has been extensively studied in residential [277] and small indoor [278] scenarios. An extension of DSC operating on APs, is presented in [279], where the APs tune the CCA threshold based on the RSSI of the inter-BSS frames and the intra-BSS frames. Nevertheless, the way that this algorithm operates may increase the outage probability, where users are out of coverage of the APs.

The second spatial reuse technique that is currently included in the IEEE 802.11ax standard, is BSS Color [280]. This feature has been adopted from the IEEE 802.11ah and is based on the PAID feature, aiming at the early identification of the BSS that a frame is transmitted from. The BSS Color scheme uses a 6-bit value carried in HE-SIG field along with the UL_Flag (1-bit value) that identifies the link direction of a frame (i.e. DL/UL), illustrated in Figure 2.11. Its value ranges from 1 to 63 and a value of 0 indicates that BSS Color is not used, thus, frame reception follows the legacy procedure. Nodes can abandon reception if a colored frame (Color $\neq 0$) is transmitted by a neighboring BSS, and based on the RSSI, to initiate a transmission to their AP. BSS Color is distributed to STAs during the association stage, while it may change during

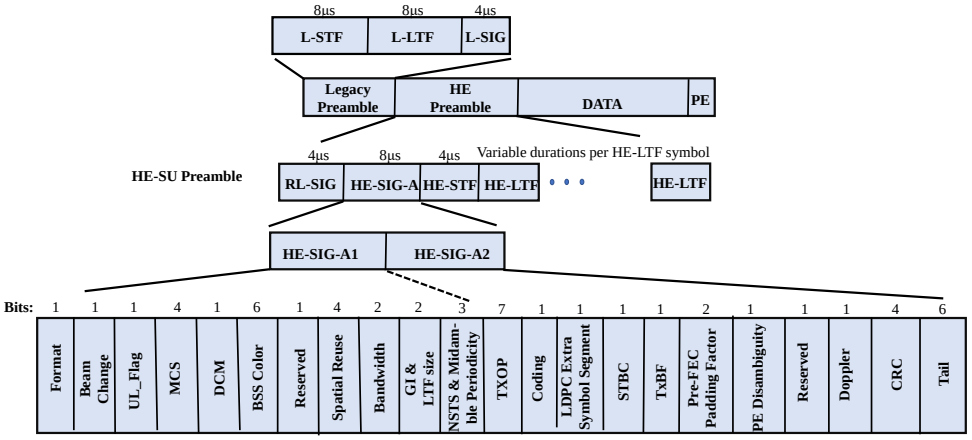

(a)

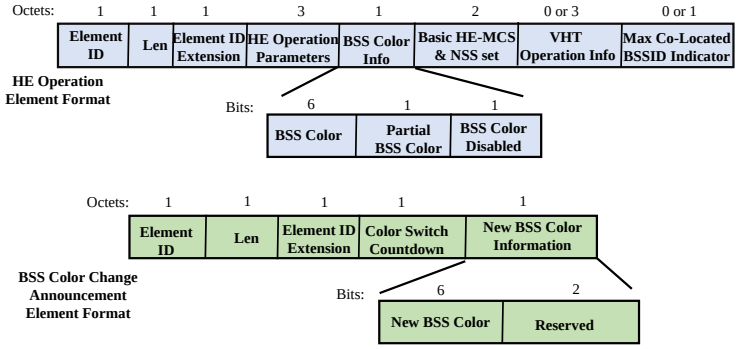

(b)

Figure 2.11: Frame structure for the a) HE-SU packet and b) management frames (HE operation Element).

operation, if color collision is detected. Both BSS Color and UL_Flag features can also be considered power-saving mechanisms, since a color or a link direction mismatch may result to the abandoning of the reception.

To assure smooth SR operation (BSS Color) two different approaches have been introduced in the IEEE 802.11ax; the OBSS / Preamble Detection (OBSS/PD) -based operation and the SRP-based operation. The latter approach is based on the transmission of a Trigger frame to initiate a data transmission from a STA for the duration of the current (ongoing) PLCP Protocol Data Unit (PDU) transmission [281]. In that case, the APs control the transmission opportunities for the associated STAs. This work

focuses on the OBSS/PD-based operation, which may function in a distributed way and does not require the exchange of control frames. An overview of the advancements proposed to enhance spectrum efficiency and the BSS Color operation is presented in this subsection.

First, the IEEE 802.11ax nodes are expected to maintain two NAVs; one for intra-BSS (intra-BSS NAV) and one for inter-BSS frames or those frames that cannot be identified (basic NAV). If both NAV timers are zero, the channel is identified as IDLE, BUSY otherwise.Although, the use of two NAVs is beneficial, especially in dense deployments, it does not fully offer protection to the ongoing transmissions. For example, in the case of Multi User (MU) operation, a hidden AP to the ongoing inter-BSS packet transmission may transmit a trigger frame to a STA for a solicit response (e.g an upcoming MU transmission with an MU-RTS). The STA then has to reset NAV timers and respond with a CTS, otherwise if the NAV reset schemes from an AP are ignored by the STAs, the NAV would overprotect AP's TxOP and would degrade the network performance [282].

Secondly, the OBSS/PD threshold is introduced to control the transmission opportunities for a node based on the inter-BSS frames' RSSI. If the inter-BSS frame's RSSI is above the OBSS/PD threshold, the node will sense the channel as BUSY, will update basic NAV, and will defer its transmission, otherwise the node may initiate a transmission (i.e. intra-BSS NAV timer is zero). In that way, the interference level introduced by multiple simultaneous transmissions (with the BSS Color) can be controlled.The OBSS/PD threshold ranges between the sensing range threshold (i.e. CCA/CS) and the CCA/ED threshold that is greater than the minimum MCS by 20 dB [245].

$$CCA/CS \leq OBSS/PD \leq CCA/ED \tag{2.1}$$

where CCA/CS equals to -82 dBm and CCA/ED to -62 dBm for a 20 MHz channel, according to the IEEE 802.11 standards. A good rule of thumb is that CCA/CS and CCA/ED thresholds should increase by 3 dB when the bandwidth doubles.

Thirdly, the Spatial Reuse Group (SRG) is another concept where multiple BSSs with different BSS Color values form a group. The nodes in an SRG can apply different rules (e.g. OBSS/PD threshold) to the inter-BSS/intra-SRG packets and to those transmitted

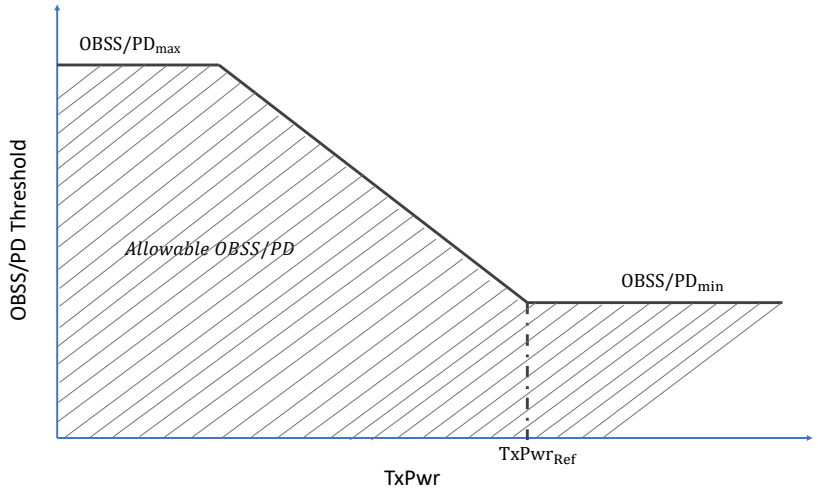

Figure 2.12: The adjustment rule for the OBSS/PD threshold and the transmit power.

from a different SRG (i.e. inter-BSS/inter-SRG). The SRG operation is more suitable for networks that are being managed by wireless access controllers or by operators that may agree beforehand on the BSS Color policies that will be using, e.g. the OBSS/PD threshold or the boundaries for the OBSS/PD etc.

Fourthly, the adjustment of the OBSS/PD threshold in conjunction with the transmit power is also proposed in the amendment to reduce the in-band emission interference to the OBSSs, thus improving the spectrum efficiency and network performance.The OBSS/PD threshold that can be applied under the OBSS/PD-based operation in relationship with the transmit power (TxPwr) is defined as:

$$\begin{aligned} OBSS/PD \quad \leq \quad & max(OBSS/PD_{min}, min(OBSS/PD_{max}, OBSS/PD_{min} \\ & +(TxPwr_{Ref} - TxPwr))) \end{aligned} \tag{2.2}$$

where $TxPwr_{Ref} = 21$ dBm for STAs and APs with less than 2 Spatial Streams (SSs) and $TxPwr_{Ref} = 25$ dBm for APs with $SS \geq 2$. The OBSS/PD threshold decreases with the increase of the transmit power level. For example, $OBSS/PD \leq -76$ dBm when a STA transmits at 15 dBm. Alternatively, a node may adjust the $TxPwr$ level

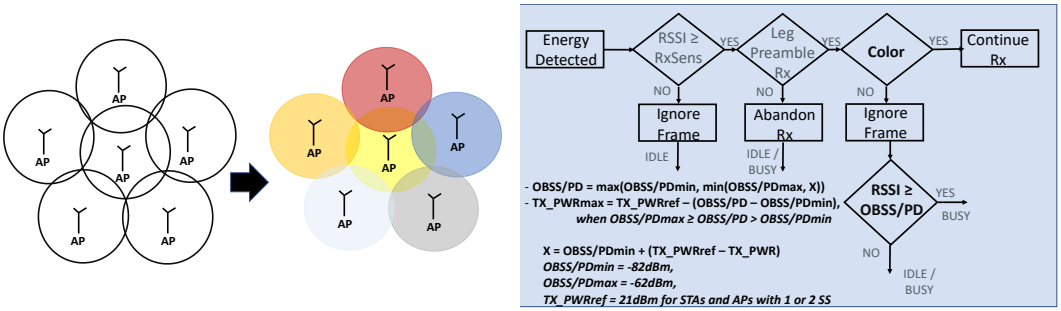

(a) (b)

Figure 2.13: IEEE 802.11ax BSS Color a) cell-layout and b) simple flow chart.

based on the OBSS/PD threshold, such as:

$$TxPwr_{max} = TxPwr_{Ref} - (OBSS/PD - OBSS/PD_{min}) \tag{2.3}$$

when $OBSS/PD_{min} < OBSS/PD \leq OBSS/PD_{max}$, otherwise it is unrestricted. Although, a low $TxPwr$ level may reduce the interference level, it could also result to a low SINR, thus a careful selection of the transmit power level is required. The rule applied for adjusting the transmit power with the OBSS/PD is illustrated in Figure 2.12.

A simple flow chart of BSS Color preamble reception procedure is illustrated in Figure 2.13.

Last, due to the absence of a specific mechanism in the amendment on how a node (e.g. STA) should select the OBSS/PD threshold, DSC was proposed to dynamically adjust the OBSS/PD level based on the beacons' RSSI [283], [284]. The OBSS/PD threshold, according to the DSC proposal is set to:

$$\begin{aligned} OBSS/PD \quad = \quad & min(OBSS/PD_{max}, max(OBSS/PD_{min}, (\overline{RSSI}_{beacon} \\ & -Margin))) \end{aligned} \tag{2.4}$$

where the value of $Margin$ (in dBs) is transmitted by the APs and is carried in a subfield of the SR parameter set element (when Equation 2.4 is applied, otherwise the subfield is not incorporated). Even though, the authors in [284] showed that by adjusting

Margin throughput gain can be achieved, their study is based on various assumptions that severely affect the performance. For example, they do not take into account the interference level and the Packet Error Rate (PER). Nevertheless, DSC does not fully exploit the BSS Color information and may also deteriorate the fairness among the cell-edge users and the rest users in terms of the transmission opportunities (reducing transmission opportunities for cell-edge users).

In contrast to the IEEE 802.11ax SR scheme, which makes decisions based on a binary identification of the detected OBSS frame, learning-based approaches have also been proposed to further improve SR and the spectrum efficiency [285], [286]. However, these schemes may increase complexity, data processing, and OPEX, hence may not be a suitable solution in residential deployments.

2.3.2.8 IEEE 802.11af - TVWS Amendment

Although, the IEEE 802.11af amendment is launched before the IEEE 802.11ax (late 2013), it is included after the IEEE 802.11ax due to its: i) different operating frequency (TVWS) and ii) main focus; seamless connectivity in rural environments and low power consumption.

It was introduced as a complementary amendment to IEEE 802.11n that takes advantage of the propagation characteristics of the TVWS spectrum and the additional bandwidth from the unused spectrum of broadcast TV services. One of the main challenges for the IEEE 802.11af amendment (a.k.a. White-Fi) is to guarantee that licensed services are not interfered by its operation [287]. Therefore, new entities were defined in the standard to support the coexistence of IEEE 802.11af (54 MHz - 698 MHz in USA, and 470 MHz - 790 MHz in Europe) and TV broadcast services.

First, a Geolocation Database (GDB), containing the allowed frequencies and the operating settings for the White Space Devices (WSDs) has been introduced in the IEEE 802.11af amendment. The available frequency bands along with the operating parameters are subjects to country/location specifics. GDB operation can be either open-loop or closed-loop. The former is mainly used in USA, where GDB provides scheduling information every 48 hours, thus, conservative transmit power levels are considered. The

latter is used in Europe and provides updates about the channel availability every 2 hours.

Secondly, the purpose of the Registered Location Secure Server (RLSS) is to maintain and provide the GDB information for a smaller area, e.g. small BSS.

Lastly, the Geolocation Database Dependent Entities (GDD) has been defined, which includes the APs and STAs, known as GDD-Enabling STAs and GDD-Dependent STAs, respectively.

The White Space Map (WSM) contains information about the available channels and the maximum transmit power that can be used in each one, based on the location. It is shared between the GDD-Enabling STAs and GDD-Dependent STAs through the Registered Location Query Protocol (RLQP), enabling STAs to effectively select the allowed channels, bandwidth, transmit power etc. GDD-Dependent STAs can also request this information (RLQP) from the RLSS, by sending a Channel Availability Query (CAQ) frame. On the other hand, the GDD-Enabling STAs request for the Channel Scheduling Management (CSM) either from RLSS or other GDD-Enabling STAs to obtain information about the available channels. Contact Verification Signal (CVS) is transmitted by the GDD-Enabling STAs to identify any GDD-Dependent STAs in their proximity. Moreover, the CVS allows the GDD-Dependent STAs to ensure that the signal was transmitted by a valid GDD-Enabling STA.

The GDD-Enablement is called the procedure where GDD-Enabling STAs transmit beacons in the available channels to establish a communication link with GDD-Dependent STAs. Three states are defined for the GDD-Dependent STAs; Unenabled, Attempting GDD-Enablement, and GDD-Enabled. In the Unenabled state, WSDs passively scan the available channels to detect a beacon. A WSD enters the Attempting GDD-Enablement state during authentication/association procedure, while it becomes GDD-Enabled when the association with the corresponding GDD-Enabling STA has been established. The last mechanism defined in the standard is the Network Channel Control, which allows WSDs to exchange information about nearby transmitters and their emissions footprints.

IEEE 802.11af adopts most of the IEEE 802.11ac features in PHY and MAC layer [288],

[289]. It is interesting to mention that three Basic Channel Units (BCUs) have been defined in IEEE 802.11af, depending on the country and spectrum availability.

2.4 Technological Solutions for M2M Communications

The ability of objects to communicate through internet without requiring human interaction, is referred as Internet of Things (IoT). The direct communication among these devices is known as Machine-Type-Communications (MTC) or M2M communications. The needs of market and industry to automate most of their process (i.e. real-time monitoring) has led to the exponential growth of the number of devices connected to internet. Emerging services, such as remote health care or learning, smart grid, and smart cities where information is efficiently collected through sensors (e.g. traffic conditions, waste collection etc.) are some of the new scenarios considered for 5G networks.

MTC will enable a plethora of applications and increase the number of devices connected to internet to millions or even more, with most of them require adequate coverage and low bandwidths to transmit small sized packets. Various standardization bodies e.g. IEEE, Internet Engineering Task Force (IETF), and 3GPP, have defined technologies to support IoT networks, with Long-Range (LoRa) [290], SigFox [291], IEEE 802.15.4g/e, IEEE 802.22 (Wi-Far), NB-IoT, IEEE 802.11ah etc. among the most well-known standards. In the following paragraphs, we provide a brief description of the technologies developed outside 3GPP and IEEE 802.11, for supporting MTC. A detailed overview of the efforts in 3GPP and IEEE 802.11x driven by MTC is presented in the next two subsections.

LoRa Wide Area Network (LoRaWAN) is a Low-Power Wide Area Network (LPWAN) technology specified to wireless battery-operated devices [292]. It operates in the Sub-1 GHz band and supports rates of up to 50 kbps and supports up to 10k devices with a single BS [293], providing up to 10 km coverage. On the other hand, SigFox, supports up to 1 million devices and provides coverage up to 50 km in suburban areas. It also, enables low energy consumption in the Sub-1 GHz spectrum. However, it provides even lower data rates than LoRaWAN (below 1 kbps).

Wi- Smart Utility Networks (Wi-SUN) consortium, established in 2011, and uses the IEEE 802.15g/e for PHY and MAC, respectively, to enable efficient management of utility services; water, gas, electricity. The Wi-SUN standard PHY layer supports three different formats; Multi-Rate Frequency Shift Keying (MR-FSK), MR- Offset Quadrature Phase Shift Keying (MR-O-QPSK), and MR-OFDM for higher data rates (i.e. from 2.4 up to 800 kbps [294]), capable of accommodating thousands of users. The IEEE 802.15.4m is another/competing standard, enabling data rates of up to 2 Mbps. It operates between the 54 and 862 MHz frequency spectrum and supports three PHY formats; FSK, OFDM, and NB-OFDM. Since most of the channels in those frequencies (TVWS), are 6 to 8 MHz wide, NB-OFDM allows the support of multiple users by dividing channels into sub-channels. Another IEEE (other than IEEE 802.11x) technology, using the TVWS bands is the IEEE 802.22, known as Wi-FAR. It is a standard for Cognitive Radio-based Wireless Regional Area Networks (WRANs) for providing broadband wireless access over large areas. It offers rates of up to 28 Mbps for an 8 MHz channel bandwidth and is suitable for use cases, such as cellular offloading, small office/home office, homeland security etc [295].

The main drawbacks of the aforementioned technologies are: i) only able to offer low data rates and operate in unlicensed bands, which makes them susceptible to interference and ii) unable to meet QoS requirements, such as high reliability and high energy efficiency. On the other hand, cellular systems can overcome those issues due to the controlled access that they offer. Moreover, LTE is a technology widely developed, offering wide coverage, high capacity, and flexibility [296], [297]. However, the enormous number of devices and diverse traffic types pose some challenges for cellular systems, as we explain in the following section.

2.4.1 3GPP LTE Enhancements for M2M Communications

Although, a first study for MTC in 3GPP, began in 2007 [298], standardization activities only started in 2010 with Rel-10 (System Architecture Group 2 (SA2) focused on MTC initially). At about the same time, the European Telecommunications Standards Institute (ETSI) and other standardization bodies (e.g. OMA, ATIS, CCSA) started

studying MTC with respect to service architecture [299].

Two types of MTC scenarios were initially defined in 3GPP; device to server and device to device through a cellular network. However, only the former was originally covered in 3GPP Rel-10. MTC services are characterized by static/low-mobility nodes, infrequent small size data transmissions, and secure connections.

Right from early stages it was realized that the main challenges for MTC services were the signaling overhead and network congestion due to massive number of devices. Therefore, 3GPP focused on addressing the overhead in C-Plane, since congestion in U-Plane is more unlikely to occur due to the advanced technologies used (i.e. CA, MIMO etc.). Approaches that are followed to tackle signaling overhead, include: i) infrequent Tracking Area Updates (TAU), due to low-mobility, ii) pull-based scheme to trigger MTC devices, iii) grouping MTC devices based on their features, iv) aggregating short messages for delay-tolerant services or when groups of MTC devices are formed, and v) support of grant/forbidden periods.

An overview of scheduling techniques used to cope with the massive number of devices, especially for UL transmissions, is presented in [300]. Although, General Packet Radio Service (GPRS) can be used for M2M communications, when voice users are active in a cell, the number of MTC devices that can be accommodated is limited. To cope with the limited resources in RACH, a new frame structure is presented in [301], supporting 10x more devices/nodes per cell than the standardized LTE/LTE-A frame structure.

One of the first schemes considered and described in 3GPP Rel-10 for addressing the substantial number of devices contending for a preamble, is the Access Class Barring (ACB) [302]. A device generates a random number is compared against an access probability number that is transmitted by the eNodeB. If the device generated number is higher than the access probability, then a device will access the channel. In that way, eNodeBs can control congestion by tuning the access probability i.e. a high access probability setting leads to low congestion but high delays, whilst a small one may result in consecutive preamble collisions that may in turn cause in extensive delays.

Other mechanisms that have been studied by 3GPP, include: i) Extended Access Barring (EAB), where delay-tolerant MTC devices do not contend for preamble, ii) dedicated

slots in RACH for MTC devices, iii) Prioritized Random Access (PRA), where each group of MTC devices applies different back-off, iv) dynamic allocation of Random Access resources, which may result to low data rates, and v) only the leaders from the groups to collect traffic and contend for access in the medium [303]. Furthermore, the importance of prioritizing Human Type Communications (HTC) during the Random Access has also been studied [304].

Two new entities have been defined in 3GPP to support M2M communications; Service Capability Servers (SCS) that connect MTC application servers to a 3GPP network and MTC-Inter-Working Function (MTC-IWF) that resides in the Home Public Land Mobile Network (HPLMN) and forwards or translates signaling protocols to enable specific functionalities in PLMN [305]. An MTC-IWF can be connected to multiple SCSs. The support of D2D communications and NFV, allowing virtual machines to carry the burden of high complexity, can be used to further enhance MTC communications.

New MTC scenarios and a new device category, namely UE category 0, were introduced in 3GPP Rel-12. To further reduce complexity and power consumption, UE Cat-0 was the only UE category to allow the support of single antenna. However, the improved efficiency in power consumption, comes at the cost of worse performance (approx. 5 dB) [305]. A new type of Half-Duplex operation (Type-B) is also considered for UE Cat-0 to further lower the cost and complexity of MTC devices. In particular, devices that belong to that category, are not allowed to skip the last OFDM symbol when switching from DL to UL transmissions as LTE devices do, due to time advance. In that way, MTC devices can reuse oscillators between receptions and transmissions. Power-Saving Mode (PSM) allows devices to remain registered in the network even when they cannot be reached by the network. It is similar to powering off, allowing devices to re-establish connectivity with eNodeBs, only when they have data to transmit. Further enhancements for MTC are also provided in the releases following 3GPP Rel-12. In particular, Rel-13 introduced enhanced MTC (eMTC), aiming at further reducing the device cost, extending coverage, and improving energy consumption. Only the minimum LTE carrier bandwidth, i.e. 1.4 MHz with 6 RBs of 180 KHz was supported. Moreover, repetition in DL and UL (PUSCH) subframes was used to improve coverage [306]. Data or control channels can be repeated for multiple subframes. Moreover, Power Spectral

Density (PSD) boosting in UL and relaxing the requirement on probability of missed detection for PRACH, were introduced to improve coverage [307]. Reduced maximum transmit power and support for simultaneous reception of multiple transmissions were also part of that release. Retransmissions are asynchronous and rely on HARQ, while frequency hopping among narrowband channels and longer transmission time that allows additional energy to be accumulated at the receiver were also included in Rel-13.

Narrowband IoT (NB-IoT) is an LPWAN technology introduced in Rel-13. Operating on a 180 kHz channel bandwidth, NB-IoT is characterized by peak data rates of less than 200 kbps, and limited mobility, an even lower power consumption and component cost. NB-IoT only supports FDD (unlike eMTC) and supports three types of communications; in-coverage, outside-coverage by using GSM carriers, and guard-band, where NB-IoT channel is placed in the Guard Band of LTE-A channels. The narrow bandwidth enables multiplexing more users in the same bandwidth in UL direction.

On the other hand, the minimum resource allocation unit is set to one subcarrier for NB-IoT nodes. Moreover, two subcarrier spacing are supported in UL; short (3.75 kHz) and the one used also in DL (15 kHz), while frequency hopping is also supported in PRACH. To meet the requirements for extended battery life (over 10 years), DRX cycle for NB-IoT devices, is extended from 2.56 seconds to approximately 3 hours [308]. A comparison between the in-coverage and outside-coverage was conducted in [309], showing that the latter scenario outperforms the former one, in terms of battery life extension, latency, and coverage.

Positioning enhancements, support of new UE categories with even lower power consumption, increased voice coverage for LTE MTC, single-cell multicast, and mobility improvements for enhancing service connectivity were the main advancements proposed in 3GPP Rel-14. Due to the power-consumption constraints, achieving less than 50m accuracy is challenging, especially in dense deployments where the low signal strength and high interference level make it even more difficult to obtain a good resolution of the time of arrival [310]. Frequency hopping was also studied for enhancing position accuracy, a scheme that can provide accuracy below 50m for a small number of hop impairments [311]. Multicast transmissions improve networks' efficiency and add more

flexibility for use cases where multiple devices require synchronous control, firmware upgrades etc.

Advancements for improving power efficiency by reducing the time that UEs monitor DL channels in idle mode, new use cases including wearables devices, and support for standalone operation are under consideration for 3GPP Rel-15 [312]. Further enhancements for mMTC scenarios that are under development for Rel-15 include: higher spectral efficiency, TDD support, latency support of at least 10 seconds, coverage enhancements, and support of 1 million devices per square km [313]. The support of additional bands for UE categories M2 and NB2 [314], while coverage enhancements in UL include the support of higher transmit power level in cases such as emergency services in rural environments [315] are under consideration in Rel-15. One of the latest techniques proposed in 3GPP, is the Early Data Transmission (EDT) [316]. It aims to reduce latency by allowing data transmissions in UL, even before RRC connection setup is complete (i.e. during Random Access). However, EDT may fail if radio quality changes, due to lack of channel estimation. The FANTASTIC-5G [317] is also a project developed by 5G-PPP Phase 1, focusing on massive MTC access and connectivity solutions. New access-scheme protocols for reducing signaling overhead and waveforms for asynchronous transmissions in UL were proposed in that project and contributed to the 5G standardization framework.

2.4.2 IEEE 802.11 Enhancements for M2M Communications

To support IoT applications, IEEE 802.11 family introduced the IEEE 802.11ah amendment (Ha-Low) in the Sub-1 GHz band (755 MHz - 928 MHz) [275]. IEEE 802.11ah takes advantage of the favorable propagation characteristics that low frequencies offer, to provide long-range communications with low power consumption, in order to satisfy one of the requirements for IoT applications.

The IEEE 802.11ah looks more like a legacy Wi-Fi technology due to the absence of licensed-spectrum services in those frequencies. It supports even smaller bandwidths than IEEE 802.11af; 1 / 2 / 4 / 8 / 16 MHz with 1 and 2 MHz most common in Europe, while an offset of 0.5 MHz in channelization is used in South Korea to prevent

interference with other wireless systems [318]. The main aim of this technology is to fill the gap of WPAN and LPWAN systems by providing adequate coverage (up to 1 km) and high data rates (peak data rates of 347 Mbps). Therefore, IEEE 802.11ah facilitates the support of various wireless technologies, by acting as backhaul network.

2.4.2.1 PHY Layer

The PHY layer specification in IEEE 802.11ah follows the IEEE 802.11ac amendment but with a down-clocked operation. For example, channel bonding is supported for 1 MHz channels to form 2 / 4 / 8 or 16 MHz (in USA) channel bandwidths. The main usage of 1 MHz channel is to extend range, thus, repetition is also considered (MCS10) to further improving coverage [319]. Even though, the channel bandwidth is doubled, the data subcarriers per OFDM symbol is more than double, due to the removal of the redundant guard band when channel bonding in contiguous bands is performed. Other PHY characteristics and a comparison of PHY characteristics between different IEEE 802.11 technologies are listed in Appendix A (Table A.1).

2.4.2.2 MAC Layer

Since inter-operability with legacy IEEE 802.11 is not required, the MAC header size in IEEE 802.11ah is reduced (by up to 20 bytes), by replacing address fields with AID values and moving some fields to PLCP header or completely removing them. One of the fields that has been removed is the Duration field, which enables a new mechanism to replace NAV when short header is used. The Response Indication Deferral (RID) mechanism, works similar to NAV, but instead of providing accurate duration for an ongoing transmission, it estimates duration from the information included in the PLCP header.

Moreover, ACKs may be sent without a MAC header, but include some useful information in their PLCP header. Those ACKs are known as NDP MAC frames [320]. Bidirectional TxOP is a feature based on the IEEE 802.11n RDP, allowing two nodes to exchange data frames within the same TxOP. However, it differs from the RDP, as the nodes may respond with data frames instead of ACKs, further reducing overhead. In

particular, all PPDU frames are marked as frames that do not need to be acknowledged, but the last one. The last PPDU may require an immediate response, where in that case, the recipient must respond with an ACK.

2.4.2.3 Power Consumption Efficiency

To reduce power consumption for STAs, the IEEE 802.11ah amendment enhances the power-saving mechanisms of legacy IEEE 802.11, by introducing TWT (described for the IEEE 802.11ax amendment). IEEE 802.11ah also extends the maximum idle period of the devices to further improve energy efficiency. In legacy IEEE 802.11, the maximum idle period where a node can be inactive before the AP disassociates it, is a 16-bit field, corresponding to $(2^{16}-1)*1000*TimeUnit = 18.64$ hours, where $TimeUnit$ is 1024μs. In IEEE 802.11ah, the two most significant bits of that field identify the scaling factor, while the remaining 14 bits are used as in the legacy one. The maximum idle period equals to $((2^{14}-1)*1000*TimeUnit)*ScalingFactor = 46600$ hours, where the values of $ScalingFactor$ are 00, 01, 10, and 11 corresponding to 1, 10, 1000, 10000, respectively.

The main challenge is how to accommodate all this information in a beacon frame, make it available to STAs. To address this issue, IEEE 802.11ah enhances the Traffic Indication Map (TIM) mechanism by introducing the page segmentation. Now, APs split the whole information (partial virtual bitmap) into consecutive beacons. For example, APs include the buffer status of grouped packets in the first beacon (Delivery TIM – DTIM), and afterwards they include the TIM information specific to a group of STAs, in the beacons. However, STAs that do not support TIM (non-TIM STAs) may stay in doze state for longer and wake whenever they have packets to transmit. Color scheme (also described for IEEE 802.11ax) was initially introduced here, but is restricted to a 3-bit value due to the need of small overhead and sporadic traffic. Moreover, APs may assign Multicast-AIDs to different user groups, to address the issue of energy consumption when all nodes stay awake to listen to broadcast messages.

In case that a BSS operates in a large bandwidth channel, while some STAs support smaller bandwidth channels due to energy consumption, IEEE 802.11ah defines the Sub-

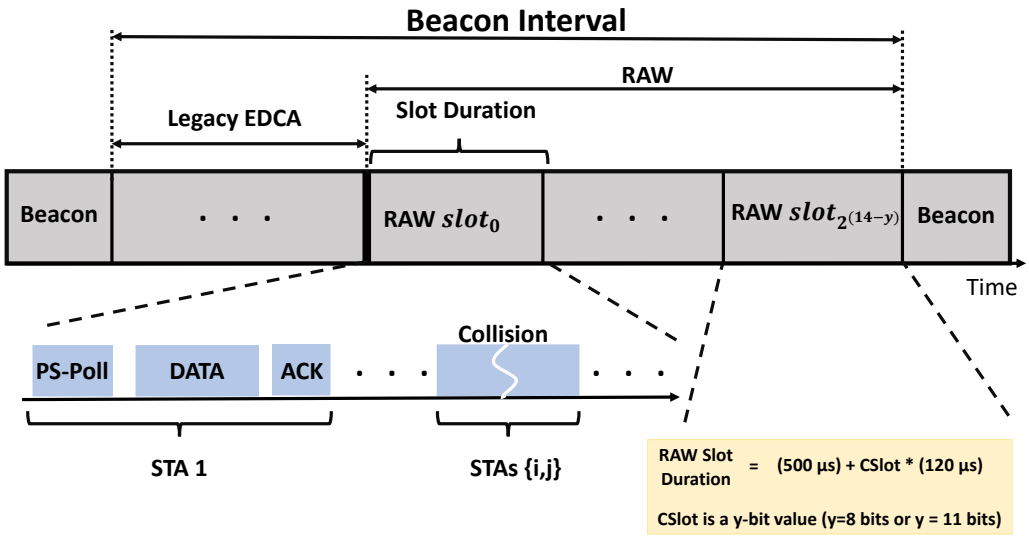

Figure 2.14: IEEE 802.11ah Restricted Access Window (RAW).

channel Selective Transmission (SST) mechanism. SST allows nodes to use subchannels instead of the whole bandwidth. It also provides flexibility to STAs, as they can select which subchannel is the best for them, which is achieved by periodic transmissions of sounding frames from APs. Multi-hop transmissions (relays) are also supported in this standard, but the number of hops is currently limited to 2. By using this technique, further reduction in power consumption is achieved. To cope with the increased delay and overhead that a relaying scheme introduces (a frame is sent over two channels), the concept of TxOP sharing was introduced. According to that feature, a relay instead of transmitting an ACK back to a STA after SIFS, it sends the data frame after SIFS, directly to the AP. The source-STA that detects this data frame (omnidirectional transmissions), will identify by the PAID value that its transmission was successful.

2.4.2.4 Advanced Technologies for Supporting Massive Number of Devices

To support enormous number of users, the AID feature has been enhanced in IEEE 802.11ah. In legacy IEEE 802.11 technology, the maximum number of users that can be accommodated is limited to 2007 due to AID range [1-2007]. By using a hierarchical AID, IEEE 802.11ah can support up to 8191 users. It comprises different fields corresponding to different STA groups. The amendment also describes two access schemes;

legacy EDCA and Restricted Access Window (RAW), illustrated in Figure 2.14. The latter is used to reduce collisions due to large-number of STAs and provide support to densely deployed IoT scenarios [321]. It is based on TDMA, where slots are specifically defined for different users or group of users. In each slot, STAs contend following EDCA procedure, hence, two different sets of EDCA are used; one backoff counter for outside RAW and one for RAW period. To better utilize channel resources, APs may allow transmissions to exceed a RAW slot. Long RAW slot durations lead to higher throughput, but also increase latency, as users need to wait longer time for their slot to come [322]. However, a dynamic RAW slot duration based on the number of STAs in each group and their requirements could improve both throughput and latency [323].

Fast Association and Authentication were also specified in IEEE 802.11ah standard, to cope with the case where thousands of users need to re-establish connectivity with an AP, after a power outage. Two methods are defined; the centralized authentication control and the locally authentication control. In the former case, an AP randomly selects a number from the range [1, 1023], called Authentication Control Threshold, and includes it in a beacon. STAs compare the Authentication Control Threshold to a number that they have randomly chosen from the range [1, 1022]; if the number is lower than the Authentication Control Threshold, they proceed to authentication, otherwise they defer their transmission. In the latter one, STAs randomly draw two number that correspond to a beacon interval and a slot, respectively, where the authentication process will be initiated (following EDCA rules). Apart from RAW scheme to group users, IEEE 802.11ah defines an alternative approach with lower complexity, namely Group Sectorization. During this operation, APs transmit sectorized beacons following the IEEE 802.11ad procedure. Those advancements in IEEE 802.11ah can lead to low energy consumption, high reliability and throughput, low delay, and capability of accommodating hundreds of users, which make it suitable for indoor or outdoor MTC scenarios [324].

2.5 Summary

High throughput, low latency, and improved network performance for all users, especially for the cell-edge ones are three of the requirements for the next generation of wireless communications. There are multiple ways for providing high capacity for the 5G applications. The most straightforward approach might be the exploitation of new available spectrum, where large bandwidth can be used for the transmissions. In particular, mmWave frequency bands offer large and unexploited bandwidth which can be utilised for short-range communications and applications that require high throughput, whereas the use of the Sub-1 GHz bands could act as the enabler for offloading traffic for specific verticals (e.g. IoT). The use of high number of antennas is also an enabler for boosting the throughput and the overall network performance, even under poor channel conditions. Last but not least, higher MCS (e.g. 1024 QAM) could potential improve the data rate by 25%.

The drivers for reducing the latency for the cellular systems include the introduction of various numerologies (i.e. different slot configurations; 1, 2, 4, 8, 16, 32 slots) smaller delay for the resource allocation schemes. On the other hand, for the WLANs, the latency can be reduced by decreasing: i) the time that a channel is idle (by increasing the transmission opportunities), ii) the number of packet collisions, and iii) the overhead introduced by the headers and/or the use of control frames. Furthermore, all the aforementioned techniques could also improve the cell-edge users' performance, along with the CoMP and/or adaptive MAC mechanisms (e.g. CCA) for the IEEE 802.11 nodes.

The contribution of this literature review that discussed and analysed in a critical manner existing works and the enabling technologies in both cellular and WLAN camps for the next generation of wireless communications, led to the identification of 4 significant gaps in respect to the IEEE 802.11 technology:

- The lack of an accurate and up to date simulator to assess the performance of the new amendments and features, such as the IEEE 802.11ax Spatial Reuse technique.

- The requirement of a mathematical model to accurately capture the behaviour of a dense deployment, showing the importance of the IEEE 802.11ax SR.
- The absence of any mechanism in the literature that exploits the Spatial Reuse feature along with other MAC functionalities and enhances the performance in dense deployments.
- The need of a mechanism to address the high MAC overhead and compensate for the packet errors under fading channels.

The aforementioned gaps of the literature study will drive the research of this thesis and will tackle each of the above significant gaps. Four distinct solutions are presented in the next four chapters, addressing each of the identified gaps. Chapters 3 and 4 present an accurate and up to date simulator that is designed and developed as part of this research. It integrates the IEEE 802.11ax MAC features, including the Spatial Reuse mechanism and a capture model for capturing the packet reception behaviour of real-world drivers and according to the TGax guidelines. Chapter 5 presents an accurate model derived from a mathematical analysis, for assessing the performance and the potential of the BSS Color scheme in IEEE 802.11 cellular-like dense deployments. Chapter 6 proposes a novel technique, one of the first that exploits the BSS Color information, for adjusting the OBSS/PD threshold for the BSS Color scheme, while Chapter 7 presents a novel rate control algorithm for dense deployments that is based on the technique for adjusting the OBSS/PD, presented in the previous chapter. Finally, a Network Coding approach to cope with the high overhead (e.g. retransmissions) over fading channels is designed and developed in Chapter 8.

References

[6] M. Tornatore, G.-K. Chang, and G. Ellinas, "Fiber-Wireless Convergence in Next-Generation Communication Networks: Systems, Architectures, and Management," *Cham: Springer International Publishing*, 2017.

[7] W. Sun et al., "Wi-Fi Could be Much More," *IEEE Communications Magazine*, vol. 52, no. 11, pp. 22–29, 2014.

[8] International Telecommunication Union, "Draft New Report ITU-R M.[IMT-2020.TECH PERF REQ] - Minimum Requirements Related to Technical Performance for IMT-2020 Radio Interface(s)," ITU, Tech. Rep., 2017. [Online]. Available: https://www.itu.int/pub/R-REP-M.2410-2017.

[9] 5G-PPP Architecture Working Group, "White Paper: View on 5G Architecture (Version 2.0)," 5G-PPP, Tech. Rep., 2017. [Online]. Available: https://5g-ppp.eu/wp-content/uploads/2017/07/5G-PPP-5G-Architecture-White-Paper-2-Summer-2017_For-Public-Consultation.pdf.

[10] K. Zheng, L. Zhao, J. Mei, M. Dohler, W. Xiang, and Y. Peng, "10 Gb/s HetsNets with Millimeter-Wave Communications: Access and Networking - Challenges and Protocols," *IEEE Communications Magazine*, vol. 53, no. 1, pp. 222–231, 2015.

[11] Ofcom, "White Paper: Update on 5G Spectrum in the UK," Ofcom, Tech. Rep., 2017. [Online]. Available: https://www.ofcom.org.uk/__data/assets/pdf_file/0021/97023/5G-update-08022017.pdf.

[12] S. Yost, "White Paper: mmWave: Battle of the Bands," National Instruments, Tech. Rep., 2016. [Online]. Available: https://www.ni.com/en-gb/innovations/white-papers/16/mmwave--the-battle-of-the-bands.html.

[13] J. Knapp, "Presentation: FCC Actions to Make Spectrum Available for 5G", 2016. [Online]. Available: https://5g-ppp.eu/wp-content/uploads/2016/11/Opening-1_Julius-Knapp.pdf.

[14] F. C. Commission, "Document (347449A1): Use of Spectrum Bands Above 24 GHz for Mobile Radio Services," Federal Communications Commission (FCC), Tech. Rep., 2019. [Online]. Available: https://www.federalregister.gov/documents/2019/02/05/2018-27975/use-of-spectrum-bands-above-24-ghz-for-mobile-radio-services.

[15] M. Cudak et al., "Moving Towards Mmwave-Based Beyond-4G (B-4G) Technology," *IEEE 77th Vehicular Technology Conference (VTC Spring)*, pp. 1–5, 2013.

[16] J. Zhang, P. Tang, L. Tian, Z. Hu, T. Wang, and H. Wang, "6-100 GHz Research Progress and Challenges from a Channel Perspective for Fifth Generation (5G) and Future Wireless Communication," *Science China Information Sciences, 60: 080301*, vol. 60, no. 8, pp. 1–18, 2017.

[17] T. S. Rappaport, Y. Xing, G. R. Maccartney, A. F. Molisch, E. Mellios, and J. Zhang, "Overview of Millimeter Wave Communication for Fifth-Generation (5G) Wireless Networks - with a focus on Propagation Models," *IEEE Transactions on Antennas and Propagation*, vol. 65, no. 12, pp. 6213–6230, 2017.

[18] M. K. Samimi, G. R. Maccartney, S. Sun, and T. S. Rappaport, "28 GHz Millimeter-Wave Ultrawideband Small-Scale Fading Models in Wireless Channels," *IEEE 83rd Vehicular Technology Conference (VTC Spring)*, pp. 1–6, 2016.

[19] 5G-PPP, "Document (H2020 - ICT - 671650): Measurement Results and Final mmMagic Channel Models", 2017. [Online]. Available: `https://bscw.5g-mmmagic.eu/pub/bscw.cgi/d202656/mmMAGIC_D2-2.pdf`.

[20] T. Wang et al., "Spectrum Analysis and Regulations for 5G," *5G Mobile Communications, Springer International Publishing*, pp. 27–50, 2017.

[21] S. Vetti, J. Olsson, and J. Copley, "White Paper: Sub-1 GHz Long-Range Communication and Smartphone Connection for IoT Applications," Texas Instruments, Tech. Rep., 2016. [Online]. Available: `http://www.ti.com/lit/wp/swry026/swry026.pdf`.

[22] U. Rehfuess, "White Paper: 5G for People and Things 700 MHz Band as Key to Success for Wide-Area 5G Services," Nokia, Tech. Rep., 2017. [Online]. Available: `https://www.itu.int/en/ITU-D/Regional-Presence/Europe/Documents/Events/2017/Spectrum%20Management/Ulrich__Nokia__5G_in%20700w.pdf`.

[23] Q. Wu, G. Y. Li, W. Chen, D. W. K. Ng, and R. Schober, "An Overview of Sustainable Green 5G Networks," *IEEE Wireless Communications*, vol. 24, no. 4, pp. 72–80, 2017.

[24] C.-X. Wang et al., "Cellular Architecture and Key Technologies for 5G Wireless Communication Networks," *IEEE Communications Magazine*, vol. 52, no. 2, pp. 122–130, 2014.

[25] R. Q. Hu and Y. Qian, "An Energy Efficient and Spectrum Efficient Wireless Heterogeneous Network Framework for 5G Systems," *IEEE Communications Magazine*, vol. 52, no. 5, pp. 94–101, 2014.

[26] F. R. Yu, X. Zhang, and V. C.-M. Leung, "Green Wireless Communications and Networking," *Green Communications and Networking, CRC Press*, 2012.

[27] A. He et al., "Green Communications: A Call for Power Efficient Wireless Systems," *Journal of Communications*, vol. 6, no. 4, pp. 340–351, 2011.

[28] P. Kamalinejad, C. Mahapatra, Z. Sheng, S. Mirabbasi, V. C. M. Leung, and Y. L. Guan, "Wireless Energy Harvesting for the Internet of Things," *IEEE Communications Magazine*, vol. 53, no. 6, pp. 102–108, 2015.

[29] P. Ramezani and A. Jamalipour, "Toward the Evolution of Wireless Powered Communication Networks for the Future Internet of Things," *IEEE Network*, vol. 53, no. 6, pp. 1–10, 2017.

[30] 5G Workgroup - Wireless Broadband Alliance, "White Paper: 5G Networks - The Role of Wi-Fi and Unlicensed Technologies," Wireless Broadband Alliance, Tech. Rep., 2017.

[31] T. S. Rappaport and J. N. Murdock, "Power Efficiency and Consumption Factor Analysis for Broadband Millimeter-Wave Cellular Networks," *2012 IEEE Global Communications Conference (GLOBECOM)*, pp. 4518–4523, 2012.

[32] P. B. Papazian, G. A. Hufford, R. J. Achatz, and R. Hoffman, "Study of the Local Multipoint Distribution Service Radio Channel," *IEEE Transactions on Broadcasting*, vol. 43, no. 2, pp. 175–184, 1997.

[33] Z. Pi and F. Khan, "An Introduction to Millimeter-Wave Mobile Broadband Systems," *IEEE Communications Magazine*, vol. 49, no. 6, pp. 101–107, 2011.

[34] T. S. Rappaport et al., "Millimeter Wave Mobile Communications for 5G Cellular: It Will Work!" *IEEE Access*, vol. 1, pp. 335–349, 2013.

[35] S. Rangan, T. S. Rappaport, and E. Erkip, "Millimeter-Wave Cellular Wireless Networks: Potentials and Challenges," *Proceedings of the IEEE*, vol. 102, no. 3, pp. 366–385, 2014.

[36] T. S. Rappaport, F. Gutierrez, E. Ben-Dor, J. N. Murdock, Y. Qiao, and J. I. Tamir, "Broadband Millimeter-Wave Propagation Measurements and Models Using Adaptive-Beam Antennas for Outdoor Urban Cellular Communications," *IEEE Transactions on Antennas and Propagation*, vol. 61, no. 4, pp. 1850–1859, 2013.

[37] M. R. Gerdisch and J. A. Kilpatrick, "Co-located Omnidirectional and Sectorized Base Station," U.S. Patent No. 6,141,566, 2000.

[38] E. S. Sousa, "Antenna Architectures for CDMA Integrated Wireless Access Networks," *Wireless: Merging onto the Information Superhighway: Proceedings of 6th International Symposium on Personal, Indoor and Mobile Radio Communications (PIMRC'95)*, vol. 3, pp. 921–925, 1995.

[39] C. A. Balanis, "Antenna Theory: A Review," *Proceedings of the IEEE*, vol. 80, no. 1, pp. 7–23, 1992.

[40] G. J. K. Moernaut and D. Orban, "Article: The Basics of Antenna Arrays," Orban Microwave Products, Tech. Rep., 2014. [Online]. Available: https://orbanmicrowave.com/the-basics-of-antenna-arrays/.

[41] ETSI, "Technical Report (ETSI TR 138912): 5G; Study of New Radio (NR) Access Technology," ETSI, Tech. Rep., 2017. [Online]. Available: https://www.etsi.org/deliver/etsi_tr/138900_138999/138912/14.00.00_60/tr_138912v140000p.pdf.

[42] 3rd Generation Partnership Project, Technical Specification Group Radio Access Network, "Document (3GPP TR 38.801 V14.0.0): Study on New Radio Access Technology: Radio Access Architecture and Interfaces," 3GPP, Tech. Rep., 2017. [Online]. Available: http://www.3gpp.org/ftp//Specs/archive/38_series/38.801/38801-e00.zip.

[43] ——, "Document (3GPP TR 38.802 V14.2.0): Study on New Radio Access Technology: Physical Layer Aspects," 3GPP, Tech. Rep., 2017. [Online]. Available: http://www.3gpp.org/ftp//Specs/archive/38_series/38.802/38802-e20.zip.

[44] 5G-PPP Phase 1 Projects, mmMAGIC. (2017). mmMAGIC: Millimetre-Wave Based Mobile Radio Access Network for Fifth Generation Integrated Communications, [Online]. Available: https://5g-ppp.eu/mmmagic/ (visited on 2017).

[45] A. Alkhateeb, O. E. Ayach, G. Leus, and R. W. Heath, "Channel Estimation and Hybrid Precoding for Millimeter Wave Cellular Systems," *IEEE Journal of Selected Topics in Signal Processing*, vol. 8, no. 5, pp. 831–846, 2014.

[46] Y. M. Tsang, A. S. Y. Poon, and S. Addepalli, "Coding the Beams: Improving Beamforming Training in mmWave Communication System," *2011 IEEE Global Telecommunications Conference (GLOBECOM 2011)*, 2011.

[47] W. Roh et al., "Millimeter-Wave Beamforming as an Enabling Technology for 5G Cellular Communications: Theoretical Feasibility and Prototype Results," *IEEE Communications Magazine*, vol. 52, no. 2, pp. 106–113, 2014.

[48] A. Alkhateeb, G. Leus, and R. W. Heath, "Limited Feedback Hybrid Precoding for Multi-User Millimeter Wave Systems," *IEEE Transactions on Wireless Communications*, vol. 14, no. 11, pp. 6481–6494, 2015.

[49] F. Rusek, D. Persson, B. K. Lau, E. G. Larsson, T. L. Marzetta, and F. Tufvesson, "Scaling Up MIMO: Opportunities and Challenges with Very Large Arrays," *IEEE Signal Processing Magazine*, vol. 30, no. 1, pp. 40–60, 2013.

[50] S. Han, C. L. I, C. Rowell, Z. Xu, S. Wang, and Z. Pan, "Large Scale Antenna System with Hybrid Digital and Analogue BF Structure," *2014 IEEE International Conference on Communications Workshops (ICC)*, pp. 842–847, 2014.

[51] S. Han, C.-L. I, Z. Xu, and C. Rowell, "Large-Scale Antenna Systems with Hybrid Analog and Digital Beamforming for Millimeter Wave 5G," *IEEE Communications Magazine*, vol. 53, no. 1, pp. 186–194, 2015.

[52] A. Alkhateeb, O. E. Ayach, G. Leus, and R. W. Heath, "Hybrid Precoding for Millimeter Wave Cellular Systems with Partial Channel Knowledge," *2013 Information Theory and Applications Workshop (ITA)*, pp. 1–5, 2013.

[53] A. F. Molisch et al., "Hybrid Beamforming for Massive MIMO: A Survey," *IEEE Communications Magazine*, vol. 55, no. 9, pp. 134–141, 2017.

[54] S.-H. Wu, L.-K. Chiu, K.-Y. Lin, and T.-H. Chang, "Robust Hybrid Beamforming with Phased Antenna Arrays for Downlink SDMA in Indoor 60 GHz Channels," *IEEE Transactions on Wireless Communications*, vol. 12, no. 9, pp. 4542–4557, 2013.

[55] I. Uchendu and J. R. Kelly, "Survey of Beam Steering Techniques Available for Millimeter Wave Applications," *Progress In Electromagnetics Research B*, vol. 68, pp. 35–54, 2016.

[56] J. Zhang, X. Ge, Q. Li, M. Guizani, and Y. Zhang, "5G Millimeter-Wave Antenna Array: Design and Challenges," *IEEE Wireless Communications*, vol. 24, no. 2, pp. 106–112, 2017.

[57] A. V. Raisanen et al., "Beam-Steering Antennas at Millimeter Wavelengths," *Proceedings of 2012 5th Global Symposium on Millimeter-Waves*, pp. 170–173, 2012.

[58] K. Zarb-Adami, A. Faulkner, J. G. B. D. Vaate, G. W. Kant, and P. Picard, "Beamforming Techniques for Large-N Aperture Arrays," *2010 IEEE International Symposium on Phased Array Systems and Technology*, pp. 883–890, 2010.

[59] V. I. Barousis, C. B. Papadias, and R. R. Muller, "A New Signal Model for MIMO Communication with Compact Parasitic Arrays," *2014 6th International Symposium on Communications, Control and Signal Processing (ISCCSP)*, pp. 109–113, 2014.

[60] R. C. Hansen, *Phased Array Antennas*. John Wiley & Sons, 2009.

[61] R. J. Mailloux, *Phased Array Antenna Handbook*. Boston: Artech House, 2005.

[62] K. Gyoda and T. Ohira, "Design of Electronically Steerable Passive Array Radiator (ESPAR) Antennas," *IEEE Antennas and Propagation Society International Symposium. Transmitting Waves of Progress to the Next Millennium. 2000 Digest. Held in conjunction with: USNC/URSI National Radio Science Meeting (Cat. No.00CH37118)*, vol. 2, pp. 922–925, 2000.

[63] H. Kawakami and T. Ohira, "Electrically Steerable Passive Array Radiator (ESPAR) Antennas," *IEEE Antennas and Propagation Magazine*, vol. 47, no. 2, pp. 43–50, 2005.

[64] A. Kalis, A. G. Kanatas, and C. B. Papadias, *Parasitic Antenna Arrays for Wireless MIMO Systems*. New York: Springer, 2014.

[65] A. L. Swindlehurst, E. Ayanoglu, P. Heydari, and F. Capolino, "Millimeter-Wave Massive MIMO: The Next Wireless Revolution?" *IEEE Communications Magazine*, vol. 52, no. 9, pp. 56–62, 2014.

[66] S. Mumtaz, J. Rodriguez, and L. Dai, *MmWave Massive MIMO: A Paradigm for 5G*. Academic Press, 2016.

[67] E. Larsson, O. Edfors, F. Tufvesson, and T. Marzetta, "Massive MIMO for Next Generation Wireless Systems," *IEEE Communications Magazine*, vol. 52, no. 2, pp. 186–195, 2014.

[68] L. Lu, G. Y. Li, A. L. Swindlehurst, A. Ashikhmin, and R. Zhang, "An Overview of Massive MIMO: Benefits and Challenges," *IEEE Journal of Selected Topics in Signal Processing*, vol. 8, no. 5, pp. 742–758, 2014.

[69] A. Ashikhmin and T. Marzetta, "Pilot Contamination Precoding in Multi-Cell Large Scale Antenna Systems," *2012 IEEE International Symposium on Information Theory Proceedings*, pp. 1137–1141, 2012.

[70] M. Feng and S. Mao, "Harvest the Potential of Massive MIMO with Multi-Layer Techniques," *IEEE Network*, vol. 30, no. 5, pp. 40–45, 2016.

[71] E. Björnson, E. G. Larsson, and T. L. Marzetta, "Massive MIMO: Ten Myths and One Critical Question," *IEEE Communications Magazine*, vol. 54, no. 2, pp. 114–123, 2016.

[72] E. Zeydan, D. Dedeoglu, and Y. Turk, "Experimental Evaluations of TDD-Based Massive MIMO Deployment for Mobile Network Operators," *IEEE Access*, vol. 8, pp. 33 202–33 214, 2020.

[73] A. Nosratinia, T. E. Hunter, and A. Hedayat, "Cooperative Communication in Wireless Networks," *IEEE Communications Magazine*, vol. 42, no. 10, pp. 74–80, 2004.

[74] M. Sawahashi, Y. Kishiyama, A. Morimoto, D. Nishikawa, and M. Tanno, "Coordinated Multipoint Transmission/Reception Techniques for LTE-Advanced [Coordinated and Distributed MIMO," *IEEE Wireless Communications*, vol. 17, no. 3, pp. 26–34, 2010.

[75] X.-H. You, D.-M. Wang, B. Sheng, X.-Q. Gao, X.-S. Zhao, and M. Chen, "Cooperative Distributed Antenna Systems for Mobile Communications [Coordinated and Distributed MIMO]," *IEEE Wireless Communications*, vol. 17, no. 3, pp. 35–43, 2010.

[76] A. K. Samingan, I. Suleiman, C. Y. Yeoh, and A. A. A. Rahman, "Receiver Antenna Synchronization and Carrier Frequency Offsets Pre-Mitigation for Distributed Massive MIMO System," *2016 22nd Asia-Pacific Conference on Communications (APCC)*, pp. 457–461, 2016.

[77] A. Dhananjay, "Iris: Mitigating Phase Noise in Millimeter Wave OFDM Systems," PhD thesis, Courant Institute of Mathematical Sciences New York, 2015.

[78] H. Mehrpouyan, A. A. Nasir, S. D. Blostein, T. Eriksson, G. K. Karagiannidis, and T. Svensson, "Joint Estimation of Channel and Oscillator Phase Noise in MIMO Systems," *IEEE Transactions on Signal Processing*, vol. 60, no. 9, pp. 4790–4807, 2012.

[79] G. Colavolpe, A. Barbieri, and G. Caire, "Algorithms for Iterative Decoding in the Presence of Strong Phase Noise," *IEEE Journal on Selected Areas in Communications*, vol. 23, no. 9, pp. 1748–1757, 2005.

[80] M. R. Khanzadi, G. Durisi, and T. Eriksson, "Capacity of SIMO and MISO Phase-Noise Channels with Common/Separate Oscillators," *IEEE Transactions on Communications*, vol. 63, no. 9, pp. 3218–3231, 2015.

[81] E. Björnson, M. Matthaiou, A. Pitarokoilis, and E. G. Larsson, "Distributed Massive MIMO in Cellular Networks: Impact of Imperfect Hardware and Number of Oscillators," *2015 23rd European Signal Processing Conference (EUSIPCO)*, pp. 2436–2440, 2015.

[82] H. V. Balan, R. Rogalin, A. Michaloliakos, K. Psounis, and G. Caire, "AirSync: Enabling Distributed Multiuser MIMO With Full Spatial Multiplexing," *IEEE/ACM Transactions on Networking*, vol. 21, no. 6, pp. 1681–1695, 2013.

[83] K. Nikitopoulos, and K. Jamieson, "FASTER: Fine and Accurate Synchronization for Large Distributed MIMO Wireless Networks," *RN 13 (2013)*, pp. 19–26, 2013.

[84] J. Xiong, K. Sundaresan, K. Jamieson, M. A. Khojastepour, and S. Rangarajan, "MIDAS: Empowering 802.11ac Networks with Multiple-Input Distributed Antenna Systems," *Proceedings of the 10th ACM International on Conference on emerging Networking Experiments and Technologies - CoNEXT 14*, pp. 29–40, 2014.

[85] F. Hu, *Opportunities in 5G Networks: A Research and Development Perspective*. CRC Press, 2016.

[86] M. Giordani, M. Mezzavilla, and M. Zorzi, "Initial Access in 5G mmWave Cellular Networks," *IEEE Communications Magazine*, vol. 54, no. 11, pp. 40–47, 2016.

[87] H. Shokri-Ghadikolaei, C. Fischione, G. Fodor, P. Popovski, and M. Zorzi, "Millimeter Wave Cellular Networks: A MAC Layer Perspective," *IEEE Transactions on Communications*, vol. 63, no. 10, pp. 3437–3458, 2015.

[88] H. Shokri-Ghadikolaei, C. Fischione, P. Popovski, and M. Zorzi, "Design Aspects of Short-Range Millimeter-Wave Networks: A MAC Layer Perspective," *IEEE Network*, vol. 30, no. 3, pp. 88–96, 2016.

[89] M. Polese, M. Giordani, M. Mezzavilla, S. Rangan, and M. Zorzi, "Improved Handover Through Dual Connectivity in 5G mmWave Mobile Networks," *IEEE Journal on Selected Areas in Communications*, vol. 35, no. 9, pp. 2069–2084, 2017.

[90] IEEE Standards Association, *ISO/IEC/IEEE International Standard for Information Technology - Telecommunications and Information Exchange Between Systems–Local and Metropolitan Area Networks - Specific Requirements - Part 11: Wireless LAN Medium Access Control (MAC) and Physical Layer (PHY) Specifications Amendment 3: Enhancements for Very High Throughput in the 60 GHz Band (adoption of IEEE Std 802.11ad-2012)*, 2012.

[91] E. Perahia, C. Cordeiro, M. Park, and L. L. Yang, "IEEE 802.11ad: Defining the Next Generation Multi-Gbps Wi-Fi," *2010 7th IEEE Consumer Communications and Networking Conference*, pp. 1–5, 2010.

[92] G. R. Muns, K. V. Mishra, C. B. Guerra, Y. C. Eldar, and K. R. Chowdhury, "Beam Alignment and Tracking for Autonomous Vehicular Communication using IEEE 802.11ad-based Radar," *IEEE INFOCOM 2019 - IEEE Conference on Computer Communications Workshops (INFOCOM WKSHPS)*, pp. 535–540, 2019.

[93] T. Nitsche, C. Cordeiro, A. Flores, E. Knightly, E. Perahia, and J. Widmer, "IEEE 802.11ad: Directional 60 GHz Communication for Multi-Gigabit-per-second Wi-Fi [Invited Paper]," *IEEE Communications Magazine*, vol. 52, no. 12, pp. 132–141, 2014.

[94] E. Perahia and M. X. Gong, "Gigabit Wireless LANs: An Overview of IEEE 802.11ac and 802.11ad," *ACM SIGMOBILE Mobile Computing and Communications Review*, vol. 15, no. 3, pp. 23–33, 2011.

[95] IEEE Standards Association, *P802.11ay™/D0.8 Draft Standard for Information Technology - Telecommunications and Information Exchange Between Systems - Local and Metropolitan Area Networks - Specific Requirements - Part 11: Wireless LAN Medium Access Control (MAC) and Physical Layer (PHY) Specifications Amendment 7: Enhanced throughput for operation in license-Exempt bands above 45 GHz*, 2017.

[96] C. Chen, O. Kedem, C. R. C. M. d. Silva, and C. Cordeiro, "Millimeter-Wave Fixed Wireless Access Using IEEE 802.11ay," *IEEE Communications Magazine*, vol. 57, no. 12, pp. 98–104, 2019.

[97] P. Zhou et al., "IEEE 802.11ay based mmWave WLANs: Design Challenges and Solutions," *IEEE Communications Surveys & Tutorials*, pp. 1–28, 2018.

[98] Y. Ghasempour, C. R. C. M. Da Silva, C. Cordeiro, and E. W. Knightly, "IEEE 802.11ay: Next-Generation 60 GHz Communication for 100 Gb/s Wi-Fi," *IEEE Communications Magazine*, pp. 1–7, 2017.

[99] K. Jo, S. Park, H. Cho, J. Kim, S. Bang, and S. G. Kim, "Document (IEEE802.11-16/0092r1): Multi-Beamforming in Polarized Channels for 11ay," IEEE, Tech. Rep., 2016. [Online]. Available: `https://mentor.ieee.org/802.11/dcn/16/11-16-0092-01-00ay-multi-beamforming-in-polarized-channels-for-11ay.pptx`.

[100] J. Luo et al., "Document (IEEE802.11-16/0393r0): Characterization of Polarimetric Scattering Effects for 802.11ay Channel Modelling," IEEE, Tech. Rep., 2016. [Online]. Available: `https://mentor.ieee.org/802.11/dcn/16/11-16-0202-04-00ay-tg-ay-march-2016-meeting-agenda.ppt`.

[101] A. Maltsev, A. Pudeyev, and J. Wang, "Document (IEEE802.11-17/1423r1): Polarization in IEEE 802.11ay," IEEE, Tech. Rep., 2017. [Online]. Available: `https://mentor.ieee.org/802.11/dcn/17/11-17-1423-01-00ay-polarization-for-11ay.pptx`.

[102] S. Gao, Q. Luo, and F. Zhu, *Circularly Polarized Antennas*. Wiley, 2014.

[103] B. Kim, B. Pan, S. Nikolaou, Y.-S. Kim, J. Papapolymerou, and M. M. Tentzeris, "A Novel Single-Feed Circular Microstrip Antenna with Reconfigurable Polarization Capability," *IEEE Transactions on Antennas and Propagation*, vol. 56, no. 3, pp. 630–638, 2008.

[104] K. M. Mak, H. W. Lai, K. M. Luk, and C. H. Chan, "Circularly Polarized Patch Antenna for Future 5G Mobile Phones," *IEEE Access*, vol. 2, pp. 1521–1529, 2014.

[105] S. Gao, Y. Qin, and A. Sambell, "Low-Cost Broadband Circularly Polarized Printed Antennas and Array," *IEEE Antennas and Propagation Magazine*, vol. 49, no. 4, pp. 57–64, 2007.

[106] F. Yang and Y. Rahmat-Samii, "A Reconfigurable Patch Antenna Using Switchable Slots for Circular Polarization Diversity," *IEEE Microwave and Wireless Components Letters*, vol. 12, no. 3, pp. 96–98, 2002.

[107] M. Allayioti and J. R. Kelly, "Multiple Parameter Reconfigurable Microstrip Patch Antenna," *2017 IEEE International Symposium on Antennas and Propagation & USNC / URSI National Radio Science Meeting*, pp. 1141–1142, 2017.

[108] D. Tuikovic, S. Sawhney, and M. Grigat, "Document (IEEE802.11-17/1022r0): Changes to IEEE 802.11ay in Support of mmW Distribution Network Use Cases," IEEE, Tech. Rep., 2017. [Online]. Available: https://mentor.ieee.org/802.11/dcn/17/11-17-1022-00-00ay-changes-to-ieee-802-11ay-in-support-of-mmw-mesh-network-use-cases.pptx.

[109] R. W. Yeung, and S. Yang, "Document (IEEE802.11-16/0317r0): BATS: Network Coding for Wireless Relay Networks," IEEE, Tech. Rep., 2016. [Online]. Available: `https://mentor.ieee.org/802.11/dcn/16/11-16-0317-00-00ay-bats-network-coding-for-wireless-relay-networks.pptx`.

[110] R. Ahlswede, N. Cai, S.-Y. Li, and R. Yeung, "Network Information Flow," *IEEE Transactions on Information Theory*, vol. 46, no. 4, pp. 1204–1216, 2000.

[111] T. Ho and D. S. Lun, *Network Coding: An Introduction*. Cambridge University Press, 2008.

[112] S. Katti, H. Rahul, W. Hu, D. Katabi, M. Medard, and J. Crowcroft, "XORs in the Air: Practical Wireless Network Coding," *IEEE/ACM Transactions on Networking*, vol. 16, no. 3, pp. 497–510, 2008.

[113] J. Zhang, Y. P. Chen, and I. Marsic, "MAC-layer Proactive Mixing for Network Coding in Multi-hop Wireless Networks," *Computer Networks*, vol. 54, no. 2, pp. 196–207, 2010.

[114] T. Ho, R. Koetter, M. Medard, D. R. Karger, and M. Effros, "The Benefits of Coding over Routing in a Randomized Setting," *Proceedings of the IEEE International Symposium on Information Theory*, p. 442, 2003.

[115] M. Taghouti et al., "Reduction of Padding Overhead for RLNC Media Distribution With Variable Size Packets," *IEEE Transactions on Broadcasting*, vol. 65, no. 3, pp. 558–576, 2019.

[116] J. Heide, M. V. Pedersen, F. H. P. Fitzek, and T. Larsen, "Network Coding for Mobile Devices - Systematic Binary Random Rateless Codes," *2009 IEEE International Conference on Communications Workshops*, pp. 1–6, 2009.

[117] S. Yang and R. W. Yeung, "Batched Sparse Codes," *IEEE Transactions on Information Theory*, vol. 60, no. 9, pp. 5322–5346, 2014.

[118] R. Bassoli, V. N. Talooki, H. Marques, J. Rodriguez, R. Tafazolli, and S. Mumtaz, "Hybrid Serial Concatenated Network Codes for Burst Erasure Channels," *2015 IEEE 81st Vehicular Technology Conference (VTC Spring)*, pp. 1–4, 2015.

[119] D. E. Lucani, M. V. Pedersen, J. Heide, and F. H. P. Fitzek, "Fulcrum Network Codes: A Code for Fluid Allocation of Complexity," *arXiv preprint arXiv:1404.6620*, pp. 1–31, 2014.

[120] Q. Huang, K. Sun, X. Li, and D. O. Wu, "Just FUN: A Joint Fountain Coding and Network Coding Approach to Loss-Tolerant Information Spreading," *Proceedings of the 15th ACM International Symposium on Mobile Ad hoc Networking and Computing - MobiHoc 14*, pp. 83–92, 2014.

[121] J. Barros, "Mixing Packets: Pros and Cons of Network Coding," *The 11th International Symposium on Wireless Personal Multimedia Communications*, pp. 1–5, 2008.

[122] A. Larmo, M. Lindstrom, M. Meyer, G. Pelletier, J. Torsner, and H. Wiemann, "The LTE Link-Layer Design," *IEEE Communications Magazine*, vol. 47, no. 4, pp. 52–59, 2009.

[123] E. Dahlman, S. Parkvall, and Skold Johan, *4G, LTE-Advanced Pro and the Road to 5G*. Elsevier, Academic Press is an imprint of Elsevier, 2016.

[124] B. Classon, A. Nimbalker, S. Sesia, and I. Toufik, *Chapter 10: Channel Coding and Link Adaptation (in LTE: The UMTS Long Term Evolution from Theory to Practice)*. Wiley, 2009.

[125] F. Capozzi, G. Piro, L. A. Grieco, G. Boggia, and P. Camarda, "Downlink Packet Scheduling in LTE Cellular Networks: Key Design Issues and a Survey," *IEEE Communications Surveys & Tutorials*, vol. 15, no. 2, pp. 678–700, 2013.

[126] L. Gavrilovska and D. Talevski, "Novel Scheduling Algorithms for LTE Downlink Transmission," *19th Telecommunications Forum (TELFOR) Proceedings of Papers*, pp. 398–401, 2011.

[127] R. Kwan, C. Leung, and J. Zhang, "Proportional Fair Multiuser Scheduling in LTE," *IEEE Signal Processing Letters*, vol. 16, no. 6, pp. 461–464, 2009.

[128] P. C. Chan et al., "The Evolution Path of 4G Networks: FDD or TDD?" *IEEE Communications Magazine*, vol. 44, no. 12, pp. 42–50, 2006.

[129] S. Chen and J. Zhao, "The Requirements, Challenges, and Technologies for 5G of Terrestrial Mobile Telecommunication," *IEEE Communications Magazine*, vol. 52, no. 5, pp. 36–43, 2014.

[130] M. Faulkner, "The Effect of Filtering on the Performance of OFDM Systems," *IEEE Transactions on Vehicular Technology*, vol. 49, no. 5, pp. 1877–1884, 2000.

[131] S. Takebuchi, T. Arai, and F. Maehara, "A Novel Clipping and Filtering Method Employing Transmit Power Control for OFDM Systems," *2012 IEEE Wireless Communications and Networking Conference (WCNC)*, pp. 221–225, 2012.

[132] N. Himayat, S. Talwar, A. Rao, and R. Soni, "Interference Management for 4G Cellular Standards [WIMAX/LTE UPDATE]," *IEEE Communications Magazine*, vol. 48, no. 8, pp. 86–92, 2010.

[133] C. Hoymann, W. Chen, J. Montojo, A. Golitschek, C. Koutsimanis, and X. Shen, "Relaying Operation in 3GPP LTE: Challenges and Solutions," *IEEE Communications Magazine*, vol. 50, no. 2, pp. 156–162, 2012.

[134] K. Pedersen, F. Frederiksen, C. Rosa, H. Nguyen, L. G. Garcia, and Y. Wang, "Carrier Aggregation for LTE-Advanced: Functionality and Performance Aspects," *IEEE Communications Magazine*, vol. 49, no. 6, pp. 89–95, 2011.

[135] M. Kottkamp, A. Roessler, and J. Schlienz, "White Paper: LTE-Advanced Technology Introduction," Rohde & Schwarz, Tech. Rep., 2010.

[136] M. F. L. Abdullah and A. Z. Yonis, "Performance of LTE Release 8 and Release 10 in Wireless Communications," *Proceedings Title: 2012 International Conference on Cyber Security, Cyber Warfare and Digital Forensic (CyberSec)*, pp. 236–241, 2012.

[137] L. Chen, W. Chen, X. Zhang, and D. Yang, "Analysis and Simulation for Spectrum Aggregation in LTE-Advanced System," *2009 IEEE 70th Vehicular Technology Conference Fall*, pp. 1–6, 2009.

[138] H. Lee, S. Vahid, and K. Moessner, "A Survey of Radio Resource Management for Spectrum Aggregation in LTE-Advanced," *IEEE Communications Surveys & Tutorials*, vol. 16, no. 2, pp. 745–760, 2014.

[139] H. Wang, C. Rosa, and K. Pedersen, "Uplink Component Carrier Selection for LTE-Advanced Systems with Carrier Aggregation," *2011 IEEE International Conference on Communications (ICC)*, pp. 1–5, 2011.

[140] C. S. Park, L. Sundström, A. Wallén, and A. Khayrallah, "Carrier Aggregation for LTE-Advanced: Design Challenges of Terminals," *IEEE Communications Magazine*, vol. 51, no. 12, pp. 76–84, 2013.

[141] 3rd Generation Partnership Project, Technical Specification Group Services and System Aspects, "Document (3GPP TR 38.834 V11.0.0): Study on Operations, Administration and Maintenance (OAM) Aspects of Inter-Radio-Access-Technology (RAT) Energy Saving (Release 11)," 3GPP, Tech. Rep., 2016. [Online]. Available: `http://www.3gpp.org/ftp/Specs/archive/32_series/32.834/32834-b00.zip`.

[142] B. Soret, Y. Wang, and K. I. Pedersen, "CRS Interference Cancellation in Heterogeneous Networks for LTE-Advanced Downlink," *2012 IEEE International Conference on Communications (ICC)e*, pp. 6797–6801, 2012.

[143] R. Irmer et al., "Coordinated Multipoint: Concepts, Performance, and Field Trial Results," *IEEE Communications Magazine*, vol. 49, no. 2, pp. 102–111, 2011.

[144] D. Feng, C. Jiang, G. Lim, L. Cimini, G. Feng, and G. Li, "A Survey of Energy-Efficient Wireless Communications," *IEEE Communications Surveys & Tutorials*, vol. 15, no. 1, pp. 167–178, 2013.

[145] C.-L. I, C. Rowell, S. Han, Z. Xu, G. Li, and Z. Pan, "Toward Green and Soft: A 5G Perspective," *IEEE Communications Magazine*, vol. 52, no. 2, pp. 66–73, 2014.

[146] T. Yang, F. Heliot, and C. H. Foh, "A Survey of Green Scheduling Schemes for Homogeneous and Heterogeneous Cellular Networks," *IEEE Communications Magazine*, vol. 53, no. 11, pp. 175–181, 2015.

[147] D. Astely, E. Dahlman, G. Fodor, S. Parkvall, and J. Sachs, "LTE Release 12 and Beyond [Accepted from Open Call]," *IEEE Communications Magazine*, vol. 51, no. 7, pp. 154–160, 2013.

[148] 4G Americas, "White Paper: Understanding 3GPP Release 12 Standards for HSPA+ and LTE-Advanced Enhancements," 4G Americas, Tech. Rep., 2015. [Online]. Available: `https://www.5gamericas.org/understanding-3gpp-release-12-standards-for-hspa-and-lte-enhancements/`.

[149] J. S. Roessler, "White Paper: LTE-Advanced (3GPP Rel. 12) Technology Introduction White Paper," München: Application Note-1MA252-Rohde & Schwarz International, Tech. Rep., 2015. [Online]. Available: `https://scdn.rohde-schwarz.com/ur/pws/dl_downloads/dl_application/application_notes/1ma252/1MA252_2e_LTE_Rel12_technology.pdf`.

[150] S.-Y. Lien, C.-C. Chien, F.-M. Tseng, and T.-C. Ho, "3GPP Device-to-Device Communications for Beyond 4G Cellular Networks," *IEEE Communications Magazine*, vol. 54, no. 3, pp. 29–35, 2016.

[151] A. Prasad, A. Kunz, G. Velev, K. Samdanis, and J. Song, "Energy-Efficient D2D Discovery for Proximity Services in 3GPP LTE-Advanced Networks: ProSe Discovery Mechanisms," *IEEE Vehicular Technology Magazine*, vol. 9, no. 4, pp. 40–50, 2014.

[152] S. Mumtaz, K. M. S. Huq, and J. Rodriguez, "Direct Mobile-to-Mobile Communication: Paradigm for 5G," *IEEE Wireless Communications*, vol. 21, no. 5, pp. 14–23, 2014.

[153] S. Andreev, A. Pyattaev, K. Johnsson, O. Galinina, and Y. Koucheryavy, "Cellular Traffic Offloading onto Network-Assisted Device-to-Device Connections," *IEEE Wireless Communications*, vol. 52, no. 4, pp. 20–31, 2014.

[154] H. Ji et al., "Overview of Full-Dimension MIMO in LTE-Advanced Pro," *IEEE Communications Magazine*, vol. 55, no. 2, pp. 176–184, 2017.

[155] C. Liang and F. R. Yu, "Wireless Network Virtualization: A Survey, Some Research Issues and Challenges," *IEEE Communications Surveys & Tutorials*, vol. 17, no. 1, pp. 358–380, 2015.

[156] R. Ratasuk, A. Prasad, Z. Li, A. Ghosh, and M. Uusitalo, "Recent Advancements in M2M Communications in 4G Networks and Evolution Towards 5G," *2015 18th International Conference on Intelligence in Next Generation Networks*, pp. 52–57, 2015.

[157] Y.-H. Nam et al., "Full Dimension MIMO (FD-MIMO) for Next Generation Cellular Technology," *IEEE Communications Magazine*, vol. 51, no. 6, pp. 172–179, 2013.

[158] Ericsson, "3GPP LTE Work Item Description (3GPP RP-121415): New Carrier Type for LTE", 2012. [Online]. Available: https://www.3gpp.org/ftp/tsg_ran/TSG_RAN/TSGR_57/Info_for_workplan/_WI/RP-121415.zip.

[159] C. Hoymann, D. Larsson, H. Koorapaty, and J.-F. Cheng, "A Lean Carrier for LTE," *IEEE Communications Magazine*, vol. 51, no. 2, pp. 74–80, 2013.

[160] J. Lee et al., "LTE-Advanced in 3GPP Rel-13/14: An Evolution Toward 5G," *IEEE Communications Magazine*, vol. 54, no. 3, pp. 36–42, 2016.

[161] Y. Kim et al., "Full Dimension MIMO (FD-MIMO): The Next Evolution of MIMO in LTE Systems," *IEEE Communications Magazine*, vol. 21, no. 2, pp. 26–33, 2014.

[162] H. Cui, V. C. M. Leung, S. Li, and X. Wang, "LTE in the Unlicensed Band: Overview, Challenges, and Opportunities," *IEEE Wireless Communications*, vol. 24, no. 4, pp. 99–105, 2017.

[163] Z. Khan, H. Ahmadi, E. Hossain, M. Coupechoux, L. Dasilva, and J. Lehtomäki, "Carrier Aggregation/Channel Bonding in Next Generation Cellular Networks: Methods and Challenges," *IEEE Network*, vol. 28, no. 6, pp. 34–40, 2014.

[164] C. Cano and D. J. Leith, "Unlicensed LTE/WiFi Coexistence: Is LBT Inherently Fairer Than CSAT?" *2016 IEEE International Conference on Communications (ICC)*, pp. 1–6, 2016.

[165] 3rd Generation Partnership Project, Technical Specification Group Radio Access Network, "Document (3GPP TR-37.857): Study on Indoor Positioning Enhancements for UTRA and LTE," 3GPP, Tech. Rep., 2016. [Online]. Available: `http://www.3gpp.org/ftp/Specs/archive/37_series/37.857/37857-d10.zip`.

[166] H. Ryden et al., "Baseline Performance of LTE Positioning in 3GPP 3D MIMO Indoor User Scenarios," *2015 International Conference on Location and GNSS (ICL-GNSS)*, pp. 1–6, 2015.

[167] F. C. Commission, "Fourth Report and Order PS Docket No. 07-114: FCC Wireless E911 Location Accuracy Requirements," Federal Communications Commission (FCC), Tech. Rep., 2019. [Online]. Available: `https://www.federalregister.gov/documents/2019/04/04/2019-06012/wireless-e911-location-accuracy-requirements`.

[168] C. Hoymann et al., "LTE Release 14 Outlook," *IEEE Communications Magazine*, vol. 54, no. 6, pp. 44–49, 2016.

[169] R. Karaki et al., "Uplink Performance of Enhanced Licensed Assisted Access (eLAA) in Unlicensed Spectrum," *2017 IEEE Wireless Communications and Networking Conference (WCNC)*, pp. 1–6, 2017.

[170] Samsung, "3GPP LTE Work Item Description (3GPP RP-160623): Enhancements on Full-Dimension (FD) MIMO for LTE," 3GPP, Tech. Rep., 2016. [Online]. Available: `http://www.3gpp.org/ftp/tsg_ran/TSG_RAN/TSGR_71/Docs/RP-160623.zip`.

[171] Y. Hu, B. L. Ng, Y. H. Nam, J. Yuan, G. Xu, and J. Y. Seol, "Distributed FD-MIMO: Cellular Evolution for 5G and Beyond," *arXiv preprint arXiv:1704.00647*, pp. 1–12, 2017.

[172] Intel Corporation, "3GPP LTE Work Item Description (3GPP RP-160603): New WID: Radiated Performance Requirements for the Verification of Multi-Antenna Reception of UEs," 3GPP, Tech. Rep., 2016. [Online]. Available: https://www.3gpp.org/ftp/tsg_ran/TSG_RAN/TSGR_71/Docs/RP-160603.zip.

[173] 3rd Generation Partnership Project, Technical Specification Group Radio Access Network, "3GPP LTE Work Item Description (3GPP TR-37.871): Multi-Band Base Station Testing with Three or More Bands," 3GPP, Tech. Rep., 2017. [Online]. Available: http://www.3gpp.org/ftp//Specs/archive/37_series/37.871/37871-e00.zip.

[174] ——, "3GPP LTE Work Item Description (3GPP TR-36.881): L2 Latency Reduction Techniques for LTE," 3GPP, Tech. Rep., 2016. [Online]. Available: http://www.3gpp.org/ftp/Specs/archive/36_series/36.881/36881-e00.zip.

[175] ——, "3GPP LTE Work Item Description (3GPP TR-36.743): L2 Latency Reduction Techniques for LTE," 3GPP, Tech. Rep., 2016. [Online]. Available: http://www.3gpp.org/ftp/Specs/archive/36_series/36.743/36743-010.zip.

[176] IEEE Standards Association, *ISO/IEC/IEEE International Standard for Information Technology - Telecommunications and Information Exchange Between Systems - Local and Metropolitan Area Networks - Specific Requirements - Part 11: Wireless LAN Medium Access Control (MAC) and Physical Layer (PHY) Specifications Amendment 6: Wireless Access in Vehicular Environments*, 2010.

[177] G. Araniti, C. Campolo, M. Condoluci, A. Iera, and A. Molinaro, "LTE for Vehicular Networking: A Survey," *IEEE Communications Magazine*, vol. 51, no. 5, pp. 148–157, 2013.

[178] H. Seo, K.-D. Lee, S. Yasukawa, Y. Peng, and P. Sartori, "LTE Evolution for Vehicle-to-Everything Services," *IEEE Communications Magazine*, vol. 54, no. 6, pp. 22–28, 2016.

[179] S. Chen et al., "Vehicle-to-Everything (v2x) Services Supported by LTE-Based Systems and 5G," *IEEE Communications Magazine*, vol. 1, no. 2, pp. 70–76, 2017.

[180] 3rd Generation Partnership Project, Technical Specification Group Services and System Aspects, "3GPP LTE Work Item Description (3GPP TS 22.261): Service Requirements for the 5G System - Stage 1 (Release 15)," 3GPP, Tech. Rep., 2018. [Online]. Available: http://www.3gpp.org/ftp//Specs/archive/22_series/22.261/22261-f70.zip.

[181] E. Pateromichelakis et al., "Service-Tailored User-Plane Design Framework and Architecture Considerations in 5G Radio Access Networks," *IEEE Access*, vol. 5, pp. 17 089–17 105, 2017.

[182] K. Abbas, K. T. Ahmed, A. Rafig, W. Song, and S. Seok, "An LTE-WiFi Spectrum Aggregation System for 5G Network: A Testbed," *2020 International Conference on Information Networking (ICOIN)*, pp. 753–755, 2020.

[183] Huawei and Hisilicon, "Document (3GPP TDoc S1-171018): Add Vehicles Platooning Requirements in eV2X TS," 3GPP, Tech. Rep., 2017. [Online]. Available: `http://www.3gpp.org/ftp/tsg_sa/WG1_Serv/TSGS1_77_Jeju/docs/S1-171310.zip`.

[184] 5G Automotive Association (5GAA), *White Paper: Toward Fully Connected Vehicles: Edge Computing for Advanced Automotive Communications*, 2017. [Online]. Available: https://5gaa.org/news/toward-fully-connected-vehicles-edge-computing-for-advanced-automotive-communications/.

[185] 3rd Generation Partnership Project, Technical Specification Group Radio Access Network, "3GPP LTE Work Item Description (3GPP TR 36.787 V15.0): Vehicle-to-Everything (V2X) New Band Combinations for LTE (Release 15)," 3GPP, Tech. Rep., 2018. [Online]. Available: `http://www.3gpp.org/ftp//Specs/archive/36_series/36.787/36787-f00.zip`.

[186] 5G-PPP Phase 2 Projects, 5GCAR, *5GCAR: Fifth Generation Communication Automotive Research and Innovation*, 2017. [Online]. Available: https://5gcar.eu/.

[187] Korea Railroad Research Institute (KRRI), "Document (3GPP TDoc S1-171079): Addition of Requirements Regarding Supported Radio Access Technologies for FRMCS," 3GPP, Tech. Rep., 2017. [Online]. Available: `https://www.3gpp.org/ftp/tsg_sa/WG1_Serv/TSGS1_77_Jeju/Docs/S1-171079.zip`.

[188] UIC, Nokia, Kapsch Carrier Com, and Ericsson, "Document (3GPP TDoc S1-171181): New Use Case on FRMCS Positioning Accuracy," 3GPP, Tech. Rep., 2017. [Online]. Available: `http://www.3gpp.org/ftp/tsg_sa/WG1_Serv/TSGS1_77_Jeju/docs/S1-171334.zip`.

[189] 3rd Generation Partnership Project, Technical Specification Group Services and System Aspects, "Document (3GPP TR 22.989 (v0.2.0)): Study on Future Railway Mobile Communication System - Stage 1 (Release 15)," 3GPP, Tech. Rep., 2017. [Online]. Available: `http://www.3gpp.org/ftp//Specs/archive/22_series/22.989/22989-020.zip`.

[190] 5G-PPP Phase 2 Projects, 5G-XCAST, *5G-Xcast: Broadcast and Multicast Communication Enablers for the Fifth Generation of Wireless Systems*, 2018. [Online]. Available: https://5g-xcast.eu/.

[191] R. I. Ansari et al., "5G D2D Networks: Techniques, Challenges, and Future Prospects," *IEEE Systems Journal*, pp. 1–15, 2017.

[192] Samsung, "Document (3GPP TDoc R1-163999): Discussion on Different Scaling Methods for NR Subcarrier Spacing," 3GPP, Tech. Rep., 2016. [Online]. Available: https://www.3gpp.org/ftp/tsg_ran/WG1_RL1/TSGR1_85/Docs/R1-163999.zip.

[193] GTI Group, "White Paper: GTI Proof of Concept of 5G System," GTI Group, Tech. Rep., 2017. [Online]. Available: http://gtigroup.org/Resources/rep/2017-08-11/10994.html.

[194] B. Wang, K. Wang, Z. Lu, T. Xie, and J. Quan, "Comparison Study of Non-Orthogonal Multiple Access Schemes for 5G," *2015 IEEE International Symposium on Broadband Multimedia Systems and Broadcasting*, pp. 1–5, 2015.

[195] 3rd Generation Partnership Project, Technical Specification Group Radio Access Networks, "Document (3GPP TR 37.863-02-01 (V0.2.0)): Dual Connectivity (DC) Band Combinations of LTE 2DL/1UL + One NR Band," 3GPP, Tech. Rep., 2018. [Online]. Available: http://ftp.3gpp.org//Specs/archive/37_series/37.716-21-21/37716-21-21-020.zip.

[196] Qualcomm, *Presentation: Making 5G NR a Commercial Reality; a Unified, more Capable 5G Air Interface*, 2017. [Online]. Available: https://www.qualcomm.com/media/documents/files/making-5g-nr-a-commercial-reality.pdf.

[197] 5G-PPP Phase 2 Projects, ONE5G, *ONE5G: E2E-aware Optimizations and Advancements for the Network Edge of 5G New Radio*, 2017. [Online]. Available: https://one5g.eu/.

[198] Nokia, Alcatel-Lucent Shanghai Bell, "Document (3GPP TDoc R1-1612284): Polar Codes for Control Channels," 3GPP, Tech. Rep., 2016. [Online]. Available: https://www.3gpp.org/ftp/tsg_ran/WG1_RL1/TSGR1_87/Docs/R1-1612284.zip.

[199] Huawei, HiSilicon, "Document (3GPP TDoc R1-1611259): Design Aspects of Polar and LDPC Codes for NR," 3GPP, Tech. Rep., 2016. [Online]. Available: https://www.3gpp.org/ftp/tsg_ran/WG1_RL1/TSGR1_87/Docs/R1-1611259.zip.

[200] Samsung, "Document (3GPP TDoc R1-1613044): Performance of LDPC and Polar Codes over Fading Channels," 3GPP, Tech. Rep., 2016. [Online]. Available: https://www.3gpp.org/ftp/tsg_ran/WG1_RL1/TSGR1_87/Docs/R1-1613044.zip.

[201] Ericsson, "Document (3GPP TDoc R1-1611319): On Robustness of Polar Codes," 3GPP, Tech. Rep., 2016. [Online]. Available: https://www.3gpp.org/ftp/tsg_ran/WG1_RL1/TSGR1_87/Docs/R1-1611319.zip.

[202] V. Bioglio, C. Condo, and I. Land, "Design of Polar Codes in 5G New Radio," *IEEE Communications Surveys & Tutorials*, pp. 1–1, 2020.

[203] E. Arikan, "Channel Polarization: A Method for Constructing Capacity-Achieving Codes for Symmetric Binary-Input Memoryless Channels," *IEEE Transactions on Information Theory*, vol. 55, no. 7, pp. 3051–3073, 2009.

[204] R. G. Maunder, "White Paper: The 5G Channel Code Contenders," Accelercomm, Tech. Rep., 2016. [Online]. Available: https://eprints.soton.ac.uk/399915/.

[205] 3rd Generation Partnership Project, Technical Specification Group Radio Access Networks, "Document (3GPP TS 37.340 (V1.1.0.1)): Evolved Universal Terrestrial Radio Access (E-UTRA) and NR; Multi-Connectivity - Stage 2 (Release 15)," 3GPP, Tech. Rep., 2018. [Online]. Available: http://www.3gpp.org/ftp//Specs/archive/37_series/37.340/37340-f30.zip.

[206] D. Ohmann, A. Awada, I. Viering, M. Simsek, and G. P. Fettweis, "Achieving High Availability in Wireless Networks by Inter-Frequency Multi-Connectivity," *2016 IEEE International Conference on Communications (ICC)*, pp. 1–7, 2016.

[207] Huawei, Intel Corporation, and China Telecom, "Document (3GPP RP-171459): Signalling Reduction to Enable Light Connection for LTE," 3GPP, Tech. Rep., 2017. [Online]. Available: http://www.3gpp.org/ftp/TSG_RAN/TSG_RAN/TSGR_76/Docs/RP-171459.zip.

[208] CATT and CMCC, "Document (3GPP RP-172365): UL Data Compression in LTE," 3GPP, Tech. Rep., 2017. [Online]. Available: http://www.3gpp.org/ftp/TSG_RAN/TSG_RAN/TSGR_78/Docs/RP-172365.zip.

[209] Nokia and Alcatel-Lucent Shanghai Bell, "Document (3GPP RP-170805): WID on Enhancing CA Utilization," 3GPP, Tech. Rep., 2017. [Online]. Available: http://www.3gpp.org/ftp/TSG_RAN/TSG_RAN/TSGR_75/Docs/RP-170805.zip.

[210] Ericsson, "Document (3GPP RP-172826): Enhanced LTE Support for Aerial Vehicles," 3GPP, Tech. Rep., 2017. [Online]. Available: http://www.3gpp.org/ftp/TSG_RAN/TSG_RAN/TSGR_78/Docs/RP-172826.zip.

[211] I. D. Silva et al., "Tight Integration of New 5G Air Interface and LTE to Fulfill 5G Requirements," *2015 IEEE 81st Vehicular Technology Conference (VTC Spring)*, pp. 1–5, 2015.

[212] A. I. Abdulshakoor, M. M. Elmesalawy, N. A. Elmosilhy, and A. M. A El-Haleem, "An LTE-WiFi Spectrum Aggregation System for 5G Network: A Testbed," *2019 42nd International Conference on Telecommunications and Signal Processing (TSP)*, pp. 307–312, 2019.

[213] M. Shariat et al., "5G Radio Access above 6 GHz," *Transactions on Emerging Telecommunications Technologies*, vol. 27, no. 9, pp. 1160–1167, 2016.

[214] I.-P. Belikaidis et al., "Multi-RAT Dynamic Spectrum Access for 5G Heterogeneous Networks: The SPEED-5G Approach," *IEEE Wireless Communications*, vol. 24, no. 5, pp. 14–22, 2017.

[215] 5G-PPP Phase 1 Projects, SPEED-5G, *Speed 5G: Quality of Service Provision and Capacity Expansion through Extended-DSA for 5G*, 2014. [Online]. Available: https://speed-5g.eu/.

[216] V. W. S. Wong, R. Schober, D. W. K. Ng, and L. C. Wang, *Key Technologies for 5G Wireless Systems*. Cambridge University Press, 2017.

[217] S. Samarakoon, M. Bennis, W. Saad, and M. Latva-aho, "Dynamic Clustering and On/Off Strategies for Wireless Small Cell Networks," *IEEE Transactions on Wireless Communications*, vol. 15, no. 3, pp. 2164–2178, 2016.

[218] S. Bassoy, M. Jaber, M. A. Imran, and P. Xiao, "Load Aware Self-Organising User-Centric Dynamic CoMP Clustering for 5G Networks," *IEEE Access*, vol. 4, pp. 2895–2906, 2016.

[219] P. Luoto, M. Bennis, P. Pirinen, S. Samarakoon, K. Horneman, and M. Latva-Aho, "Vehicle Clustering for Improving Enhanced LTE-V2X Network Performance," *2017 European Conference on Networks and Communications (EuCNC)*, pp. 1–5, 2017.

[220] I. D. Silva et al., "Impact on Network Slicing on 5G Radio Access Networks," *2016 European Conference on Networks and Communications (EuCNC)*, pp. 1–5, 2016.

[221] P. Rost et al., "Network Slicing to Enable Scalability and Flexibility in 5G Mobile Networks," *IEEE Communications Magazine*, vol. 55, no. 5, pp. 72–79, 2017.

[222] R. H. Tehrani, S. Vahid, D. Triantafyllopoulou, H. Lee, and K. Moessner, "Licensed Spectrum Sharing Schemes for Mobile Operators: A Survey and Outlook," *IEEE Communications Surveys & Tutorials*, vol. 18, no. 4, pp. 2591–2623, 2016.

[223] K. Katsalis, N. Nikaein, E. Schiller, A. Ksentini, and T. Braun, "Network Slices toward 5G Communications: Slicing the LTE Network," *IEEE Communications Magazine*, vol. 55, no. 8, pp. 146–154, 2017.

[224] 3rd Generation Partnership Project, Technical Specification Group Services and System Aspects, "Document (3GPP TS 23.501 (V15.4.0)): System Architecture for the 5G System; Stage 2 (Release 15)," 3GPP, Tech. Rep., 2018. [Online]. Available: `http://www.3gpp.org/ftp//Specs/archive/23_series/23.501/23501-f40.zip`.

[225] X. Li et al., "Network Slicing for 5G: Challenges and Opportunities," *IEEE Internet Computing*, vol. 21, no. 5, pp. 20–27, 2017.

[226] 5G-PPP Phase 2 Projects, SLICENET, *SLICENET: End-to-End Cognitive Network Slicing and Slice Management Framework in Virtualised Multi-Domain, Multi-Tenant 5G Networks*, 2017. [Online]. Available: https://slicenet.eu/.

[227] ETSI, "Group Report (ETSI GR mWT 016 (V1.1.1)): Applications and Use Cases of Software Defined Networking (SDN) as Related to Microwave and Millimetre Wave Transmission," ETSI, Tech. Rep., 2017. [Online]. Available: https://www.etsi.org/deliver/etsi_gr/mWT/001_099/016/01.01.01_60/gr_mWT016v010101p.pdf.

[228] ——, "Group Specification (ETSI GS NFV-EVE 005 (V1.1.1)): Network Functions Virtualisation (NFV) Ecosystem: Report on SDN Usage in NFV Architectural Framework," ETSI, Tech. Rep., 2015. [Online]. Available: https://www.etsi.org/deliver/etsi_gs/NFV-EVE/001_099/005/01.01.01_60/gs_NFV-EVE005v010101p.pdf.

[229] ——, "Technical Specification (ETSI TS 128 628 (V14.0.0)): Universal Mobile Telecommunications System (UMTS); LTE; Telecommunication management; Self-Organizing Networks (SON) Policy Network Resource Model (NRM) Integration Reference Point (IRP); Information Service (IS) (3GPP TS 28.628 version 14.0.0 Release 14)," ETSI, Tech. Rep., 2017. [Online]. Available: https://www.etsi.org/deliver/etsi_ts/128600_128699/128628/14.00.00_60/ts_128628v140000p.pdf.

[230] ——, "Group Specification, (ETSI GS MEC (011 V1.1.1)): Mobile Edge Computing (MEC); Mobile Edge Platform Application Enablement," ETSI, Tech. Rep., 2017. [Online]. Available: https://www.etsi.org/deliver/etsi_gs/MEC/001_099/011/01.01.01_60/gs_MEC011v010101p.pdf.

[231] ——, "Group Specification, (ETSI GS NFV-IFA (011 V2.3.1)): Network Functions Virtualisation (NFV) Release 2; Management and Orchestration; VNF Packaging Specification," ETSI, Tech. Rep., 2017. [Online]. Available: https://www.etsi.org/deliver/etsi_gs/NFV-IFA/001_099/011/02.01.01_60/gs_NFV-IFA011v020101p.pdf.

[232] H. Abou-zeid, F. Pervez, A. Adinoui, M. Aljlayl, and H. Yanikomeroglu, "Cellular V2X Transmission for Connected and Autonomous Vehicles Standardization, Applications, and Enabling Technologies," *IEEE Consumer Electronics Magazine*, vol. 8, no. 6, pp. 91–98, 2019.

[233] 5G-PPP Phase 2 Projects, 5G ESSENCE, *5G ESSENCE: Embedded Network Services for 5G Experiences*, 2016. [Online]. Available: http://www.5g-essence-h2020.eu/.

[234] 5G-PPP Phase 1 Projects, SELFNET, *SELFNET: A Framework for Self-Organized Network Management in Virtualized and Software Defined Networks*, 2014. [Online]. Available: https://selfnet-5g.eu/.

[235] 5G-PPP Phase 1 Projects, CHARISMA, *CHARISMA: Converged Heterogeneous Advanced 5G Cloud-RAN Architecture for Intelligent and Secure Media Access*, 2014. [Online]. Available: http://www.charisma5g.eu/.

[236] 3rd Generation Partnership Project, Technical Specification Group Radio Access Network, "Document (3GPP TR 36.742 (V15.0.0)): Study on Self-Organizing Networks (SON) for enhanced Coordinated Multi-Point (eCoMP) (Release 15)," 3GPP, Tech. Rep., 2017. [Online]. Available: `http://www.3gpp.org/ftp//Specs/archive/36_series/36.742/36742-f00.zip`.

[237] M. Agiwal, A. Roy, and N. Saxena, "Next Generation 5G Wireless Networks: A Comprehensive Survey," *IEEE Communications Surveys & Tutorials*, vol. 18, no. 3, pp. 1617–1655, 2016.

[238] J. Moysen and L. Giupponi, "From 4G to 5G: Self-Organized Network Management Meets Machine Learning," *arXiv preprint arXiv:1707.09300*, pp. 1–25, 2017.

[239] K. Tsagkaris, A. Katidiotis, and P. Demestichas, "Neural Network-Based Learning Schemes for Cognitive Radio Systems," *Computer Communications*, vol. 31, no. 14, pp. 3394–3404, 2008.

[240] C. Jiang, H. Zhang, Y. Ren, Z. Han, K.-C. Chen, and L. Hanzo, "Machine Learning Paradigms for Next-Generation Wireless Networks," *IEEE Wireless Communications*, vol. 24, no. 2, pp. 98–105, 2017.

[241] ITU-T, *Group: Focus Group-Machine Learning 5G*, 2017. [Online]. Available: https://www.itu.int/en/ITU-T/focusgroups/ml5g/Pages/default.aspx.

[242] E. Bastug, M. Bennis, and M. Debbah, "Living on the Edge: The Role of Proactive Caching in 5G Wireless Networks," *IEEE Communications Magazine*, vol. 52, no. 8, pp. 82–89, 2014.

[243] F. B. Mismar and B. L. Evans, "Deep Reinforcement Learning for Improving Downlink mmWave Communication Performance," *IEEE Journal of Selected Topics in Signal Processing*, pp. 1–8, 2017.

[244] ——, "Partially Blind Handovers for mmWave New Radio Aided by Sub-6 GHz LTE Signaling," *IEEE International Conference on Communications Workshop on Evolutional Technologies & Ecosystems for 5G Phase II*, pp. 1–5, 2018.

[245] IEEE Standards Association, *802.11-2012-IEEE Standard for Information Technology–Telecommunications and Information Exchange Between Systems Local and Metropolitan Area Networks–Specific Requirements Part 11: Wireless LAN Medium Access Control (MAC) and Physical Layer (PHY) Specifications*, 2012.

[246] ——, *ISO/IEC/IEEE International Standard for Information Technology - Telecommunications and Information Exchange Between Systems - Local and Metropolitan Area Networks - Specific Requirements - Part 11: Wireless LAN Medium Access Control (MAC) and Physical Layer (PHY) Specifications Amendment 5: Television White Spaces (TVWS) Operation*, 2013.

[247] E. Perahia and R. Stacey, *Next Generation Wireless LANs: 802.11n and 802.11ac*. Cambridge University Press, 2015.

[248] E. Lopez-Aguilera, E. Garcia-Villegas, and J. Casademont, "Evaluation of IEEE 802.11 Coexistence in WLAN Deployments," *Wireless Networks*, pp. 1–18, 2017.

[249] IEEE Standards Association, *802.11e-2005 - IEEE Standard for Information Technology - Local and Metropolitan Area Networks - Specific Requirements - Part 11: Wireless LAN Medium Access Control (MAC) and Physical Layer (PHY) Specifications Amendment 8: Medium Access Control (MAC) Quality of Service Enhancements*, 2005.

[250] Y. Bejerano, H.-G. Choi, and S.-J. Han, "Fairness Analysis of Physical Layer Capture Effects in IEEE 802.11 Networks," *13th International Symposium on Modeling and Optimization in Mobile, Ad Hoc, and Wireless Networks (WiOpt)*, pp. 323–330, 2015.

[251] J. Lee et al., "An Experimental Study on the Capture Effect in 802.11a Networks," *Proceedings of the Second ACM International Workshop on Wireless Network Testbeds, Experimental Evaluation and Characterization - WinTECH 07*, pp. 19–26, 2007.

[252] O. Ekici and A. Yongacoglu, "IEEE 802.11a Throughput Performance with Hidden Nodes," *IEEE Communications Letters*, vol. 12, no. 6, pp. 465–467, 2008.

[253] D. Shukla, L. Chandran-Wadia, and S. Iyer, "Mitigating the Exposed Node Problem in IEEE 802.11 Ad Hoc Networks," *Proceedings of the 12th International Conference on Computer Communications and Networks (IEEE Cat. No.03EX712)*, pp. 157–162, 2003.

[254] J. Deng, B. Liang, and P. Varshney, "Tuning the Carrier Sensing Range of IEEE 802.11 MAC," *IEEE Global Telecommunications Conference, GLOBECOM 04*, vol. 5, pp. 2987–2991, 2004.

[255] G. Anastasi, E. Borgia, M. Conti, and E. Gregori, "Wi-Fi in Ad Hoc Mode: A Measurement Study," *Proceedings of the Second IEEE Annual Conference on Pervasive Computing and Communications*, pp. 145–154, 2004.

[256] P. C. Ng, S. C. Liew, K. C. Sha, and W. T. To, "Experimental Study of Hidden Node Problem in IEEE 802.11 Wireless Networks," *Sigcomm Poster*, 2005.

[257] Z. Zhong, P. Kulkarni, F. Cao, Z. Fan, and S. Armour, "Issues and Challenges in Dense Wifi Networks," *2015 International Wireless Communications and Mobile Computing Conference (IWCMC)*, pp. 947–951, 2015.

[258] Y. Xiao, "IEEE 802.11n: Enhancements for Higher Throughput in Wireless LANs," *IEEE Wireless Communications*, vol. 12, no. 6, pp. 82–91, 2005.

[259] B. Ginzburg and A. Kesselman, "Performance Analysis of A-MPDU and A-MSDU Aggregation in IEEE 802.11n," *2007 IEEE Sarnoff Symposium*, pp. 1–5, 2007.

[260] D. Skordoulis, Q. Ni, H.-H. Chen, A. P. Stephens, C. Liu, and A. Jamalipour, "IEEE 802.11n MAC Frame Aggregation Mechanisms for Next-Generation High-Throughput WLANs," *IEEE Wireless Communications*, vol. 15, no. 1, pp. 40–47, 2008.

[261] IEEE Standards Association, *802.11ac-2013 - IEEE Standard for Information Technology - Telecommunications and Information Exchange between Systems Local and Metropolitan Area Networks - Specific Requirements - Part 11: Wireless LAN Medium Access Control (MAC) and Physical Layer (PHY) Specifications Amendment 4: Enhancements for Very High Throughput for Operation in Bands below 6 GHz*, 2013.

[262] E. H. Ong, J. Kneckt, O. Alanen, Z. Chang, T. Huovinen, and T. Nihtila, "IEEE 802.11ac: Enhancements for Very High Throughput WLANs," *2011 IEEE 22nd International Symposium on Personal, Indoor and Mobile Radio Communications*, pp. 849–853, 2011.

[263] Aruba Networks, "White Paper: 802.11ac In-Depth," Aruba Networks, Tech. Rep., 2014. [Online]. Available: `https://www.arubanetworks.com/assets/wp/WP_80211acInDepth.pdf`.

[264] R. Liao, B. Bellalta, M. Oliver, and Z. Niu, "MU-MIMO MAC Protocols for Wireless Local Area Networks: A Survey," *IEEE Communications Surveys & Tutorials*, vol. 18, no. 1, pp. 162–183, 2016.

[265] M. S. Afaqui, E. Garcia-Villegas, and E. Lopez-Aguilera, "IEEE 802.11ax: Challenges and Requirements for Future High Efficiency WiFi," *IEEE Wireless Communications*, vol. 24, no. 3, pp. 130–137, 2017.

[266] B. Bellalta, "IEEE 802.11ax: High-Efficiency WLANs," *IEEE Wireless Communications*, vol. 23, no. 1, pp. 38–46, 2016.

[267] IEEE Standards Association, *IEEE P802.11ax/D2.0 Standard for Information Technology - Telecommunications and Information Exchange between Systems Local and Metropolitan Area Networks - Specific Requirements - Part 11: Wireless LAN Medium Access Control (MAC) and Physical Layer (PHY) Specifications Amendment 6: Enhancements for High Efficiency WLAN*, 2017.

[268] S. Vermani et al., "Document (IEEE 802.11-15/1309r1): Extended Range Support for 11ax," IEEE, Tech. Rep., 2015. [Online]. Available: https://mentor.ieee.org/802.11/dcn/15/11-15-1309-01-00ax-extended-range-support-for-11ax.pptx.

[269] L. Wihelmsson and M. Wang, "Document (IEEE 802.11-14/1452r0): Frequency Selective Scheduling in OFDMA," IEEE, Tech. Rep., 2014. [Online]. Available: https://mentor.ieee.org/802.11/dcn/14/11-14-1452-00-00ax-frequency-selective-scheduling-in-ofdma.pptx.

[270] K. Oteri, A. Sahin, F. Xi, H. Lou, R. Yang, "Document (IEEE 802.11-15/0568r2): Frequency Selective Scheduling (FSS) for TGax OFDMA," IEEE, Tech. Rep., 2015. [Online]. Available: https://mentor.ieee.org/802.11/dcn/15/11-15-0568-02-00ax-frequency-selective-scheduling-fss-for-tgax-ofdma.pptx.

[271] Ericsson, "Document (IEEE 802.11-15/0868r0): Impact of Frequency Selective Scheduling Feedback for OFDMA," IEEE, Tech. Rep., 2015. [Online]. Available: https://mentor.ieee.org/802.11/dcn/15/11-15-0868-00-00ax-impact-of-frequency-selective-scheduling-feedback-for-ofdma.pptx.

[272] Q. Li, P.-k. Huang, X. Chen, and Y. Zhu, "Aggregation of Multiuser Frames," U.S. Patent No. 20170149523, 2017.

[273] D. Lim, E. Park, W. Lee, J. Choi, J. Chun, and H. Cho, "Document (IEEE 802.11-14/0801r0): Envisioning 11ax PHY Structure - Part II," IEEE, Tech. Rep., 2014. [Online]. Available: https://mentor.ieee.org/802.11/dcn/14/11-14-0801-00-00ax-envisioning-11ax-phy-structure-part-ii.pptx.

[274] Y. Fang, K. Lv, and B. Sun, "Document (IEEE 802.11-17/0340r6): Comment Resolution for CIDs on Dual Beacon Operation," IEEE, Tech. Rep., 2017. [Online]. Available: https://mentor.ieee.org/802.11/dcn/17/11-17-0340-06-00ax-cr-for-11-1-3-10.docx.

[275] IEEE Standards Association, *IEEE 802.11ah-2016 Standard for Information Technology -Telecommunications and Information Exchange between Systems Local and Metropolitan Area Networks - Specific Requirements - Part 11: Wireless LAN Medium Access Control (MAC) and Physical Layer (PHY) Specifications Amendment 2: Sub 1 GHz License Exempt Operation*, 2016.

[276] G. Smith, "Document (IEEE 802.11-13/1012r4): Dynamic Sensitivity Control V2," IEEE, Tech. Rep., 2013. [Online]. Available: `https://mentor.ieee.org/802.11/dcn/13/11-13-1012-04-0wng-dynamic-sensitivity-control.pptx`.

[277] M. S. Afaqui, E. Garcia-Villegas, E. Lopez-Aguilera, G. Smith, and D. Camps, "Evaluation of Dynamic Sensitivity Control Algorithm for IEEE 802.11ax," *2015 IEEE Wireless Communications and Networking Conference (WCNC)*, pp. 1060–1065, 2015.

[278] Z. Zhong, F. Cao, P. Kulkarni, and Z. Fan, "Promise and perils of Dynamic Sensitivity control in IEEE 802.11ax WLANs," *2016 International Symposium on Wireless Communication Systems (ISWCS)*, pp. 439–444, 2016.

[279] M. S. Afaqui, E. Garcia-Villegas, E. Lopez-Aguilera, and D. Camps-Mur, "Dynamic Sensitivity Control of Access Points for IEEE 802.11ax," *2016 IEEE International Conference on Communications (ICC)*, pp. 1–7, 2016.

[280] M. Fischer et al., "Document (IEEE 802.11-13/1207r1): CID 205 BSSID Color Bits," IEEE, Tech. Rep., 2013. [Online]. Available: `https://mentor.ieee.org/802.11/dcn/13/11-13-1207-01-00ah-partial-aid-color-bits.pptx`.

[281] M. Fischer, J. Wang, Y. Seok, and R. Porat, "Document (IEEE 802.11-17/0075r8): SRP-Based Operation," IEEE, Tech. Rep., 2017. [Online]. Available: `https://mentor.ieee.org/802.11/dcn/17/11-17-0075-08-00ax-srp-based-sr-summary-and-update.pptx`.

[282] P.-K. Huang, "Document (IEEE 802.11-16/1173r2): Comment Resolution on Two NAVs - Part II," IEEE, Tech. Rep., 2016. [Online]. Available: `https://mentor.ieee.org/802.11/dcn/16/11-16-1173-02-00ax-comment-resolution-on-two-navs-part-ii.docx`.

[283] G. Smith and L. Cariou, "Document (IEEE 802.11-18/0617r4): Dynamic OBSS_PD level," IEEE, Tech. Rep., 2018. [Online]. Available: `https://mentor.ieee.org/802.11/dcn/18/11-18-0617-02-00ax-dynamic-obss-pd-level.docx`.

[284] T. Ropitault, "Document (IEEE 802.11-16/1161r1): Simulation-based Evaluation of OBSS_PD-based SR Default Parameters," IEEE, Tech. Rep., 2016. [Online]. Available: https://mentor.ieee.org/802.11/dcn/16/11-16-1161-01-00ax-simulation-based-evaluation-of-obss-pd-based-sr-default-parameters.pptx.

[285] B. Yin, K. Yamamoto, T. Nishio, M. Morikura, and H. Abeysekera, "Learning-Based Spatial Reuse for WLANs With Early Identification of Interfering Transmitters," *IEEE Transactions on Cognitive Communications and Networking*, vol. 6, no. 1, pp. 151–164, 2020.

[286] B. Wilhemi, et al., "A Flexible Machine-Learning-Aware Architecture for Future WLANs," *IEEE Communications Magazine*, vol. 58, no. 3, pp. 25–31, 2020.

[287] A. B. Flores, R. E. Guerra, E. W. Knightly, P. Ecclesine, and S. Pandey, "IEEE 802.11af: A Standard for TV White Spectrum Sharing," *IEEE Communications Magazine*, vol. 51, no. 10, pp. 92–100, 2013.

[288] D. Lekomtcev and R. Maršálek, "Comparison of 802.11af and 802.22 Standards-Physical Layer and Cognitive Functionality," *Elektro Revue*, vol. 3, no. 2, pp. 12–18, 2012.

[289] H.-S. Chen and W. Gao, "Document (IEEE 802.11-10/0258r0): MAC and PHY Proposal for 802.11af," IEEE, Tech. Rep., 2010. [Online]. Available: https://mentor.ieee.org/802.11/dcn/10/11-10-0258-00-00af-mac-and-phy-proposal-for-802-11af.pdf.

[290] SigFox. (2018). The Global Communications Service Provider for the Internet of Things (IoT), [Online]. Available: https://www.sigfox.com/en (visited on 2018).

[291] LoRa Alliance. (2018). Wide Area Networks for IoT, [Online]. Available: https://www.lora-alliance.org/ (visited on 2018).

[292] M. Centenaro, L. Vangelista, A. Zanella, and M. Zorzi, "Long-Range Communications in Unlicensed Bands: The Rising Stars in the IoT and Smart Grid City Scenarios," *IEEE Wireless Communications*, vol. 23, no. 5, pp. 60–67, 2016.

[293] LoRa Alliance - Wide Area Networks for IoT, "White Paper: Streetlight Control Solution Successfully Passes Field Trials in Szada, Hungary," LoRa Alliance, Tech. Rep., 2016. [Online]. Available: https://intelilight.eu/intelilight-lora-streetlight-control-solution-successfully-passes-field-trials-szada-hungary/.

[294] K. Shah et al., "White Paper: Smart Grid Task Group - Sub 1 GHz," IEEE 802.24 Vertical Applications Technical Advisory Group, Tech. Rep., 2016. [Online]. Available: http://www.ieee802.org/24/Smart%20Grid%20Standards%20for%20Operation%20in%20Sub-1%20GHz%20Bands_white%20paper.pdf.

[295] C.-S. Sum, H. Harada, F. Kojima, Z. Lan, and R. Funada, "Smart Utility Networks for TV White Space Spectrum Sharing," *IEEE Communications Magazine*, vol. 49, no. 7, pp. 132–139, 2011.

[296] A. Ali, W. Hamouda, and M. Uysal, "Next Generation M2M Cellular Networks: Challenges and Practical Considerations," *IEEE Communications Magazine*, vol. 53, no. 9, pp. 18–24, 2015.

[297] F. Ghavimi and H.-H. Chen, "M2M Communications in 3GPP LTE/LTE-A Networks: Architectures, Service Requirements, Challenges, and Applications," *IEEE Communications Surveys & Tutorials*, vol. 17, no. 2, pp. 525–549, 2015.

[298] 3rd Generation Partnership Project, Technical Specification Group Services and System Aspects, "Document (3GPP TR 22.868 (V8.0.0)): Study on Facilitating Machine to Machine Communication in 3GPP Systems (Release 8)," 3GPP, Tech. Rep., 2007. [Online]. Available: `http://www.3gpp.org/ftp/Specs/archive/22_series/22.868/22868-800.zip`.

[299] T. Taleb and A. Kunz, "Machine Type Communications in 3GPP Networks: Potential, Challenges, and Solutionss," *IEEE Communications Magazine*, vol. 50, no. 3, pp. 178–184, 2012.

[300] A. G. Gotsis, A. S. Lioumpas, and A. Alexiou, "M2M Scheduling over LTE: Challenges and New Perspectives," *IEEE Vehicular Technology Magazine*, vol. 7, no. 3, pp. 34–39, 2012.

[301] A. Ijaz et al., "Enabling Massive IoT in 5G and Beyond Systems: PHY Radio Frame Design Considerations," *IEEE Access*, vol. 4, pp. 3322–3339, 2016.

[302] S.-Y. Lien, K.-C. Chen, and Y. Lin, "Toward Ubiquitous Massive Accesses in 3GPP Machine-to-Machine Communications," *IEEE Communications Magazine*, vol. 49, no. 4, pp. 66–74, 2011.

[303] M. Hasan, E. Hossain, and D. Niyato, "Random Access for Machine-to-Machine Communication in LTE-Advanced Networks: Issues and Approaches," *IEEE Communications Magazine*, vol. 51, no. 6, pp. 86–93, 2013.

[304] K. Zheng, S. Ou, J. Alonso-Zarate, M. Dohler, F. Liu, and H. Zhu, "Challenges of Massive Access in Highly Dense LTE-Advanced Networks with Machine-to-Machine Communications," *IEEE Wireless Communications*, vol. 21, no. 3, pp. 12–18, 2014.

[305] H. Shariatmadari et al., "Machine-Type Communications: Current Status and Future Perspectives toward 5G Systems," *IEEE Communications Magazine*, vol. 53, no. 9, pp. 10–17, 2015.

[306] A. Rico-Alvarino et al., "An Overview of 3GPP Enhancements on Machine to Machine Communications," *IEEE Communications Magazine*, vol. 54, no. 6, pp. 14–21, 2016.

[307] Ericsson, "Document (3GPP RP-141865): Further LTE Physical Layer Enhancements for MTC," 3GPP, Tech. Rep., 2014. [Online]. Available: `https://www.3gpp.org/DynaReport/TDocExMtg--RP-66--30567.htm`.

[308] R. Ratasuk, N. Mangalvedhe, Y. Zhang, M. Robert, and J.-P. Koskinen, "Overview of Narrowband IoT in LTE Rel-13," *2016 IEEE Conference on Standards for Communications and Networking (CSCN)*, pp. 1–7, 2016.

[309] R. Ratasuk, B. Vejlgaard, N. Mangalvedhe, and A. Ghosh, "NB-IoT System for M2M Communication," *2016 IEEE Wireless Communications and Networking Conference*, pp. 1–5, 2016.

[310] S. Hu, A. Berg, X. Li, and F. Rusek, "Improving the Performance of OTDOA Based Positioning in NB-IoT Systems," *GLOBECOM 2017 - 2017 IEEE Global Communications Conference*, pp. 1–7, 2017.

[311] J. A. D. Peral-Rosado, J. A. Lopez-Salcedo, and G. Seco-Granados, "Impact of Frequency-Hopping NB-IoT Positioning in 4G and Future 5G Networks," *2017 IEEE International Conference on Communications Workshops (ICC Workshops)*, pp. 1–6, 2017.

[312] Huawei and HiSilicon, "Document (3GPP RP-171428): Revised WID on Further NB-IoT Enhancements," 3GPP, Tech. Rep., 2017. [Online]. Available: `http://www.3gpp.org/ftp/TSG_RAN/TSG_RAN/TSGR_76/Docs/RP-171428.zip`.

[313] Ericsson, "Document (3GPP R1-1703865): on 5G mMTC Requirement Fulfilment, NB-IoT and eMTC Connection Density," 3GPP, Tech. Rep., 2017. [Online]. Available: `https://www.3gpp.org/ftp/tsg_ran/WG1_RL1/TSGR1_88/Docs/R1-1703865.zip`.

[314] ATT and T-Mobile USA, "Document (3GPP RP-172078): New WID on Additional LTE Bands for UE Category M2 and/or NB2 in Rel-15," 3GPP, Tech. Rep., 2017. [Online]. Available: `http://www.3gpp.org/ftp/TSG_RAN/TSG_RAN/TSGR_77/Docs/RP-172078.zip`.

[315] Motorola Solutions, Home Office, BT, and Telstra, "Document (3GPP RP-161871): New Work Item Proposal: Add Power Class 1 UE to B3/B20/B28 for LTE," 3GPP, Tech. Rep., 2016. [Online]. Available: https://www.3gpp.org/ftp/tsg_ran/TSG_RAN/TSGR_73/Docs/RP-161871.zip.

[316] LG Electronics Inc., "Document (3GPP R2-1709457): Early Data Transmission Failure Handling in NB-IoT," 3GPP, Tech. Rep., 2017. [Online]. Available: https://www.3gpp.org/ftp/TSG_RAN/WG2_RL2/TSGR2_99/Docs/R2-1709457.zip.

[317] 5G-PPP Phase 1 Projects, FANTASTIC-5G. (2017). FANTASTIC-5G–Flexible Air iNTerfAce for Scalable service delivery wiThin wIreless Communication networks of the 5th Generation, [Online]. Available: https://5g-ppp.eu/fantastic-5g/ (visited on 2017).

[318] S. Aust, R. V. Prasad, and I. G. M. M. Niemegeers, "IEEE 802.11ah: Advantages in Standards and Further Challenges for Sub 1 GHz Wi-Fi," *2012 IEEE International Conference on Communications (ICC)*, pp. 6885–6889, 2012.

[319] W. Sun, M. Choi, and S. Choi, "IEEE 802.11ah: A Long Range 802.11 WLAN at Sub 1 GHz," *Journal of ICT Standardization*, vol. 1, no. 1, pp. 83–108, 2013.

[320] E. Khorov, A. Lyakhov, A. Krotov, and A. Guschin, "A Survey on IEEE 802.11ah: An Enabling Networking Technology," *Computer Communications*, vol. 58, pp. 53–69, 2015.

[321] L. Tian, S. Deronne, S. Latré, and J. Famaey, "Implementation and Validation of an IEEE 802.11ah Module for ns-3," *Proceedings of the Workshop on ns-3 - WNS3 16*, pp. 49–56, 2016.

[322] L. Tian, J. Famaey, and S. Latre, "Evaluation of the IEEE 802.11ah Restricted Access Window Mechanism for Dense IoT Networks," *2016 IEEE 17th International Symposium on A World of Wireless, Mobile and Multimedia Networks (WoWMoM)*, pp. 1–9, 2016.

[323] N. Nawaz, M. Hafeez, S. Zaidi, D. Mclernon, and M. Ghogho, "Throughput Enhancement of Restricted Access Window for Uniform Grouping Scheme in IEEE 802.11ah," *2017 IEEE International Conference on Communications (ICC)*, pp. 1–7, 2017.

[324] T. Adame, A. Bel, B. Bellalta, J. Barcelo, and M. Oliver, "IEEE 802.11ah: The WiFi Approach for M2M Communications," *IEEE Wireless Communications*, vol. 21, no. 6, pp. 144–152, 2014.

Chapter 3

On the Performance of the IEEE 802.11ax Spatial Reuse Features

This chapter presents a performance assessment of the IEEE 802.11ax SR technique (i.e. BSS Color) in dense deployments. It also shows the design and development of the SR feature as the IEEE 802.11ax amendment evolves. An insight into the BSS Color operation and its potential to enhance network performance is given and simulations are carried to assess its performance under various dense deployments. The evaluation of the BSS Color and the advancements introduced in the simulation tool aim to identify the drawbacks of the SR feature and give an introduction into the novel SR algorithms for the BSS Color that are presented in later chapters.

3.1 Introduction

The interference levels in dense WLAN deployments are expected to increase, thus severely affecting the network performance. The authors in [257] study and present an interference analysis in dense networks. They argue that due to densification, the number of packet collisions, interference from neighbouring Basic Service Sets (BSSs), and the hidden/exposed node problem significantly degrade the network performance.

There are several approaches that have been proposed in the literature in order to

enhance the network throughput by improving the spatial reuse. The main two techniques proposed are the TPC and tuning the Physical Carrier Sensing (PCS) threshold. TPC is essential for decreasing the energy consumption in a station and reducing the interference level to the neighbouring nodes. However, it requires a sufficient number of power transmit levels [325], and coordination among the users, otherwise the SINR at the receiver could be extremely low, leading to outage. Furthermore, the maximum transmit power is constrained by the regulatory bodies e.g. Federal Communications Commission (FCC). A PCS scheme could also be an effective way to enhance the spatial reuse in a network, whilst it does not require any modifications to the hardware or the IEEE 802.11 standard.

Even though there is a considerable amount of work in the literature (e.g. [326], [327]), performance of PCS in dense networks, has not been adequately evaluated, in the past. The DSC and the BSS Color scheme are the two main schemes under consideration by the IEEE 802.11ax working group, for improving spectral reuse, due to the potential gains they can provide. To the best of our knowledge, the performance of these schemes in such dense deployments along with the PAID [261], feature of IEEE 802.11ac, have not been yet fully evaluated in the literature.

This chapter presents an evaluation of the aforementioned schemes in a high density wireless network, using ns-3 simulation tool [328] assuming multi-cell deployment scenarios, identified in the IEEE 802.11ax standard [329]. Furthermore, a design where the aforementioned schemes are enabled together is also proposed and presented here.

The rest of the chapter is organized as follows. Section 3.2, overviews the spatial reuse approaches that have been proposed in the literature. Section 3.3, describes the DSC algorithm, the PAID feature, and the BSS Color scheme as were initially proposed and developed, while Section 3.4 presents the simulation scenario and Section 3.5 analyses the simulation results. Finally, Section 3.6 concludes this chapter where the need for further developing and advancing the ns-3 tool as the IEEE 802.11ax amendment continues to evolves is also identified.

3.2 Background

This section discusses about the related works for the SR presented in the TGax. It initially presents the IEEE 802.11 carrier sensing mechanisms and the equations describe them. Then it overviews the related works that have been proposed in the literature and DSC is based on. Finally, the SR features that were designed and developed following the TGax guidelines, while in their initial stage, conclude this section.

The carrier sensing mechanism in IEEE 802.11, supports two schemes; the mandatory PCS and the optional Virtual Carrier Sensing (VCS), which sets the NAV on the MAC layer, based on the RTS/CTS frames. The former scheme, which is also known as CCA, determines whether the medium is IDLE or BUSY. CCA monitors the channel for preambles and returns BUSY when the received energy from the concurrent transmissions is above a certain threshold (CCA/ED_{th}), and can be expressed as:

$$\sum_{n=1}^{k} TxPwr_r^{n,i} \geq CCA/ED \tag{3.1}$$

where k is the number of the total interferers to the node i and $Pr^{n,i}$ is the received power from the transmitter n to the node i. The received power at a distance d, assuming that the ratio of the antenna gain to the antenna loss is equal to 1, in both the transmitter and receiver, and only the signal attenuation due to path loss is considered, then the received power is:

$$TxPwr_r = \frac{TxPwr}{d^{\alpha}} \tag{3.2}$$

where α is the path loss exponent (typical values 2-4) and $TxPwr$ the transmit power of the transmitter. It is assumed that the transmission power is the same for all nodes. The carrier sensing range is the minimum distance that allows two concurrent transmissions and occurs when $Pr = CCA/ED$. Specifically, from Equation 3.2, the energy sensing range can be expressed as:

$$CCA/ED_{range} = \Big(\frac{TxPwr}{CCA/ED}\Big)^{\frac{1}{\alpha}} \tag{3.3}$$

However, in a dense network due to the accumulative interference, the CCA/ED_{range} must be equal to the distance between the intended transmitter (i) and its furthest interferer node (ri), in order for the node i to initiate a transmission and not cause any interference to the ongoing transmissions. Let $A = (TxPwr_r^{n,i})_{n=1}^{k}$ be the set of the received powers from the interferers of the node i. Assuming that α is the same for all nodes and each of them experiences the same channel conditions, the minimum received power corresponds to the furthest interferer node. If Equation 3.1 holds, then:

$$CCA/ED_{range}^{i} = \Big(\frac{TxPwr}{\min A}\Big)^{\frac{1}{\alpha}} \tag{3.4}$$

A node can detect and decode (with high probability based on the MCS) a signal, if the RSSI is above a threshold named receiver sensitivity (or Signal Detection or Carrier Sensing). The maximum transmission range where a Wi-Fi signal can be detected, can be derived from Equation 3.3:

$$CCA/CS_{range} = \Big(\frac{Pt}{CCA/CS}\Big)^{\frac{1}{\alpha}} \tag{3.5}$$

As mentioned in Section 2.3.2.1 $CCA/ED > CCA/CS$ with the values of -62 and -82 dBm defined in the standard. If $RSSI \geq CCA/CS$ it does not mean that the channel will set as BUSY, unless the duration field is successfully decoded or $RSSI \geq CCA/ED$.

That is, the higher the CCA/ED is, the smaller the CCA/ED_{range} is, and the nodes are more aggressive in accessing the medium. An extremely low CCA/ED increases the number of exposed nodes in a network. On the other hand, a very high threshold increases the number of hidden nodes. It has been shown that these nodes severely affect the spatial reuse [330], reducing the network capacity. The authors in [254], [331] show that the optimal CCA/ED, which maximizes the network throughput allows a certain number of hidden end exposed nodes to exist. Furthermore, they argue that there is a balance between these nodes and the capacity which can be achieved by tuning the CCA thresholds.

The authors in [332] introduce the K-APCS algorithm that incorporates the IEEE 802.11k radio resource management to obtain the metrics needed to tune the CCA

threshold. The CDPCS algorithm presented in [333], adjusts CCA based on the area that a particular node is. It requires the use of the RTS/CTS frames to define the area. Both algorithms, however, introduce overheads in order to tune CCA.

The authors in [334], propose a decentralized approach for setting CCA, based on the beacon's RSSI, similar to the DSC scheme. However, DSC differs from the algorithm in [334], as it uses a moving average to compute the threshold, and it also decrements it after X consecutive missed beacons. The authors in [277] evaluate the DSC scheme in a multi-floor residential building, considering only uplink transmissions, and tuning only the CCA/CS.

The authors in [335] study the performance of the DSC and the BSS Color scheme for uplink transmissions. The same authors in [336] evaluate the performance of the BSS Color scheme if a 2nd threshold is used when color mismatched occurs. In both cases, DSC outperforms over the BSS Color technique, however they argue that the throughput gain increases when these two techniques are combined. However, they consider a 19-cell deployment with spatial reuse factor 3 in their simulations. They do not consider the wrap-around scheme, which can potentially lead in overestimating the network performance. On the contrary, this chapter evaluates both schemes in a high density deployment with spatial reuse factor 1 (with wrap-around) for both uplink and downlink transmissions. Furthermore, the joint tuning of the CCA/CS and the CCA/ED and also its combination with the BSS Color scheme.

3.3 Description of the schemes

This section provides an overview of the DSC algorithm, the PAID feature, and the BSS Color scheme as was initially conceived. The DSC algorithm, tunes the carrier sensing range and the transmission range in every STA, locally. In particular, it does not require any information from the neighbouring STAs, thus it does not introduce any overhead. The main idea derives from the fact that stations at the edge of a cell should use lower CCA than those placed close to their associated AP. This is because the cell-edge nodes should increase their sensing range to eliminate the hidden nodes, increasing the probability of correct transmissions. On the other hand, STAs placed

close to an AP have higher probability of a successful transmission due to their short distance to the AP. The DSC algorithm sets an *UpperLimit* that corresponds to the maximum CCA that a node can have, to prevent the stations placed close to an AP to gain access more often than the others. It also sets a decrement value by which the threshold decreases, after X consecutive missed beacons. DSC records the beacons' RSSI and calculates the thresholds using a moving average over the last x RSSI recorded values, according to $CCA = \overline{RSSI} - Margin$. The value of the *Margin* must be carefully selected. In particular, an extremely small value could increase the number of disassociations (high CCA/CS) or the number of collisions (high CCA/ED). On the other hand, an extremely big value could degrade the network performance due to the increased number of exposed nodes (or failure transmissions, as a STA might lock onto frames from neighbouring BSSs).

PAID is a power-saving feature, built on AID of the IEEE 802.11n. Contrary to the AID feature, PAID value is not unique for every STA and is carried in the PLCP header. In that way, a STA quickly identifies and drops large frames not intended for it. This allows a STA to reduce its power consumption by switching to sleep or doze mode for the duration of the transmission. Although the initial intention of PAID was to reduce the power consumption, the most important benefit is that the likelihood of an erroneous reception following a successful preamble reception reduces. In particular, a node uses the EIFS to initiate a transmission following an erroneous reception, instead of DIFS, where $EIFS = DIFS + SIFS + ACKTxTime_{LowestMandRate}$. For a transmission from a STA to an AP, the PAID is the last 9 bits of the BSSID, while for the reverse link, PAID combines the AID and the BSSID.

Due to ambiguity issues (a STA might decode a frame destined to an AP), the authors in [280] proposed the BSS Color, as an extension of the PAID feature. According to the BSS Color technique every PLCP header, carries the color id and the uplink id. The former id, is used only in a downlink transmission to assist a station in identifying the BSS from which a frame was sent. The uplink id (*Uplink Indication*) identifies the type of link. Specifically, a value of 1 corresponds to an uplink transmission, while 0 to a downlink transmission. Moreover, the color id values range from 0 to 7, identifying groups of (at most) 8 BSSs and is given to a STA, during the association stage. The

Table 3.1: Simulation parameters

Parameter	Value
Scenario / Channel	Outdoor (SR1) / TGax channel model ([337])
Number of APs / STAs	127 / 1431
Number of Rings	6 (Wrap-Around [338])
STA density	770 STAs per km^2
Shadowing	Disabled
Inter AP distance	130 m
Mobility	Disabled
AP / STA Tx Power	20 / 15 dBm
AP / STA antenna gain	0 / -2 dBi
Number of antennas (AP, STA)	1 (SISO)
Noise figure	7 dB
PHY rate	Minstrel [339] (IEEE 802.11g)
Traffic	UDP, Full buffer
RTS/CTS	Disabled
Max number of retransmissions	10
Packet	1464 bytes
Beacon Interval	102.4 ms
CCA/CS, CCA/ED	-82 dBm, -62 dBm

procedure that an AP has to follow to select the color id is not specified in [275], leaving the developers to make this decision.

3.4 Simulation Setup

The outdoor dense scenario (Scenario 4), specified in IEEE 802.11 TGax [329] is considered. Furthermore, a large enough simulation time and number of runs were conducted, in order to get more accurate results. The aforementioned schemes are evaluated under full buffer conditions in both directions; using only Uplink or only Downlink traffic. All STAs share the same MAC and PHY characteristics, apart from the DSC and BSS Color schemes, which are enabled only for the IEEE 802.11ax nodes. It is assumed that the additional color or PAID info are carried in the PLCP header without increasing their transmission time and are used in all unicast frames (including ACKs). Moreover, there is no *BSS Color Collision*, and the OBSS/PD threshold is equal to -82 dBm. Furthermore, a STA is disassociated from its AP when the packet delivery ratio is more than 99% (referred as disassociation mechanism). The MAC and PHY parameters are listed in Table 3.1. The reader can refer to Appendix D for more information about

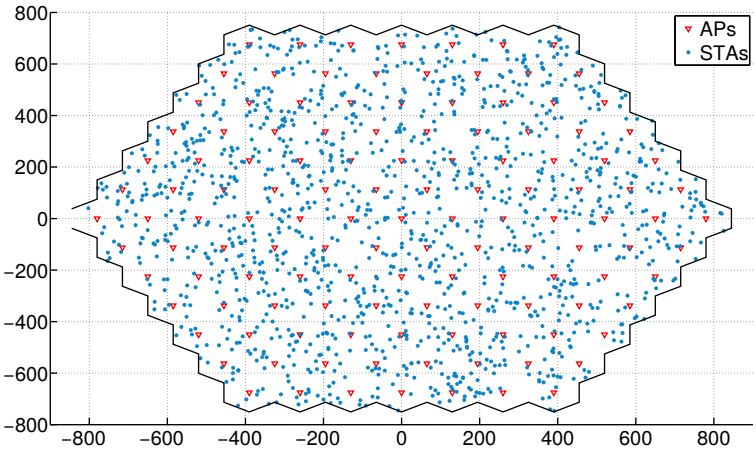

Figure 3.1: Simulated scenario where the axes units are in meters (approximately 1.85 km^2).

ns-3 and the Wi-Fi module used in this work.

Moreover, a wrap-around technique [340] is applied, so that BSSs located at the outer rings experience a similar interference as those at the inner rings. The original hexagonal network is extended to a cluster of 6 virtual copies of the original layout. These virtual copies are placed around the original network. In that way, a small fraction of a larger deployment can be studied instead of the entire large network. If wrap-around is not used, then the performance only of the simulated layout and not the entire network can be assessed. The optimal number of rings required (for the simulation scenarios considered), is determined according to [338]. It is also assumed that all nodes establish the Block Ack Agreement instantly and disassociation do not occur (*Missed Beacons* is set to infinite). Figure 3.1 illustrates a layout of the simulation scenario.

3.5 Simulation results

This section presents the performance of a) the DSC algorithm, b) the BSS Color scheme with and without the PAID feature in order to study the impact of EIFS in terms of throughput, and c) a combination of the aforementioned techniques normalised per km^2.

3.5.1 DSC performance

First, the DSC algorithm for different settings is evaluated, in a specific scenario where all STAs are assumed to be IEEE 802.11ax (SR is enabled), to reveal the values that utilize the network throughput. The values used for the DSC are: $UpperLimit$ $(-35, -40, -45)$ in dBms, $Margin(5, 10, 15, 20, 25)$ in dB, and $Decrement(1, 3, 5)$ in dB. The DSC is evaluated in the DL and the UL case, while only the CCA/CS and the CCA/ED is tuned at a time. In particular, in the DL case, the CCA/CS has greater impact than the CCA/ED on the performance, as the STAs do not contend for channel access and thus, are not required to sense the channel. In UL case, as most of the transmitted frames are on the uplink direction, the STAs sense the channel before initiating a transmission. That is, in that scenario, the CCA/ED severely affects the performance.

Figure 3.2a illustrates DSC's throughput against various settings. Only the results for different $Margin$ values are presented, as the throughput does not vary significantly for different values of the *UpperLimit* or the *Decrement*. The highest throughput in DL and UL scenarios, is achieved for different values of *Margin*; 5 in downlink 5, while 25 in uplink. The closer the CCA/CS value is to the RSSI from the associated AP, the higher the probability a STA may drop any received frame originated by a neighbouring AP. That is, the probability of a successful transmission from the associated AP increases. On the contrary, larger values of *Margin* for the CCA/ED, lead to larger carrier sensing ranges, decreasing the number of hidden nodes. However, this might come at the cost of decreasing fairness among the users due to the lower CCA/ED.

Figure 3.2b depicts the impact of the $Margin$ value on overheads. Note that *"Other"* represents the transmitted probes, association requests/responses and the retransmitted data, normalised over the total transmitted traffic. Overheads decrease with the decrease (increase) of the $Margin$ value for the CCA/CS (CCA/ED) in the downlink (uplink). However, even a very high *Margin* value (e.g. 25) is not sufficient enough to compensate for the large number of frame retransmissions in the UL case (approx. 70% of the total transmitted traffic is due to retransmissions).

To measure the system fairness for each setting, in terms of transmitted traffic (UL case) and throughput (DL case), the Jain's Fairness Index (JFI) [341], is applied where

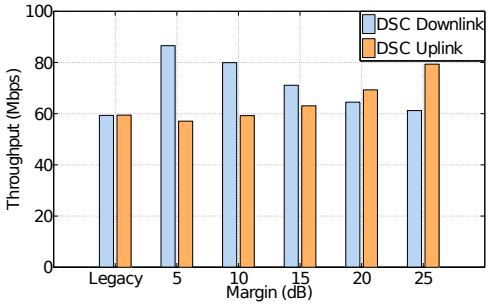

(a) Throughput.

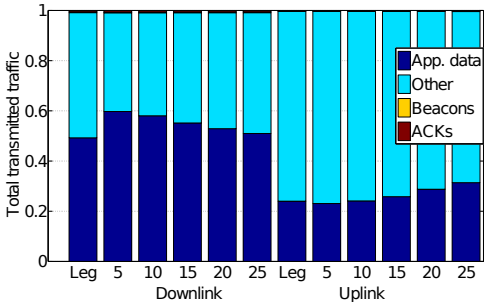

(b) Impact of DSC on overheads (normalised).

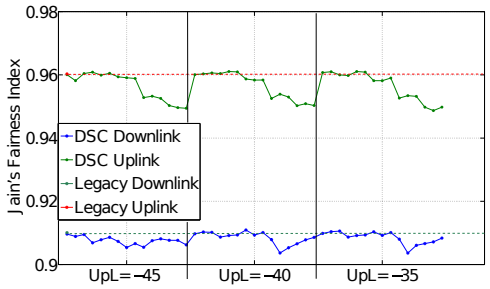

(c) Fairness Index.

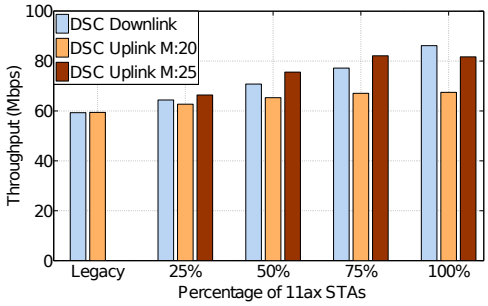

(d) Throughput with Leg. STAs.

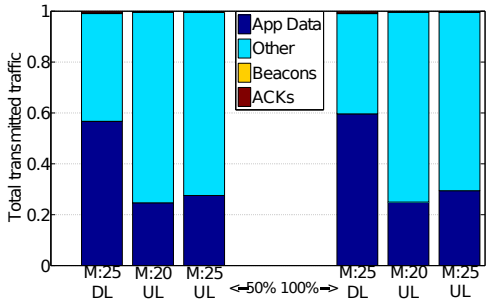

(e) Impact of Leg. STAs on overheads (normalised).

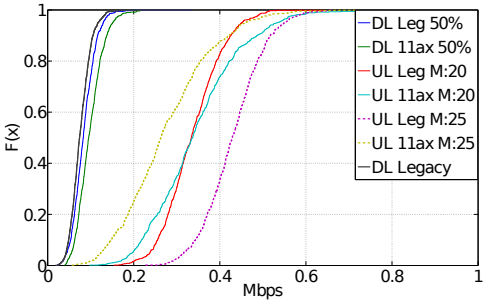

(f) Ecdf (averaged) for Rx and Tx traffic (50%11ax).

Figure 3.2: DSC metrics for various *Margin* values.

it ranges from 0 to 1, with its maximum value being when all users receive the same allocation. Figure 3.2c depicts the results for the JFI. The red asterisk stands for the Legacy mode in uplink, while the green for the different settings of DSC. The light blue and the dark blue stand for the legacy and DSC mode, respectively, in downlink. Note that first the *Decrement* value is gradually increased, then the *Margin* and lastly the *UpperLimit*. For example, the first leftmost DSC asterisk corresponds to *DSC(-45,5,1)*

while the last rightmost to *DSC(-35,25,5)*, where *DSC(UpperLimit,Margin,Decrement)*. An important outcome is that for small $Margin$ values, the JFI is close to the legacy's one, while for large values, the *UpperLimit* and *RSSI Decrement* parameters affect the fairness index. A low value of the CCA/CS or CCA/ED leads the cell-edge users to lock onto frames originated by neighbouring APs or defer their transmissions more frequently than the others nodes. As a result, fairness issues emerge between the cell-edge users and those located close to their associated AP.

An evaluation of DSC in the presence of legacy STAs, when DSC jointly tunes the CCA/CS and CCA/ED, is presented in Figure 3.2d. In particular, a value of $Margin = 5$ is applied for the CCA/CS, while 20 and 25 for the CCA/ED. It can be observed that as the number of the IEEE 802.11ax nodes increases, the network throughput increases too. The CCA/ED values for the IEEE 802.11ax nodes range from -60 (or -65 when $Margin = 25$) to -82 dBm, reducing the number of hidden nodes (better channel quality). By comparing the 75% to 100% cases in uplink, it can be seen that high $Margin$ values favour the legacy nodes, as the throughput slightly drops. The throughput gain for $Margin = 25$ compared to the case when $Margin = 20$ is due to the reduced number of overhead, as it is depicted in Figure 3.2e.

Even though, the throughput gain increases for $Margin = 25$, it comes at the cost of decreased fairness (in terms of transmitted bits) in uplink, compared to $Margin = 20$, Figure 3.2f. In downlink, DSC improves the legacy performance as well, due to the higher Packet Delivery Ratio (PDR). The results only for the 50% case (50% of the STAs are legacy) are presented in Figure 3.2f.

After closely analysing the DSC performance in both DL and UL transmissions, it is recommended different *Margin* values for the CCA/CS and the CCA/ED. In particular, it is recommended values of 5 and 25 (or 20 for preserving fairness) as the values for tuning the aforementioned thresholds, $UpperLimit = -40$, and $Decrement = 5$ show high throughput gain and may preserve fairness among the users. In order to use a small *Margin* for the CCA/CS, the DSC algorithm should use a large value for the *Decrement* parameter (e.g. 5) to result in smaller number of consecutive missed beacons ($X \leq 10$).

3.5.2 BSS Color performance

Five cases are considered for the BSS Color scheme; Legacy, 0%, 25%, 50%, 75%, and 100%. In the former case all APs and STAs operate in the legacy mode, while in the other cases, the percentage of the nodes operating in the IEEE 802.11ax mode is gradually increased. In line with the IEEE specification, it is considered that the legacy nodes process only the frames transmitted by or destined to legacy nodes (we refer to them as legacy frames). They also, drop the colored frames and set *CCA IDLE* when the predicted duration based on the *TxTime* has elapsed. It should be noted that an IEEE 802.11ax node processes not only the frames destined to it, but the legacy frames too.

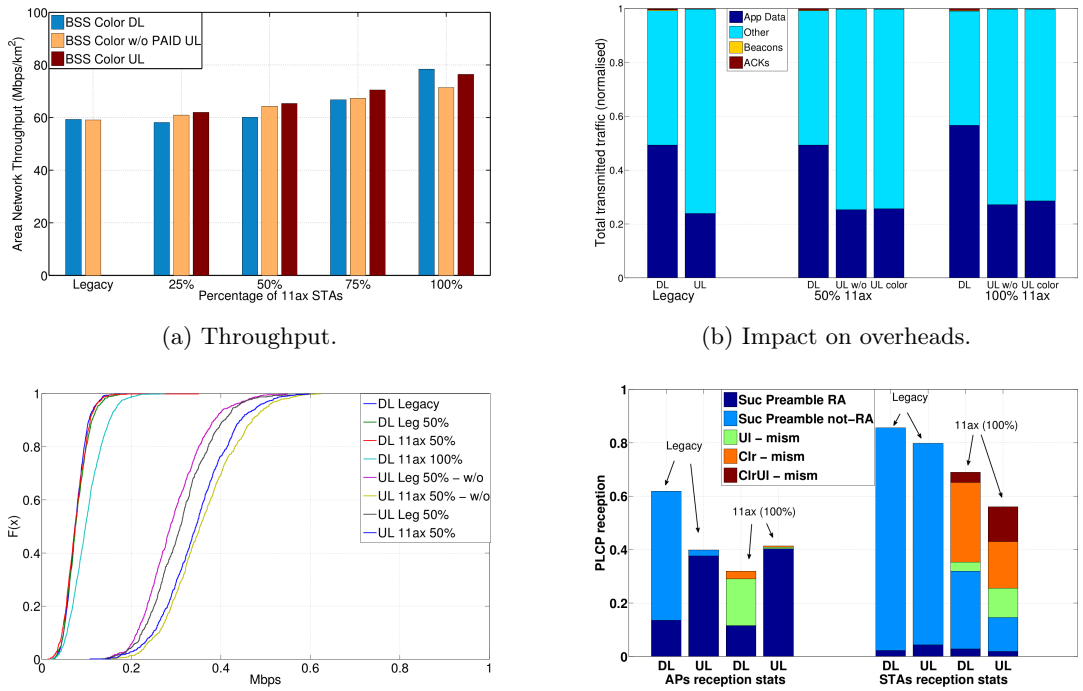

(a) Throughput.

(b) Impact on overheads.

(c) Ecdf (averaged) for Rx and Tx traffic.

(d) PLCP reception stats.

Figure 3.3: BSS Color (& BSS Color *w/o PAID*) metrics.

Figure 3.3a depicts the performance of the Color scheme in the presence of legacy STAs when PAID is used in the unicast frames transmitted by the APs and when it is not (*w/o PAID* on the DL frames). The results for the *BSS Color w/ PAID* only for the UL case is presented, as for the DL the performance is similar to the *BSS Color*

w/o PAID. This is due to the fact, that STAs benefit from the PAID only when they transmit frames. To clarify, in the UL case, a STA drops every ACK originated by its associated AP and destined to another STA. In that way, a STA initiates a transmission following a successful reception of the ACK preamble using DIFS instead of EIFS, thus improving the performance. In the DL case an AP has to process all frames (ACKs in the DL scenario) originated by its associated STAs, and drop all the other frames (PAID carries a different BSSID) originated by a neighbouring BSS. In that case, a STA drops a data frame intended to a different STA and it transmits an ACK only if the frame was intended to it. A potential throughput gain of PAID could also be observed in a mixed-traffic (UL and DL transmissions) scenario, however in this work such a scenario is not considered.

In the UL case, it can be observed that the performance gradually improves with the increase in the percentage of the IEEE 802.11ax STAs. This is because the likelihood of at least one transmission per BSS increases. Furthermore, PAID enhances the throughput by improving the PDR (Figure 3.3b, *"Color"* bar), which validates the previous argument about the benefits of PAID.

Although, BSS Color increases the number of concurrent transmissions within a network as depicted in the Figure 3.3a, it can be seen that when the number of legacy nodes is more than the IEEE 802.11ax in downlink, the network throughput slightly degrades compared to the legacy mode. This might be due to the high number of disassociated STAs (edge-cell users) for the legacy mode, improving the network throughput or an AP drops all the colored frames originated by neighbouring BSSs, while it locks onto all legacy frames with *RSSI* greater than the CCA/CS. As the percentage of the IEEE 802.11ax nodes increases, the likelihood an AP to lock onto a legacy frame originated by a neighbouring BSS drops. That means that an AP might sense the channel as *IDLE*, initiating a transmission to a node (legacy or not) which has already been locked onto a legacy frame. In the above example, the RSSI of the legacy frame is not sufficient enough to trigger one of the *CCA* thresholds and block the AP from transmission, while one of the colored frames might be above the CCA/CS but still not to satisfy Equation 3.1. The only difference as the number of IEEE 802.11ax increases, is that the likelihood of a legacy frame transmission drops. Note that when there is a balance

between the number of legacy and IEEE 802.11ax STAs, the network throughput is similar to the *"Legacy"* case. Moreover, the PDR for these two cases is the same, while it further increases as the IEEE 802.11ax are more than the legacy, Figure 3.3b. BSS Color preserves the fairness among the legacy and the IEEE 802.11ax STAs, as it can be seen in Figure 3.3c for the *50%* case (in DL). However, as the number of concurrent transmissions increase, the Color favours the nodes located close to the associated AP, due to the high interference that the edge-cell users face, from neighbouring APs. This is validated by observing the steep incline of the slope *"DL 11ax 100%"*.

Note that the 5 leftmost ecdfs in Figure 3.3c, stand for the throughput in downlink, whereas the 4 rightmost ecdfs for the transmitted bits in uplink when PAID is used and when it is not. It is worth noting that PAID feature enhances the fairness between the users in terms of transmission opportunities. If an error occurs at the payload, following a successful reception of a preamble will not affect a STA if it is not the intended recipient of that frame. In that way, the group of STAs that will initiate a transmission after EIFS reduces, preserving fairness among the users of the same BSS. Moreover, in UL case, as expected the color technique favors the STAs that use it, increasing their transmission opportunities. This can be observed by comparing the throughput per legacy and IEEE 802.11ax STA in UL for the *50%* case (Figure 3.3c).

Figure 3.3d illustrates the successfully received PLCP headers over the total detected preambles. *"Suc PLCP RA"* represents the percentile of the correctly received PLCP headers that are destined to that node, whilst *"Suc PLCP not-RA"* the percentile of the successfully received PLCP headers that are intended for a different node. In particular, the percentile of these two categories represents the percentage of the frames that a node locks onto. *"UL - mism"* stands for the case where the *Uplink Id* is not correct. It occurs whenever an AP correctly receives a frame from another AP, or a STA from another STA from the same BSS. *"Clr - mism"* stands for the Color Mismatched, namely the successfully received PLCP headers that are sent by a neighbouring BSS, while the *Uplink Id* is correct. *"ClrUl - mism"* shows the percentage of the correctly received PLCP headers by a STA that are originated by a STA belonging to a neighbouring BSS. To summarise, a node is interested only in the *"Dark blue"* PLCP headers.

Three important conclusions can be drawn from that figure in downlink. First, the interference caused by neighbouring APs (*"UL - mism"* for the APs and *"Clr - mism"* for the STAs). Second, the significant high percentage of *"Clr - mism"* in an AP, compared to *"Suc PLCP RA"*, which indicates the importance of the color field in both directions (in UL the color corresponds to the PAID). Lastly, the amount of frames that a STA proceeds which are not destined to it (*"Suc PLCP not-RA"*). The throughput gain of BSS Color scheme against BSS Color *w/o PAID* derives from the fact that a STA will drop these packets (due to PAID).

Due to the fact that the transmission probability per BSS increases, an AP mostly locks onto frames transmitted by its associated STAs. This can be observed in Figure 3.3d for the uplink transmissions. Furthermore, it can be seen that a STA experiences the same "interference" from the STAs belonging on the same and neighbouring BSSs.

3.5.3 Combining the BSS Color with the DSC

In this section an evaluation of the DSC scheme and the BSS Color when applied together is presented, in order to compensate for the high interference that the latter technique introduces (especially in the UL case). The following settings for the DSC scheme are used; *DSC (-40, -5, -20, 5)* and *DSC (-40, -5, -25, 5)*, where $DSC(Upperlimit, Margin-CCA/CS, Margin-CCA/ED, Decrement)$.

Figure 3.4a illustrates the performance of the BSS Color, when it is used along with the DSC algorithm. By tuning the CCA/CS and the CCA/ED accordingly, the total network throughput increases (compared to Figure 3.3a), and the PDR (Figure 3.4b) too. In the DL case, the throughput gain is much lower compared to the UL case, because in BSS Color scheme an IEEE 802.11ax node drops all colored frames originated by a neighbouring BSS. Thus, DSC additionally drops only a small number of frames (i.e. broadcasts with RSSI below CCA/CS) from the neighbouring BSSs. However, the network throughput in the DL case, is still lower than the one when only DSC is applied (Figure 3.2a). When only DSC is used, a transmission from an AP might prevent the neighbouring APs from transmitting, as the DSC applies only at the STAs. On the contrary, the BSS Color scheme does not block its neighbouring APs from transmitting,

increasing the interference levels.

A lower CCA/ED achieves higher throughput gain in uplink compared to the cases where the spatial reuse schemes are used individually. This is due to the higher carrier sensing range, resulting in less hidden nodes. However, that comes at the cost of deteriorating the fairness among the users.

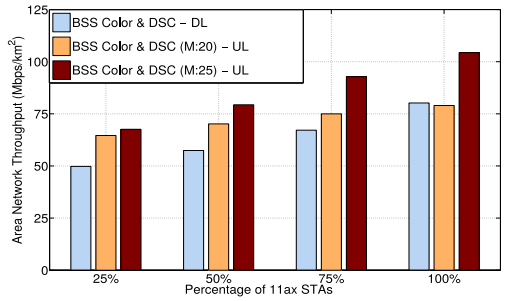

(a) Throughput.

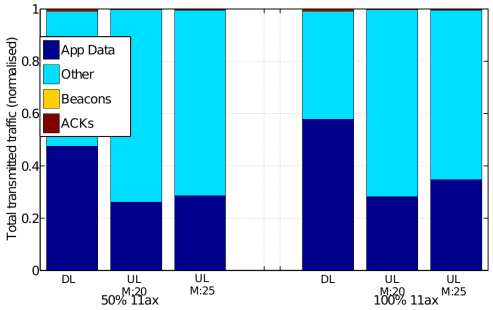

(b) Impact on overheads.

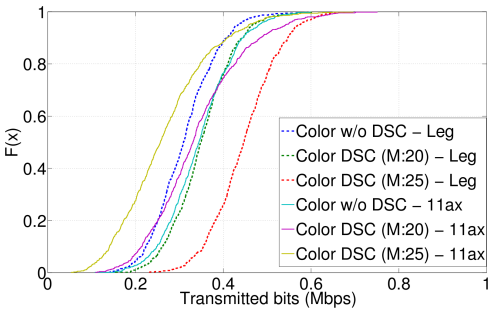

(c) Ecdf (averaged) for Tx traffic (50% IEEE 802.11ax).

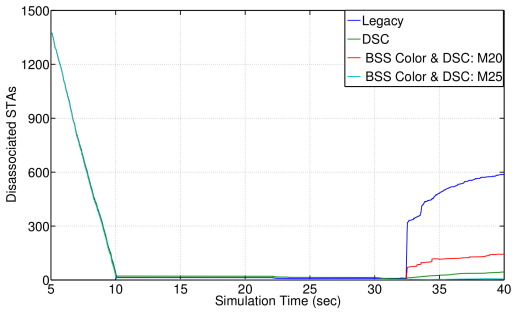

(d) Disassociated STAs.

Figure 3.4: BSS Color along with DSC, metrics.

Also, it can be observed in Figure 3.4c that as the number of the IEEE 802.11ax increases, the fairness among the users deteriorates, while the throughput per station increases. On the contrary, the legacy performance slightly improves, compared to the BSS Color scheme where the DSC mechanism is not used. This is mainly, due to the lower CCA/ED for the IEEE 802.11ax STAs. A value of 25 for the *Margin* improves the legacy performance, due to the lower CCA/ED for the IEEE 802.11ax STAs and the higher PDR.

Figure 3.4d presents the number of the disassociated STAs in the UL case, for the first

40 seconds of the simulation. Only the UL case is presented, because it is the worst case in terms of contention. It is interesting that when the data traffic starts (30^{th} second), the number of the disassociated stations increases. In particular, more than 25% of the STAs disassociate from their APs in the Legacy mode. On the contrary, when DSC is applied, the stations mostly lock onto frames originated by their associated APs, leading to less disassociations. Another important outcome is that a $Margin$ value of 20 for the CCA/ED is not enough to compensate for the high interference level introduced by the BSS Color scheme. When $Margin = 25$, the number of the disassociated STAs throughout the simulation remains constant. However, the high number of the disassociated STAs for the legacy case, may be due to the use of the disassociation mechanism.

After analysing the results, it can be concluded that the BSS Color scheme with the DSC algorithm can significantly enhance the network throughput, and the spatial reuse. It is recommended 25 as the optimal value for the $Margin$ of the CCA/ED (*DSC(-40, -5, -25, 5)*). However, this might come at the cost of slightly decreased fairness among the users. In order to compensate for the high interference that the cell-edge users experience, especially in the UL case, a TPC algorithm should be used in the APs and IEEE 802.11ax STAs.

3.6 Conclusion

This chapter investigated the performance of DSC algorithm, BSS Color scheme, PARTIAL -AID feature, and a combination of the aforementioned techniques. They were evaluated in both uplink and downlink transmissions, in a dense outdoor network with IEEE 802.11ax and legacy nodes. By utilizing the DSC scheme and using different *Margin* values for the CCA/CS and the CCA/ED, the network throughput improves and the fairness between the nodes can be preserved. It also showed that only when the number of the IEEE 802.11ax STAs is higher than the legacy, the BSS Color technique enhances the network performance. The performance of PAID feature was also assessed, which improves the throughput by reducing the erroneous received frames. By jointly using the aforementioned techniques, it was showed that the network throughput can

be further improved, especially for the uplink transmissions.

The development of the IEEE 802.11ax features and the simulation scenarios constitute the first step towards understanding the potential of the SR mechanism and the challenges that the future WLANs will face. However, as the IEEE 802.11ax amendment evolves, there is a need for the simulation tools to keep pace with this evolution to correctly assess the performance of the active amendment. Apart from the new features and advancements that are keeping introduced by the TGax, the lack of ns-3 to correctly capture the behaviour of the off-the-shelf devices could have significant implications on the assessment of the IEEE 802.11 performance. The Physical Layer Capture (PLC) has been shown that has a significant impact on throughput and may cause fairness issues between the nodes [250], [342], [343].

References

[325] T.-S. Kim, H. Lim, and J. C. Hou, "Improving Spatial Reuse through Tuning Transmit Power, Carrier Sense Threshold, and Data Rate in Multihop Wireless Networks," *Proceedings of the 12th Annual International Conference on Mobile Computing and Networking (ACM)*, pp. 366–377, 2006.

[326] B. Alawieh, Y. Zhang, C. Assi, and H. Mouftah, "Improving Spatial Reuse in Multihop Wireless Networks - A Survey," *IEEE Communications Surveys & Tutorials*, vol. 11, no. 3, pp. 71–91, 2009.

[327] C. Thorpe and L. Murphy, "A Survey of Adaptive Carrier Sensing Mechanisms for IEEE 802.11 Wireless Networks," *IEEE Communications Surveys & Tutorials*, vol. 16, no. 3, pp. 1266–1293, 2014.

[328] Network Simulator 3 (ns-3). (2015). A Discrete-Event Network Simulator for Internet Systems, [Online]. Available: `https://www.nsnam.org/` (visited on 2020).

[329] S. Merlin et al., "Document (IEEE 802.11-14/0980r16): TGax Simulation Scenarios," IEEE, Tech. Rep., 2014. [Online]. Available: `https://mentor.ieee.org/802.11/dcn/14/11-14-0980-16-00ax-simulation-scenarios.docx`.

[330] Z. Zeng, Y. Yang, and J. C. Hou, "How Physical Carrier Sense Affects System Throughput in IEEE 802.11 Wireless Networks," *IEEE INFOCOM 2008 - The 27th Conference on Computer Communications*, pp. 1445–1453, 2008.

[331] J. Zhu, B. Metzler, X. Guo, and Y. Liu, "Adaptive CSMA for Scalable Network Capacity in High-Density WLAN: A Hardware Prototyping Approach," *Proceedings of the 25th IEEE International Conference on Computer Communications (IEEE INFOCOM 2006)*, pp. 1–10, 2006.

[332] S. M. C. Thorpe and L. Murphy, "IEEE802. 11k Enabled Adaptive Physical Carrier Sense Mechanism for Wireless Networks (K-APCS)," *Proceedings of the 4th ACM workshop on Performance monitoring and measurement of heterogeneous wireless and wired networks*, pp. 209–215, 2009.

[333] X. Zhang, G. Qiu, Z. Dai, and D. K. Sung, "Coordinated Dynamic Physical Carrier Sensing Based on Local Optimization in Wireless ad hoc Networks," *2013 IEEE Wireless Communications and Networking Conference (WCNC)*, pp. 398–403, 2013.

[334] I. Jamil, L. Cariou, J.-F Helard, "Efficient MAC protocols optimization for future high density WLANs," *Wireless Communications and Networking Conference (WCNC), 2015 IEEE*, pp. 1054–1059, 2015.

[335] T. Itagaki, Y. Morioka, M. Mori, "Document (IEEE802.11-14/1403r0): Performance Analysis of BSS Color and DSC," IEEE, Tech. Rep., 2014. [Online]. Available: `https://mentor.ieee.org/802.11/dcn/14/11-14-1403-00-00ax-performance-analysis-of-bss-color-and-dsc.pptx`.

[336] T. Itagaki, Y. Morioka, M. Mori, K. Ishihara, S. Shinohara, Y. Inoue, "Document (IEEE802.11-15/0045r0): Performance Analysis of BSS Color and DSC," IEEE, Tech. Rep., 2015. [Online]. Available: `https://mentor.ieee.org/802.11/dcn/15/11-15-0045-00-00ax-performance-analysis-of-bss-color-and-dsc.pptx`.

[337] J. Liu et al., "Document (IEEE802.11-14/0882r04): TGax Channel Models," IEEE, Tech. Rep., 2014. [Online]. Available: `https://mentor.ieee.org/802.11/dcn/14/11-14-0882-04-00ax-tgax-channel-model-document.docx`.

[338] M. Filo, R. Edgar, S. Vahid, R. Tafazolli, "Document (IEEE802.11-15/1049): Implications of Wrap-Around for TGax Scenario 3 and Scenario 4," IEEE, Tech. Rep., 2015. [Online]. Available: `https://mentor.ieee.org/802.11/dcn/15/11-15-1049-01-00ax-implications-of-wrap-around-for-tgax-scenario-3-and-scenario-4.pptx`.

[339] The MadWifi project (Minstrel). (2007). Minstrel: Rate Control Algorithm, [Online]. Available: `https://sourceforge.net/p/madwifi/svn/HEAD//tree/madwifi/trunk/ath_rate/minstrel/minstrel.txt` (visited on 2019).

[340] T. Hytönen, "Optimal Wrap-around Network Simulation," Helsinki University of Technology Institute of Mathematics, Tech. Rep., 2001. [Online]. Available: `https://research.aalto.fi/en/publications/optimal-wraparound-network-simulation(defc5b96-f90c-4902-9bc9-2ec28445d916).html`.

[341] R. K. Jain, D.-M. Chiu, and W. R. Hawe, *A Quantitative Measure of Fairness and Discrimination for Resource Allocation in Shared Computer System*. Eastern Research Laboratory, Digital Equipment Corporation, Hudson, MA, 1984.

[342] A. Kochut, A. Vasan, and A. U. Agrawala, "Sniffing out the Correct Physical Layer Capture Model in 802.11b," *In Proceedings of the 12th IEEE International Conference on Network Protocols (ICNP 2004)*, pp. 252–261, 2004.

[343] K. Pahlavan and A.-H. Levesque, *Topology, Medium Access, and Performance Wireless Information Networks (501-579)*. John Wiley & Sons, Inc., 2005.

Chapter 4

Exploiting the Capture Effect on the IEEE 802.11ax Spatial Reuse Features

Understanding the behaviour of real-world devices can provide valuable insights into developing mechanisms to address the challenges of the future WLANs. That requires to continuously advance the simulator tools that can give a first taste of the performance and behaviour of the mechanisms proposed for the upcoming technologies. Simulation tools can steer the research to the right direction by identifying the needs and challenges of the current technologies. The early identification of the issues and the continuous assessment of the newly proposed features are crucial and are considered to play major role in the formation of the new amendments, before they are finalised and commercial products hit the market. For example, the IEEE 802.11ax BSS Color has been advanced since it was initially conceived, with a lot new features to support its smooth operation.

This chapter overviews the latest advancements proposed to support the BSS Color operation. It also, presents a PLC model developed according to the TGax guidelines and integrated into the ns-3. It then, shows the impact of PLC on the network performance in terms of throughput and fairness in simple scenarios where it can more easily be assessed. Finally, an evaluation of the PLC model and its impact on the IEEE 802.11ax

SR features is presented in an indoor deployment.

4.1 Introduction

The main reason why WLANs are a commodity to our daily lives is their inherent advantages against other technologies, such as their cost efficiency and easy deployability in diverse environments, including residential apartments, offices, public transportation, outdoor hotspots etc. as illustrated in Figure 4.1, and the fact they can provide ever increasing high data rates. In scenarios, where multiple APs are deployed and hundreds of STAs associate with them, it is inevitable transmissions not to interfere with OBSSs. Of a particular interest, is the case of the already congested 2.4 GHz band where there are only three non-overlapping 20 MHz channels and yet most of the devices continue operate in this frequency.

Fortunately, in most of the cases STAs associate with the strongest APs, which means that the received signal will be stronger than the interfering ones. The ability of a receiver to lock onto the strongest signal and may successfully decode it, it is very beneficial for the devices, especially in dense deployments. According to the IEEE 802.11 standard, once a receiver locks onto a packet, it shall continue receiving it for the duration of the transmission. This means that the devices will not try to decode or lock onto a different preamble. However, the receive state machine implemented by many vendors, differentiates from what it is described in the standard [344].

Figure 4.1: Scenarios for the future WLANs.

In the case of a stronger signal arriving during the reception of a frame, instead of losing both packets due to collision, the receiver could re-synchronize to the stronger one, as it has higher probability of surviving the collision. Thus, the system throughput could increase, whilst unfairness among the cell-edge and the rest users could aggravate. Although, PLC is implemented on the off-the-shelf devices, the effects of PLC have not been yet fully evaluated in the literature and most of the studies are based on the assumption that both packets are lost in a collision [345]. Due to its implications on the network performance and the impact on the SR mechanisms, PLC was described in TGax and was incorporated in the [346] where the simulation scenarios and the methodology for evaluating the new features are overviewed.

This chapter presents the development of the PLC in ns-3, according to the TGax guidelines and its evaluation in terms of throughput and fairness on simple scenarios. Furthermore, it overviews the latest developments on the IEEE 802.11ax SR schemes that were also integrated in ns-3. Finally, the impact of PLC on the two SR schemes, DSC and BSS Color, in a dense indoor (hexagonal-like) deployment is also presented here.

The rest of the chapter is organised as follows. Section 4.2 presents related work and describes the PLC. Section 4.3 presents the simulation scenario, while Section 4.4 analyses the simulation results. Finally, Section 4.5 concludes this chapter.

4.2 Background

Although, SR mechanisms could reduce the probability of frame collisions, there might still be occasions due to the nature of the wireless medium and CSMA/CA mechanism that packets collide. Especially, in dense deployments the probability of users initiating a transmission at the same time slot increases. In the event of a collision, the receiver might still be able to successfully decode the strongest signal, even if it arrives later than the weaker signals. This event is known as PLC [347].

The works in [342], [348] show the fairness issues caused by PLC and investigate the performance of different capture models. Experimental studies of PLC are also pre-

sented in [251], [349]. The authors in [251] show the relationship between the packet arriving time and collided packet that could be successfully decoded, whereas in [349] a technique to detect and recover the collided frames is presented. In [250] the authors analyse the fairness issues among the nodes caused by PLC, and its impact on MAC protocol, whereas a simulation-based study in [350] shows that PLC favors all users, especially the cell-edge users which are more likely to detect an OBSS transmission and lock onto. The authors in [351] propose to mitigate unfairness introduced by PLC, through adjusting the MAC parameters. They show that fairness can be restored by tuning the retransmission limit, the contention window, the TxOP, and the AIFS.

A more recent work with respect to the PLC is presented in [344]. The authors studied the impact of the PLC on various off-the-shelf devices, deployed in a testbed. The findings of this work can be summarised in: i) all the devices (from those studied, i.e. Broadcom, Intel, Qualcomm) support the PLC during the preamble reception and ii) only in a few Qualcomm devices, PLC is realised during the payload. The former is beneficial for the case when nodes grant access to the channel at the same time slot (BackOff counter is zero), whereas the latter is for the case of hidden nodes where transmissions can be initiated during the whole duration of a packet.

The capture model implemented in this work follows the procedure described in [346]. In particular, a receiver captures the strongest signal detected within a capture window. This capture window has a duration of 800ns and it starts at the first arrival frame with RSS above the Rx Sensitivity. At the end of the capture window, the receiver locks onto the strongest signal whose preamble is to be decoded. If a frame arrives after the end of the capture window and within the preamble duration of the strongest signal, it is considered as interference. Following a successful reception of the preamble, the capture phase starts again. This time, the window, a.k.a. Pre-emption Window, has duration equal to the duration of the frame whose preamble has been successfully decoded. If a new frame arrives during the Pre-emption Window, the receiver will lock onto it, if its RSS is at least XdB above the RSS of the current reception ($RSS_{new} \geq (RSS_{cur} + X)$). X is known as the capture threshold, and a value of 10 dB is used [346]. Then, the current reception terminates, the receiver captures the newly arrived frame, and the capture procedure starts again. The starting time and duration of the capture and

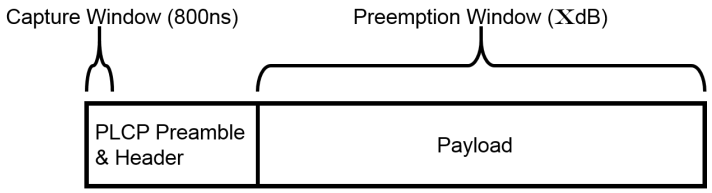

Figure 4.2: Duration of capture and pre-emption window.

pre-emption window with respect to a receiving frame, are illustrated in Figure 4.2.

4.3 Simulation Setup

To test fairness and throughput performance of WLAN with the effect of capture model, three scenarios are created: two small-scale ad-hoc topologies, illustrated in Figure 4.3. In the small-scale scenarios, each circle represents the carrier sensing range of each node. In the former case (*Case 1*), there is only one receiver (R) and two hidden senders (S1, S2) which are equidistant from the receiver. Whilst, in the latter test case (*Case 2*), there are two senders (R0, R1) hidden from each other, transmitting traffic destined to S0 and S1, respectively. S1 node is an exposed node, since both R0 and R1 are within its carrier sensing range. That means, S1 could lock to a frame originated by R0 or R1, and could transmit a frame when both R0 and R1 do not transmit any frame. Moreover, S1 is placed closer to R1 than to R0, such that $RSS\_R1 = RSS\_R0 + 0.11$ when both R0 and R1 transmit at the same power level. In both simulations, the senders are hidden from each other, hence can transmit simultaneously, whereas the capture threshold is set equal to 0.1 dB to capture the ideal case where a receiver is capable to detect any signal stronger than the current one that is locked to. Both Broadcast and Unicast traffic are considered in order to study the impact of PLC on MAC layer.

Then, the performance of DSC and BSS Color in a dense deployment consisted only of 11ax nodes (nodes that support DSC or BSS Color) is evaluated. The APs are placed in fixed location, whilst STAs randomly placed in a reference area, as illustrated in Figure 4.3c. In particular, this reflects to Scenario 3 from the list of TGax baseline scenarios [329], an indoor small deployment. The wrap-around technique is also applied, while it is assumed that all nodes establish the Block Ack Agreement instantly and dis-

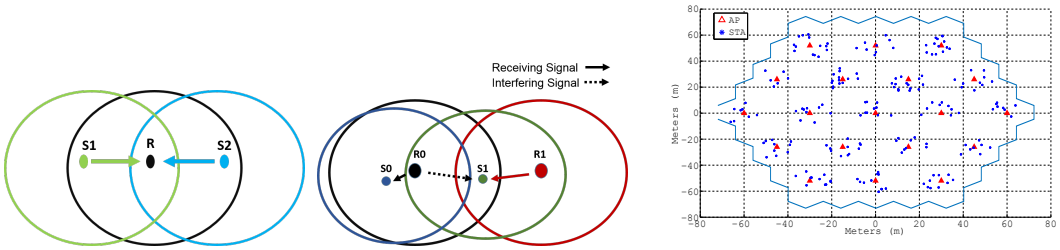

(a) (b) (c)

Figure 4.3: Simulation Scenarios: a) hidden nodes (packets to the same receiver), b) hidden nodes (packets to different receivers), and c) SCE3 (SR3 and Rings 2).

association do not occur (*Missed Beacons* is set to infinite). The simulation parameters used in this study are listed in Table 4.1.

DSC is also implemented following [276] with the addition of two *Margin* values for *CCA/ED* and *RxSensitivity* (CCA/CS) as described on the previous section. On the other hand, no color collisions are assumed and the Color id is carried on the PLCP header without increasing its transmission time, since the IEEE 802.11ac physical layer is used. Specifically, it is included in the HE-SIG-A1 field, that means it is the first field following the legacy portion of the preamble. In ns-3 the whole preamble is for now considered as a standalone sub-frame. However, part of the development in this work includes the separation of the preamble reception based on the fields included in it, to gradually incorporate (correctly) the IEEE 802.11ax features and BSS Color fields. In that way, a node may identify a color mismatched earlier instead of waiting until the end of the whole preamble. Furthermore, if a field is not successfully detected, then a node sets CCA threshold or the channel as *BUSY* according to PHY receive state machine flowchart [245]. Lastly, once receivers successfully decode a preamble, they lock onto that transmission until the last A-MPDU frame, which also means that Pre-emption window's duration extends until the end of the last A-MPDU frame.

Table 4.1: Simulation parameters

Parameter	Value
Scenario / ICD [m] / Rings / SR	SCE3 / 17.32 / 2 / 3 (Wrap Around)
Frequency band [GHz]	TGax SCE3 / 5 (Bandwidth 20MHz)
Number of APs/STAs	19/197
Shadowing	Disabled
AP/STA Tx Power [dBm]	20/15 , unless otherwise specified
AP/STA antenna gain [dBi]	0/-2
Antennas (AP, STA)	1 (SISO)
Noise figure [dB]	7
PHY rate [data/control frames]	VHT-(MCS5/MCS0), unless otherwise specified
Traffic per BSS [Mbps]	100 (UDP)
RTS/CTS	Disabled
Max retransmissions	10
Packet at APP Layer [bytes]	1472, unless otherwise specified
Max A-MPDU [frames]	32 or 5.484ms, unless otherwise specified
Beacon Interval [ms]	102.4
CCA/CS, CCA/ED [dBm]	-82, -62, unless otherwise specified,
Simulation Time per run [s]	50 (40 Runs)

4.4 Simulation Results

This section presents the performance evaluation of a) PLC, b) DSC, and c) BSS Color schemes in the aforementioned small and large-scale scenarios, in terms of fairness, average user and aggregated throughput. The fairness for the small-scale scenarios is defined as the user throughput ratio, whereas in the large-scale scenario can be observed from the gradient of the cumulative distribution function (cdf) lines. The aggregated throughput in the large-scale deployment is per channel (20MHz) and normalised per km^2 due to the use of wrap-around.nNote that for the assessment of PLC, two different packet sizes has been applied as representative of small and large packet sizes, whilst for the DSC and BSS Color performance the packet size is set according to the TGax guidelines.

4.4.1 PLC Impact

First, the impact of PLC is studied in the scenarios *Case 1* and *Case 2* with data rate VHT-MCS0. Figures 4.4a to 4.4c present the impact of PLC in terms of user and aggregated throughput for broadcast and unicast traffic for *Case 1*, depicted in

Figure 4.3a. The x-axis represents the difference of the Transmit Powers between S2 (STA2) and S1 (STA1); $TxPwr\_S2 - TxPwr\_S1$. As S2 increases its Transmit Power, fairness deteriorates since S2 throughput improves whereas that of S1 reduces. It is also observed that fairness between S1 and S2 further deteriorates with PLC (*CapWin: 1*, i.e. PLC is enabled), especially for small packet sizes. Smaller packet sizes have higher probability of successful reception with or without PLC. Thus, when a receiver locks onto a small packet, the transmission will be most probably successful. However, this is not the case for large packets as they have lower probability of successful transmission. This is the main reason, PLC has more impact on smaller packets in terms of throughput and fairness. Unfairness is even higher in unicast traffic due to MAC retransmissions and Contention Window size. It is only presented the aggregated throughput for broadcast traffic, as for unicast traffic *throughput gain* $\approx 1\%$ for PLC.

Figures 4.4d to 4.4f depict the results obtained for *Case 2*, illustrated in Figure 4.3b. In that case, fairness improves since throughput of S1 approximates this of S0 when PLC is modelled. The aggregated throughput gain is significant higher than in *Case 1*, as PLC increases the number of successful concurrent transmissions. That is, PLC can improve throughput and fairness, especially for the cell-edge users in specific scenarios.

The impact of PLC in a dense deployment is assessed, for various packet size, data rate, capture threshold, and transmission link; DL only and UL only. Since the signal strength difference required for PLC depends on MCS and there are techniques to tune PLC properties [352], [353], three different capture thresholds are applied, namely: 1, 5, and 10 dB [348]–[350].

Figure 4.5 illustrates the aggregated and gain throughput of PLC against various data rates and packet sizes. Figure 4.5a presents the impact of different data rates when capture threshold is set to an extremely large value (PLC is disabled). As it is expected, throughput improves as higher data rate is used, even for large frame sizes. That means SINR is sufficient for successful transmissions in that specific case. In Figure 4.5b the throughput gain of various capture thresholds is depicted. It can be observed that throughput gain further improves as the frame size increases. This is due to the combination of low data rate which is more robust to interference and the duration

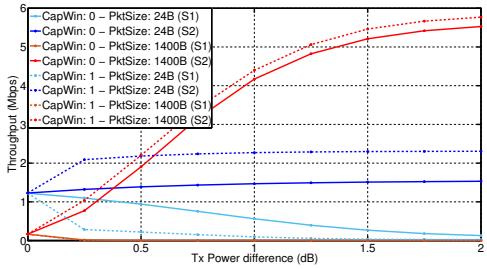

(a) Broadcast traffic (Case 1).

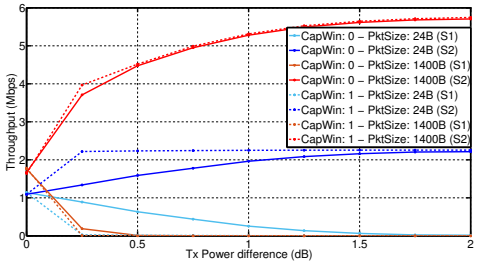

(b) Unicast traffic (Case 1).

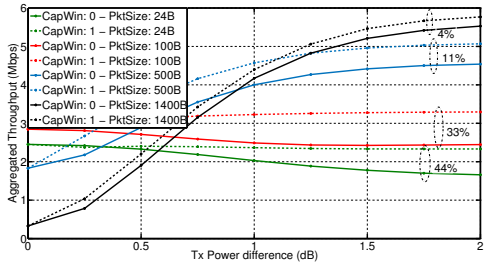

(c) Broadcast traffic (Case 1) - Aggr. Thr.

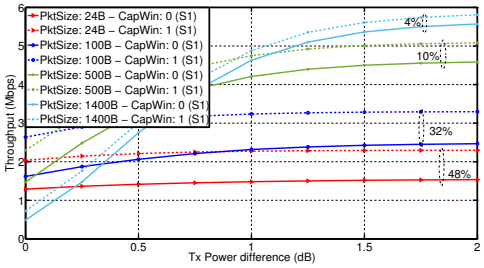

(d) Broadcast traffic (Case 2).

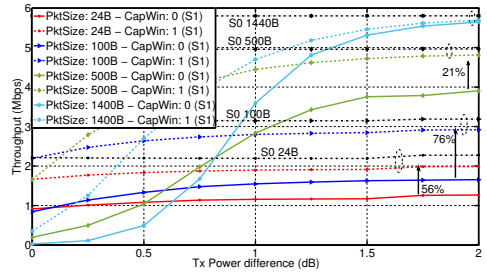

(e) Unicast traffic (Case 2).

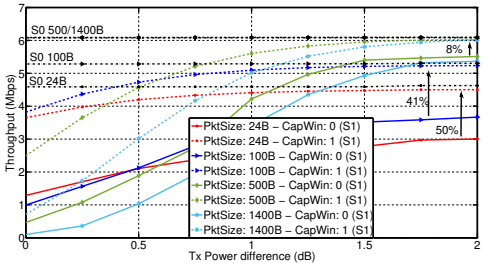

(f) Unicast traffic (Case 2) - A-MPDU: 5.

Figure 4.4: Impact of PLC in terms of aggregated throughput or throughput per STA [notated as aggregated throughput or throughput, respectively] and fairness.

of PLC windows. Especially, the ratio of PLC windows and the time window between them, that PLC is not used (No PLC). As the frame size increases, the ratio of PLC and No PLC window increases, which means that the probability of a frame arriving within the PLC windows increases. Two important outcomes can be derived from Figure 4.5c. First, the gain decreases as data rate increases, since higher data rates require higher SINRs for successful transmissions. Second, as data rate increases, a higher capture threshold results in a higher throughput gain.

On the other hand, in UL case, high data rates and large packet sizes result in a poor

performance, Figure 4.5d, since they are more susceptible to low SINR. The number of nodes, now, competing to grant access to channel is 10x times than in DL case, increasing interference. This is also, the main reason that throughput gain is higher for smaller frame sizes, as illustrated in Figure 4.5e.

A throughput loss can be observed in Figure 4.5f for large frame sizes and high data rates due to the strong interference (see Appendix D for the packet reception model). After, closely analysing that behaviour it was found that the loss is due to max A-MPDU number, due to longer transmitted packets (hence, longer transmission times), resulting in more packets being lost due to insufficient SINR (and the preceding packets before the PLC kick in). By restricting the number of A-MPDU to 1 frame for VHT-MCS7 and setting the capture threshold to 5, a gain could be observed. Let us assume a STA that initiates a transmission (*Tx0*) to AP. If the packet preamble is successfully decoded by all STAs within the BSS then they will defer their transmissions until the end of the ongoing transmission. In case that at least one STA fails to decode preamble, then it might initiate a transmission (*Tx1*) after a specific number of time slots, depending on the interference level and *CCA/ED* threshold. *Tx1* may interfere with *Tx0* depending on the transmission duration of the latter one. Now, the AP will lock onto the newly arrived frame based on the capture threshold. In case that capture threshold is set to a small value, SINR might not be sufficient enough to successfully decode the newly arrived packet or even its preamble. This could result both STAs to transmit Block-Ack requests or even retransmit all their frames even though some of them might have been correctly received. If PLC is disabled, then the AP would acknowledge the first STA and inform it about the number of successfully received frames, reducing the overhead of retransmissions.

The throughput gain of PLC in DL case is mainly due to the fact that STAs drop frames transmitted by OBSSs when a stronger signal arrives, as in *Case 2*. Whilst, in UL case, there are multiple senders that could be hidden to each other, transmitting to the same receiver which could result to a throughput loss in specific cases. In such cases, appropriate CCA thresholds could eliminate the concurrent transmissions within the same BSS.

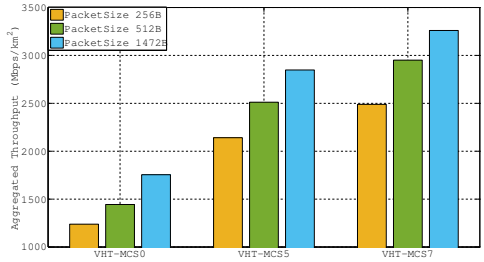

(a) Aggregated Throughput DL (No PLC).

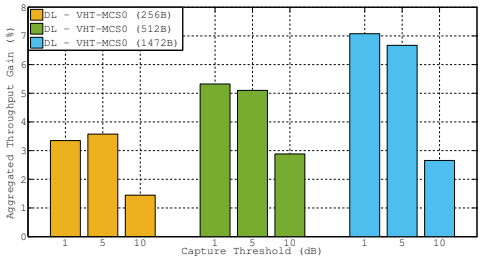

(b) Throughput gain DL (VHT-MCS0).

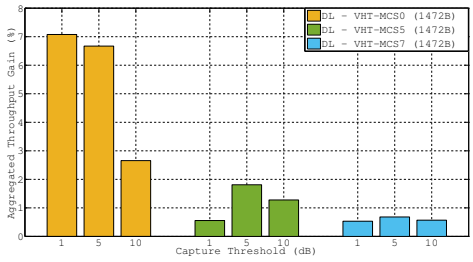

(c) Throughput gain DL (1472B).

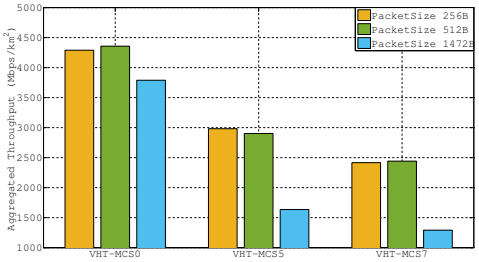

(d) Aggregated Throughput UL (No PLC).

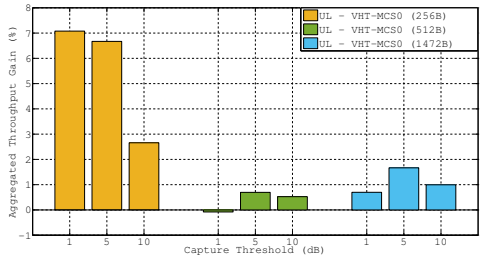

(e) Throughput gain UL (VHT-MCS0).

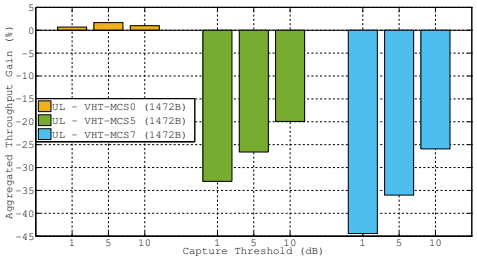

(f) Throughput gain UL (1472B).

Figure 4.5: Impact of PLC in terms of aggregated throughput and aggregated throughput gain in SCE3.

4.4.2 DSC Evaluation

DSC is evaluated now, for 5 different *Margin* values, whereas *UpperLimit* is set to *-40* for all cases. The *Margin* values are depicted in Figure 4.6a, while a capture threshold of 10 dB is used. In DL case, only *CCA/CS* is tuned whereas a *Margin* value of 20 is used for *CCA/ED*. In UL, a similar approach is followed but this time, *CCA/ED* is tuned whilst a *Margin* value of 5 is used for *CCA/CS*. It can be observed in this figure, that different values of *Margin* have negligible impact on throughput in DL case. The throughput gain in that case is marginal ($\leq 1\%$) due to PLC. Specifically, even if a node

locks onto a signal originated by an OBSS, it may abandon this reception if detects a stronger signal which was possibly transmitted by its associated AP, unless that frame arrives between Capture and Pre-emption window. Since the duration between Capture and Pre-emption window is small compared to the total duration of those windows, the probability of receiving a stronger frame within that duration is extremely small, hence the low throughput gain. A potential higher throughput gain could be observed though, in a bi-directional case when a STA has also frames to transmit. In UL case, as *Margin* increases, carrier sensing range also expands, increasing the probability of successful transmissions, eliminating the concurrent transmissions of STAs within the same BSS. However, an extremely low *Margin* results in a negative throughput gain compared to Legacy one, due to the hidden node problem.

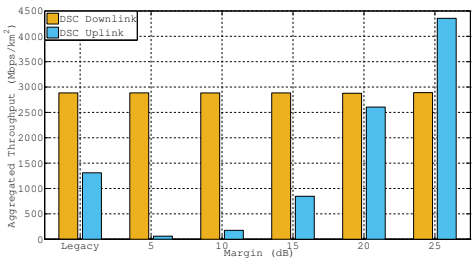

(a) Aggregated Throughput.

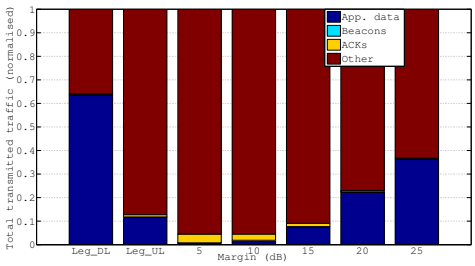

(b) Impact of DSC on overheads.

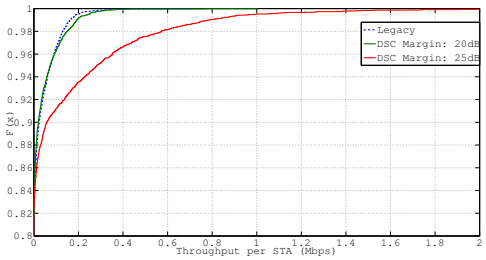

(c) Ecdf for UL transmissions.

Figure 4.6: DSC metrics.

Figure 4.6b depicts the impact of *Margin* on overheads. The first bar represents the DL case, whereas *Other* the retransmitted data. Only one bar for DL is presented, since the results do not significantly vary for different *Margin* values. In UL case, a high percentage of ACKs transmissions and retransmissions for small *Margin* can be observed due to the extremely small carrier sensing range. One important outcome,

is the packet delivery ratio (PDR) that can be derived from this figure. A value of 20 offers an almost two-fold better PDR than the legacy does, whereas when $Margin = 25$, PDR further improves.

Figure 4.6c presents the average throughput per STA in UL case. Three important conclusions can be drawn from that figure. First, throughput has been generated by less than 20% of the total STAs. Second, the throughput gain of $Margin = 20$ is due to a small fraction of the STAs ($\approx 3\%$) that takes advantage of the smaller carrier sensing range. They are located close to the APs as their signal should be strong enough to trigger PLC and also survive collisions. Lastly, a value of 25 favours a bigger portion of the STAs, not only those located very close to an AP. However, it can be argued that fairness deteriorates for these STAs due to the gentle slope. After closely analysing the results, a *Margin* value of 25 for *CCA/ED* seems more suitable for the specific scenario, whereas a small one for *CCA/SD* could potentially increase the transmission opportunities for a STA assuming low-mobility in a bi-directional (DL and UL) scenario.

4.4.3 BSS Color Evaluation

On the other hand, BSS Color is evaluated for different $OBSS/PD_{thr}$ and transmit power levels, while a capture threshold of 10 dB is used. In particular, a specific transmit power for a node is set, while $OBSS/PD_{thr}$ is adjusted using Equation 2.2. Figure 4.7a illustrates BSS Color performance in terms of throughput for DL and UL cases. The x-axis represents the transmit power for APs and STAs, $(TxPwr\_AP, TxPwr\_STA)$. For example, when $(TxPwr\_AP, TxPwr\_STA) = (20, 15)$, then the threshold is $(OBSS/PD^{AP}_{thr}, OBSS/PD^{STA}_{thr}) = (-81, -76)$. In DL case, it can be seen that for the $(20, 15)$ and $(17, 12)$ cases throughput slightly decreases compared to *Legacy*, whereas a further reduction in transmit power results in extremely low throughput. First, reducing transmit power might improve spatial reuse by increasing the number of concurrent transmissions, which could lead to higher interference level. In addition, BSS Color increases the transmission opportunities which could result in low SINR that is not sufficient enough for successful transmissions. A similar behaviour is observed in UL case. However, this time throughput decreases more rapidly as transmit level reduces. In

addition to high interference level from OBSSs, in UL case, due to the high CCA/ED there are hidden nodes within the same BSS that could further increase the probability of collisions or decrease SINR.

Figure 4.7b presents the impact of BSS Color on overheads. The four left-hand bars stand for DL case, whereas the rest four for UL. Two outcomes can be derived from this figure. First, PDR decreases with the transmit power. Secondly, as transmit power reduces, the ACK portion increases, indicating the high number of retransmissions. Especially, in UL case, the high number of acknowledgements could be due to PLC as described in Section 4.4.1.

Figure 4.7c depicts the average throughput per STA in UL case. Even though BSS Color increases the transmission opportunities, especially for the cell-edge users that could lock onto a frame originated from an OBSS, it can be observed that the throughput of these nodes dramatically drops. Their performance becomes even worse as $OBSS/PD_{thr}$ increases. This is due to lower transmit power, which could reduce interference level to OBSSs but it might increase the number of hidden nodes within the BSS.

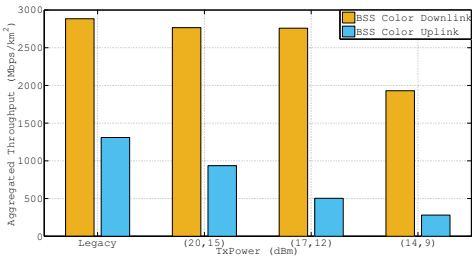

(a) Aggregated Throughput.

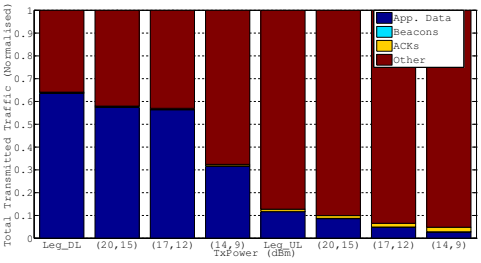

(b) Impact of BSS Color on overheads.

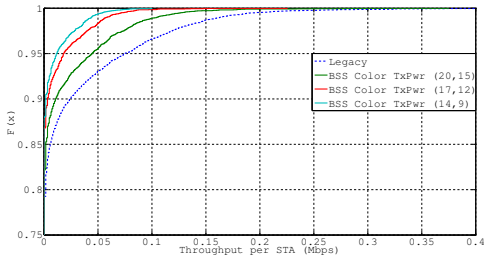

(c) Ecdf for UL transmissions.

Figure 4.7: BSS Color metrics.

To cope with the hidden node problem, BSS Color is now applied along with DSC. DSC reduces the probability of concurrent transmissions within a BSS through *CCA/ED* and the probability of a node locking onto a preamble originated by an OBSSs through *CCA/CS*. On the other hand, the main advantage of BSS Color is blocking the reception of OBSS frames and increasing transmission opportunities through *OBSS/PD* and *CCA/ED*. The *Margin* values used in that case are; 5 for *CCS/CS* and 20, 25 for *CCA/ED*.

Figure 4.8a illustrates the performance of BSS Color along with DSC algorithm in DL transmissions. The results when *Margin* = 20 for *CCA/ED* are presented, since the results for a value of 25 dB do not vary significantly. It can be observed that DSC has a negligible impact in that case. This is because, DSC is only applied on STAs, which means that it does not block APs from transmitting. The small deviation in throughput gain observed in that case, is due to the expanded carrier sensing range for the STAs and the small share of the traffic transmitted in the UL link (Block-Acks).

On the other hand, in UL case, as most of the traffic is transmitted from STAs, DSC highly affects the system performance as depicted in Figure 4.8a. Two important outcomes can be drawn from this figure. First, the great impact of adjusting the carrier sensing range compared to the case where only BSS Color is used. Secondly, a *Margin* value of 20 dB achieves higher throughput gain than 25 dB, compared to the case where only DSC is applied with the same values. This is because BSS Color blocks all OBSS frames, whilst DSC does not and due to transmission opportunities through *OBSS/PD* and *CCA/ED*. A very low *CCA/ED* will force a STA to defer its transmission, even if the received signal of an OBSS frame is below *OBSS/PD*. This is the main reason that throughput gain is approx. 10% and 1% for a value of 20 and 25 dB, respectively, compared to DSC.

After analysing the results, it can be argued that DSC outperforms over BSS Color, whereas by combing these schemes, a higher throughput gain can be observed. The main difference between BSS Color and DSC is that the latter scheme does not distinguish the packets (i.e. inter-BSS or intra-BSS packets), treating them equally, which means that inter-BSS transmissions may block STAs from transmitting if the energy detected

is above the CCA/ED threshold. On the other hand, BSS Color blocks the STAs from transmitting only when inter-BSS packets are detected, which may lead to packet collisions due to hidden nodes within the BSS. The poor performance of BSS Color could be due to PLC in addition to small ICD and low SINR for the data rate used in this study.

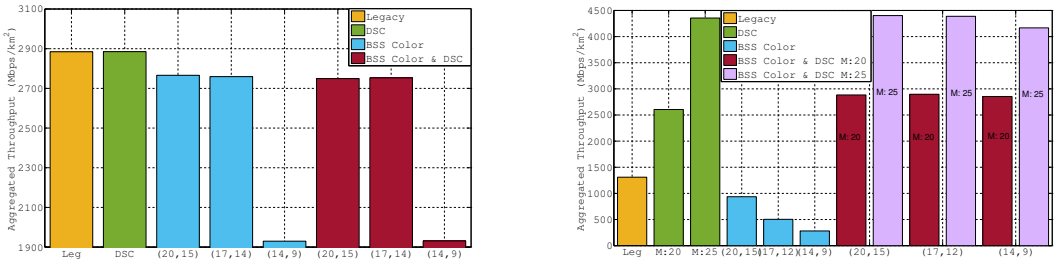

(a) DL transmissions.

(b) UL transmissions.

Figure 4.8: BSS Color along with DSC.

4.5 Conclusion

This chapter investigated the performance of DSC, BSS Color, and a combination of these schemes when the PLC is modelled. PLC is not mentioned in the IEEE 802.11 amendments and it breaks some of the IEEE 802.11 reception rules, but it is a mechanism used in most off-the-shelf devices. First, an overview of the PLC model is presented and a study of the PLC developed in ns-3, in a small and large-scale scenario. The fairness issues caused by PLC can be observed, reported also in previous works, but a case where PLC improves fairness is also introduced. Following that, an evaluation of the performance of DSC and BSS Color in a large deployment for both downlink and uplink transmissions is presented. It is showed that, by utilizing DSC, the system throughput enhances, whereas the reasons of BSS Color's poor performance in the specific scenario are listed. By jointly applying the aforementioned schemes, network throughput can be further increased.

The throughput loss observed by the use of BSS Color in this chapter, it opens the door to the research community to contribute toward the IEEE 802.11ax SR enhancements.

Further, a mechanism for setting the $OBSS/PD$ threshold has not yet been defined in the amendment and was left to the discretion of the IEEE 802.11 drivers and chipsets manufacturers. A naïve approach would be to integrate DSC as the algorithm that defines the $OBSS/PD$ threshold. DSC has been extensively studied for adjusting the CCA thresholds in various scenarios and it is a well known technique in the TGax community. However, the two main drawbacks for DSC are: i) fairness issues for the cell-edge users and ii) does not take into account the interference level from the OBSSs, where the $OBSS/PD$ is based on. Nevertheless, the potentials for the BSS Color scheme are still unknown, hence an analysis of this scheme is presented in the next chapter.

References

[344] E. Khorov, A. Kureev, I. Levitsky, and A. Lyakhov, "Testbed to Study the Capture Effect: Can We Rely on This Effect in Modern Wi-Fi Networks," *2018 IEEE International Black Sea Conference on Communications and Networking (BlackSeaCom)*, pp. 1–5, 2018.

[345] G. Bianchi, "Performance Analysis of the IEEE 802.11 Distributed Coordination Function," *IEEE Journal on Selected Areas in Communications*, vol. 18, no. 3, pp. 535–547, 2000.

[346] R. Porat et al., "Document (IEEE 802.11-14/0571r12): TGax Evaluation Methodology," IEEE, Tech. Rep., 2014. [Online]. Available: `https://mentor.ieee.org/802.11/dcn/14/11-14-0571-12-00ax-evaluation-methodology.docx`.

[347] M. Soroushnejad and E. Geraniotis, "Probability of Capture and Rejection of Primary Multiple-access Interference in Spread-spectrum Networks," *IEEE Transactions on Communications*, vol. 39, no. 6, pp. 986–994, 1991.

[348] C. Ware, J. Chicharo, and T. Wysocki, "Modelling of Capture Behaviour in IEEE 802.11 Radio Modems," *IEEE International Conference on Telecommunications*, pp. 1–6, 2001.

[349] K. Whitehouse, A. Woo, F. Jiang, J. Polastre, and D. Culler, "Exploiting the Capture Effect for Collision Detection and Recovery," *The Second IEEE Workshop on Embedded Networked Sensors (EmNetS-II)*, pp. 45–52, 2005.

[350] V. Ferdowsi and D. Lee, "Document (IEEE 802.11-15/1302): System Level Simulator Evaluation with/without Capture Effect," IEEE, Tech. Rep., 2015. [Online]. Available: `https://mentor.ieee.org/802.11/dcn/15/11-15-1302-02-00ax-system-level-simulator-evaluation-with-without-capture-effect.pptx`.

[351] S. Ganu, K. Ramachandran, M. Gruteser, M. Seskar, and J. Deng, "Methods for Restoring MAC Layer Fairness in IEEE 802.11 Networks with Physical Layer Capture," *Proceedings of the 2nd International Workshop on Multi-hop Ad Hoc Networks: from Theory to Reality*, pp. 7–14, 2006.

[352] I. Bruyland, "The Influence of Finite Bandwidth on the Capture Effect in FM Demodulators," *IEEE Transactions on Communications*, vol. 26, no. 6, pp. 776–784, 1978.

[353] J. Ward and R. T. Compton, "Improving the performance of a slotted ALOHA packet radio network with an adaptive array," *IEEE Transactions on Communications*, vol. 40, no. 2, pp. 292–300, 1992.

Chapter 5

An Analytical Model for the IEEE 802.11ax BSS Color

Previous chapter presented the advancements introduced in the ns-3 tool being in line with the TGax recommendations. This chapter strives to shed some light on the potentials of BSS Color by analysing its performance based on Markov chains in small-cell scenarios. First, it shows an extended model of the one presented in [345] by taking into account the busy duration of the states in a multi-BSS scenario. Finally, an evaluation of the model is presented against ns-3 in various scenarios.

5.1 Introduction

In the case of a single BSS, Bianchi [345] presented a model based on a Discrete Time Markov Chain (DTMC) to assess the performance of the network in terms of throughput. The model is based on the assumption that hidden and exposed nodes do not exist in the network and that transmissions are not exposed to BER and therefore packet losses occur only due to packet collisions. In a scenario like that, there are not asynchronous transmissions and therefore one Markov chain can describe the whole network. Bianchi's model is mostly for a single BSS scenario and is shown to give accurate results based on these assumptions.

Analysing scenarios with multiple OBSSs operating on the same channel is challenging. To capture the interactions between the OBSSs, Continuous Time Markov Chain (CTMC) has been proposed in [354]–[356]. However, the number of possible states in a CTMC is a function of the number of OBSSs. This means that constructing the CTMC is challenging and a complex task, as the number of possible states grows rapidly with the number of OBSSs. In order to reduce complexity, this study focuses on a DTMC model, and tries to provide an accurate model in a scenario with multiple OBSSs.

The rest of the chapter is organised as follows. Section 5.2 presents the analytical model, while Section 5.3 provides the performance analysis in various topologies. Finally, Section 5.4 concludes this chapter.

5.2 Throughput Analysis

The analytical model described in this section is based on the assumption of small cells, where the STAs are located close to the APs and experience good channel conditions, hence the transmission are always considered successful (i.e. no collisions) and the APs have always packet to transmit (saturation conditions). In the analysis, DL traffic is only considered with multiple APs, whilst each AP associates with one STA. Further, an aggressive CCA/ED threshold is applied, which means that when the packet preamble is missed it will not trigger busy channel. Finally, the physical capture model described in the previous chapter is also applied in this analysis, and only the basic access is considered.

5.2.1 Bianchi's model

Under saturation conditions, each node has always a packet to transmit, but each packet has to wait for DIFS and a random backoff interval as described in the previous section. The state of each node; idle, busy, transmit and the backoff stage are illustrated in Figure 5.1. Note that the state of busy probability is also included in the figure, in contrast to Bianchi's model.

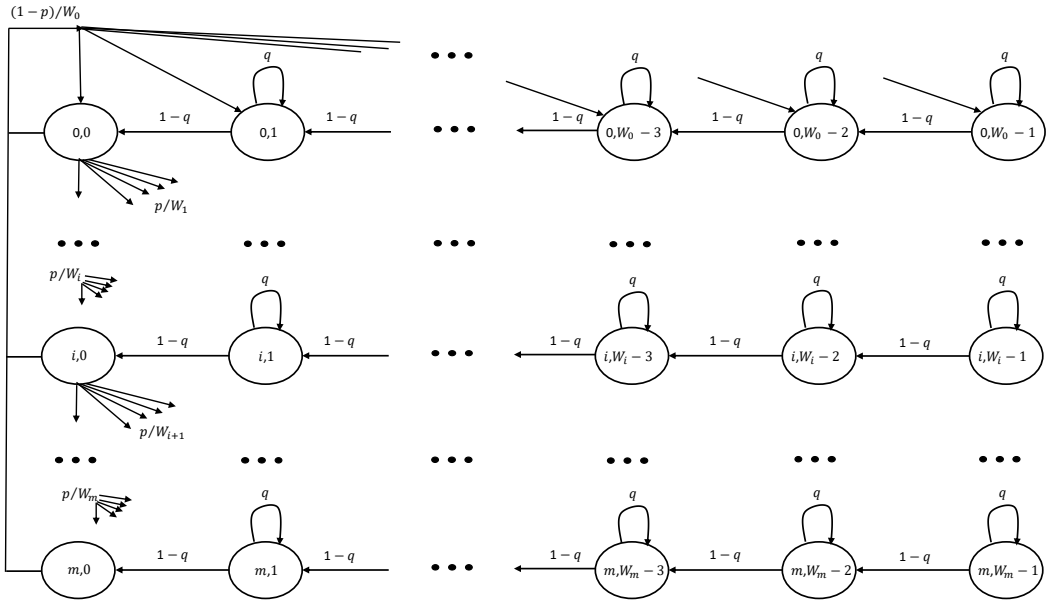

Figure 5.1: Markov chain for for the backoff window size.

Let q be the busy probability, where a node senses the channel busy due to an ongoing transmission. In that case, the backoff freezes and resumes once the channel is sensed idle. Let m be the maximum backoff stage such that $CW_{max} = 2^m W$, where W is the minimum Contention Window. The backoff window in an i backoff stage is therefore given as $W_i = 2^i W$, with $i \in (0, m)$.

After a packet collision, the node will increase its backoff stage (e.g. move from i to $i+1$) and will select a random backoff interval from the new stage with a probability of p/W_{i+1}, where p is the collision probability. The transition probabilities are given by:

$$\begin{cases} P\{i,k \mid i,k+1\} = 1 \text{ - q}, & k \in (0, W_i - 2) \text{ and } i \in (0,m) \\ P\{0,k \mid i,0\} = (1-p)/W_0, & k \in (0, W_i - 1) \text{ and } i \in (0,m) \\ P\{i,k \mid i-1,0\} = p/W_i, & k \in (0, W_i - 1) \text{ and } i \in (1,m) \\ P\{m,k \mid m,0\} = p/W_m, & k \in (0, W_m - 1) \end{cases} \tag{5.1}$$

The first case in Equation 5.1 stands for the fact, that in each slot a node decrements its backoff counter, with probability of $1-q$ or in other words the backoff counter freezes with probability q. The second case accounts for the case when a randomly backoff

counter is selected following a successful transmission (stage 0). The two other cases stand for the selection of the backoff counter after a collision at the stage $i-1$ and m, respectively. This study focuses on the first two cases to analyse the network performance in the absence of collisions, given that the STAs are located close to their APs where the increased interference that BSS Color may introduce (due to the concurrent transmission of inter-BSS packets) does not severely affect these STAs.

Let τ be the transmission probability, that can be expressed as the sum of the left-most states (when a transmission happens):

$$\tau = \sum_{i=0}^{m} b_{i,0} \tag{5.2}$$

In the absence of collisions, Equation 5.2 can be simplified and be rewritten as:

$$\tau = b_{0,0} \tag{5.3}$$

Let b_t be the stochastic process representing the backoff time counter for a given station. Now, $b_{0,0}$ can be found by making use of the following equation and given that $p = 0$:

$$\sum_{k=0}^{W_i-1} b_{0,k} = 1 \tag{5.4}$$

where the probability of $b_{0,k}$ is expressed in relationship to $b_{0,0}$ as:

$$\begin{cases} b_{0,k} = q \cdot b_{0,k} + b_{0,0} \cdot (1/W_0), & \text{with } k = W_0 - 1 \\ b_{0,k} = q \cdot b_{0,k} + b_{0,0} \cdot (1/W_0) + (1-q) \cdot b_{0,k+1}, & \text{with } k \in (1, W_0 - 2) \end{cases} \tag{5.5}$$

Finally, the transmission probability by using Equations 5.3 - 5.5 is given as:

$$\tau = \frac{2 \cdot (1-q)}{2 \cdot (1-q) + W_0 - 1} \tag{5.6}$$

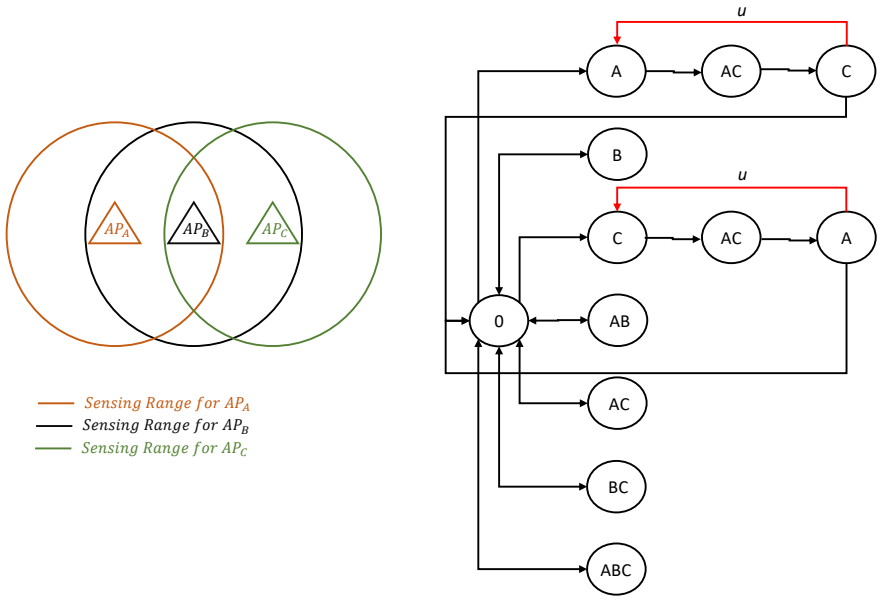

Figure 5.2: Network with exposed node and the possible states.

The only unknown in Equation 5.6 is the probability q, which is the probability that in a given time slot, at least one of the remaining nodes within the sensing range will transmit and its transmission will be seen by the node of interest:

$$q = 1 - (1 - \tau)^{n-1} \tag{5.7}$$

where $n - 1$ is the number of remaining nodes withing the sensing range.

5.2.2 Modifications to Bianchi's model

However, Equation 5.7 holds if there are no exposed and hidden nodes. In the presence of exposed nodes, the probability q for these nodes, should be higher than the one obtained from Equation 5.7 to account for the asynchronous transmissions due to the hidden nodes. In other words, the exposed node will remain in the busy state (q) for longer compared to the rest of the nodes.

A simple scenario with an exposed node is depicted in Figure 5.2, where the states for this scenario are also illustrated to visualise the impact of the extended busy duration. Note that for the exposed node, the transition probability from state C to A given

that the system was previously in AC because of BSS_A initially granting access to the medium, needs to be found. Let u be this transition probability, defined as the probability that the exposed node (i.e. B) will stay longer in the busy state due to a transmission from A or C. In particular, when the system transits from the idle state to state A, then due to the fact that BSS_A and BSS_C are hidden, it will evolve to AC and finally to C (similar behaviour is observed when the system transits from idle to C).

The transition probability u can be defined as the probability for the BSS_A recapturing the channel, with BSS_B staying in the busy state due to the late and asynchronous transmission from BSS_C. In order for BSS_B not to have the opportunity to identify the channel as idle and compete for it, BSS_A has to grant access to the medium before the end of BSS_C' transmission. Let $P\{A\}$ be the probability of the following event:

$$BO'_A < BO_C - x \tag{5.8}$$

where BO'_A is the newly selected backoff for BSS_A and BO_C the one that used by BSS_C for its late transmission and x is expressed in terms of slots with $x = DIFS/slot$. Apart from the $P\{A\}$, the probability u is also affected by the data duration, that is also expressed as $y = DIFS/Data$. Finally, u is given as:

$$u = y \cdot P\{A\} \tag{5.9}$$

Lastly, by making use of Equations 5.7 and 5.9, the busy-period probability converts to:

$$q' = (1 - (1 - \tau)^{n-1} + l \cdot u)/k \tag{5.10}$$

where l is the number of asynchronous transmissions that will extend the busy duration for the exposed node that is locked on an ongoing transmission and k is the total number of asynchronous transmissions that can occur in the deployment based on the assumption that a transmission is not seen once its preamble is missed. Further, τ is the

transmission probability for the nodes within the sensing range. For example, $l = 1$ and $k = 2$ in the case of Figure 5.2, which means that only half of the transmission will be detected by the exposed node given that it uses a very aggressive CCA/ED threshold.

Now, the throughput can be expressed as the ratio:

$$S = \frac{E[payload\ information\ transmitted\ in\ a\ time\ slot]}{E[length\ of\ a\ time\ slot]} \tag{5.11}$$

with the numerator ($E[P]$) being the average payload information transmitted in a time slot, and the denominator the average length of a time slot. The former is equal to $P_{tr} \cdot P_s \cdot E[P]$, since the probability of a successful transmission in a time slot (P_s) is $P_{tr} \cdot P_s$, where P_{tr} is the transmission probability (i.e. τ). The latter is calculated considering that a slot is idle with probability $(1-q') \cdot (1-P_{tr})$, busy with probability q', contains a successful transmission with probability $P_{tr} \cdot P_s$, and collision with $P_{tr} \cdot (1-P_s)$. Therefore Equation 5.11 becomes:

$$S = \frac{P_{tr} \cdot P_s \cdot E[P]}{slot \cdot (1-q') \cdot (1-P_{tr}) + q' \cdot T_{tr} + P_{tr} \cdot P_s \cdot T_s + P_{tr} \cdot (1-P_s) \cdot T_c} \tag{5.12}$$

where all variables in regard to time are expressed in the same units. Since in this study, collisions [3] are not considered, Equation 5.12 can be simplified to:

$$S = \frac{P_{tr} \cdot P_s \cdot E[P]}{slot \cdot (1-q') \cdot (1-P_{tr}) + q' \cdot T_s + P_{tr} \cdot P_s \cdot T_s} \tag{5.13}$$

Now, the only unknown variable to obtain throughput is T_s, which for the basic access scheme is found as:

$$T_s = H + E[P] + SIFS + \delta + ACK + \delta + DIFS \tag{5.14}$$

with H being the packet header and equal to $H = PHY_{hdr} + MAC_{hdr}$, and δ the propagation delay.

[3] The modeling of collisions is not a trivial task due to complex SNR model that ns-3 uses.

The throughput for BSS Color can be obtained based on two cases: i) if the inter-BSS packet's RSSI is above OBSS/PD, then the previous equation can be used [4] and ii) if the inter-BSS packet's RSSI is above the receiver's sensitivity but below OBSS/PD threshold then Equation 5.13 is expressed as:

$$S = \frac{P_{tr} \cdot P_s \cdot E[P]}{slot \cdot (1 - q') \cdot (1 - P_{tr}) + q' \cdot T_b + P_{tr} \cdot P_s \cdot T_s} \tag{5.15}$$

where T_b is the time required for a node to drop a frame due to the color mismatched. This is the busy interval for the BSS Color, which is equal to the time interval that is required for a node to detect the BSS Color field (HE-SIG-A1). Furthermore, l for this case is equal to the number of the maximum transmissions that a node can sense (e.g. $l = n - 1$), whilst $k = 1$ since now the packets are dropped and the node considers the channel as idle. In that case, the node starts sensing the channel activity for a duration of DIFS and then the BO mechanism is triggered again.

5.3 Model Validation and Performance Evaluation

This section presents a validation of the model against the results obtained from ns-3. The simulation settings and parameters values used in the analytical model are listed in Table 5.1. Figure 5.3 illustrates the initial scenarios to validate the analytical model.

Figure 5.4 illustrates an evaluation of the analytical model against the simulation results, obtained from ns-3. Due to the different interactions that the outer and the inner BSSs experience, different τ and q should be applied to capture these interactions. Since the inner BSSs behave similarly, based on the assumption of symmetric networks, one Markov chain is required for the inner BSSs and one for the outer BSSs. The four lines represent the simulation results for the four cases, depicted in Figure 5.3, whilst the markers are for the results obtained by the analytical model. Note that the packet size

[4] Even though the packet is dropped, the node remains in the busy state until the end of the ongoing transmission.

[5] Lock to the strongest signal during PHY Preamble and PHY HDR, whilst the Preemption Window is set to 10 dB.

[6] AIFS replaces DIFS for QoS nodes, and $DIFS = AIFS = 3 \cdot slot$, for AC_BE traffic.

Table 5.1: Simulation Parameters

Parameter	**Value**
Channel Model / Shadowing	TGax SCE3 / Disabled
Number of APs / STAs	varies / 1 per AP
Frequency Band [GHz] / Bandwidth [MHz]	5.58 / 20
Physical Capture Model	Enabled [5]
AP/STA Tx Power [dBm]	20/20, unless otherwise specified
AP/STA Antenna Gain [dBi]	0/0 (SISO)
Noise Figure [dB]	7
PHY rate [data, control]	[HE-MCS0, HE-MCS0]
Guard Interval [us]	0.8
Traffic	UDP and full buffer
RTS/CTS	Disabled
Retransmissions	Disabled
Contention Window [min,max]	varies
Packet at APP Layer [bytes]	1458, unless otherwise specified
Max A-MPDU [no. of frames]	1
Beacon	Disabled
CCA/SD, CCA/ED, OBSS/PD [dBm]	-82,50, (-82,-62)
slot, SIFS, DIFS [us]	9, 16, 27 [6]
Busy interval (BSS Color) [us]	32

at the MAC layer is 1500 bytes, including the MAC header, which is 34 bytes. The analytical model shows good match with the simulation results for various CW values, as depicted in Figure 5.4. Even for *Case (d)*, where the analytical results differ from the simulation ones by approx. 2 Mbps, on per node basis analytical results are within a range of 0.4 Mbps compared to the simulation results.

Finally, Figure 5.6 shows the performance of BSS Color against the legacy scheme for the scenario illustrated in Figure 5.5, where the ISD varies. The analytical results are also included in the figure for various packet sizes, indicated by the markers. Similar here, two Markov chains are applied, one for the central BSS and one for the outer ring. That said, only the values for l and k are accordingly set and the number of nodes within the sensing range. For convenience, the equations are listed below:

$$\begin{cases} \tau_0 = \frac{2\cdot(1-q_0)}{2\cdot(1-q_0)+W_0-1} \\ \tau_1 = \frac{2\cdot(1-q_1)}{2\cdot(1-q_1)+W_0-1} \\ q_0 = (1-(1-\tau_1)^{n_0-1}+l\cdot u)/k \\ q_1 = (1-(1-\tau_0)\cdot(1-\tau_1)^{n_1-1}+l\cdot u)/k \end{cases} \tag{5.16}$$

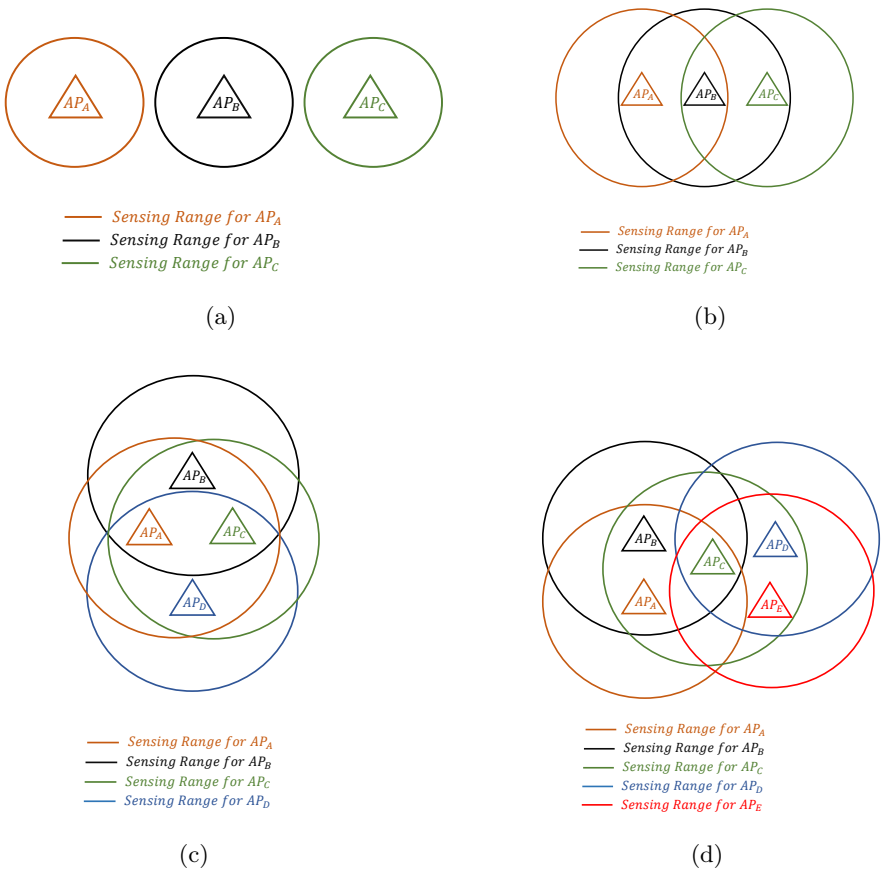

Figure 5.3: Validation Scenarios: a) non-overlapping ($l = 0$ and $k = 1$), b) partial-overlapping with one exposed node ($l = 1$ and $k = 2$), c) partial-overlapping with two exposed nodes ($l = 1$ and $k = 2$), and d) partial-overlapping with one exposed node and four hidden nodes ($l = 1$ and $k = 2$).

where $[\tau_0, q_0]$ and $[\tau_1, q_1]$ correspond to the [transmission probability, busy probability] for the central and outer BSS, respectively. Further, n_0 and n_1 stand for the nodes within the sensing range for the central and outer BSSs, respectively. In particular, the values for $[l, k, n_0, n_1]$ as the ISD decreases are $[0, 1, 0, 0], [2, 3, 6, 2], [1, 2, 6, 4]$, and $[0, 1, 6, 5]$. In order to get the maximum from the BSS Color scheme in an ideal scenario, the $OBSS/PD$ threshold should always be higher than the inter-BSS packet's RSSI, when applicable, such that a node to drop and ignore the OBSS packet and to access the channel. Therefore, the Pt for BSS Color is tuned such that $OBSS/PD > RSSI_{OBSS}$, with $OBSS/PD_{max} = -62$.

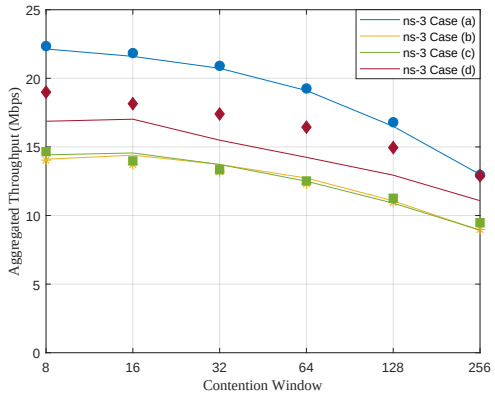

Figure 5.4: Throughput evaluation for various Contention Window sizes (number of slots), analysis versus simulation.

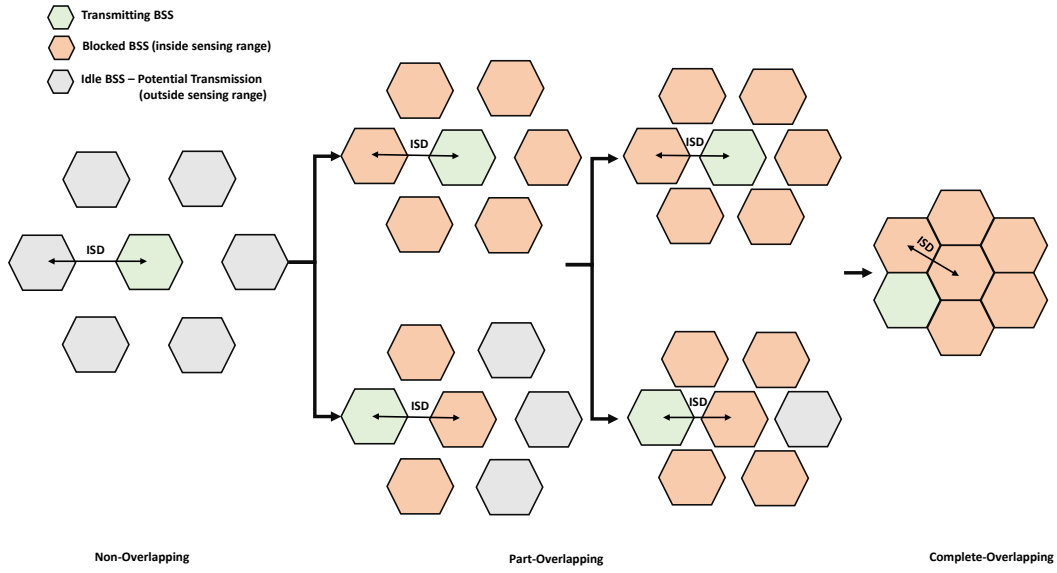

Figure 5.5: One ring deployment for various ISD values.

Three conclusions can be drawn from Figure 5.6. First, the analytical model provides good match with ns-3 under the various cases, with the accuracy improving as the packet size and/or CW increase. Secondly, it can clearly be seen that with BSS Color the throughput curve shifts to the right, meaning that the high throughput is maintained for smaller ISD, given the ideal conditions. This is the advantage of BSS Color for using OBSS/PD threshold and tuning the transmit power accordingly. Finally, the throughput gain for BSS Color is affected by the busy period that is sensed by the

nodes, which drops with the size of CW and increases with the length of packet. To capture the BSS Color performance, one can set $[l, k]$ according to the sensing range (i.e. $[1, 1]$ for both partial-overlapping scenarios).

5.4 Conclusion

This chapter provided an analytical model based on UDP traffic, which can be used as a generic framework to describe the performance of a network consisting by multiple OBSSs. The model is shown to provide good accuracy with simulation results for small cell deployments, where the nodes experience good channel conditions. The same model can also be applied to obtain the throughput for the BSS Color, by taking into consideration the OBSS/PD threshold and transmit power with respect to the sensing range. Moreover, the good potentials for the BSS Color under ideal channel conditions were observed, showing throughput gain over 100% in some cases, highlighting the importance of this SR feature on improving network performance.

Note that to accurately capture the impact of TCP on the IEEE 802.11 performance, the probability distribution functions of the TCP data segments and TCP ACK packets need to be derived. However, based on the simplified framework presented in [357], the aggregated throughput achieved by the TCP flows would be n times lower than the one achieved by n UDP flows, and is independent of the total number of persistent TCP connections.

Although, the analytical model provides good accuracy with the complex ns-3 tool, it needs to be further extended to account for packet collisions that nodes may experience, especially in large cell deployments. Furthermore, packet losses due to channel conditions need also to be accounted for, to obtain correct throughput for a network, as the increased number of concurrent transmissions that this SR feature introduces may severely affect the BSS Color performance. Also, the importance for tuning the OBSS/PD threshold is highlighted in this section that could boost network performance. To address the inherent limitations of DSC and to exploit the information carried in the BSS Color field, a new mechanism for adjusting the OBSS/PD threshold is introduced in the next chapter.

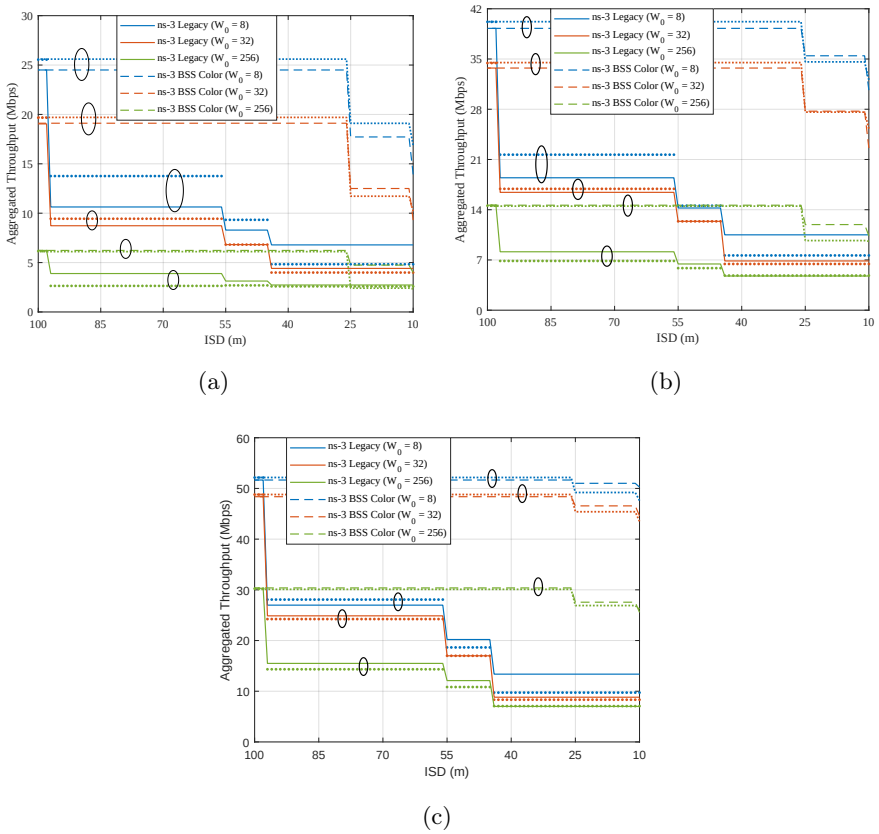

Figure 5.6: Throughput analysis in 1-ring deployment for various ISD and packet size (including MAC HDR): a) 200 bytes, b) 500 bytes, and c) 1500 bytes.

References

[354] T. Begin, B. Baynat, I. G. Lassous, and T. Abreu, "Performance Analysis of Multi-hop Flows in IEEE 802.11 Networks: A Flexible and Accurate Modeling Framework," *Elsevier*, pp. 12–32, 2016.

[355] A. Faridi, B. Bellalta, and A. Checco, "Analysis of Dynamic Channel Bonding in Dense Networks of WLANs," *IEEE Transactions on Mobile Computing*, vol. 16, no. 8, pp. 2118–2131, 2017.

[356] B. Bellalta, "Throughput Analysis in High Density WLANs," *IEEE Communications Letters*, vol. 21, no. 3, pp. 592–595, 2017.

[357] R. Bruno, M. Conti, and E. Gregori, "CThroughput Analysis and Measurements in IEEE 802.11 WLANs with TCP and UDP Traffic Flows," *IEEE Transactions on Mobile Computing*, vol. 7, no. 2, pp. 171–186, 2008.

Chapter 6

Control OBSS/PD Sensitivity Threshold for IEEE 802.11ax BSS Color

Previous chapter presented an analytical model and the good potentials for the BSS Color. However, static settings for the MAC features (e.g. CCA) have proven to provide poor performance, similar to what was observed for the BSS Color in the previous chapter. This chapter presents a novel algorithm for adjusting the $OBSS/PD$ threshold for the IEEE 802.11ax devices, by considering the channel conditions. The chapter gives significant insight into the operation of the algorithm and presents design rules that offer the flexibility of re-using and integrating the algorithm along with other MAC features. The operation and performance of the mechanism are evaluated through extensive simulations in a TGax scenario under various cases.

6.1 Introduction

Adaptive CCA thresholds and TPC have drawn increasing attention by both the research and industry communities. Nevertheless, only the usage of TPC is so far standardised by IEEE 802.11h-2003. In particular, IEEE 802.11h-2003 defines the rules

for the maximum transmit power in a region. However, TPC is selfless, meaning that nodes that applying TPC will not benefit from it (may experience low SINR), but the neighbouring nodes that do not use it (transmit at the maximum power level), will directly be at an advantage [358]. This is the main reason that TPC is not widely used in the networks and it is only applied on APs with wireless controllers. On the other hand, tuning the carrier sensing threshold would be beneficial for all nodes in a network [359], but has not been standardised due to the restrictions imposed by the IEEE 802.11 standards (i.e. reception rules and false alarm).

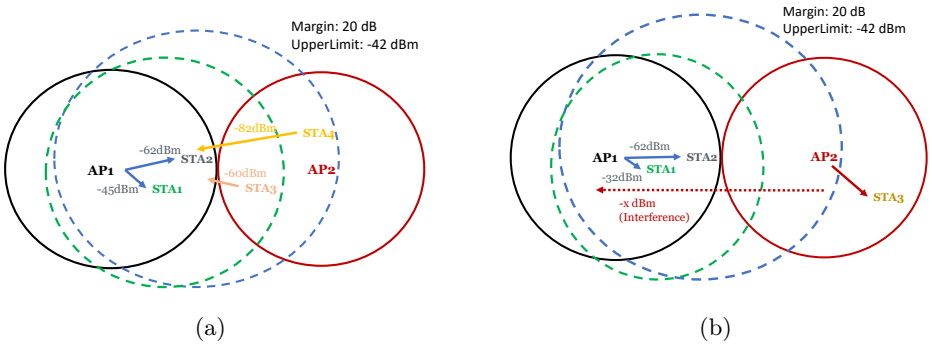

Figure 6.1: DSC limitations a) first case and b) second case.

Although, DSC was originally proposed in TGax as an SR technique for tuning CCA thresholds, it was also, recently proposed for tuning OBSS/PD [284], [360]. The main drawback for DSC is that STAs close to the AP have higher probability of accessing the medium due to higher RSSI that results into smaller carrier sensing range [278]. This case is illustrated in Figure 6.1a, where STA2 transmits only when STA4 does not transmit, even though a concurrent transmission from these STAs could be successful. Moreover, assuming that DSC is applied for OBSS/PD, then in a scenario such as the one depicted in Figure 6.1b, STA1 initiates a transmission to AP1 whereas STA2 must defer its transmission due to lower OBSS/PD. Assuming that SINR at AP1 is the same from both STA1 and STA2 (i.e. $Tx\_PWR_{STA1} = 1dBm, Tx\_PWR_{STA2} = 21dBm$), then by applying Equation 2.3 or DSC, it becomes obvious that transmission opportunity for cell-edge users further decreases for the same SINR level and the probability of a false alarm increases too. Lastly, DSC applies only at STAs and does not take into

account any changes on the OBSSs, hence it does not fully exploit BSS Color. An iterative algorithm is developed that leverages BSS Color information and the interference level measured at a node. The algorithm is able to adjust the OBSS/PD threshold and adopt to channel conditions and the interference level, by continuously monitoring the channel and recording the RSSI and interference levels.

The rest of the chapter is organised as follows. Section 6.2 presents the proposed algorithm, Control OBSS/PD Sensitivity Threshold (COST), while Section 6.3 presents the simulation scenario. Section 6.4 analyses the simulation results. Finally, Section 6.5 concludes this chapter.

6.2 Control OBSS/PD Sensitivity Threshold (COST)

To overcome DSC's limitations, the Control OBSS/PD Sensitivity Threshold (COST) algorithm is presented, which sets OBSS/PD based on the inter-BSS and intra-BSS RSSI. COST is designed to operate at both APs and STAs. The main goals for COST are: i) protecting ongoing transmissions, ii) preserving cell-edge users from starvation, and iii) preserving fairness for all nodes in terms of channel contention (roughly the same probability of transmission for all nodes). A flow chart of COST algorithm is depicted in Figure 6.2. COST is initialised following a conservative approach (OBSS/PD is set to its minimum value) for detecting majority of nodes in its vicinity. Its basic functionalities are highlighted below.

The first step (*A*) is to check BSS Color value in the HE-SIG-A field and identify whether the frame is intra-BSS (BSS) or inter-BSS (OBSS). This step is also included in the HE frame reception, nevertheless, nodes now (steps *B1, B2*), record the RSSI before abandoning or continuing the reception. In steps *C1, C2*, nodes accumulate the recorded RSSI for BSS and OBSS frames using any moving average scheme, such as Exponential Moving Average (EMA). The *WindowSize* defines the window size for the moving average scheme. If the elapsed time has exceeded *UpdatePeriod*, COST proceeds to step *E*, otherwise it awaits for the next frame to be received. For example, *UpdatePeriod* could be equal to N beacon intervals.

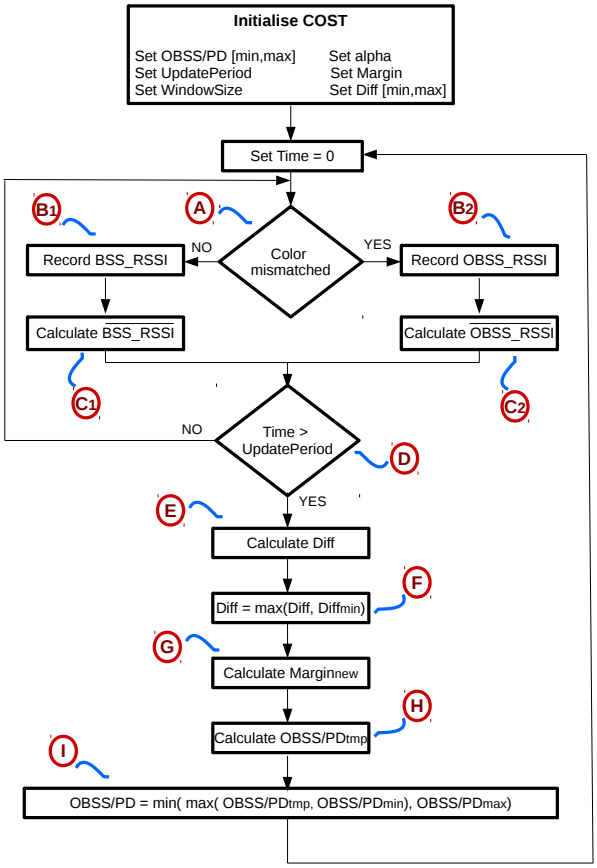

Figure 6.2: Flow chart of COST algorithm operating at both APs and STAs.

In step E, the following equation is applied:

$$Diff = \overline{BSS\_RSSI} - \overline{OBSS\_RSSI} \tag{6.1}$$

The main idea behind Equation 6.1 is the identification whether BSS STAs are closer to or not to OBSS interferers rather their BSS recipient(s), an information that is used in step G. Step F is essential to avoid a division by zero in step G, where $Margin_{new}$ is calculated according to:

$$Margin_{new} = \frac{Margin}{Diff^{alpha^{-1}}} + Margin \tag{6.2}$$

where *alpha* is an integer value that is introduced to further increase *Margin* value. Note that *Margin* operates in a similar manner as in DSC (the concept of using *Margin* derives from DSC). In some cases, a higher *Margin* might be required for a successful transmission to a cell-edge user or when high data rates are used. Thus, instead of the APs advertising the new *Margin* values, they can tune *alpha* instead, hence reducing the overhead transmitted over the channel. Figure 6.3a presents the $MarginFactor = 1/Diff^{alpha^{-1}}$, whereas Figure 6.3b the $Margin_{new}$ value for various *alpha* and *Diff* values. Four outcomes can be observed from these Figures. First, a high *alpha* value results to high $Margin_{new}$ in respect to the advertised *Margin* even for large *Diff* values ($Margin_{new} > 1.8 \cdot Margin$). Secondly, as *alpha* increases, the *Diff* value has low impact on the final $Margin_{new}$ value. Thirdly, high *Diff* values have negligible effect on $Margin_{new}$ irrespective of *alpha* and *Margin*. This can be observed by comparing the yellow and purple lines in Figure 6.3b. Lastly, the higher *Margin* is, the higher the difference of two $Margin_{new}$ values for different *Diff* values.

Due to the nature of the wireless deployments, OBSS STAs' RSSI might be higher than BSS STAs' RSSI at an AP, either because they are closer or due to shadowing. APs must ensure that BSS STAs will successfully receive the frames in the presence of OBSS STAs, hence the following calculation is performed in step *H*:

$$OBSS/PD_{tmp} = \min(\overline{BSS\_RSSI}, \overline{OBSS\_RSSI}) - Margin_{new} \tag{6.3}$$

Before setting OBSS/PD, the threshold is confined between the minimum and maximum OBSS/PD thresholds, which can be seen in step *I*. Note that, to reduce implementation complexity whilst preserving most of the gains that COST algorithm offers, some steps can be skipped for COST operating at STAs. For example, the recording of RSSI from BSS frames and step *G* can be skipped, while $\overline{BSS\_RSSI}$ can be replaced with $\overline{OBSS\_RSSI}$ in step *H*.

An additional (optional) step at STAs for setting the minimum OBSS/PD threshold could also be deployed for preserving transmission opportunity for cell-edge users. A cell-edge user can benefit from a higher OBSS/PD threshold than a user not located at the cell-edge, when roughly the same interference level is sensed by the two users. The

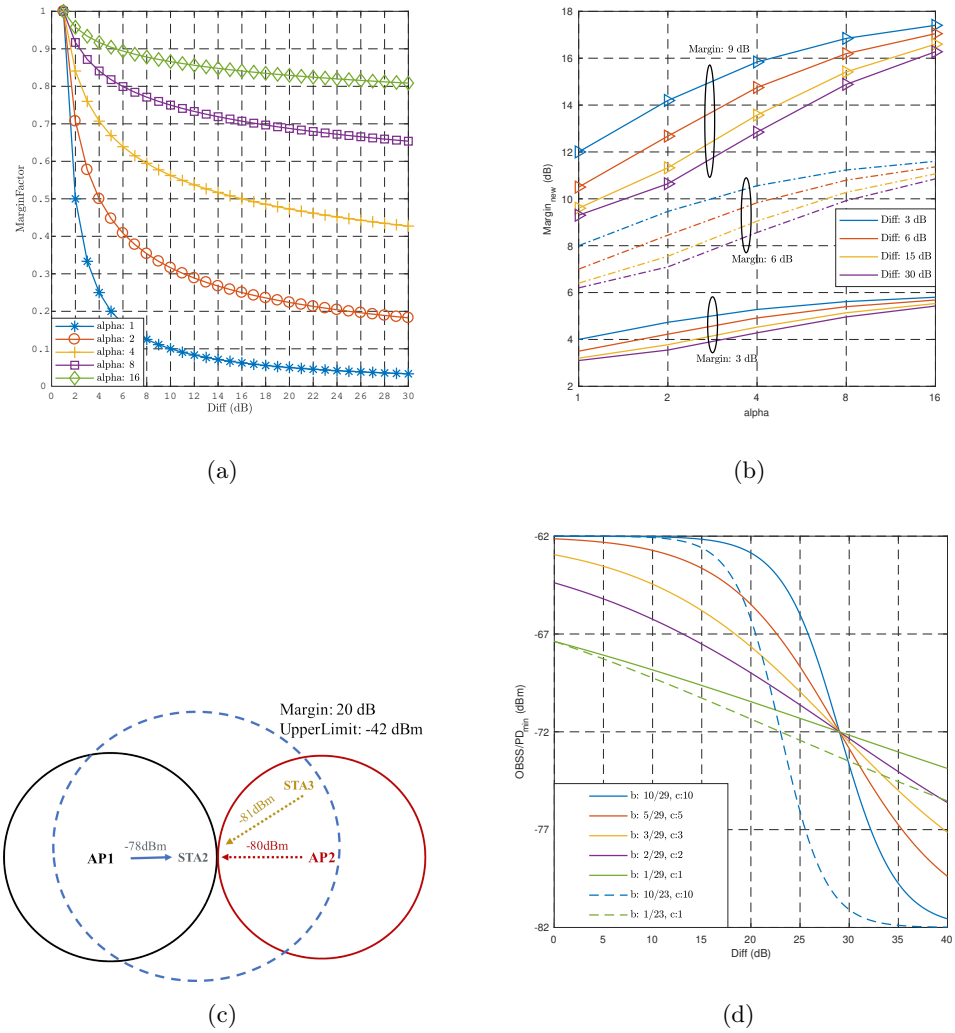

Figure 6.3: COST parameters: a) an example for *Margin Factor*, b) an example for $Margin_{new}$, c) a scenario example for the optional feature of COST at STAs, and d) an example of $OBSS/PD_{min}$.

main idea is to define a function that preserves cell-edge users from using an extremely conservative threshold, which could lead to extremely low transmission opportunities. For example, the following equation can be followed for setting the minimum OBSS/PD threshold:

$$OBSS/PD_{min} = OBSS/PD_{def} + \frac{Diff_{max}}{1 + \exp(b \cdot x - c)} \tag{6.4}$$

where $OBSS/PD_{def}$ is the default minimum value for OBSS/PD (i.e. -82 dBm for 20 MHz channel bandwidth), $Diff_{max}$ is the maximum value that can be subtracted from $OBSS/PD_{def}$. Parameter x could be either the average beacons' RSSI from the associated AP or *Diff*. *Diff* tends to zero as a user moves away from the AP, since interference level inclines whereas RSSI from the AP decays, assuming that neighbouring BSSs exist. Moreover, the parameters b and c can be adjusted accordingly, based on the decay rate or threshold we need to achieve. An example of the decrement factor of Equation 6.4 for $Diff_{max} = 20$ dB and $x = Diff$ is illustrated in Figure 6.3d. *Diff* shall be zero if $\overline{OBSS\_RSSI} > \overline{BSS\_RSSI}$. Note that the values for b and c highly affect the decline rate and the breakpoint.

6.3 Simulation Setup

The scenario illustrated in Figure 6.4 is considered, to evaluate BSS Color, DSC, and COST schemes in terms of throughput and fairness. In particular, this scenario corresponds to the Box 5 scenario from the list of TGax baseline scenarios. Four different cases are considered, including both DL and UL traffic and different patterns of the BSSs that are being enabled, following the procedure as described in [361]–[363]. In particular, the first three cases (i.e. *DL/DL*, *DL/UL*, *UL/UL*) refer to the scenarios when only BSSs A and B are enabled, whereas the last case (*DL/DL/DL*) refers to the scenario when all the BSSs are enabled. It is also assumed no color collisions, which means that BSS Color is unique for each BSS. Preamble reception and capture effect are also modelled, following the procedure described in Chapter 4. Two different data rates are used, the robust High-Efficiency Modulation and Coding Scheme 0 (HE-MCS0) and HE-MCS5, whereas the propagation model is the one defined for Scenario 3 (SCE3) in TGax. The simulation parameters used in this study are listed in Table 6.1. Note that when DSC is enabled, Equation 2.2 is applied at the APs, since DSC operates only at STAs. Moreover, a warm-up period is also considered, hence, the statistics are collected from the last 50 seconds per simulation run.

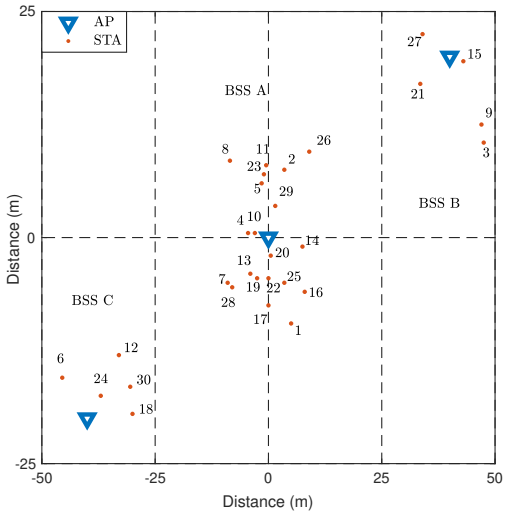

Figure 6.4: Simulation Scenario (Box 5).

Table 6.1: Simulation Parameters

Parameter	**Value**
Scenario / Channel model	Indoor (Box5) / TGax SCE3
Number of BSSs	3
Frequency Band [GHz] / Bandwidth [MHz]	2.4 / 20
Shadowing [dB]	5
Physical Capture Model	800ns/10dB
AP/STA Tx Power [dBm]	20/15
AP/STA Antenna Gain [dBi]	0/-2
Number of Antennas	1
Noise Figure [dB]	7
PHY rate [data]	HE-MCS0, HE-MCS5
PHY rate [control]	HE-MCS0
Traffic	Full Buffer
RTS/CTS	Disabled
Max Retransmissions	10
Contention Window [min,max]	[15,255]
Packet at APP Layer [bytes]	1472
Max A-MPDU [no. of frames]	32
TxOP [ms]	5.484 (AC_BE)
Beacon Interval [ms]	102.4
CCA/SD, CCA/ED [dBm]	-82,-62
OBSS/PD (min, max) [dBm]	(-82, -62)
Simulation Time per run [s]	200 (20 Runs)

6.4 Simulation Results

This section presents the performance evaluation of a) DSC and COST for various *Margin* values and b) against BSS Color (enabled and disabled) in terms of fairness and aggregated throughput. For the fairness, the Jain's Fairness Index (JFI) [341] is considered and is based on the average user throughput per BSS.

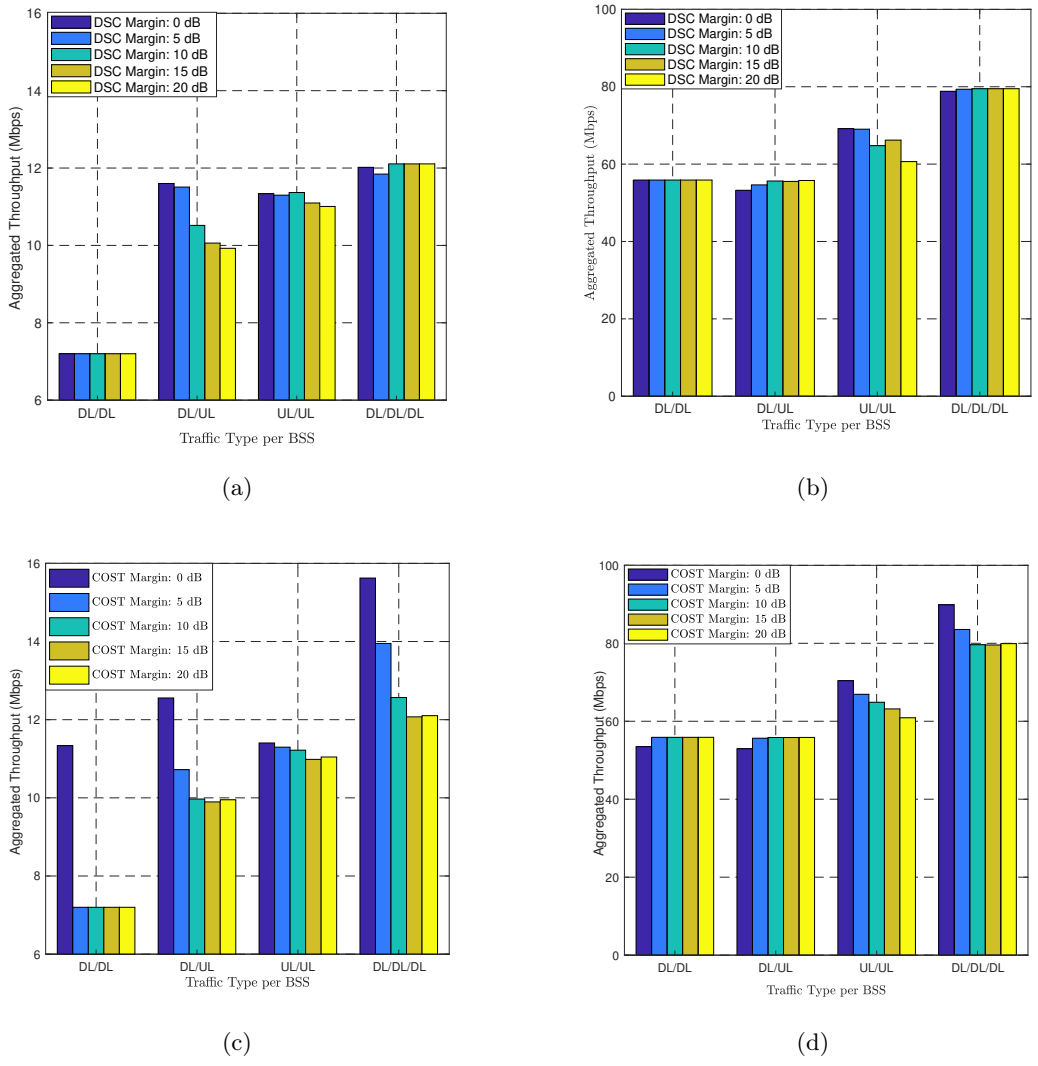

Figure 6.5: Aggregated throughput for various *Margin* values of: a) DSC for HE-MCS0, b) DSC for HE-MCS5, c) COST for HE-MCS0, and d) COST for HE-MCS5.

Figure 6.5 illustrates the aggregated throughput of DSC and COST schemes for various

Margin values. It can be observed that COST outperforms DSC in all cases, especially when a DL flow is enabled, since DSC operates only at STAs. The highest throughput for both COST and DSC when HE-MCS0 is used, is achieved for aggressive OBSS/PD thresholds (*Margin = 0*). On the other hand, when higher MCS is applied (HE-MCS5), the highest throughput is not always achieved for an aggressive OBSS/PD threshold. This is due to the higher SINR requirement for HE-MCS5, where a more conservative threshold might be required for protecting transmissions. For example, if the *DL/DL* case is compared, it can be seen that two concurrent DL transmissions can be successful when HE-MCS0 is applied, but not when HE-MCS5 is used.

Figure 6.6 depicts a comparison of the highest throughput achieved for COST and DSC with the default BSS Color and BSS Color disabled performances. Six important conclusions can be drawn from that Figure. First, with *BSS Color ON*, a throughput gain can be observed compared to *BSS Color OFF*. However, it is highly affected by the traffic type and scenario, since the use of a conservative OBSS/PD threshold might have no impact on network performance as it can be seen for the *DL/DL* case. Secondly, a higher throughput gain can be achieved by tuning OBSS/PD threshold. Thirdly, COST achieves the highest throughput gain in all the cases among the aforementioned techniques, with the exception of the *UL/UL* scenario. In particular, up to 57% throughput gain can be observed for the *DL/DL* case when COST is applied, compared to DSC, *BSS Color ON*, and *BSS Color OFF* techniques. Fourthly, throughput loss for the *UL/UL* is observed when BSS Color is enabled. This is due to the high number of contending STAs in BSS A, as it is explained in the next paragraph. Fifthly, fairness is highly affected due to the enabling of BSS Color as it can be observed in Figure 6.6c. Apart from the *UL/UL* case, in all other simulated cases, fairness among BSSs improves by the use of COST, as transmission probability among BSSs is roughly the same (e.g. *DL/DL/DL*). Note that JFI is presented only for HE-MCS0, since it does not vary significantly for HE-MCS5. Lastly, the small throughput gain in *DL/DL* for HE-MCS5 when BSS Color is enabled, is due to Extended Interframe Spacing (EIFS) that is applied after a failed reception for protecting the transmission of ACKs. In particular, when BSS Color is enabled and after a color mismatch, a node abandons the reception and does not experience EIFS. Note that EIFS has no impact in throughput when HE-MCS0 is used, as

that data rate is more resilient to low SINR.

The *UL/UL* case is now studied when the aforementioned techniques are applied, Figure 6.6d. When BSS Color is enabled, the number of contending STAs in BSS A increases compared to *BSS Color OFF*, especially for COST algorithm. On the other hand, when BSS Color is disabled, the STAs in BSS A that are located in between BSS A and BSS B may sense the channel as *BUSY* when an UL transmission in BSS B occurs, reducing the number of contending STAs in BSS A. An efficient way to reduce the collision rate in BSS A is by tuning the contention window along with CCA for intra-BSS frames. However, since tuning contention window size and CCA threshold are out of the scope of this section, the contention is decreased by reducing the number of STAs in BSS A. In particular, the number of STAs in BSS A to 6 (*STAs (1, 2, 5, 7, 25, 26)*) and to 4 (*STAs (5, 7, 25, 26)*) is reduced. A *Margin* value of 0 for both DSC and COST is used, while Equation 6.4 is also applied to limit the $OBSS/PD_{min}$ value. The values used for adjusting $OBSS/PD_{min}$ are: $OBSS/PD_{def} = -82$, $b = 3/29$, and $c = 3$. As the number of STAs within BSS A decays and the contention decreases, BSS Color performance improves. DSC outperforms COST due to the fact that the former algorithm reduces transmission opportunity for the cell-edge user, resulting in lower contention. However, when the $OBSS/PD_{min}$ is accordingly adjusted (contention may reduce), then throughput gain for COST is higher and outperforms DSC when the number of STAs in both BSSs is roughly the same.

Finally, COST is evaluated in the scenario described in [284], against the DSC algorithm for adjusting the OBSS/PD threshold, Figure 6.7. To be fair, a fixed MCS was applied for all schemes (i.e. conventional color, COST, DSC) as it was outlined in that document. It can be seen that COST outperforms DSC, but both schemes show throughput loss against the conventional HE (BSS Color is disabled). This is due to the increased interference along with the (high) fixed data rate (i.e. HE-MCS5) that cannot cope with the interference level.

After analysing the results, it can be argued that OBSS/PD threshold should be adjusted similar to CCA in order to improve network performance and to fully exploit BSS Color. The value of *Margin* for tuning OBSS/PD is an important parameter for

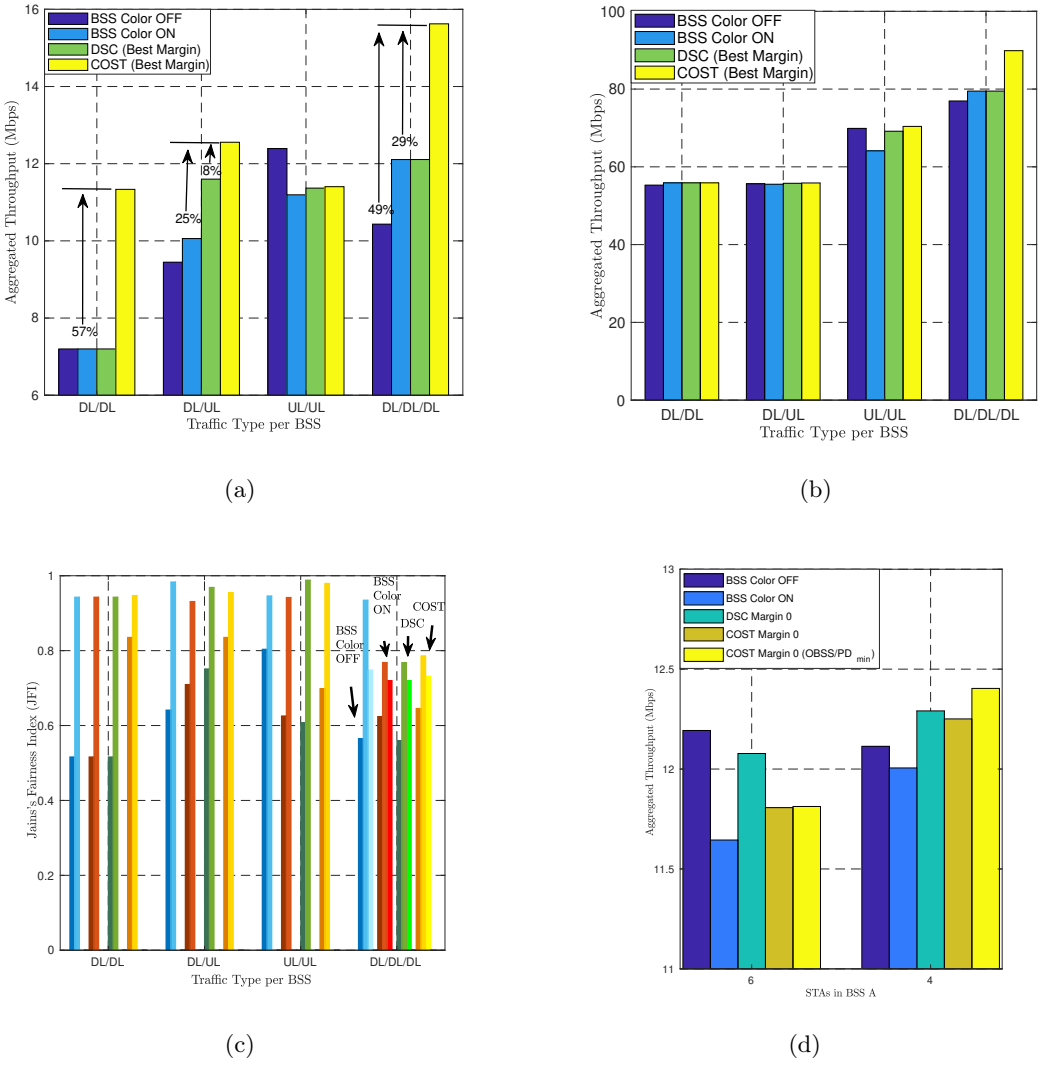

Figure 6.6: Comparison of BSS Color ON/OFF with DSC and COST schemes in terms of throughput and fairness: a) aggregated throughput for HE-MCS0, b) aggregated throughput for HE-MCS5, c) JFI for HE-MCS0, and d) study of *UL/UL* case for different BSS A STA density.

both the DSC and COST algorithms and has significant impact on throughput gain. COST achieves higher throughput gain than DSC in most of the cases (up to 57% for *DL/DL* case), as it takes into account changes occurring in OBSSs. On the other hand, by preserving fairness for users in a BSS, contention among them increases, hence, the throughput loss observed in Figure 6.6a for the *UL/UL* case. However, contention

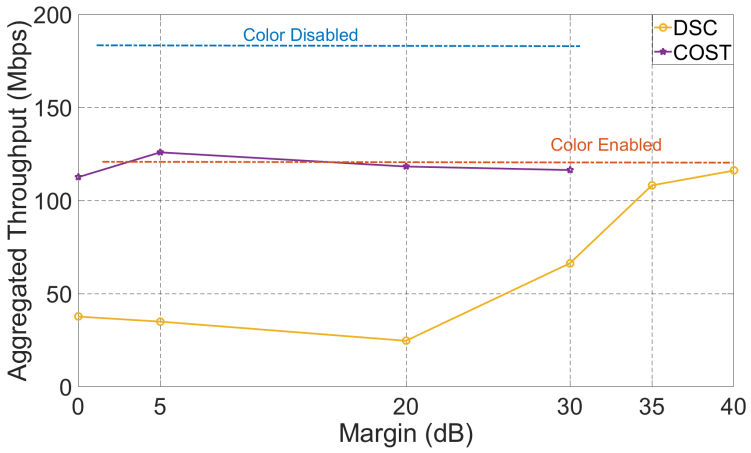

Figure 6.7: Performance evaluation of COST and DSC in a dense deployment.

among users can be managed by other means specifically designed to cope with it (i.e. CCA, contention window etc.).

6.5 Conclusion

This chapter investigated the performance of a newly introduced IEEE 802.11ax feature, i.e. BSS Color and the impact of OBSS/PD threshold in various cases. COST, an algorithm for adjusting OBSS/PD at both APs and STAs that does not require major modifications in MAC layer is also proposed and introduced here. In particular, the main modifications required on MAC layer to support the COST algorithm include: i) signalling of RSSI and interference level from PHY to MAC layer and ii) an internal signalling to update the OBSS/PD threshold. Due to the use of *alpha*, the *Margin* value could be advertised only with the beacons sent by the APs, therefore the overhead can be considered negligible.

COST adjusts OBSS/PD based on the interference level observed and the RSSI from the associated recipient(s). It was also compared against DSC, an algorithm that was initially proposed for adjusting CCA, but was also proposed in TGax for OBSS/PD threshold adjustment. It was showed that COST outperforms the aforementioned schemes (up to 57% in terms of throughput gain) in most of the simulated cases, while preserving fairness among the users. On the other hand, COST increases the transmission oppor-

tunities for STAs (roughly the same probability for all users within a BSS), resulting in higher contention level too. However, user contention can be managed by other means that are specifically designed to deal with it, such as the CCA threshold and the contention window size.

Although, COST improves the performance in terms of throughput and fairness, the main challenge is to correctly set the *Margin* value based not only on the interference level but on the MCS. The rationale behind this is the different SNR (SINR) requirements for the various MCSs. The higher the MCS is, the higher the *Margin* value should be to protect the transmission. This means, the nodes should be capable of selecting the *Margin* locally, based on the available information and the rate they use. To this extend, a new novel rate control algorithm that incorporates COST, is developed and presented in the next chapter.

References

[358] G. Smith, "Document (IEEE 802.11-18/1531r3): TGax Spatial Reuse DSC and TPC," Tech. Rep., 2018. [Online]. Available: `https://mentor.ieee.org/802.11/dcn/18/11-18-1531-03-00ax-spatial-reuse-dsc-and-tpc.pptx`.

[359] J. Zhu, X. Guo, L. L. Yang, and W. S. Conner, "Leveraging Spatial Reuse in 802.11 Mesh Networks with Enhanced Physical Carrier Sensing," *IEEE International Conference on Communications (IEEE Cat. No.04CH37577), Paris*, vol. 11, pp. 4004–4011, 2004.

[360] G. Smith, "Document (IEEE 802.11-17/0163r3): DSC as OBSS_PD," Tech. Rep., 2017. [Online]. Available: `https://mentor.ieee.org/802.11/dcn/17/11-17-0163-03-00ax-dsc-as-obss-pd.pptx`.

[361] J. Pang, H. Su, C. Ma, J. Zhang, "Document (IEEE 802.11-14/1177r2): Discussion about Box5 Calibration," Tech. Rep., 2014. [Online]. Available: `https://mentor.ieee.org/802.11/dcn/14/11-14-1177-02-00ax-box5-calibration-discussion.pptx`.

[362] ——, "Document (IEEE 802.11-14/1441r0): Simulation Setting of Box5 Calibration," Tech. Rep., 2014. [Online]. Available: `https://mentor.ieee.org/802.11/dcn/14/11-14-1441-00-00ax-simulation-setting-of-box5-calibration.pptx`.

[363] S. Kim et al., "Document (IEEE 802.11-14/1392r1): Simulation Results for Box 5 Calibration," Tech. Rep., 2014. [Online]. Available: https://mentor.ieee.org/802.11/dcn/14/11-14-1392-01-00ax-simulation-results-for-box-5-calibration.ppt.

Chapter 7

Damysus; A Practical IEEE 802.11ax BSS Color Aware Rate Control Algorithm

Previous chapter presented a novel algorithm, namely COST, for dynamically adjusting the OBSS/PD threshold based on the interference level. Although, COST could improve throughput and fairness for the nodes, it does not completely operate locally. The value of *Margin* may significantly affect the performance, was left to the discretion of the manufacturers. This means that either a static value could be set based on the type of a node (i.e. AP or STA) or the value could be obtained from the APs (information carried on the header of the management frames, e.g. beacons). Either way would result in un-utilised spectrum and overhead.

This chapter presents Damysus, an algorithm proposed here to cope with the additional overhead that COST may introduce. Damysus is a rate control algorithm that functions in a completely local way by incorporating COST mechanism for tuning the OBSS/PD threshold. Along with the OBSS/PD threshold, Damysus determines *Margin* based on the rate used for a transmission. The operation and performance of Damysus are explained and evaluated through extensive simulations in various TGax scenarios against other off-the-shelf rate control algorithms.

7.1 Introduction

The main motivation to advance COST and to develop a rate control algorithm is due to the diverse environments, each one with different challenges and requirements. This chapter introduces Damysus, a rate control algorithm that operates hand in hand with the BSS Color scheme and leverages the SR features.

The rest of the chapter is organised as follows. Section 7.2 presents related work with respect to the available rate control algorithms. Section 7.3 overviews the concept and design of the proposed rate control algorithm for further improving the network performance in the presence of BSS Color, while Section 7.4 analyses the simulation results in various scenarios. Finally, Section 7.5 concludes the chapter.

7.2 Background

Multirate selection algorithms are an efficient approach to improve network performance. The IEEE 802.11 standard does not mandate the use of a specific rate selection algorithm, which is left to the discretion of the IEEE 802.11 drivers and chipsets manufacturers. This has led to the design of various rate selection algorithms that follow different strategies to adapt the rate.

These strategies fall into two categories; the packet loss-based and the SNR-based approaches. There are in general, two possible causes of packet loss: i) packet collisions due to the hidden nodes problem and ii) weak received signal due to channel fading (low SNR) or strong interference (low SINR). There have been proposed a few schemes that aim to differentiate the cause of packet loss and they mainly rely on the use of control frames (i.e. RTS/CTS). The SNR-based algorithms adapt the rate based on the RSSI measurements. However, there might be an up to 14 dB uncertainty of estimating the SNR due to multipath and link asymmetry (i.e. DL and UL) [364]. This uncertainty can be addressed by incorporating the IEEE 802.11k amendment where nodes can request for the Radio Management capability Information Element in the beacon (e.g. RSSI measurements).

The first rate selection algorithm ever introduced for the IEEE 802.11 WLANs is the Auto Rate Fallback (ARF) [365]. The ARF scheme is an easy to implement algorithm that selects the rate based on the number of successful transmissions. In particular, ARF moves to the next highest rate after X successful transmissions (where the default $X = 10$) or to the next lowest rate after a packet transmission failure. The Adaptive ARF (AARF) [366], is a variant of the ARF algorithm that was introduced to improve the network performance in stable environments. AARF uses the history of the channel to adapt the threshold of the successful transmissions before selecting a higher rate. Similar to the ARF algorithm, the AARF reduces the rate after an unacknowledged transmission, while it doubles the threshold when the first transmission with the new selected rate fails (i.e. $2 \cdot X$). Otherwise, the threshold is reset to its default value. In that way, the AARF algorithm produces fewer rate fluctuations than the ARF scheme and enhances the performance under stable channels [367]. Although, these approaches (ARF variants) offer low complexity and are easy to implement, they provide poor performance as they do not differentiate the packet losses (collision or not), thus a lower rate may increase the probability of packet loss due to the longer transmission time (i.e. in the presence of hidden nodes).

Onoe [368] is a well known algorithm that was the first developed and integrated into the MadWifi drivers (Linux kernel drivers for WLANs). Onoe is a credit-based algorithm that adapts the credit threshold at the end of each cycle (i.e. 1 seconds), based on the transmission statistics collected in this cycle. The rate is deducted when at least 1 retransmission on average (for each packet) has occurred and is increased when the credit exceeds a predefined threshold (e.g. 10). Now, the credit is increased when less than 10% of the packets required a retransmission. Although, Onoe is less sensitive to packet failures than the ARF algorithm, it is more conservative and shows slow responsiveness to changes in the channel conditions (i.e. it will take up to 10 seconds to increase the rate). In contrast to Onoe, the SampleRate [369] algorithm selects the rate based on the number of successful transmissions, the number of failures, and the transmission time. It calculates the success probabilities using the Exponential Weighted Moving Average (EWMA) and selects the rate that provides the highest throughput. SampleRate periodically also transmits packets on a different rate to estimate their per-

formance (training). The main drawback of SampleRate is its slow response to changes in the channel (mobile or fast-fading), as the training phase may take up a few seconds (approximately 30 seconds).

Minstrel [339] can be considered as an advancement to the SampleRate algorithm that is based solely on the acknowledgment feedback and its historical data for a specific rate. It was developed for the MadWifi drivers to address the slow responsiveness and reliability issues of SampleRate. Although, it was introduced more than a decade ago, it is the one that is currently used in most of the devices (i.e. Linux distros, mobile devices etc.). Note that rate control algorithms are not part of the IEEE 802.11 standardisation, but is left to the discrepancy of the manufacturers. Nevertheless, Minstrel has been extended to support the IEEE 802.11n/ac rates (i.e. Minstrel HT), which is its current status. Minstrel also makes use of the EWMA mechanism to smooth the probability estimation and uses a smoother function than SampleRate for the throughput estimation [370]. To avoid excessive sampling, only 10% of the frames are used for sampling new rates and the transmission of two consecutive probes is prohibited. Minstrel also supports a multi-rate retry chain to quickly respond to channel changes. First, it transmits on the data rate that achieves the highest throughput for a specific number of attempts (e.g. c0). If the transmissions are not successful, then it will select a random rate and will try for c1 times ($min(random, highest_{throughput})$). The third rate to be selected if none of the aforementioned have succeeded is the one with the highest successful rate (c2 attempts) and the last in the list is the lowest available rate (c3 attempts). However, Minstrel's tendency to select high data rates has one major drawback: it shows a poor performance when the channel conditions deteriorate and the RSSI falls from high to low values [371].

Collision-Aware Rate Adaptation (CARA) [372] relies on RTS/CTS to differentiate packet losses (i.e. due to the channel conditions or due to packet collisions). Although, CARA is introduced for IEEE 802.11 WLANs with multiple nodes, the use of the control frames has a significant impact on the network performance and only partially eliminates the hidden node problem. The authors in [373] propose a joint TPC and rate control algorithm for improving the spatial reuse and the network throughput in dense deployments. It requires the explicit coordination among the APs for setting

the same transmit power level due to the selfless behaviour of the TPC schemes. The work in [374] presents the Rate Selection for Industrial Networks (RSIN) algorithm, aiming at minimizing the Packet Error Rate (PER), while taking into account the delay restrictions on per-packet basis. RSIN can be considered as an optimisation problem that relies on the SNR value that is attached as an additional field on the packets' header, the PER for a specific rate and SNR, and the delay requirements.

The proposed algorithm, Damysus was conceived by observing i) the lack of most rate control algorithms to integrate fundamental MAC functionalities and incorporate new techniques introduced in the recent amendments and ii) the throughput loss for Minstrel when the BSS Color is enabled (Minstrel could not cope with the higher interference level).

7.3 The Damysus Algorithm

The development of Damysus is based on the observation that most of the available control algorithms do not fully exploit the MAC features (e.g. CCA adaptation) and the available information that can be extracted from the IEEE 802.11 packets. Furthermore, existing approaches provide poor performance under various dense deployments as they were initially designed for simple (small) indoor scenarios and they offer limited flexibility when it comes to integrating features introduced in the latest amendments (e.g. IEEE 802.11ax).

To address these challenges, Damysus attempts to select a rate that is characterised by high delivery probability, given the network conditions (e.g. SNR, interference level etc.). It also exploits the SR mechanism of the IEEE 802.11ax by integrating the COST scheme, introduced in the previous chapter, that adapts the OBSS/PD threshold and jointly adjusts the transmit power level. The main goals for Damysus are: i) select an appropriate rate close to the maximum achievable one that also provides stable results, ii) show robustness when channel conditions deteriorate (e.g. reduce the rate by selecting a lower one) where Minstrel fails and ameliorate the network performance in the presence of BSS Color, iii) select the rate without any additional overhead introduced, and iv)

exploit the SR mechanism of the IEEE 802.11ax to improve efficiency and network throughput in dense deployments.

The first step for Damysus is to construct a table and map the SNR with the MCS and the PER. This step is optional and can be disregarded from Damysus to reduce complexity. Further, the algorithm records the RSSI from the recipient node (e.g. the associated AP/STA) and accumulates the recorded value, using any moving average scheme, such as the Exponential Weighted Moving Average (EWMA) used for the DSC algorithm. The estimation of the path loss can be obtained by incorporating the TPC feature of the IEEE 802.11h that defines the maximum transmit power level for the specific BSS. The IEEE 802.11h specifies two ways to obtain the TPC information [375]: i) advertising the maximum transmit power in the management frames (i.e. beacons and probe responses) and ii) requesting the TPC Report element, a frame that holds information about the transmit power and the link margin. Note that the control and managements frames are all sent using the highest allowable transmit power level and all the statistics obtained are held on per associated node-basis.

When the algorithm initiates its first transmission (e.g. after an association), if it does not possess any statistics, it will make use of the next highest available rate that the control frames (e.g. association frames) were transmitted (i.e. HE-MCS1). Furthermore, based on the selected rate, Damysus will tune the transmit power level to protect inter-BSS transmissions while the SNR requirement is satisfied. To cope with the SNR uncertainty due to the multipath, a margin is added to the path loss estimation (e.g. 9 dB).

Damysus also exploits the IEEE 802.11ax BSS Color by distinguishing the inter-BSS and intra-BSS frames and recording the corresponding RSSI values. Those values are used to estimate the interference level, an information that is applied for adjusting the OBSS/PD threshold according to the COST algorithm.

Now, focusing on the rate selection, Damysus uses two thresholds (i.e. *succThres* and *failThres*) that correspond to the minimum number of consecutive successful and failed transmissions respectively, before the selection of a new rate. The rationale for using those two thresholds is to achieve stability and prohibit Damysus from using an inap-

propriate rate. A transmission is considered successful when it is acknowledged for the case of non A-MPDU and when a sufficient number of packets have been successfully delivered in the case of the Block-Ack mechanism (under aggregation and TxOP). For the latter case, the *ampduSucces* variable is defined, that specifies the success rate threshold (in %), which determines the outcome of the transmission under a Block-Ack (success or not). For example, if 10 packets are aggregated and 8 of them have been correctly received, with $ampduSucces = 70$ the transmission will be defined as successful.

Furthermore, Damysus keeps the historical data for a specific rate per node (i.e. recipient that associates with) and calculates per interval (e.g. 100ms) and per cycle (where cycle > interval, e.g. 1sec when the OBSS/PD is updated) the following:

- *intervalRateSuccess*, the number of packets succeeded per interval,
- *intervalRateTxFrames*, the total number of the packets transmitted per interval,
- *numRateTxFrames*, the number of packets transmitted per cycle,
- *numRateTxAttempts*, the total number of transmission attempts per cycle (aggregated frame transmission is considered as 1),
- *throughput*, based on the packets transmitted and the success rate per interval and smoothed out with a moving average scheme,
- *ewmaProb*, the success rate probability based on the success rate per interval and smoothed out with the EWMA.

The *throughput* and *ewmaProb* variables are initialized to zero during the association/dissociation or after long periods of inactivity. The *ewmaProb* is calculated based on the Equation 7.1:

$$ewmaProb = \frac{succProbTrans \cdot (100 - ewmaLevel) + ewmaProb \cdot ewmaLevel}{100} \tag{7.1}$$

where the *ewmaLevel* is the EWMA (e.g. $ewmaLevel = 75$) and

$$succProbTrans = 100 \cdot \frac{intervalRateSuccess}{intervalRateTxFrames} \tag{7.2}$$

Apart from the metrics per node related to rate, Damysus maintains statistics also per node unrelated to rate, such as:

- *nSuccess*, the number of successful transmission attempts,
- *nFail*, the number of failed transmission attempts,
- *lastMcs*, the last MCS used for a specific recipient,
- *avPL*, the path loss per recipient,
- *lastTxPwr*, the last transmit power level used for a specific recipient,
- *TxPwrFlag*, determines whether the transmit power level can be decreased and the minimum power level.

The *TxPwrFlag* variable is set to false when the transmit power level has been increased after a few failure attempts in order to prevent an immediate deduction of the power level after a few successful transmissions. It is also set to true and the TPC is allowed, only when the current rate statistics are sufficient good (e.g. high *ewmaProb*).

After the *succThres* condition is triggered, the algorithm will either select a higher rate (if certain conditions are met) or keep the current rate and may adjust the transmit power level and/or the OBSS/PD threshold. Damysus maintains the same rate when the current rate has good properties (i.e. high *ewmaProb* that is also higher enough than the next highest rate's) and both the current and the next highest rates have a sufficient number of attempts per cycle. In that case, Damysus will report (internally) a high interfering OBSS signal (i.e. $RSSI = OBSS/PD_{max}$) to influence the selection of the OBSS/PD threshold towards a more aggressive threshold and may decrease the transmit power level by a specific value (e.g. *TxPowerStep*) if the new transmit power is sufficient enough for the given rate.

On the other hand, the rate is increased in two cases: i) when both the current and the next highest rates are characterised by good properties or the latter rate has a low number of packet transmissions and attempts or never used before, and there is a transmit power level for the next rate (that does not exceed the maximum allowed

transmit power) and ii) when a non suitable transmit power level has been found for the next highest rate, Damysus will search among a few higher rates and will select the one (if any) that meets the following criteria: it has high *ewmaProb* and is the highest among the rates that are being looked at or it provides the highest *throughput*. A more detailed description of the Damysus operation in the case of the *succThres* is given in the Appendix B. Furthermore, the upper limit for the rates range that Damysus will be looking at in the (ii) case, is restricted by the following equation:

$$UpperMCS = round(\frac{(MaxGroupMCS - 1) - lastMcs}{4}) \tag{7.3}$$

where *round* will return the nearest possible integer value that is greater than or equal to a given argument and *MaxGroupMCS* is the maximum number of MCSs supported for a specific group of rates (i.e. 12 MCSs are supported per group for the IEEE 802.11ax). For example, the space that Damysus will search for a new rate (under condition (ii)) when $lastMcs = 0$ is [MCS1, MCS3]. Note that *round* could be replaced with *ceil* to make Damysus more aggressive in choosing higher rates.

In the case that the *failThres* condition is triggered, i.e. after X failed transmissions, Damysus will undergo the recovery operation for selecting a lower rate or searching for a rate that is characterised by good properties. To prevent Damysus from slowly adapting the rate, especially when the $failThres$ is set to a high value, the algorithm will first try to address the packet losses by increasing the transmit power level and reducing the OBSS/PD threshold, thus improving SINR. If the number of failed transmissions has reached the 30% of the *failThres*, Damysus will increase the transmit power level exponentially and influence the selection of the OBSS/PD threshold towards a more conservative value. The transmit power level for that case is set according to:

$$TxPwr = min(TxPwr + ceil(e^{(TxPwr_{step} + ceil(0.3 \cdot failed))}), TxPwr_{max}) \tag{7.4}$$

where $TxPwr_{step}$ is the step for tuning the transmit power level and *failed* is the number of failed transmissions. If the rate for *failed* is above 30% and the *failed* number below

the *failThres*, the transmit power level is defined as:

$$TxPwr = min(TxPwr + (factor \cdot TxPwr_{step}), TxPwr_{max}) \tag{7.5}$$

where $factor = failThres - failed$. If the transmit power level is tuned according to one of the Equations 7.4 and 7.5 then the *TxPwrFlag* is set to false.

Once the *failThres* is triggered, there are three cases in respect to the rate: i) use of a lower rate, ii) set the rate based on the statistics collected, and iii) maintain the same rate. First, Damysus will check whether the current rate has few tries and bad properties (i.e. $ewmaProb_c < ewmaTemp$). If so, it will search for potential rates based on the $TxPwr_{max}$ and the interference level according to:

$$rate_{interf} = min(max(mcs_c - max(mcs_c - diff, 0), 0), 11) \tag{7.6}$$

where $rate_{interf}$ is confined between $[0, 11]$ that is the range for the HE-MCS, mcs_c is the current rate, and diff is given from:

$$diff = 6 - \frac{min(|Interference - OBSS/PD_{max}|, 20)}{4} \tag{7.7}$$

where $Interference$ is the recorded interference level based on the color mismatch. The parameter *diff* is confined between $[1, 6]$ to avoid high fluctuations on the rate selection. If $Interference > OBSS/PD_{max}$ then $diff$ is deducted by 1 to account for the high interference level. The $rate_{PwrMax}$ that was selected based on the $TxPwr_{max}$, is adjusted based on the:

$$rate_{PwrMax} = min(max(rate_{PwrMax} \cdot ewmaProb, 0), 11) \tag{7.8}$$

The rate selected under this first condition is finally given by the:

$$rate = \begin{cases} max(rate_{interf}, rate_{PwrMax}), & \text{if } nSuccess \geq 0.6 \cdot succThres \\ max(rate_{interf}, rate_{PwrMax}) - 1, & \text{if } nSuccess \geq 0.4 \cdot succThres \\ min(ceil(((rate_{interf} + rate_{PwrMax})/2), & \\ max(rate_{interf}, rate_{PwrMax}) - 1), 0), & \text{otherwise} \end{cases} \tag{7.9}$$

The constant values 0.6 and 0.4 that define the thresholds, have been found to provide good performance in various scenarios. In particular, if a conservative value is used (i.e. > 0.9, the node will never try (in most of the real-world scenarios) a higher MCS. On the other hand, an extremely low constant value would result to higher probability for Damysus of using the higher MCSs, falling into the same pitfalls that MinstrelHT does.

The second condition that will be checked against, accounts for the case where $mcs_c = 0$ with quite a few tries on that rate and bad properties. In that case, the rate will not change, whilst the transmit power level will be set to its maximum value and the OBSS/PD threshold will be reduced (influencing the selection of the threshold).

If none of the above two conditions are true, Damysus will search all available rates for a potential rate, based on the statistics collected. If less than two rates have been tried in the last interval whilst the statistics for the *ewmaProb* and *throughput* are not yet available, Damysus will reduce the rate by 1 for the new set of transmissions due to the uncertainty about the channel conditions. If the statistics for more than 4 rates are available and $ewmaProb_{best} < 50$ then the new rate will be set according to:

$$rate = \frac{mcs_{best} \cdot 0.1 + ewmaMcs_{best} \cdot 0.1 + mcs_c \cdot 0.2 + rate_{PwrMax} \cdot 0.6}{4} \tag{7.10}$$

where mcs_{best} is the rate with the highest throughput and $ewmaMcs_{best}$ the rate with the highest *ewmaProb*. Else if the current rate has either high *ewmaProb* or high interval success rate, it will be maintained the same for the next transmissions. Finally, if Damysus fails to trigger one of the above conditions, it will select the mcs_{best} or the

$ewmaMCS_{best}$ based on their properties. A more detailed description for the case of the *failThres* is given in Appendix C.

Apart from the rate and the TPC, Damysus also controls the OBSS/PD threshold by using the core functionality of the COST algorithm. However, Damysus advances COST's functionality by adapting the *Margin* value, specific to channel conditions and the rates used. The rationale for this operation is to protect the transmissions in the presence of high interference and/or when high MCS is to be used, by enabling a more conservative OBSS/PD threshold (i.e. higher *Margin*). Hence, the following equations, operations, and the constant variables for adapting the *Margin* are defined.

In particular, Damysus calculates the channel occupancy of the inter-BSS packets based on the BSS Color by using any moving average scheme. It also records the channel occupancy (for the inter-BSS packets) for the downlink transmissions by exploiting the *UL_Flag* feature and computes the first potential *Margin* as:

$$Margin_{first} = \begin{cases} \frac{chan_{occ}}{10} + 3, & \text{if } chan_{occ}^{DL} > chan_{occ}^{UL} + 3 \\ \frac{chan_{occ}}{10}, & \text{otherwise} \end{cases} \tag{7.11}$$

where $chan_{occ}$ is the channel occupancy for the inter-BSS packets. In the case that inter-BSS DL packets dominate the channel, an additional 3 dB value is added in the $Margin_{first}$ to protect the transmissions to the STAs. Note that in the literature [376]–[378], a value of between 1-4 dB is typically considered as the minimum SNR required for a Wi-Fi signal to be detected (preamble), hence the value of 3 dB. Equation 7.11 is applied only when $chan_{occ} > limitThres$, where it is set $limitThres = 20 * 0.6 = 12$, for 60% MAC efficiency and 20% occupancy from the OBSSs. The second *Margin* value is calculated based on the recorded inter-BSS and intra-BSS $\overline{RSSI}$. First, the *Margin* for the intra-BSS $\overline{RSSI}$ is calculated as:

$$Margin_{second} = beta \cdot (|\overline{RSSI}| - alpha)^3 + ceta \tag{7.12}$$

where *alpha* is a constant variable confined in the space [42 82]. The default values of *alpha* are 42 (aggressive value) and 62 (moderate value) for the STAs and APs, respectively. Note that a power of 3rd is applied, due to the properties of x^3. In

particular, when a STA is located close to an AP, the term $(|\overline{RSSI}|-alpha)^3$ would result in a very low value, hence a small $Margin_{second}$, meaning that the STA could use an aggressive $Margin_{second}$ for the inter-BSS packets. On the other hand, as the STA moves further from the AP, the $Margin_{second}$ would gradually increase, after some point where the increase would be exponential (i.e. cell-edge STA). The variable *beta* is given by the Equation 7.13:

$$beta = \frac{Margin_{max}}{(RSS_{max} - alpha)^3 - (RSS_{min} - alpha)^3} \tag{7.13}$$

with $RSS_{max} = 82$, $RSS_{min} = 42$, and $Margin_{max} = 12$. The *ceta* argument is defined according to the following equation (following the same principle of Equation 7.12):

$$ceta = -1 \cdot beta \cdot (RSS_{min} - alpha)^3 \tag{7.14}$$

with its value acting as a guard for the $Margin$ calculation (e.g. given the values described earlier, higher guard value will be applied for the APs due to *alpha*, in order to protect transmissions to cell-edge STAs).

The calculation for the inter-BSS $\overline{RSSI}$ *Margin* follows the Equation 7.12, but this time $alpha = 72$ and 42 for the STAs and APs, respectively and it is combined with the $Margin_{first}$:

$$Margin_{first} = Margin_{const} - (Margin_{first} + Margin_{second}) \tag{7.15}$$

where $Margin_{const} = 15$ and 10 (in dB) for the STAs and APs, respectively. The values for $Margin_{const}$ were defined in a way to confine the $Margin$ between [3, 21] for the APs and [6, 21] for the STAs. This means that $Margin$ will never be 0, hence to protect any inter-BSS transmissions and will be no higher than 21 dB (i.e. based on the values that have been found for $Margin$ when applied on DSC [284], [335] and the equation provided in [267] where transmit power is inversely proportional to OBSS/PD with a value of 21 being used as a reference). Finally, the value of the *Margin* is defined as:

$$Margin = max(Margin_{first}, Margin_{second}) + Margin_{mcs} \tag{7.16}$$

where $Margin_{mcs}$ is the additional *Margin* due to the MCS used. In particular, this extra *Margin* is applied to ensure that low OBSS/PD threshold is used with high MCSs and it is given as:

$$Margin_{mcs} = \overline{MCS} \cdot (\frac{OBSS/PD_{step}}{OBSS/PD_{step} + 0.5}) \tag{7.17}$$

From the Equation 7.16 the minimum *Margin* can be derived for the APs and STAs, which are 3 dBs and 6 dBs, respectively. The maximum *Margin* is approximately 21 dBs, given that the highest MCS is used (i.e. $\overline{MCS} = 11$, HE-MCS11).

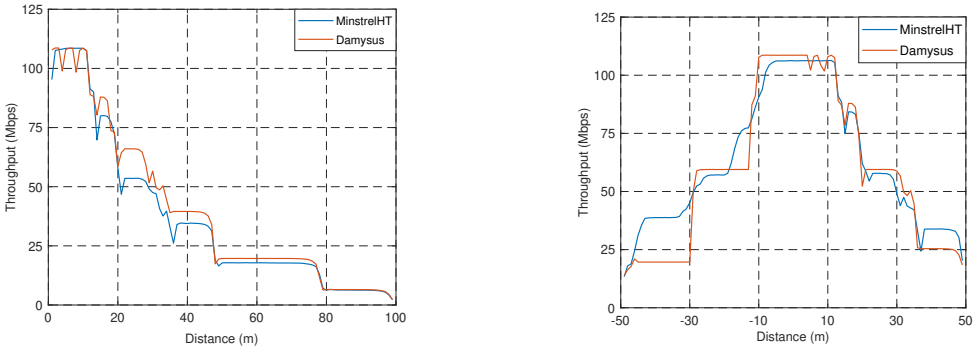

(a) (b)

Figure 7.1: Performance of Damysus against MinstrelHT for a user moving from: a) high to low RSSI and b) low to high RSSI.

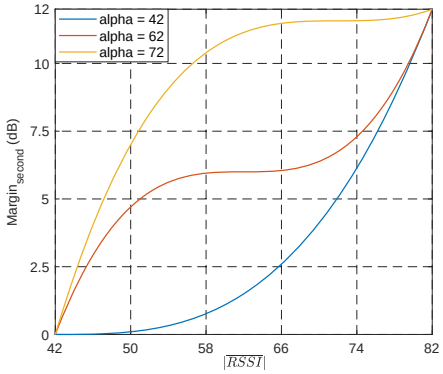

Figure 7.2: Impact of the various *alpha* values on teh caluclation of $Margin_{second}$

An assessment of Damysus against MinstrelHT [7], as a user moves from high to low

[7]MinstrelHT is the Minstrel variance for the IEEE 802.11n/ac, whilst it was developed to also

and from low to high RSSI values is illustrated in Figure 7.1 (with *succThres* = 10 and *failThres* = 10). For this simulation, the BSS Color is not enabled and there is no interference, thus Damysus is semi-functional as many of its functions and Equations described earlier do not apply now. Four important conclusion can be drawn from this figure. First, the validation of MinstrelHT's poor performance when the RSSI falls from high to low values, as also reported in [371]. Secondly, Damysus outperforms MinstrelHT in most of the locations (Figure 7.1a) as the channel conditions deteriorate. Third, the slow start of Damysus under poor channel conditions when most of the rates have not been probed. Although, Damysus will try transmitting on higher rates, the use of *succThres* and *failThres* thresholds along with the absence of interference and the BSS Color affect Damysus's response. In particular, high values for both of the threshold, will provide stability and prevent Damysus from fluctuating. On the other hand, lower values will make Damysus more aggressive and may provide higher throughput when the channel conditions improve. Finally, even though Damysus was more stable than MinstrelHT during the multiple runs, its sawtooth behaviour is due to the use of TPC (can be seen when the STA is close to the AP) along with the thresholds for the consecutive successful or failed transmissions. Figure 7.2 shows the impact of the different values for the *alpha* parameter on the calculation of $Margin_{second}$.

7.4 Simulation Setup

The scenarios as defined in the IEEE 802.11ax document [329] and in [379] are considered, to evaluate the performance of Damysus against MinstrelHT. The scenarios (layout and propagation models) are developed according to the IEEE 802.11ax guidelines and are integrated into the ns-3 and correspond to a residential, an enterprise, a small indoor, and a large outdoor scenario, each one with the propagation model as defined in the same document. Two different cases are considered per scenario, one for DL traffic and one for the UL. To assure full buffer conditions, User Datagram Protocol (UDP) traffic is generated in a constant bit rate of 40 Mbps per BSS. It is also assumed no color collisions (apart from the scenarios where BSSs > 64), which means

support the IEEE 802.11ax rates.

Table 7.1: Simulation Parameters

Parameter	**Value**
Frequency Band [GHz] / Bandwidth [MHz]	2.4 / 20
Shadowing [dB]	5 (SCE1/2/3) and 3/4 (SCE4 LOS/NLOS)
Physical Capture Model	800ns/10dB
AP/STA Tx Power [dBm]	20/15 (max. TxPwr for Damysus too)
AP/STA Antenna Gain [dBi]	0/-2
Number of Antennas	1
Noise Figure [dB]	7
Guard Interval (GI) [ns]	1600 (SCE1/2/3) and 3200 (SCE4)
PHY rate	MinstrelHT / Damysus
Traffic	UDP - Full Buffer (40 Mbps per BSS)
RTS/CTS	Disabled
Max Retransmissions	10
Contention Window [min,max]	[15,1023]
Packet at APP Layer [bytes]	1472
Max A-MPDU [no. of frames]	64
TxOP [ms]	5.484 (AC_BE)
Beacon Interval [ms]	102.4
CCA/SD, CCA/ED [dBm]	-82,-62
OBSS/PD (min, max) [dBm]	(-82, -62)
Damysus (*succThres*, *failThres*)	(10, 10)
Damysus *ampduSucces*	80%
Simulation Time per run [s]	32 (40 Runs)

that BSS Color is unique for each BSS. Moreover, only the OBSS/PD-based operation is considered, which means that the same rules are applied in all OBSSs (the SRG-based operation is not considered). Preamble reception and capture effect are also modelled, following the procedure in Chapter 4. The common simulation parameters used in this study for all the scenarios are listed in Table 7.1. Finally, a sufficient large period is allowed for the STAs' association, whereas the block acknowledgment agreement is instantly established with the association. Also, a warm-up period is also considered, hence, the statistics are collected from the last 8 seconds per simulation run.

7.4.1 Residential Scenario

This subsection presents the performance evaluation of MinstrelHT and Damysus in a residential environment as illustrated in Figure 7.3a. This multi-floor building comprises 5 floors with 2x10 apartments per floor, each one with size of 10m x 10m x 3m. One AP and five STAs are randomly placed in each apartment in an unplanned fashion (at 1.5m above the floor). Although, TGax defines 2 STAs per AP, a more recent study [380] showed that a higher number of STAs per apartment should be considered

(5 to 6 devices) based on the data collected from real environments. Moreover, each AP is randomly assigned in one of the 3 non-overlapping 20 MHz channels. Figure 7.3b presents the path loss model used for the residential scenario, that is defined as:

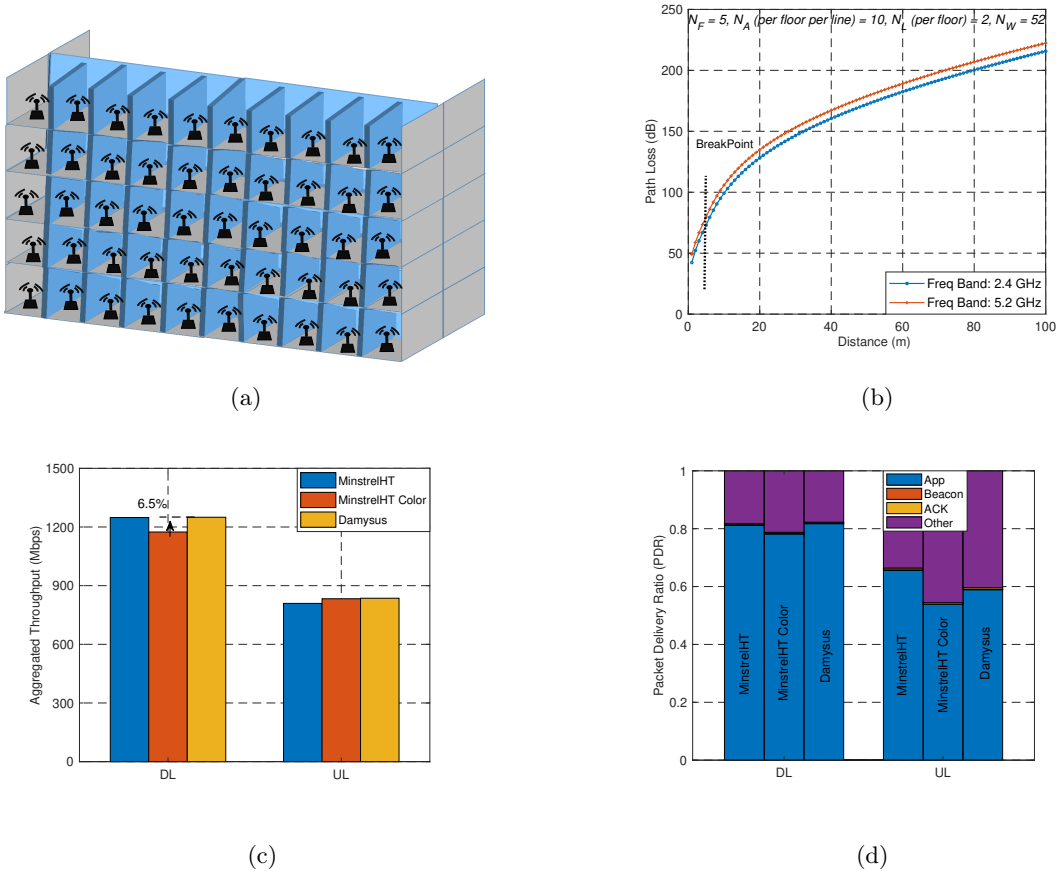

Figure 7.3: Residential scenario (SCE1): a) topology, b) path loss model, c) aggregated throughput, and d) packet delivery ratio.

$$PL_{sce1}(dB) = 40.05 + 20 \cdot \log_{10}(\frac{f_c}{2.4}) + 20 \cdot \log_{10}(\min(d, d_{BP})) + 18.3 \cdot (\frac{d}{N_F})^{\frac{\frac{d}{N_F}+2}{(\frac{d}{N_F}+1)-0.46}} + 5 \cdot \frac{d}{N_W} + \mathbb{1}(d > d_{BP}) \cdot 35 \cdot \log_{10}(\frac{d}{d_{BP}}) \quad (7.18)$$

where f_c is the frequency in GHz, d_{BP} is the breakpoint in meters with $d_{BP} = 5$, d is the 3D distance (in meters) between two nodes, N_F the number of floors, N_W the number of walls per floor, and $\mathbb{1}(d > d_{BP})$ the indicator function equal to 1 if $d > d_{BP}$

and 0 otherwise. The number of walls is given by:

$$N_W = ((N_A \cdot 4) - (N_A - 1)) + ((N_L - 1) \cdot (N_A \cdot 3) - (N_A - 1)) \tag{7.19}$$

where N_L is the number of apartment rows per floor (e.g. 2 in our scenario) and N_A is the number of apartments per floor and N_L (e.g. 10 in our scenario).

Figure 7.3c presents the total aggregated throughput for the three algorithms in DL and UL. It can be observed that BSS Color has negative impact on the performance for the MinstrelHT algorithm for DL (channel conditions deteriorate due to the higher interference), whereas the performance does not significantly vary for the UL case. On the other hand, Damysus achieves slightly higher throughput against MinstrelHT in both directions. The presence of the BSS Color along with the unmanaged deployment of the APs (i.e. random position and random channel) increase the interference level. A similar behaviour observed also in [381], where different BSSs react very differently to specific settings in the residential scenario. Figure 7.3d depicts the impact of the algorithms on the overhead. Note that *Other* represents the transmitted probes, association requests/responses, and the retransmitted data. Two conclusions can be drawn from that figure. First, overheads increase with the use of BSS Color when the MinstrelHT is applied, which is due to the higher interference. Secondly, Damysus achieves better Packet Delivery Ratio (PDR) against MinstrelHT- Color as it takes into account the interference level.

7.4.2 Enterprise Scenario

The second TGax scenario (SCE2), an office environment is presented in Figure 7.4a. It comprises a floor with 8 offices, each one covering an area of 20m x 20m and containing 64 cubicles. Each cubicle has size of 2m x 2m and contains 4 STAs that are randomly placed at height of 1m. Furthermore, 4 APs are installed per office, in predefined locations, on the ceiling (i.e. 3m above the floor). There are in total 32 APs with 64 STAs per AP. Three non-overlapping channels in the 2.4 GHz band are assigned for this scenario, with the following allocation (per office): $AP_0 \leftarrow Channel\ 1$, $AP_1 \leftarrow Channel\ 6$, $AP_2 \leftarrow Channel\ 11$, $AP_3 \leftarrow Channel\ 11$, $AP_4 \leftarrow Channel\ 1$, $AP_5 \leftarrow Channel\ 6$, $AP_6 \leftarrow Channel\ 11$, and $AP_7 \leftarrow Channel\ 11$.

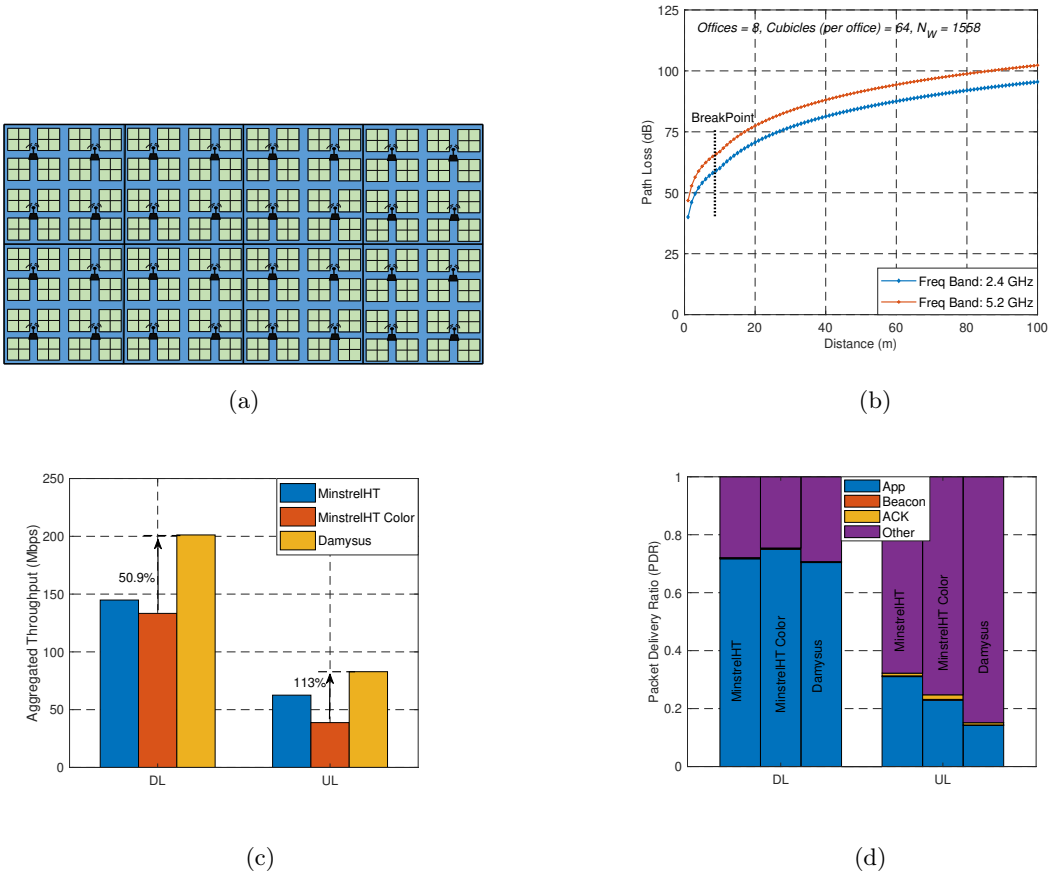

Figure 7.4: Enterprise scenario (SCE2): a) topology, b) path loss model, c) aggregated throughput, and d) packet delivery ratio.

Figure 7.4b presents the path loss model for this specific scenario, where the number of walls has been found to be 1558. The model for the path loss is given by the following equation:

$$\begin{aligned} PL_{sce2} &= 40.05 + 20 \cdot \log_{10}(\frac{f_c}{2.4}) + 20 \cdot \log_{10}(min(d, d_{BP})) + 7 \cdot \frac{d}{N_W} \\ &+ \mathbb{1}(d > d_{BP}) \cdot 35 \cdot \log_{10}(\frac{d}{d_{BP}}) \end{aligned} \tag{7.20}$$

where $d_{BP} = 10$ (m).

Figure 7.4c illustrates the aggregated throughput of the rate control algorithms for the Enterprise scenario. It can be observed that Damysus takes advantage of the good

link between the AP and the associated STAs and outperforms MinstrelHT (w/wo the Color) in both links with over 50% throughput gain in DL and 113% for UL. The poor performance of MinstrelHT is not because of the low RSSI but due to the high interference level and packet collisions (UL case). The PDR can also be observed in Figure 7.4d. Although, it remains fairly high in DL for all algorithms, it rapidly degrades when it comes in UL transmissions. The main reason behind this degradation is the high contention among the STAs, which is even higher for Damysus due to the adaptive OBSS/PD threshold, resulting in lower PDR.

7.4.3 Indoor Small BSSs Scenario

A more challenging case is that of crowded places; i.e. a stadium or dense indoor deployments (i.e. airport, train station, auditorium), where thousands of people are concentrated in a small area. In such deployments, hundreds of APs are needed to serve a large number of STAs. For example, the traffic density for a medium size stadium is expected to be over 1 Tbps, mostly in uplink [382], with spectators sharing High-Definition (HD) video to social media. For this case, TGax has defined SCE3. The APs' deployment is planned in a hexagonal layout with Inter Cell Distance (ICD) of 17.32m. A frequency reuse pattern is also considered with SR3 to be more representative than SR1, even though, SR1 should also be considered as some regions might have very low available bandwidth. In this study, SR3 is considered, whereas the APs and the STAs are placed at a height of 3m and 1.5m, respectively. For both SR patterns, 19 co-channel cells are considered with one AP per cell, forming a 2-ring deployment, as depicted in Figure 7.5a. Moreover, 570 STAs are randomly placed inside the hexagonal area illustrated in Figure 7.5a and associate to the strongest RSSI from the APs. This means that 30 STAs on average, associate with each AP.

Figure 7.5b illustrates the path loss model defined in TGax for SCE3 and used in this study. The path loss model for this specific scenario is defined as:

$$PL_{sce3} = 40.05 + 20 \cdot \log_{10}(\frac{f_c}{2.4}) + 20 \cdot \log_{10}(min(d, d_{BP})) + \mathbb{1}(d > d_{BP}) \cdot 35 \cdot \log_{10}(\frac{d}{d_{BP}}) \quad (7.21)$$

where $d_{BP} = 10$ (m).

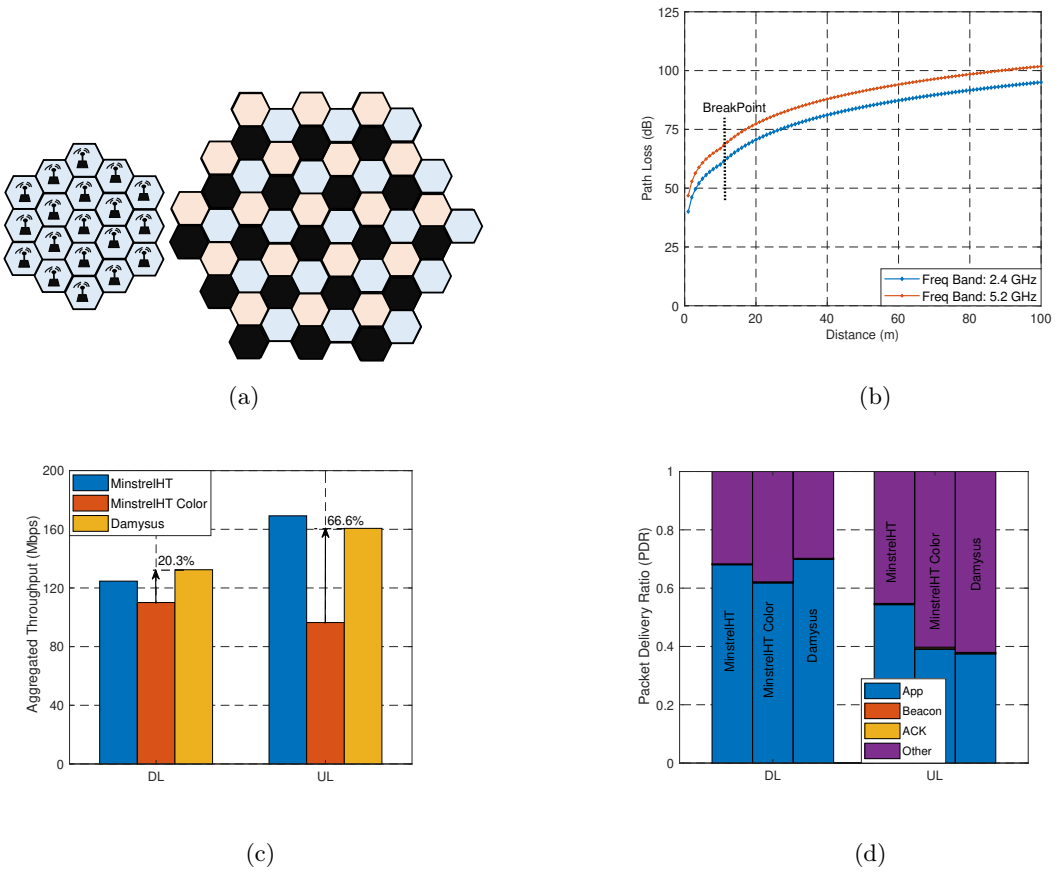

Figure 7.5: Indoor Small BSSs scenario (SCE3): a) topology, b) path loss model, c) aggregated throughput, and d) packet delivery ratio.

Figure 7.5c depicts the aggregated throughput of Damysus and MinstrelHT in SCE3. Two conclusions can be drawn from this figure. First, Damysus achieves higher throughput against the *MinstrelHT - Color* for both DL and UL cases, with a gain of approx. 20% and 66%, respectively. Secondly, the impact of BSS Color in both MinstrelHT and Damysus. The increased transmission opportunities with the BSS Color result to more packet collisions. Although, SCE2 and SCE3 are quite similar in terms of the path loss models and the high number of STAs per BSS, they differ in one major thing: the STAs in SCE3 associate with the strongest AP which is not necessarily the closest one and they are placed in a wider area that could introduce hidden nodes. Those two reasons are the main causes of the throughput loss observed in the UL case and the failure of both algorithms to cope with that. The PDR achieved by Damysus is equal to or higher

than the *MinstrelHT - Color*, as illustrated in Figure 7.5d.

7.4.4 Outdoor Large BSS Scenario

WLAN technology is expected to be extensively used in urban outdoor scenarios, e.g. outdoor hotspots. In that case, the AP deployment is more likely to be managed and used for offloading traffic through Wi-Fi. To capture an outdoor cell deployment where the distance between APs is high and the cell-edge users experience low SNR, SCE4 was formulated by the TGax. The ICD is 130m and 19 APs are placed at 10m height, forming again hexagonal cells (Figure 7.5a). In contrast to the indoor scenario (SCE3), SR1 is more suited here, whilst 950 STAs are randomly placed now in the hexagonal area, that corresponds to 50 STAs (on average) per AP. Similar to SCE3, the STAs associate with the strongest AP.

Figure 7.6a shows the Line-of-Sight (LOS) probability for the Urban Micro-cell (UMi) and Urban Macro-cell (UMa) deployments. The LOS probability for the UMi and UMa deployments is given by the following equation:

$$LOS_{prob} = \begin{cases} min(\frac{18}{d}, 1) \cdot (1 - e^{\frac{-d}{36}}) + e^{\frac{-d}{36}}, & \text{UMi} \\ min(\frac{18}{d}, 1) \cdot (1 - e^{\frac{-d}{63}}) + e^{\frac{-d}{63}}, & \text{UMa} \end{cases} \tag{7.22}$$

In this study, it has been considered the UMi channel model as it is the one preferred by the TGax group and does not take into account the building height and street width. The path loss model is depicted in Figure 7.6b for both the LOS and non-LOS (NLOS) cases. Note that the *LOS-adv* and *NLOS-adv* are the models applied in our study (the *UMi LOS* and *UMi NLOS* can be found in [329]) and are defined as:

$$PL^{LOS}_{sce4/UMi} = \begin{cases} 21 \cdot \log_{10}(\sqrt{d^2 + (TX_z - RX_z)^2}) + 32.4 + 20 \cdot log_{10}(f_c), \ d \leq d_{BP} \\ 40 \cdot \log_{10}(\sqrt{d^2 + (TX_z - RX_z)^2}) + 32.4 + 20 \cdot log_{10}(f_c) \\ - \ 9.5 \cdot \log_{10}((d_{BP})^2 + (TX_z - RX_z)^2), \qquad d > d_{BP} \end{cases} \tag{7.23}$$

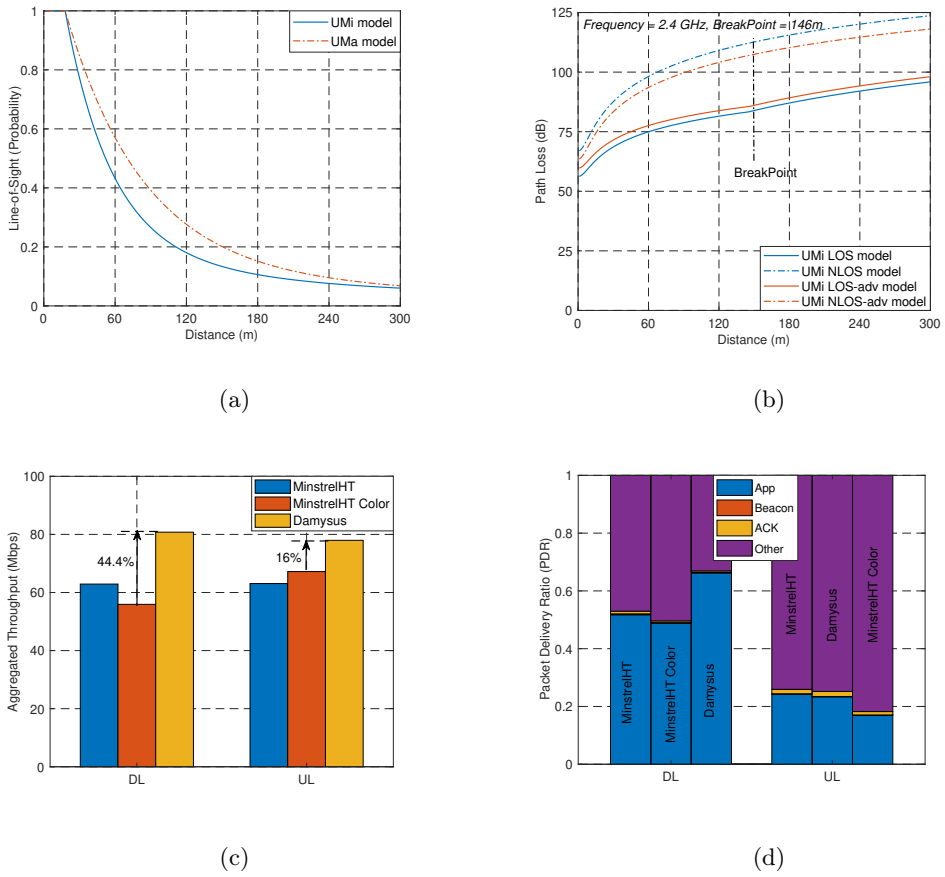

(a) (b)

(c) (d)

Figure 7.6: Outdoor Large BSS scenario (SCE4): a) Line-of-Sight (LOS) probability, b) path loss model c) aggregated throughput, and d) packet delivery ratio.

where TX_z, RX_z is the height (in m) of the transmitter and receiver, respectively, d is the 2D distance now, and the Breakpoint distance (in m) is given by:

$$d_{BP} = \frac{4 \cdot (TX_z - 1) \cdot (RX_z - 1) \cdot (f_c \cdot 10^9)}{C} \tag{7.24}$$

where C is the speed of light (299792458 m/s) and the f_c is in Hz that time (only for the Equation 7.24). For more details in respect to the UMi and UMa channel models, the reader can refer to [383] (Table A1-2) and [384] (Note 1 in Table 7.4.1-1).

In contrast to SCE3, where the STAs experience high SNR, in SCE4 there will be a lot of STAs experiencing poor channel conditions (i.e. low RSSI and high interference). Two conclusions can be drawn from Figure 7.6c. First, Damysus's capability of sensing

the channel and recording the RSSI along with the interference level result in better performance. In particular, Damysus achieves up to 44% higher throughput gain than the *MinstrelHT - Color* in DL and 16% for the UL case. Secondly, MinstrelHT fails to adapt to the low SNR conditions (one of the main drawbacks for Minstrel) that many of the STAs will experience, resulting in poor performance. Moreover, Damysus improves PDR for the DL case whereas maintains a similar level of PDR for the UL. Note that PDR for the UL case is approximately 20%, which means that approx. 4 out of 5 transmitted data were retransmissions, which is due to the high number of contending STAs (high number of hidden nodes) along with the poor channel conditions.

Figure 7.7 illustrates the throughput per STA in DL and UL for the 4 scenarios described earlier. It is interesting to see that in all scenarios, the percentage of STAs that could not get served is quite high. Note that only for SCE1 and SCE4 there are STAs that cannot associate with the APs (approx. 11% and 3% of the STAs for SCE1 and SCE4, respectively). Almost in all cases, Damysus improves the throughput perceived by the STAs against MinstrelHT Color, for those experiencing lower SINR and those that are close to the APs. Throughput loss for Damysus can be observed in SCE3 (UL case) for the cell-edge users, whilst a significant throughput gain is achieved for the users located closer to the APs and experience higher SINRs. This could be due to the hidden nodes (compared to SCE2, where a similar propagation model is applied) as explained earlier. Table 7.2 presents the statistics collected for the three algorithms in all the scenarios, including all nodes (i.e. APs and STAs). Note that *Average Tx packet size* may be below the data packet size because it accounts for all transmitted traffic. Moreover, each cell holds the statistics per algorithm for all 4 scenarios and link directions (i.e. DL / UL).

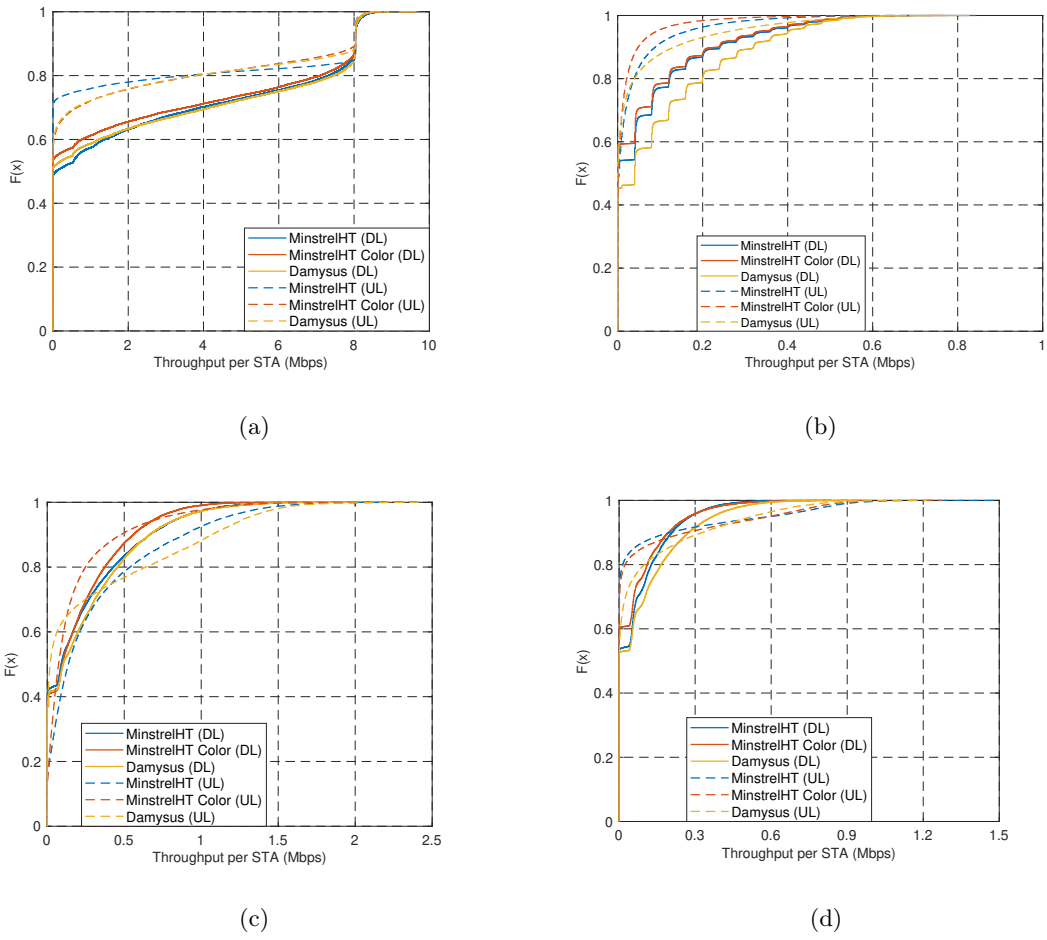

Figure 7.7: Throughput per STA for a) SCE1, b) SCE2, c) SCE3, and d) SCE4.

Table 7.2: Statistics on key performance metrics' results

Parameter	MinstrelHT	MinstrelHT Color	Damysus
Average Rate [Mbps]	56.3 / 55.0	54.1 / 45.0	63.3 / 53.6
	38.9 / 13.7	37.1 / 09.4	64.5 / 64.5
	32.4 / 18.9	28.2 / 13.7	45.4 / 46.2
	22.3 / 15.2	19.7 / 12.3	25.6 / 30.7
Average Tx packet size [bytes]	3375 / 1386	3145 / 2052	2816 / 1815
	9708 / 2040	8797 / 1301	10961 / 2664
	9823 / 4863	7494 / 3455	8341 / 3744
	3969 / 1168	3348 / 1106	3762 / 1722
Average Tx Power [dBm]	17.7 / 17.1	17.7 / 16.9	16.5 / 16.7
	18.0 / 16.4	18.0 / 16.1	18.0 / 15.8
	17.9 / 17.1	17.9 / 16.9	17.8 / 16.8
	18.3 / 16.0	18.2 / 15.8	18.2 / 15.7
Average OBSS/PD [dBm]	N/A / N/A	-78.7 / -78.5	-80.4 / -80.0
	N/A / N/A	-79.0 / -77.1	-80.5 / -77.7
	N/A / N/A	-78.9 / -77.9	-79.5 / -71.8
	N/A / N/A	-79.2 / -76.8	-81.8 / -81.3

7.5 Conclusion

This chapter assessed the performance of Spatial Reuse mechanism in various dense deployments when MinstrelHT is applied. By enabling BSS Color, it was found that network performance degrades due to the higher interference level introduced in the channel. MinstrelHT is a well known off-the-shelf rate control algorithm that can provide near optimal performance in the absence of interference. However, the inability of MinstrelHT to accurately select a rate when channel conditions deteriorate and in the presence of interferers have led to the introduction of a new rate control algorithm. Damysus is a rate control algorithm that was developed and proposed in this chapter to cope with the challenges that dense deployments face and address the poor performance of MinstrelHT. Damysus exploits the Spatial Reuse mechanism and adjusts the rate by taking advantage of the available information that the Spatial Reuse mechanism provides. It also uses a TPC and adjusts the OBSS/PD threshold based on the interference level observed and the RSSI from the associated recipient(s).

Damysus was also compared against MinstrelHT in four different scenarios identified by the IEEE 802.11ax Task Group (i.e. Residential, Enterprise, Indoor Small BSS, and Outdoor Large BSSs) and in all of them outperformed MinstrelHT (up to 113% throughput gain). However, Damysus increases the transmission opportunities due to the adaptive OBSS/PD threshold that it uses, resulting in higher contention level inside a BSS. To ameliorate its performance and control the contention and interference levels, the use of RTS/ CTS might be inevitable for some scenarios. Furthermore, a mechanism for adjusting the CCA thresholds accordingly to cope with the high number of hidden nodes is required. However, such a mechanism should be carefully designed and incorporated into Damysus as it may significantly affect some of its operations (e.g. the selection of the OBSS/PD) and/or break some of the rules defined in the IEEE 802.11ax amendment. Finally, the SRP-based operation and the SRG concept should also be investigated, especially in the scenarios where throughput loss due to the BSS Color is observed.

Apart from the aim for higher throughput, reliable communications is another aspect of interest for the research and industry communities. In the environments where the

channel conditions rapidly change, e.g. due to mobility, packet retransmissions will take the lion's share of the available resources (spectrum and transmission time). Also, in the event of static users it was found in this chapter that most of the packets transmitted were retransmissions. In most of the scenarios, the PDR was relative low that indicates that resources are wasted to retransmitted packets and hence, control frames (Block-ACKs, ACKs). One approach to provide reliable communications, that was also discussed in Chapter 2 is the Network Coding. The next chapter presents a network coding scheme that was developed and was integrated in ns-3 for the IEEE 802.11 module.

References

[364] M. Z. Brodsky and R. T. Morris, "In Defense of Wireless Carrier Sense," *ACM*, vol. 39, no. 4, pp. 147–158, 2009.

[365] A. Kamerman and L. Monteban, "WaveLAN-II: a High-performance Wireless LAN for the Unlicensed Band," *Bell Labs technical journal*, vol. 2, no. 3, pp. 118–133, 1997.

[366] M. Lacage, M. H. Manshaei, and T. Turletti, "IEEE 802.11 Rate Adaptation: A Practical Approach," *In Proceedings of the 7th ACM International Symposium on Modeling, Analysis and Simulation of Wireless and Mobile System*, pp. 126–134, 2004.

[367] S. Biaz and S. Wu, "Rate Adaptation Algorithms for IEEE 802.11 Networks: A Survey and Comparison," *In IEEE Computers and Communications (ISCC)*, pp. 130–136, 2008.

[368] The MadWifi project. (), [Online]. Available: `http://madwifi-project.org/wiki/UserDocs/RateControl` (visited on 2020).

[369] J. C. Bicket and R. T. Morris, "Bit-rate Selection in Wireless Networks," PhD thesis, Master's thesis, Massachusetts Institute of Technology (MIT), 2005.

[370] A. Mcgregor and D. Smithies, "Rate Adaptation for 802.11 Wireless Networks", 2010. [Online]. Available: `http://blog.cerowrt.org/papers/minstrel-sigcomm-final.pdf`.

[371] D. Xia, J. Hart, and Q. Fu, "Evaluation of the Minstrel Rate Adaptation Algorithm in IEEE 802.11g WLANs," *In IEEE International Conference on Communications (ICC)*, pp. 2223–2228, 2013.

[372] J. Kim, S. Kim, S. Choi, and D. Qiao, "CARA: Collision-Aware Rate Adaptation for IEEE 802.11 WLANs," *In Infocom*, vol. 6, pp. 1–11, 2006.

[373] S. Tang, H. Yomo, A. Hasegawa, T. Shibata, and M. Ohashi, "Joint Transmit Power Control and Rate Adaptation for Wireless LANs," *In Wireless Personal Communications Springer*, vol. 74, no. 2, pp. 469–486, 2014.

[374] F. Tramarin, S. Vitturi, and M. Luvisotto, "A Dynamic Rate Selection Algorithm for IEEE 802.11 Industrial Wireless LAN," *In IEEE Transactions on Industrial Informatics*, vol. 13, no. 2, pp. 846–855, 2017.

[375] D. Qiao and S. Choi, "New 802.11h Mechanisms can Reduce Power Consumption," *In IT Professional*, vol. 8, no. 2, pp. 43–48, 2006.

[376] MCS, SNR, and RSSI. (), [Online]. Available: `https://d2cpnw0u24fjm4.cloudfront.net/wp-content/uploads/802.11n-and-802.11ac-MCS-SNR-and-RSSI.pdf` (visited on 2020).

[377] D. Halperin, W. Hu, A. Sheth, D. Wetherall, "Predictable 802.11 packet delivery from wireless channel measurements," *ACM SIGCOMM Computer Communication Review*, vol. 40, no. 4, pp. 159–170, 2010.

[378] K. D. Huang, D. Malone, and K. R. Duffy, "The 802.11g 11 mb/s rate is more robust than 6 mb/s," *IEEE Transactions on Wireless Communications*, vol. 10, no. 4, pp. 1015–1020, 2011.

[379] T. Adame, M. Carrascosa, and B. Bellalta, "The TMB Path Loss Model for 5 GHz Indoor WiFi Scenarios: On the Empirical Relationship between RSSI, MCS, and Spatial Streams," *In IEEE 2019 Wireless Days (WD)*, pp. 1–8, 2019.

[380] C. Ansley, "Document (IEEE 802.11-16/0355r0): Snapshot of Residential Wi-Fi Activity," Tech. Rep., 2016. [Online]. Available: `https://mentor.ieee.org/802.11/dcn/16/11-16-0355-00-00ax-snapshot-of-residential-use-2016.pptx`.

[381] K. Odman, "Document (IEEE 802.11-15/0357r4): 802.11ax scenario 1 CCA," Tech. Rep., 2015. [Online]. Available: `https://mentor.ieee.org/802.11/dcn/15/11-15-0357-04-00ax-scenario-1-cca-simulation.pptx`.

[382] N. Alliance, "White Paper: 5G White Paper - Next Generation Mobile Networks," NGMN Alliance, Tech. Rep., 2015. [Online]. Available: `https://www.ngmn.org/work-programme/5g-white-paper.html`.

[383] ITU-R, "Technical Report (M2135-1): Guidelines for Evaluation of Radio Interface Technologies for IMT-Advanced," ITU-R, Tech. Rep., 2009. [Online]. Available: https://www.itu.int/dms_pub/itu-r/opb/rep/R-REP-M.2135-1-2009-PDF-E.pdf.

[384] 3rd Generation Partnership Project, Technical Specification Group Radio Access Network, "Document (3GPP TR-38.901): Study on Channel Model for Frequencies from 0.5 to 100 GHz," 3GPP, Tech. Rep., 2018. [Online]. Available: http://www.3gpp.org/ftp//Specs/archive/38_series/38.901/38901-f00.zip.

Chapter 8

Reducing the Use of IEEE 802.11 Acknowledgements; A Network Coding Approach

Network Coding is an efficient concept to improve the network capacity under lossy channels. This chapter presents a scheme based on Serially Concatenated Code (SCC) that has been proposed in the literature and comprises an outer fountain code and Random Linear Network Coding (RLNC) as an inner code to allow intermediate nodes to re-encode the information. We have placed SCC in a shim layer between the MAC and Network layers where the (de-)coders operate. Furthermore, a header for the SCC scheme was also introduced that carries the information required for decoding the information. Simulation results in a fading IEEE 802.11 channel and an analysis based on the IEEE 802.11 basic access scheme, show that SCC can indeed improve the performance when it is carefully designed and can provide a means of enabling robust communications without the use of ACKs and retransmissions (i.e. multicast/broadcast communications).

8.1 Introduction

In WLANs, packets may be lost due to the poor channel conditions (e.g. high interference, weak received signal etc.), degrading the achievable throughput. Existing network protocols rely on packet retransmissions based on feedback provided to cope with packet losses and guarantee reliable communications (i.e. TCP).

The use of erasure codes [385]–[390] is another approach that can be followed to compensate for the channel errors. Erasure codes break the data into smaller blocks (chains), and encode them (data blocks) by adding redundant information for fault tolerance. In particular, they are considered Forward Error Correction (FEC) codes under the assumption of bit erasures. Erasure codes are used not only in the telecommunications to protect the original data when transmitted over lossy (wireless/wired) channels, but also in storage. For example, data replication provides a robust solution against data losses by ensuring that the data are available in more than one server. However, replication is expensive in terms of storage resources, hence, many providers rely on the use of erasure codes.

A class of erasure codes that has gain a lot of attention by the research community is that of fountain codes (e.g. Luby Transform (LT) [385] and Raptor [386] codes), where the transmitter sends the encoded packets at a receiver without any knowledge of which packets have been received. Fountain codes are suitable for multicast and broadcast transmissions, as they do not require feedback, they are rateless and are characterised by low overhead and low complexity. The authors in [391] show that an LT-code approach can provide up to 20% throughput gain when compared to a traditional ARQ scheme. On the downside, fountain codes' performance significantly degrades with the number of hops (i.e. multihop topology), since the intermediate nodes just forward the received frames without re-encoding them [120]. The destination node is able to decode (with high probability) the original message only after collecting sufficient information (typically, it is slightly larger than the original message) irrespective of which packets are arrived.

On the other hand, Network Coding (NC) is considered to be an enabling technique

to cope with the packet losses over multihop wireless erasure networks. It relies on the pioneering work of Ahlswede et al. [110] showing that by combining and coding information from different flows at an intermediate node, instead of simply routing or encoding (e.g. amplify-and-forward) can significantly improve the network throughput, energy efficiency, and provide high-reliability communications [111]. By combining a fountain code with RLNC has shown to provide higher performance in terms of decoding success rate, as it was discussed in Chapter 2.

This chapter presents a comprehensive simulation-based study on the performance of the serially concatenated code (SCC) presented in [118], in a single-hop IEEE 802.11 network over fading channel. Furthermore, an analysis of the NC scheme against the legacy IEEE 802.11 based on the access method (i.e. transmission duration, interframe spaces etc.) is presented here. The ns-3 simulation tool is used to carry out this study, wherein the NC scheme is implemented.

The rest of the chapter is organised as follows. Section 8.2 overviews the concept and design of the framework applied in an IEEE 802.11 system, while Section 8.3 presents the simulation scenario. Section 8.4 provides and analyses the simulation results in various scenarios. Finally, Section 8.5 concludes the chapter.

8.2 Serially Concatenated Codes: Design

This section presents the design of the Serially Concatenated Codes (SCCs) used in this work [8]. In contrast to the analytical work in [118], here, the SCC scheme is studied in a more realistic environment by using the well known ns-3 simulator and taking into consideration the IEEE 802.11 characteristics.

The SCC mechanism lies on top of the higher MAC due to advantages that this layer offer, as explained earlier. SCC scheme also supports operation of LT, RLNC, and systematic RLNC as stand alone schemes. The outer code is LT, a rateless fountain code, whereas the inner code is RLNC to incorporate the benefits of NC into our system.

[8] Part of the code developed for this study was applied in a real environment for the SWARMs project (http://www.swarms.eu/).

The major modification required on MAC to enable SCC would be to stream the flows of data through this shim layer (i.e. from the upper and lower layers) and a signalling mechanism to inform the lower MAC whether an ACK mechanism should be used or not. In this work, SCC signals the lower MAC to completely disable the use of an ACK, hence MAC could mimic multicasting/broadcasting modes. Furthermore, the APs should include their SCC capabilities on beacon's header to inform the STAs, whilst during the initial association handshake, STAs could inform whether or not SCC is supported.

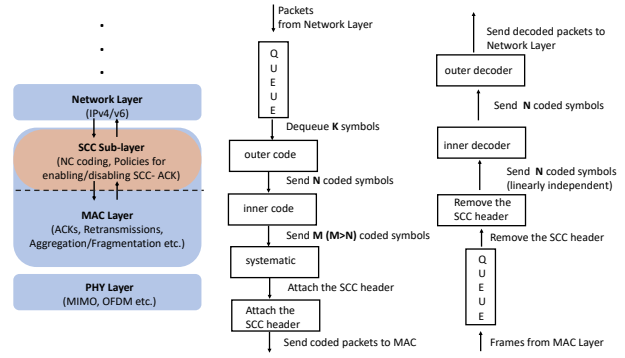

(a)

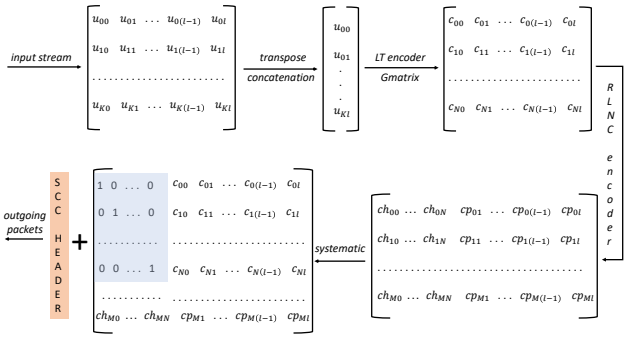

(b)

Figure 8.1: SCC design a) layer overview and b) coding procedure.

Packets received from the higher layers in the SCC shim layer are buffered in the SCC queue and are sent to the LT encoder once a threshold has been reached (a sufficient number of packets has been buffered). This queue is used to provide SCC with the flexibility to adapt the number of input symbols into LT accordingly. The architecture of the SCC mechanism is illustrated in Figure 8.1a.

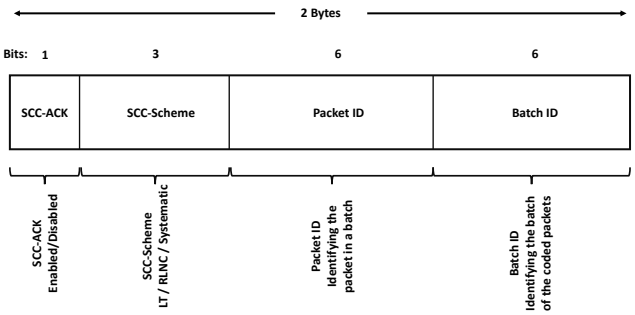

(a)

Figure 8.2: The SCC header.

Let us consider now, that K_p packets are sent in the LT encoder, where each packet consists of l symbols in $\mathbb{F}_q$ (finite field, with $q = 2^m$), hence every symbol has l_m bits. First, the $K_p \times l$ matrix (K symbols) of the input packets is then transformed into a single-column $(K_p \cdot l) \times 1$ matrix and is sent to the LT encoder. Secondly, the LT encoder produces an $N_p \times l$ matrix (N symbols), which is sent to the inner code (where N_p is the outgoing packets from LT). The RLNC now, multiplies the incoming symbols with coefficients selected from a finite field and attaches the coefficient vector at the headers of the encoded packets. Since we use a systematic approach, the product of the encoding procedure, consists of the LT coded packets and a specific number of the RLNC coded packets, as depicted in Figure 8.1b. Note that the identity matrix attached to the LT packets, is not transmitted but it is generated only for the decoding process.

At the receiver, once the number of the frames buffered in the queue (belonging in the same batch) is sufficient (i.e. frames received $\geq K$, the higher the number of the frames received, the higher the probability of recovering the initial information), the decoding procedure initiates with the frames sent to the RLNC decoder (identity matrix is attached to the LT coded frames only). In the case that the number of linearly independent frames received is not sufficient, then the RLNC decoder is skipped and the frames (only the LT coded frames) are sent straight to the LT decoder.

At the receiver in order to decode the frames, a header that is attached to each coded frame has been created, as illustrated in Figure 8.2. It is a 2-byte header that carries the batch id (e.g. 6-bit), the packet id (e.g. a 6-bit value that identifies each packet

in the batch) used to prevent packet duplication and help with packet ordering (i.e. re-sequencing performed during the LT decoding procedure), and 3 bits that identify whether LT, RLNC, systematic are enabled. Furthermore, the SCC scheme can be used either in acknowledgment mode or in the multicast/broadcast mode where the acknowledgement is disabled. This information is also included in the SCC header (1-bit). If the SCC-ACK is used, then the recipient transmits an SCC-ACK informing the transmitting node that a specific batch has been decoded and no additional frames (belonging in the same batch) are required. In that way, any coded frames left in the queues (i.e. SCC, MAC) are discarded. Note that a mapping between the transmitting node MAC address and the batch id is also required for supporting multiple SCC users. Moreover, the SCC header might be used to accommodate the information required for designing the degree distribution of the LT codes in both the transmitter and the receiver (i.e. seed number), that would require one more field.

8.3 Simulation Setup

First, the degree distribution for the LT codes is analysed and designed, since their performance is highly affected by the degree distribution. Although, there are quite a few optimisations and designs for the degree distribution in the literature, the Robust Soliton Distribution (RSD) that was originally introduced in [385], is applied here.

A good degree distribution should provide a sufficient number of degree-one symbols (i.e. symbols that depend only on one neighbour), meaning that during the decoding process, the decoder can retrieve the information of its unique neighbour. The set of the degree-one symbols that have not yet processed are called the ripple. The decoding process stops when the ripple set is empty (i.e. the decoder cannot decode further symbols). The decoding is considered successful when all symbols are retrieved and failure otherwise (i.e. there are still symbols that cannot be recovered). Hence, the objective is to design a degree distribution that i) as few encoding symbols as possible will be required for successful recovery of the original information (keep the overhead low) and ii) the number of symbol operations to recover a symbol is as low as possible (i.e. average degree per symbol). RSD is a degree distribution that satisfies the aforementioned

Table 8.1: Simulation Parameters

Parameter	Value
Scenario	IEEE 802.11 Single-hop
Channel	TGn Channel B [392] (slow fading)
Number of APs/STAs	1/1
Frequency Band [GHz]	5 (20 MHz at channel 36 (i.e. 5.18 GHz)
Guard Interval [ns]	3200
AP/STA Tx Power [dBm]	16/16
Number of Antennas	1
Noise Figure [dB]	7
PHY rate [data/control]	[HE-MCS0/HE-MCS0]
Traffic	Full Buffer (Constant Bit Rate), Video [393]
RTS/CTS	Disabled
Max Retransmissions	10 (Legacy only)
Contention Window [min,max]	[15,1023]
Packet at APP Layer [bytes]	[128/484/1024]
Max A-MPDU [no. of frames]	1
Beacon Interval [ms]	102.4
CCA/SD, CCA/ED [dBm]	-82,-62
Simulation Time per run [s]	10 (20 Runs)

constraints as described in [385].

The next step is to evaluate SCC performance against LT, RLNC and S-RLNC, where a burst erasure channel is considered. In particular, a matrix of symbols (each symbol is considered a byte) is created and then errors are randomly introduced to mimic a burst erasure channel. Further, the matrix is sent to the decoder (i.e. LT or RLNC) that tries to retrieve the original information. The above procedure is performed for a large number of iterations (i.e. 10^6) to get accurate results.

Secondly, an analysis based on the IEEE 802.11 access scheme (CSMA/CA) is provided, to show the benefits of applying an NC scheme (SCC in our case) to compensate for the channel errors. That is, it is shown when an NC scheme is beneficial based on the packet error rate, packet size, MCS and interframe spaces (i.e. frequency band).

Finally, SCC is evaluated in a IEEE 802.11 fading channel, where the RSSI fluctuates during the simulation. The Doppler spread and the coherence time ($T_c = 0.423/f_d$) used in this simulation are 3 Hz and 141ms to mimic a slow walking device (1.35 Km/h). Furthermore, the MAC-ACK has been completely disabled when coded packets are transmitted and we study SCC in the multicast/broadcast mode. The simulation parameters used for the study of this last case are summarised in Table 8.1.

8.4 Simulation Results

This section presents a) a performance evaluation of the coding schemes used in this study, in terms of decoding rate, b) an analysis of an NC (based on SCC) scheme against the legacy access scheme, and c) a performance evaluation of SCC in a fading channel.

8.4.1 Decoding Rate of the Coding Schemes

There are two important parameters in RSD, namely *delta* and c, which greatly affect the performance of the LT codes in terms of decoding capabilities and complexity (especially for small length packets due to the inherent limitation of LT codes, i.e. performance is optimised for large block sizes). The former parameter represents the failure probability of the decoding process, whereas the latter one is a positive constant usually smaller than 1. Both parameters influence the overhead required, the average degree per symbol, and the ripple size ($R = c \cdot \ln K/delta \cdot \sqrt{K}$). We can observe from the Figure 8.3, that as *delta* and c increase, the complexity (average degree per symbol, i.e. operations per symbol) and the overhead required to recover the original information decays. However, the failure probability for the decoding also inclines as *delta* increases. We believe that $delta < 1$ and $c < 0.1$ can offer a good trade off between complexity/overhead and decoding probability for our case study.

The coding schemes used in this study are evaluated and compared in terms of decoding capabilities. The packet size for this simulation is 156 bytes (to be inline with the results in Figure 8.3), whereas the number of input and outgoing packets from the LT encoder are 3 and 4/5, respectively (i.e. $K = 468, N = 624$ and $N = 780$). Figures 8.4a and 8.4b depict the decoding rate for the LT codes, as burst errors are artificially introduced in the matrix sent to the decoder. Three important conclusions can be drawn from these two figures. First, it can be observed how the values of c and *delta* greatly affect the decoding capabilities of the LT codes. Secondly, it can be seen that the values of 0.01 and 0.9 for c and *delta*, respectively, achieve the highest decoding rate among the rest. Lastly, as the overhead (i.e. outgoing packets) is increased from 4 to 5, LT decoding capability greatly improves. Figure 8.4c illustrates the decoding rate for the RLNC

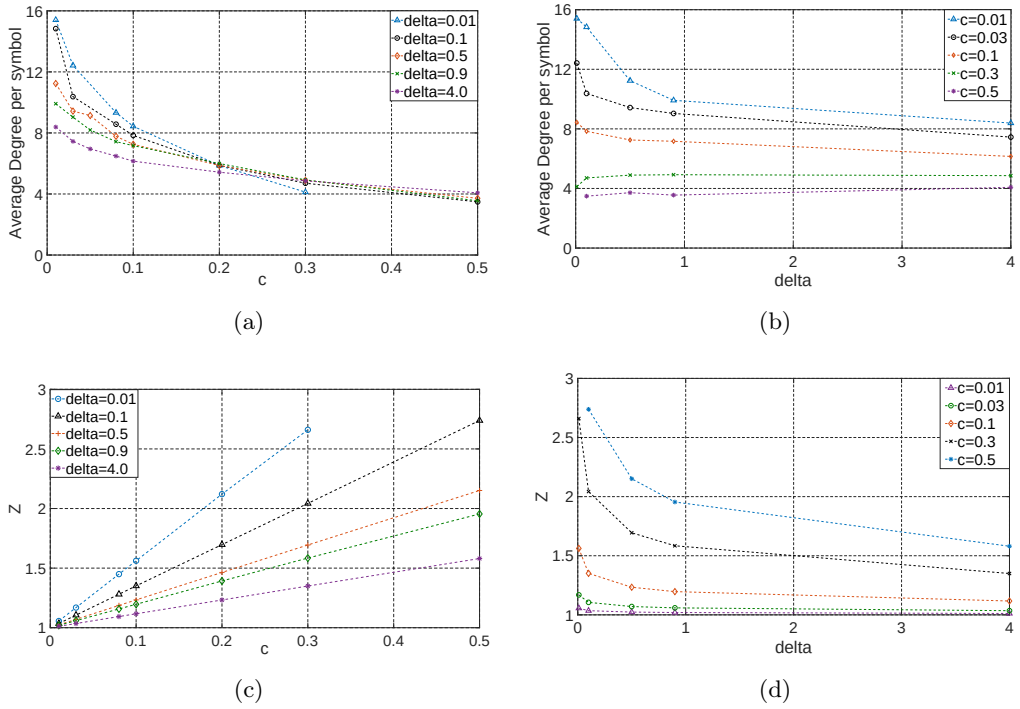

Figure 8.3: Impact of the *delta* and c parameters (Robust Soliton Distribution) on the average degree per symbol as a) c varies and b) *delta* varies and on the overhead (Z) as c) c varies and d) *delta* varies for $K = 468$ and $N = 780$.

and S-RLNC schemes. By adding additional overhead, it can be observed that RLNC performance improves, whilst S-RLNC does not provide any significant gains. Finally, when the systematic SCC mechanism is used, where the benefits of the both LT and RLNC are combined, the error probability for the decoder can be maintained at or close to 0, as illustrated in Figure 8.4d.

8.4.2 Benefits of NC in an IEEE 802.11 environment

IEEE 802.11 is an asynchronous technology that relies on the CSMA/CA protocol. According to CSMA/CA, every node senses the channel prior a transmission; if the channel is sensed as idle then it proceeds to the transmission of a frame, otherwise the transmission is deferred. Further, to minimize the probability of frame collisions, where nodes initiate a transmission to the same recipient at exactly the same time slot (hidden nodes are not assumed), a node randomly draws a number within a window (i.e.

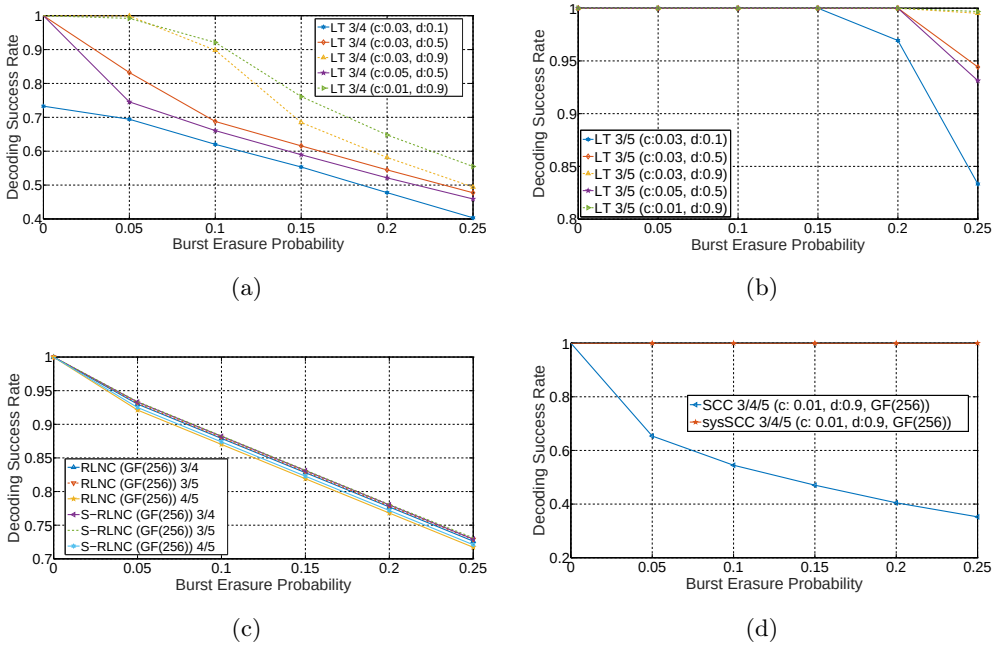

Figure 8.4: Comparison of the coding schemes for various burst erasure probabilities: a) LT for $K = 468$ and $N = 624$, b) LT for $K = 468$ and $N = 780$, c) RLNC and S-RLNC for [InPackets, OutPackets] = [3,4] and [3,5], and d) SCC and sysSCC.

CW) indicating the number of time slots that it has to wait before it transmits. This procedure is known as back-off mechanism and is characterised by the size of the CW that doubles for every retransmission whilst resets to its initial size after a successful transmission. The basic access scheme for IEEE 802.11 is illustrated in Figure 8.5a. If the channel is sensed busy during the back-off, then the counter freezes and resumes when the channel is sensed idle for a DIFS. The successful reception of a data frame is followed by the transmission of an acknowledgment from the recipient to the initial sender (ACK is transmitted after the SIFS). A failure in the transmission of the frame is triggered after an ACK timeout and the node then doubles its CW size for the retransmission. On the other hand, under the SCC scheme, a node follows the basic access scheme to grant access to the medium, but instead of retransmitting a frame after a failed transmission, it transmits a sufficient number of coded frames to compensate for the frame losses. A comparison of the legacy basic and SCC access schemes is illustrated in Figure 8.5b.

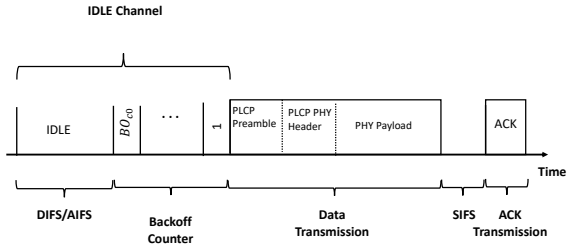

(a)

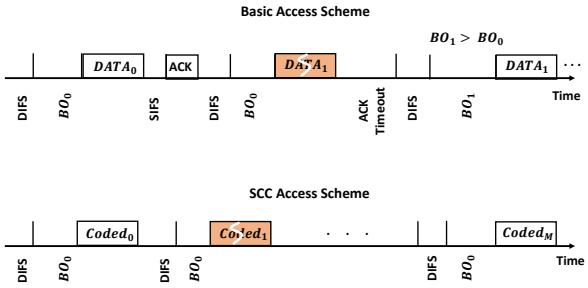

(b)

Figure 8.5: Basic Access Scheme for IEEE 802.11 a) conventional and b) compared to SCC access scheme.

Based on the access schemes for the conventional and SCC mechanisms, the SCC approach could provide gains compared to the conventional on the following cases: i) when the access probability is small and transmissions occur under an aggregation scheme or the TxOP mechanism (e.g. dense deployments), ii) when $M \cdot (DIFS + BO + CodedData) < K_p \cdot (DIFS + BO + Data + SIFS + ACK)$, where M is the number of the transmitted coded packets required to recover the original K_p packets, and iii) when the time for frames to be correctly received is higher than the time required for the coded packets due to retransmissions (e.g. lossy channels). This study focuses on the second and third cases, as for the first case, the access probability per node decays with the number of nodes (under full buffer conditions). A single STA and a single AP is the scenario investigated here.

For example, if the second case under ideal channel conditions where no retransmissions

take place is considered and the systematic SCC with $[K_p, N_p, M] = [3, 4, 5]$ is used, the transmission duration of the *CodedData* would be:

$$CodedData < \frac{SIFS + (3 \cdot ACK) - 2 \cdot (BO + 2 \cdot TimeSlot)}{2} \tag{8.1}$$

where $DIFS = SIFS + 2 \cdot TimeSlot$, $ACK = 44$ μs ([328]), $CodedData \approx Data$. It can clearly be seen from Equation 8.1 that under the ideal scenario with $M = 5$, the systematic SCC can never outperform the legacy (*CodedData* can never be below 0). However, considering that only 4 packets are required to successfully decode the batch (systematic SCC [3,4,4]) then the transmission duration of the *CodedData* is given by:

$$CodedData < 2 \cdot (SIFS - TimeSlot) + (3 \cdot ACK) - BO \tag{8.2}$$

This time Equation 8.2 gives $CodedData < 83\mu$s (5GHz bands). In the case of [3,4,5] and under the acknowledgment mode, the transmission duration of the *CodedData* should be less than 23μ in order to outperform the legacy operation (legacy ACK applied). Note that 20μs out of the 83μs is for the physical preamble, whilst the HE physical header is 20μs (at least 20μs since it depends on the number of HE-LTF), which implies that SCC under acknowledgment mode is impossible to outperform the legacy operation (given the ideal conditions and settings described earlier). For example, it would require the MCS2 (i.e. 26 Mbps) or MCS11 to transmit 68 and approx. 500 bytes (including MAC headers), respectively, for the SCC to outperform the conventional IEEE 802.11ax (SCC [3,4,4]). The useful payload after removing all headers would be less than the values mentioned earlier. Note that the IEEE 802.11ax amendment (a.k.a. High Efficiency (HE)) supports data rates of up to 143 Mbps for a 20 MHz channel bandwidth with Guard Interval (GI) of 800ns in a SISO system and operation on the 5 GHz bands.

Figure 8.6 presents the performance of systematic SCC compared to the conventional IEEE 802.11ax operating on the 5GHz band, for the third case when GI of 3200ns is used. This figure illustrates the achievable throughput for the systematic SCC when the settings of Figure 8.4d are used, against the legacy IEEE 802.11ax where retransmissions

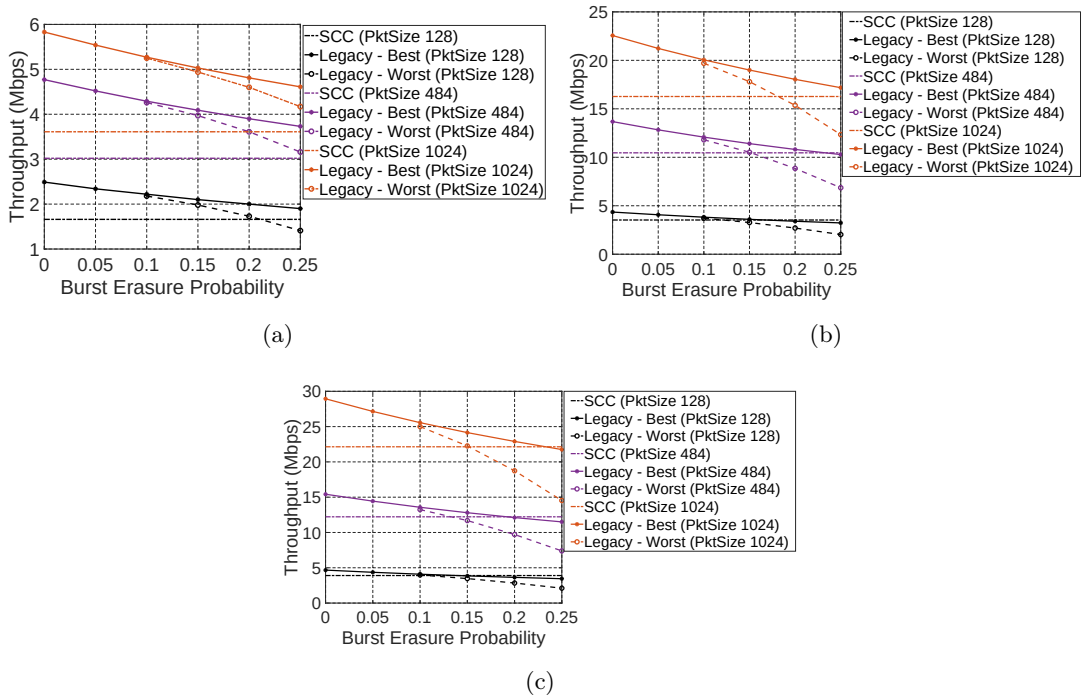

Figure 8.6: Comparison of the systematic SCC against conventional IEEE 802.11ax operating at 5GHz band when aggregation is disabled (GI=3200ns) for a) HE-MCS0, b) HE-MCS5, and c) HE-MCS11.

occur. Note that *Legacy-Best* and *Legacy-Worst* correspond to the cases where all the corrupted frames (unsuccessful transmissions in the first attempt/transmission) are successfully received in the first retransmission and for the case that the maximum number of retransmissions is required to correctly receive the frame(s). For example, if 20 frames transmitted are assumed and the burst erasure probability is 0.25 (i.e. burst errors introduced based on the Burst Error model in ns-3 (following a uniform distribution), with 0.25 meaning that 25% of the bits transmitted are lost) then either five frames corrupted in the first transmission will be successfully received or one frame will be retransmitted five times. Moreover, it is not considered any ACKs lost, implying that the transmitter of the data/coded frames does not experience the EIFS ($EIFS > DIFS$). Two important conclusions can be drawn from this figure. First, operating in the lowest MCS (in our case HE-MCS0) throughput gain for SCC can only be achieved under high burst erasure probability and for small frames, assuming that EIFS is not

used at the transmitting node. Secondly, as the data rate increases, higher throughput gain can be observed even for larger frames. For example, systematic SCC achieves a 33% and 45% throughput gain when HE-MCS11 is used for packet sizes of 128 and 1024 bytes, respectively. If aggregation is enabled then higher transmission rates will be required for the transmission of the data frames to compensate for the use of Block-ACKs (e.g. wider channel bandwidth, MIMO etc.).

8.4.3 Performance of Systematic SCC in IEEE 802.11 Fading Channel

The SCC is now evaluated in a scenario described in Table 8.1. The main difference now, that should greatly affect the decoding capabilities is that instead of the burst erasure channel used earlier, a packet either is correctly received or not received at all due to low RSSI or SNR. The node is placed in various locations such that the packet error probability is allowed to vary (i.e. ≈ 0 to ≈ 0.3). Note that the packet error rate is measured only at the receiver of the data frames. That means that if an ACK is lost during the reception, the node experiences EIFS instead of DIFS for the retransmission. Further, the same settings to SCC as the ones used in the previous sub-section (i.e. $delta = 0.9$, $c = 0.01$ and systematic SCC with $[K_p, N_p, M] = [3, 4, 5]$) are applied. Any errors that have not been recovered by the SCC decoder are handled in the higher layers (e.g. errors in the IPv4 header etc.). Lastly, the lowest HE-MCS was used, first as the worst case scenario for the SCC performance and secondly to meet the full buffer requirements without increasing the complexity of the simulations (i.e. higher HE-MCS would mean higher number of encoding/decoding operations).

Figure 8.7a illustrates the goodput (i.e. focusing on useful data only (i.e. excluding any headers), hence measured at the application layer) of SCC against the conventional IEEE 802.11ax for three different packet sizes; 128, 484, and 1024 bytes (at the application layer). It is expected that for a packet size of 128 bytes, the SCC mechanism would have shown the highest throughput gain against the legacy scheme, nevertheless, SCC shows an extremely poor performance in this case. This is mainly due to the fragile decoding capabilities of LT when performing over small number of input symbols. The channel used now, needs to also be taken into consideration, which differs from

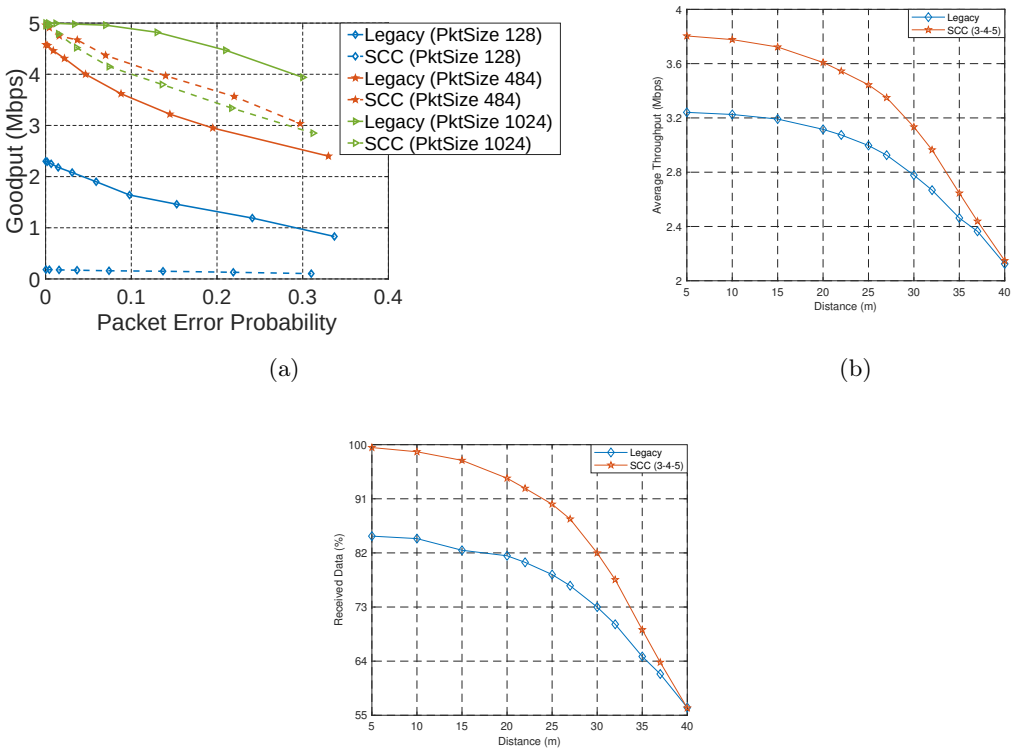

Figure 8.7: SCC performance against conventional IEEE 802.11ax in a fading channel a) Aggregation is disabled (HE-MCS0), b) throughput for AMPDU = 4 (emulating video traffic), and c) data received for AMPDU = 4 (emulating video traffic).

the burst erasure one. On the other hand, for the packet sizes of 484 and 1024 bytes, SCC decoding rate is maintained high (slightly higher than the goodput), which means that the usage of the higher LT packet sizes, result in acceptable performance by SCC. Although, for a packet size of 484 bytes, SCC offers a throughput gain of only up to 20% compared to the legacy scheme, when a packet size of 1024 bytes is used the benefits of SCC start to diminish. This effect is due to the access scheme and the low MCS (i.e. HE-MCS0) used for the transmission of such large frames (Sub-Section 8.4.2).

On the other hand, when aggregation is enabled and video traffic (burst traffic) is emulated, a clear improvement can be observed in Figures 8.7b and 8.7c in terms of throughput and reliability (data received), respectively. This is due to the traffic pattern

and the reduction in overhead when sending multiple coded data as an aggregated single packet.

8.5 Conclusion

This chapter investigated the performance of a network coding scheme, a.k.a. Serially Concatenated Codes (SCC), that comprises an outer digital fountain code (i.e. LT) and an inner coded that is based on the RLNC. Encoding is performed at the transmitter side, whilst the use of RLNC as an inner code allows intermediate nodes to re-encode the information based on the RLNC. The SCC mechanism lies in a shim layer between the MAC layer and the Network layer and allows a node to encode/decode information with or without the use of an ACK. Reliable communications in the absence of ACKs are ensured and provide a means of applying the SCC or any other powerful coding scheme for multicast/broadcast transmissions. It is showed that SCC can improve the decoding capabilities of both the LT and RLNC when used as a standalone codes under a burst erasure channel. Further, the potential benefits of SCC when applied in an IEEE 802.11 environment are studied, by looking at the access scheme and the procedure followed for the retransmissions. SCC was also compared against the conventional IEEE 802.11ax in a fading channel where the RSSI varies during the simulation to mimic a slow walking station. Directions for future study include the optimisation of SCC for small packet sizes, the study of aggregation against SCC and the impact of the SCC-ACK on the overall system performance, and extensions to other scenarios (e.g. dense deployments).

References

[385] M. Luby, "LT Codes," *Proceedings of the 43rd Annual IEEE Symposium on Foundations of Computer Science*, pp. 271–280, 2002.

[386] A. Shokrollahi, "Raptor Codes," *IEEE/ACM Transactions on Networking (TON)*, vol. 14, no. SI, pp. 2551–2567, 2006.

[387] I. S. Reed and G. Solomon, "Polynomial Codes over Certain Finite Fields," *Journal of the Society for Industrial and Applied Mathematics*, vol. 8, no. 2, pp. 300–304, 1960.

[388] M. Luby, "Tornado Codes: Practical Erasure Codes Based on Random Irregular Graphs," *International Workshop on Randomization and Approximation Techniques in Computer Science (Springer)*, p. 171, 1998.

[389] P. Maymounkov, "Online Codes (Technical Report," New York University, Tech. Rep., 2002. [Online]. Available: `http://www.academia.edu/download/32108691/maymounkov-online.pdf`.

[390] R. Gallager, "Low-Density Parity-Check Codes," *IRE Transactions on Information Theory 8.1*, pp. 21–28, 1962.

[391] W. Liu, Y. Yang, and M. Zhu, "Research on Inter Hospital and Ambulance Data Transmission Using LT-coding over VANET," *2013 ICME International Conference on Complex Medical Engineering*, pp. 119–123, 2013.

[392] V. Erceg et al., "Document (IEEE 802.11-03/940r4): TGn Channel Models," IEEE, Tech. Rep., 2004. [Online]. Available: `https://www.iitk.ac.in/mwn/papers/11-03-0940-01-000n-tgn-channel-models.pdf`.

[393] W.Y. Campo-Muñoz, E. Astaiza-Hoyos, and L. F. Muñoz-Sanabria, "Traffic Modelling of the Video-on-Demand Service through NS-3," *2017 Dyna*, pp. 55–64, 2017.

Chapter 9

Conclusion

9.1 Summary of the Thesis

The main purpose of this research study was to understand the potentials and challenges that the new IEEE 802.11 amendments will face in dense deployments. To this extend, IEEE 802.11 has introduced a new amendment to address users' demands and requirements in populated areas. This new amendment, namely IEEE 802.11ax (a.k.a. Wi-Fi 6), is coming out with a lot new features aiming at improving not only throughput performance but also spectrum efficiency in dense areas. This study focused on the Spatial Reuse feature introduced in IEEE 802.11ax, which is a completely new mechanism coping with the exposed node problem, hence improving the network performance. Exposed nodes incur some major challenges in dense scenarios and poor performance, by reducing the number of concurrent transmissions. This in turn, would lead to low throughput and spectrum inefficiency, nodes being blocked from transmissions.

In this research, a tutorial on the directions that both 3GPP and IEEE 802.11 camps are looking at, was provided. The most straightforward approach to provide higher throughput for the users, is the exploitation of new available spectrum and might use higher Modulation and Coding Scheme (MCS) (e.g. 1024 QAM). Although, mmWave frequency bands can potential offer large and unexploited bandwidth, they can mainly be used for short-range communications, similar with the higher MCSs. On the other hand, following the paradigm of IEEE 802.11ah, an amendment for IoT, the IEEE 802.11ax introduces OFDMA and BSS Color, a Spatial Reuse scheme, for utilising the

spectrum in the already congested 2.4 and 5 GHz bands and coping with the high number of users. Moreover, the latency can also reduced for the WLANs by decreasing: i) the time that a channel remains idle, ii) the number of packet collisions, and iii) the overhead introduced by the headers and control/management frames. Even though, a noticeable number of works were included in this tutorial, the area of Spatial Reuse in dense deployments is still at the initial stage of development.

The development of the IEEE 802.11ax features and the simulation scenarios constitute the first step towards understanding the potential of the SR mechanism and the challenges that the future WLANs will face. However, as the IEEE 802.11ax amendment evolves, there is a need for the simulation tools to keep pace with this evolution to correctly assess the performance of the active amendment. Therefore, the IEEE 802.11ax SR features were developed in a well known simulator (a.k.a. ns-3) and assessed in various scenarios, according to the TGax guidelines. Apart from the new features and advancements that are keeping introduced by the TGax, the lack of ns-3 to correctly capture the behaviour of the off-the-shelf devices could have significant implications on the assessment of the IEEE 802.11 performance. The Physical Layer Capture (PLC) has been shown that has a significant impact on throughput and may cause fairness issues between the nodes, especially for the cell-edge users, which was also developed in this work. Furthermore, an analytical model was proposed to capture the behaviour of IEEE 802.11 in dense deployments that gave insights of the good potentials for the BSS Color.

Based on the analytical and simulation results, the increased interference level introduced by the higher number of concurrent transmissions from the BSS Color scheme can severely affect the network performance and lead to low throughput. To this extent, a novel algorithm was proposed that takes into account the channel conditions to adjust the thresholds for BSS Color. It is the first ever algorithm proposed based on BSS Color that aims at improving throughput, whilst preserving fairness for the cell-edge users in terms of transmission opportunities. It is solely based on the interference level and the RSSI from the associated recipient(s) to adjust the thresholds in regard to the BSS Color. Simulation results showed of up to 57% throughput gain in various scenarios, when the proposed algorithm is applied along with the BSS Color scheme.

The lack of most rate control algorithms to integrate fundamental MAC functionalities and incorporate new techniques introduced in the recent amendments, as well as the poor performance of the off-the-shelf rate control algorithms (e.g. MinstrelHT) have led to the development and design of a new rate control algorithm. This algorithm proposed in this thesis, attempts to select a rate in a distributed way that is characterised by high delivery probability, given the network conditions and it also exploits the IEEE 802.11ax Spatial Reuse features. It integrates the algorithm mentioned earlier for controlling the BSS Color scheme and jointly adjusts the transmit power level. Simulation results in various dense deployments show a clear gain (up to 113%) of the novel rate control algorithm against MinstrelHT.

Apart from the aim for higher throughput, reliability is another aspect of interest for the research and industry communities. In the environments where the channel conditions rapidly change, e.g. due to mobility, packet retransmissions will take the lion's share of the available resources. Also, in the event of static users, it was found in this research that most of the packets transmitted were retransmissions with the packet delivery ration in most of the dense scenarios being relative low. One approach to provide reliable communications (apart from the use of acknowledgements) is to apply Network Coding. In this study, Serially Concatenated Codes (SSC) were developed and designed to operate on the higher MAC layer and enable reliable communications. In particular, the SCC mechanism lies in a shim layer between MAC and Network layers and allows a node to encode/decode information with or without the use of an ACK. It is showed that SCC can improve performance and provide reliable communications in the absence of ACKs, whilst can enable multicast/broadcast transmissions (due to the absence of ACKs), hence efficiently utilising the spectrum resources.

9.2 Research Directions

The mathematical model proposed in this study, is more suitable to analyse throughput for small cells, where users experience good channel conditions. A possible direction that this work can take in the future is to extend the analytical model to account for the packet collisions/losses due to the channel conditions, where users may experience,

especially in large cell deployments. This means that SINR needs to be taken into account, while relaxing other assumptions made in this work will also lead to more accurate results (e.g. CCA/ED threshold).

This work showed the importance and the benefits for designing new rate control algorithms that exploit the newly proposed features of the IEEE 802.11 amendments. In this work, Damusys was proposed that is aware of the OBSS transmissions and the interference level by exploiting the BSS Color information. A possible direction for further improving Damusys's performance is to introduce a mechanism to dynamically adjust the CCA thresholds, as it has been shown that the adjustment of these thresholds may provide significant throughput gain. However, this poses a challenge since it may break the rules defined on the IEEE 802.11 standards for static thresholds during the frame reception. Therefore, this mechanism should carefully be designed by taking into account the OBSS/PD threshold and transmit power levels.

Another challenge for the future WLANs is the high interference, due to the dense deployments and the increased number of transmissions introduced for example by BSS Color. One way to address the increased interference in dense deployments could be, by enabling schedulers in the MAC layer that are interference-aware. By introducing intelligence in the MAC queue and selecting a packet that has higher probability of being successfully received than randomly selecting one. These scheduling policies could be applied along with the BSS Color, where the Access Points (APs) are aware of inter-BSS transmissions and their interference level. The AP may classify its associated STAs based on their RSSI into, e.g. three zones; short distance, intermediate distance, and cell-edge users. Once a colored packet is dropped and a concurrent transmission is allowed, the AP will select its next recipient based on the interference level (e.g. inter-BSS frame's RSSI). In particular, under strong interference, the AP will select a short distance user, when a weak inter-BSS RSSI is recorded it will transmit to a cell-edge user, otherwise an intermediate distance node will be served. In order to preserve fairness for the users in a zone, a scheduling mechanism (e.g.round-robin) can be applied per zone, following the paradigm of 3GPP for addressing the substantial number of devices contending for a preamble.

A third challenge that can be further investigated is this of Network Coding. This work shed some light on the potentials of Network Coding in terms of improving throughput, reliability, and enabling broadcastin/multicasting transmissions, but there is still a lot of work that needs to be done to fully collaborate Network Coding with the existed ACK/ARQ mechanisms. For example, the IEEE 802.11aa has been introduced to enable video multicasting where frames are repeated to ensure high reliability over lossy channels. A performance assessment of Network Coding against the IEEE 802.11aa for multicasting transmissions would be beneficial for the research and industry communities.

Finally, another hurdle that needs to be tackled in the next generation of WLANs is the huge overhead that the headers add, due to backward compatibility issues. It was shown in this study, that MAC efficiency is severely affected by the extremely long PHY headers, leading to lower throughput. One way to cope with this, would be to follow the paradigm of IEEE 802.11ah for the MAC headers, applied in the PHY headers too. Nevertheless, this would also require the "mutual collaboration" of the old devices, since the channel sensing is based on these headers.

Appendices

Appendix A

PHY characteristics of IEEE 802.11 amendments

Table A.1: Comparison of PHY characteristics for IEEE 802.11ad/ac/ax/af/ah technologies.

Parameter	**IEEE 802.11ad**	**IEEE 802.11ac**	**IEEE 802.11ax**	**IEEE 802.11af**	**IEEE 802.11ah**
Frequency Spectrum [GHz]	Between 57 - 66	5	Between 1 - 7	0.54 - 0.698 in USA and 0.47 - 0.79 in Europe	Sub-1
Channel Bandwidth [MHz]	2160	20 / 40 / 80 / 160 / (80+80)	20 / 40 / 80 / 160 / (80+80)	6 / 7 / 8 / 12 / 14 / 16 / 24 / 28 / 32, where the first three are the BCUs	1 / 2 / 4 / 8 / 16

Spectrum Sharing	SC-OFDM/ OFDM	OFDM	OFDM/ DL-UL OFDMA	OFDM	OFDM
Subcarriers per Channel (useful subcarriers)	355, where 336 are data subcarriers, 16 are pilot subcarriers, and 3 are Direct Current subcarriers	56 / 114 / 242 / 484, where 52 / 108 / 234 / 468 are data subcarriers and 4 / 6 / 8 / 16 are pilot subcarriers, for 20 / 40 / 80 / 160 (continuous or not), respectively	$N_{ST} = N_{SRU} * N_{RU}$, N_{SRU} is the number of Subcarriers per RU; 26 / 52 / 106 / 242 / 484 / 996 / 1992 and N_{RU} the number of RUs per channel width, that varies from 1 to 74, depending on channel width and N_{SRU}	114, where 108 are data subcarriers and 6 are pilot subcarriers	26 / 56 / 114 / 242 / 484, where 24 / 52 / 108 / 234 / 468 are the data subcarriers and 2 / 4 / 6 / 8 / 16 the pilot subcarriers, respectively
Modulation	Up to 64-QAM	Up to 256-QAM	Up to 1024-QAM	Up to 256-QAM	Up to 256-QAM

Coding Rates	1/2 (with/ without preamble repetition), 5/8, 3/4, 13/16	1/2, 2/3, 3/4, 5/6	1/2, 2/3, 3/4, 5/6	1/2, 2/3, 3/4, 5/6	1/2, 2/3, 3/4, 5/6
FFT Length	512	64 / 128 / 256 / 512	256 / 512 / 1024 / 2048	64 / 128 / 256 / 512 / 1024, with the latter two to be optional	32 / 64 / 128 / 256 / 512
Spatial Multiplexing/Spatial Streams/ Beamforming	N/A / 1 / Supported	DL MU-MIMO / Up to 8 / Supported	DL-UL MU-MIMO / Up to 8 / Supported	DL MU-MIMO / Up to 4 / Supported	DL MU-MIMO / Up to 4 / Supported
Symbol Duration (IDFT/DFT period) [μs]	0.194	3.2	3.2 / 6.4 / 12.8	BCUs (6 / 7 MHz): 30, BCU (8 MHz): 22.5	36 / 40 / 48
Guard Interval [μs]	0.0484	0.4 / 0.8 / 1.6	0.8 / 1.6 / 3.2	BCUs (6 / 7 MHz): 6, BCU (8 MHz): 4.5	4 / 8 / 16

Subcarrier Frequency Spacing [kHz]	5156.25	312.5	78.125	BCUs (6 / 7 MHz): 41*(2/3), BCU (8 MHz): 55*(5/9)	31.25
Max PPDU Duration [ms]	2	5.484	5.484	20	27.84
Max PSDU Length [bytes]	262143	4692480	6500631	1065600	797160
Slot time [μs]	5	9	9 / 20 in 2.4 and 5 GHz band, respectively	BCUs (6 / 7 MHz): 24, BCU (8 MHz): 20	52
SIFS/DIFS [μs]	3 / 13	16 / 34	2.4 GHz: 10 / 28, 5 GHz: 16 / 34	BCUs (6 / 7 MHz): 120, BCU (8 MHz): 90	160 / 264

BUSY indication [μs]	within 3	within 4 (primary 20 MHz channel) and 25 (non-primary 20 MHz channel)	within 4 (primary 20 MHz channel) and 25 (non-primary 20 MHz channel)	BCUs (6 / 7 MHz): 94, BCU (8 MHz): 70	within 40 (primary 1 MHz channel with RSSI $\geq$ -98 dBm for type 1 channels or -89 dBm for type 2 channels) and 212 (primary 1 MHz channel with RSSI $\geq$ -89 dBm for type 1 channels or -86 dBm for type 2 channels, and non-primary 1 MHz portion of the primary 2 MHz)

Min Receiver Sensitivity [dBm]	-78 for MCS0, PER less than 5%, for a PSDU size of 256B and -68 for all other MCSs with PER less than 1% for a PSDU size of 4096B	-82 for 20 MHz	-82 for 20 MHz	BCUs (6 / 7 MHz): -88, BCU (8 MHz): -87 with PER less than 10% for a PSDU size of 4096B	-98 / -95 for 1 MHz & repetition on / off with PER less than 10% for a PSDU size of 256B
Max Peak Rate [Mbps]	6756.75	6933.3	9608	570	347

Appendix B

Damusys Algorithm (after successful transmissions)

The following variables are defined and used in Damysus after X successful/failed transmissions:

- mcs_c : the current rate
- mcs_{pwr} : the rate based on the transmit power level
- $newRate$: the new assigned rate
- $newPower$: the power required for the next rate
- $TxPwr$: the new assigned transmit power level
- $TxPwr_c$: the current transmit power level
- $TxPwr_{max}$: the maximum transmit power level
- $TxPwr_{step}$: the step for tuning the transmit power level
- $OBSS/PD_{step}$: the step for influencing the OBSS/PD
- $OBSS/PD$: the OBSS/PD threshold

- $OBSS/PD_{max}$: the maximum OBSS/PD
- $succThres$: the successful threshold (e.g. 10)
- $failThres$: the failure threshold (e.g. 10)
- $succeed$: the number of successful transmissions ($succeed \geq succThres$)
- $failed$: the number of failed transmissions ($failed \leq failThres$)
- $ewmaTemp$: the $ewmaProb$ threshold (e.g. 75)
- $ewmaProb_c$: the $ewmaProb$ of the current rate
- $ewma_{best}$: the rate with the best $ewmaProb$
- $throughput_c$: the $throughput$ of the current rate
- $throughput_{best}$: the rate with the highest throughput
- $rateFlag_n$: is true when a higher rate exists

Algorithm 1 Damysus algorithm

1: **procedure** SUCCESS
2: $succeed \leftarrow 0$
3: $failed \leftarrow 0$
4: **if** $mcs_c < mcs_{max} - 1$ **then**
5: $ewmaProb_n \leftarrow$ the $ewmaProb$ of next rate (i.e. $n = c + 1$)
6: $succProbInter_n \leftarrow$ the success probability of the next rate
7: $numRateTxFrames_n \leftarrow$ the $numRateTxFrames$ of the next rate
8: $numRateTxAttempts_n \leftarrow$ the $numRateTxAttempts$ of the next rate
9: $throughput_n \leftarrow$ the $throughput$ of the next rate
10: $intervalRateTxFrames_n \leftarrow$ the $intervalRateTxFrames$ of the next rate
11: **end if**
12: **if** $rateFlag_n$ AND $ewmaProb_c > ewmaTemp$ AND ($ewmaProb_n > ewmaTemp$ OR $numRateTxFrames_n < 30 * succThres$ OR $numRateTxAttempts_n < 3 * succThres$ OR $throughput_n > throughput_c$) AND $failed < 0.5 * failThres$ **then**
13: **go to** IncreaseRate ($mcs_{c+1}, newPower$)
14: **else if** ($numRateTxFrames_c > 30 * succThres$ OR $numRateTxAttempts_n > 3 * succThres$) AND $ewmaProb_c > ewmaTemp$ AND $ewmaProb_c > ewmaProb_n + 2$ AND $failed < 0.4 * failThres$ **then**
15: **comment:** keep the same rate unless it has very good properties (then $mcs_c + 1$)
16: $newPower \leftarrow$ the power required for the current rate
17: **if** $TxPwr_c - TxPwr_{step} > newPower$ **then**
18: $newPower \leftarrow TxPwr_c - TxPwr_{step}$
19: **end if**
20: **if** $OBSS/PD + OBSS/PD_{step} < OBSS/PD_{max}$ **then**
21: **go to** DoReportObssSignal ($OBSS/PD_{max}$)
22: **end if**
23: **else**
24: $UpperMCS \leftarrow$ Equation 7.3
25: **for** $ii \leftarrow UpperMCS$ to 1 **do**
26: **if** $intervalRateTxFrames_{c+ii} > 0$ **then**
27: **comment:** find rate with the highest $intervalRateSuccess > ewmaTemp$
28: **else if** ($ewmaProb_{c+ii} > ewmaTemp$ AND $throughput_{c+ii} > throughput_c$) OR $ewmaProb_{c+ii} == 0$ **then**
29: **comment:** find rate with the highest $intervalRateSuccess > ewmaTemp + (c + ii)$ (guard to avoid high fluctuations)
30: **end if**
31: **end for**
32: **comment:** if new rate has been found then **go to** IncreaseRate ($newRate, TxPwr_{max}$) and set $TxPwrFlag$ to true if $ewmaProb_c > min(ewmaTemp + 15.0, 95.0)$
33: **end if**
34: **end procedure**
35: **procedure** INCREASERATE($mcs, newPower$)
36: **comment:** Increase rate and power
37: **end procedure**
38: **procedure** DOREPORTOBSSSIGNAL($OBSS/PD_{max}$)
39: **comment:** Influence the calculation of OBSS/PD to use a more aggressive value
40: **end procedure**

Appendix C

Damusys Algorithm (after failed transmissions)

Algorithm 2 Damysus algorithm

procedure FAILURE
  $succeed \leftarrow 0$
  $failed \leftarrow 0$
  if $ewmaProb_c < ewmaTemp$ AND ($numRateTxFrames_c < 30 * failThres$ OR $numRateTxAttempts_c < 3 * failThres$ OR $TxPwr < TxPwr_{max}$) **then**
    $newPower \leftarrow TxPwr_{max}$
    DoReportObssSignal ($OBSS/PD_{min}$)
    $newRate \leftarrow Equations$ 7.6 − 7.9
  else if $mcs_c == 0$ AND ($numRateTxFrames_c > 30 * failThres$ OR $numRateTxAttempts_c > 3 * failThres$) AND $ewmaProb_c < ewmaTemp$ **then**
    $newPower \leftarrow TxPwr_{max}$
    DoReportObssSignal ($OBSS/PD_{min}$)
  else
    comment: from the statistics collected, find the $ewma_{best}$ and the $throughput_{best}$ that have the highest $ewmaProb$ and achieve the highest throughput, respectively.
    if less than two rates have been tried in the last interval **then**
      $newRate \leftarrow mcs_c - 1$
    else if more than 4 rates have been used AND $ewmaProb_c < 80$ **then**
      $newRate \leftarrow Equation$ 7.10
    else if ($ewmaProb_c > ewmaTemp$ AND $intervalRateSuccess_c > 65$) OR ($ewmaProb_c < ewmaTemp$ AND $intervalRateSuccess_c > ewmaTemp$) **then**
      comment: maintain the same settings
    else
      if $mcs_c - 1 == 0$ AND $intervalRateSuccess_c > 65$ **then**
        comment: avoid using the lowest MCS, maintain the same settings
      else if $mcs_{pwr} \neq mcs_c$ AND ($ewmaProb_{pwr} > ewmaProb_c + 2$ OR $throughput_{pwr} > throughput_c$) **then**
        $newRate \leftarrow mcs_{pwr}$
      else if $throughput_{best} \leq mcs_c + 3$ AND ($ewmaProb_{throughputBest} > ewmaTemp$ OR ($ewmaProb_{throughputBest} > ewma_{best} - 2$ AND $ewmaProb_{throughputBest} > ewmaProb_c + 2$)) **then**
        $newRate \leftarrow throughput_{best}$
      else if $ewma_{best} \leq mcs_c + 3$ AND ($ewma_{best} > ewmaTemp$ OR ($ewma_{best} > ewmaProb_{throughputBest} + 2$ AND $ewma_{best} > ewmaProb_c + 2$)) **then**
        $newRate \leftarrow ewma_{best}$
      else if ($ewmaProb_{mcsPwr} == 0$ OR $ewmaProb_{mcsPwr} > ewmaTemp$) AND ($intervalRateTxFrames_{mcsPwr} == 0$ OR $intervalRateSuccess_{mcsPwr} > 65$) **then**
        comment: find the $|mcs_c - mcsPwr|$ and normalise it by 2 (i.e. $rate_{norm}$). Switch to the $rate_{norm}$ only if $mcs_c > mcsPwr$
      else
        comment: switch to either $mcs_c - 1$ or to the rate found based on Equations 7.6 - 7.9, whom provides the best properties.
      end if
    end if
  end if
end procedure

Appendix D

ns-3; Network Simulator

The simulation tool used throughout this work is ns-3, a discrete-event network simulator used by both the academia and industry. It is based mostly on C++, whilst Python scripts may also be used. The major advantage of ns-3 is that it uses parallel and distributed simulation technology, utilizing the memory and allowing a single simulation over multiple processors, hence simulations of large and dense networks are possible.

The ns-3 software tool consists of the modules that are built as separate software libraries, and the models that are abstract representations of real-world objects, protocols, devices etc.

This work focuses on the Wi-Fi module, which implements an abstraction of the IEEE 802.11 standard, attempting to provide an accurate MAC and PHY layer of the standard, illustrated in Figure D.1. It is worth noting that as new standards are introduced, new features are developed and are incorporated in the Wi-Fi module, aiming to capture the basic functionality of an IEEE 802.11 device.

The Physical layer is abstracted in ns-3 in the following way: The reception of a packet is binary, in a way that the packet received is probabilitically evaluated for the outcome of the reception; successful or failed. Now, this probability depends on the modulation, the SINR, and the state of the physical layer (e.g. if the device transmits then any received packet during that period of time will be lost). A packet is evaluated when the first bit has been received, whether its energy is above the CCA/CS threshold and

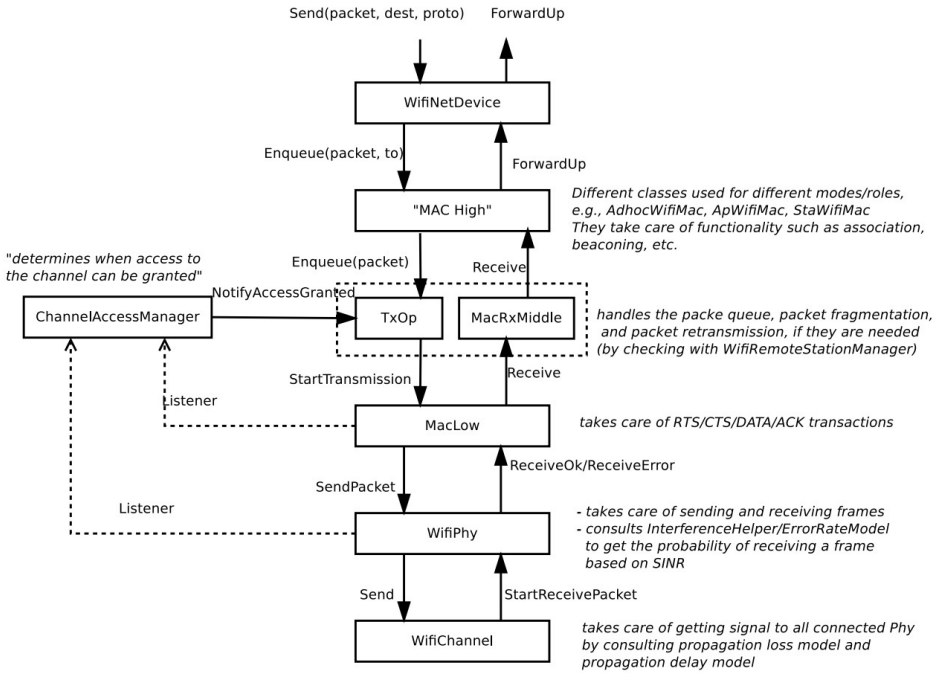

Figure D.1: The Wi-Fi module in ns-3.

then at the end of the PHY header based on the aforementioned probability. If the header is successfully received, the reception will continue with the rest bits of the packet. Finally, the end of the packet triggers again the probabilistic model, where if the reception is successful, the device will forward the packet to the higher layers (i.e. MAC). The physical model used in ns-3 is based on the one described in [394].

The MAC layer provides the core functionalities of MAC as described in the standards, taking care of the transmission of the packets (i.e. data, control, and management frames). It implements the DCF and EDCA (for QoS), whilst retransmissions, and packet aggregation are also handled by this layer.

The main contributions made on ns-3 in regard to the IEEE 802.11ax development, in this work can be summarised:

- PHY layer: The development of a physical capture model as described in Chapter 4 based on the document [346]. Furthermore, a received packet is probabilitically evaluated not only at the end of the PHY header and at the end of the packet, but also at the end of each header field. This is to provide a more accurate

packet reception scheme and evaluate the BSS Color field at the right time (i.e. when it is received and not after a few microseconds). However, this comes at the cost of increased complexity and longer simulation time. Also, the HE (IEEE 802.11ax) preamble and PHY header was developed, that carries all the related information (e.g. BSS Color). Finally, the OBSS/PD threshold has been incorporated as a function at this layer, similar to the CCA/CS and CCA/ED accounting only for the OBSS packets.

- MAC layer: Enable the support of IEEE 802.11ax frames and correctly assign to these packets this information. In particular, the Spatial Reuse is handled by this layer and the BSS Color id assignment.
- Channel models: The channel models developed too, as described in Chapter 7 based on the document [329].
- Simulation scenarios: The scenarios applied in this work, were developed again according to the document [329].

Furthermore, SISO systems are only considered in this work.The default antenna model is used in this study, which is the *IsotropicAntennaModel* from ns-3. This antenna radiation pattern model provides a unitary gain (0 dB) for all direction [395]. Note that at least 30 runs per simulations with a long simulation time per run were allowed according to the guidelines of ns-3 and IEEE 802.11ax. Finally, a sufficient warm-up period (until the simulator reaches a stable condition) was applied in this work, with all prerequisite operations (e.g. nodes' association, Block-ACK establishment) taking place during this period.

References

[394] M. Lacage and T. R Henderson, "Yet Another Network Simulator," *2006 Workshop on ns-2*, pp. 1–10, 2006.

[395] Network Simulator 3 (ns-3). (2020). Antenna Design in ns-3, [Online]. Available: `https://www.nsnam.org/docs/models/html/antenna-design.html` (visited on 2020).

Appendix E

TGax Simulation Scenarios

The simulation scenarios that have been developed and have been used in this work, follow the TGax recommendations as described in [329]. There are two different sets of the TGax simulation scenarios: i) scenarios to capture real-world dense deployments and ii) scenarios for calibration purpose. For each scenario, TGax specifies some models and settings such as:

- Topology: The location of the APs and STAs (layout) and the propagation model.
- Traffic model: Either UL (i.e. STA - AP) or DL (i.e. AP - STA). Note that mixed traffic in dense deployments is not recommended due to its high complexity to analyse the results, only for the calibration scenarios is allowed mixed traffic (i.e. DL and UL).
- PHY & MAC parameters:
  - ⋆ Transmit power [dBm]: APs at 20 dBm and STAs at 15 dBm (not EIRP).
  - ⋆ Antenna Gain [dBi]: 0 dBi and -2dBi for APs and STAs, respectively.
  - ⋆ Number of antennas: Default values of STAs is 1, whilst 2 for the APs.
  - ⋆ Noise figure [dB]: 7 for both APs and STAs.
  - ⋆ Bandwidth [MHz]: Either 20 at 2.4 GHz or 20/80 at 5 GHz.
  - ⋆ RTS/CTS: Disabled.

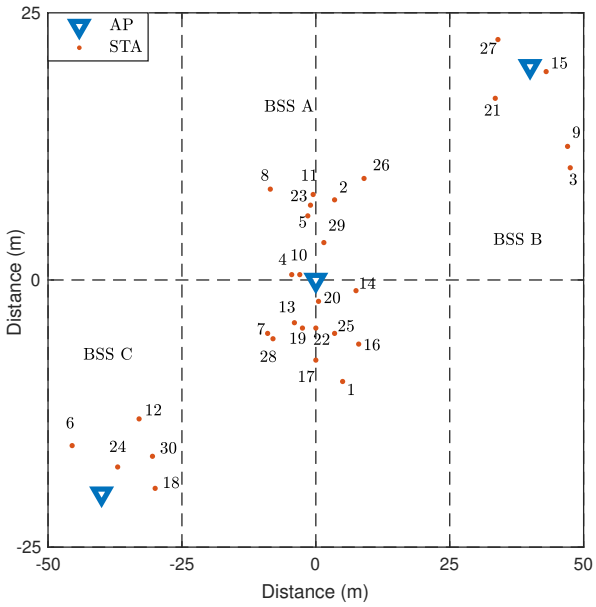

Figure E.1: Box5 calibration scenario.

- ⋆ Packet aggregation: Either 1 A-MPDU or maximum size of A-MPDU.
- ⋆ Traffic: UDP traffic is recommended (as TCP will skew the results when studying the lower layers, i.e. PHY and MAC).
- ⋆ Traffic conditions: Full-buffer.
- ⋆ Packet size: The maximum that can be supported (i.e. 1500 bytes).

E.0.1 Calibration scenarios

The calibration scenario has been introduced to allow various organisations to finely tune their simulation tools. For this scenario shadowing is not considered (although 5 dB standard deviation per link might be used, but is not recommended). Figure E.1 illustrates the layout for this calibration scenario (i.e. Box5). Note that only DL, only UL, and mixed traffic (where a few STAs transmit only UL) are supported, whereas the propagation model applied here follows the one described for SCE3 (as described in the next Section). This scenario was applied for calibrating and assessing the performance of COST algorithm (see Chapter 6).

E.0.2 Dense deployments

Five scenarios have been introduced by TGax to capture real-world deployments:

- Residential scenario (SCE1): SCE1 has been proposed by TGax, representing a multi-floor building with 5 floors as depicted in Figure E.2a. Each floor comprises of 2x10 apartments, each one with a size of 10x10x3m and an AP randomly placed in the apartment in an unplanned fashion. Each AP is randomly assigned in one of the 3 non-overlapping channels (when operating in 2.4 GHz), 11 otherwise. The main challenge here is the severe co-channel interference due to the uncontrolled and unmanaged deployment.

- Enterprise scenario (SCE2): SCE2 represents an office environment, which comprises a floor with 8 offices as depicted in Figure E.2b. Each office has an area of 20m x 20m and contains 64 cubicles, with 4 STAs and 4 APs placed per cubicle and per office, respectively. There are in total 32 APs with 64 STAs per AP. Three non-overlapping channels in the 2.4 GHz band are assigned for this scenario, with the following allocation (per office): $AP_0 \leftarrow Channel\ 1$, $AP_1 \leftarrow Channel\ 6$, $AP_2 \leftarrow Channel\ 11$, $AP_3 \leftarrow Channel\ 11$, $AP_4 \leftarrow Channel\ 1$, $AP_5 \leftarrow Channel\ 6$, $AP_6 \leftarrow Channel\ 11$, and $AP_7 \leftarrow Channel\ 11$.

- Indoor small BSS (SCE3): SCE3 represents dense indoor deployments (i.e. crowded statium, airport, auditorium etc.), where thousands of people are concentrated in a small area. The APs' deployment is planned in a hexagonal layout with ISD of 17.32m, and the APs are placed at 3m height. A frequency reuse pattern is also considered with SR3 to be more representative than SR1, even though, SR1 should also be considered as some regions might have very low available bandwidth. For both SR patterns, 19 co-channel cells are considered with one AP per cell, forming a 2-ring deployment, as depicted in Figure E.2c.

- Outdoor large BSS (SCE4): SCE4 captures an outdoor deployment (i.e. hotspot areas), where the distance between the APs is high, i.e. ISD of 130m is recommended. Similar to SCE3, 19 APs are planned in a hexagonal layout at 10m height.

- Outdoor large BSS and Residential scenario (SCE4a): SCE4a represents a of an outdoor and a residential scenario. However, in this scenario only 7 BSSs are used with one residential building deployed per BSS, as depicted in Figure E.2d. Note that each building comprises one floor.

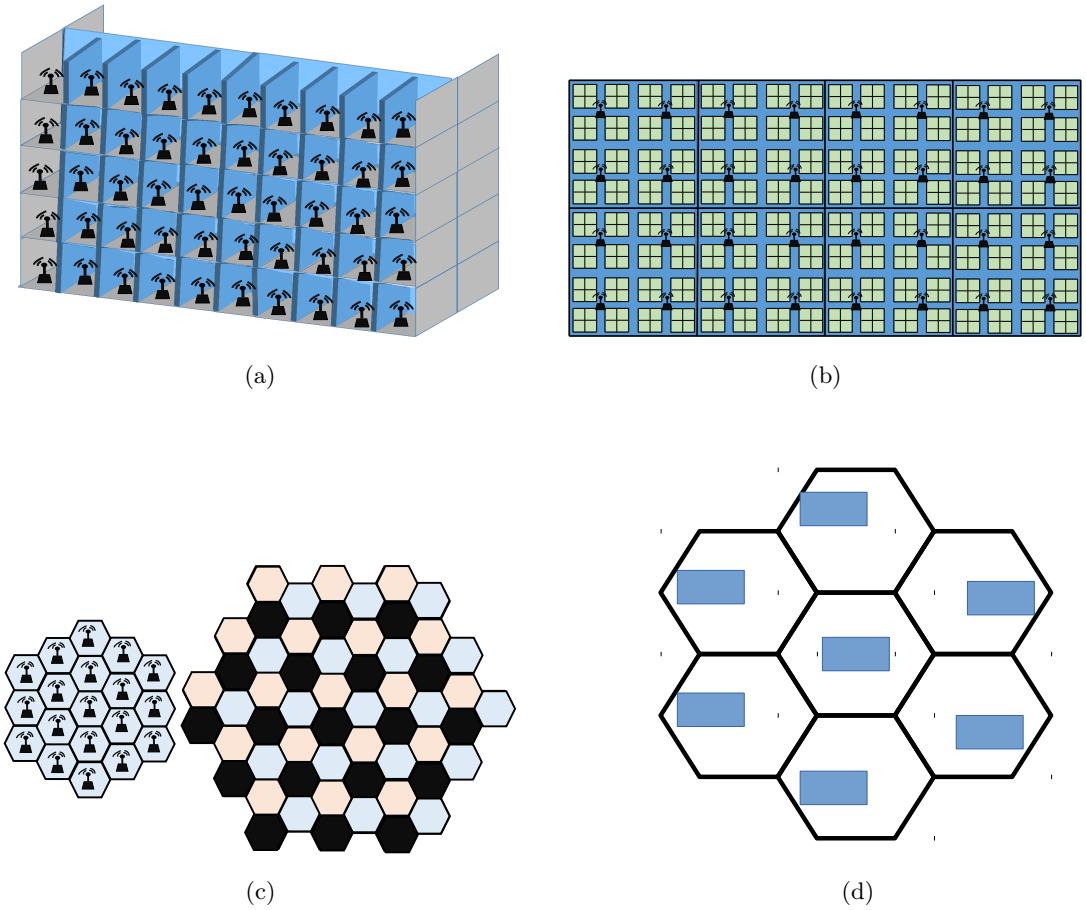

(a) (b)

(c) (d)

Figure E.2: TGax scenarios for dense deployments: a) SCE1 layout, b) SCE2 layout, c) SCE3 and SCE4 layout, and d) SCE4a layout.

In this work, scenarios Box5, SCE1, SCE2, SCE3, and SCE4 were developed and the performance of the proposed algorithms was assessed in these scenarios. In particular, SCE4 was used in Chapter 3 with some modifications, such as 127 APs were deployed forming a 6-ring deployment with the wrap-around technique enabled as described in [329], [338]. Chapter 4 studies the impact of BSS Color in SCE3 with the wrap-around technique enabled as well. Chapter 6 assesses the performance of the

proposed COST algorithm in Box5, whilst Chapter 7 evaluates the performance of the proposed rate control algorithm, namely Damysus, in SCE1, SCE2, SCE3, and SCE4. Finally, the path loss models used in each scenario are also specified in [329]:

- Path loss for SCE1:

$$\begin{aligned} PL_{sce1}(dB) &= 40.05 + 20 \cdot \log_{10}(\frac{f_c}{2.4}) + 20 \cdot \log_{10}(\min(d, d_{BP})) + 18.3 \cdot (\frac{d}{N_F})^{\frac{\frac{d}{N_F}+2}{(\frac{d}{N_F}+1)-0.46}} \\ &\quad + 5 \cdot \frac{d}{N_W} + \mathbb{1}(d > d_{BP}) \cdot 35 \cdot \log_{10}(\frac{d}{d_{BP}}) \end{aligned} \tag{E.1}$$

  with,

  PL: The path loss (in dB)

  f_c: The frequency (in GHz)

  d_{BP}: The breakpoint distance (5m)

  N_F: The number of floors

  N_W: The number of walls per floor

  N_A: The number of apartment per floor and N_L

  N_L: The number of apartment rows per floor

- Path loss for SCE2:

$$\begin{aligned} PL_{sce2} &= 40.05 + 20 \cdot \log_{10}(\frac{f_c}{2.4}) + 20 \cdot \log_{10}(min(d, d_{BP})) + 7 \cdot \frac{d}{N_W} \\ &\quad + \mathbb{1}(d > d_{BP}) \cdot 35 \cdot \log_{10}(\frac{d}{d_{BP}}) \end{aligned} \tag{E.2}$$

  where $d_{BP} = 10$ (m).

- Path loss for SCE3:

$$PL_{sce3} = 40.05 + 20 \cdot \log_{10}(\frac{f_c}{2.4}) + 20 \cdot \log_{10}(min(d, d_{BP})) + \mathbb{1}(d > d_{BP}) \cdot 35 \cdot \log_{10}(\frac{d}{d_{BP}}) \tag{E.3}$$

  where $d_{BP} = 10$ (m).

- Path loss for SCE4:

$$LOS_{prob} = \begin{cases} min(\frac{18}{d}, 1) \cdot (1 - e^{\frac{-d}{36}}) + e^{\frac{-d}{36}}, & \text{UMi} \\ min(\frac{18}{d}, 1) \cdot (1 - e^{\frac{-d}{63}}) + e^{\frac{-d}{63}}, & \text{UMa} \end{cases} \tag{E.4}$$

where $d_{BP} = 146$ (m).

$$PL^{LOS}_{sce4/UMi} = \begin{cases} 21 \cdot \log_{10}(\sqrt{d^2 + (TX_z - RX_z)^2}) + 32.4 + 20 \cdot log_{10}(f_c), \ d \leq d_{BP} \\ \\ 40 \cdot \log_{10}(\sqrt{d^2 + (TX_z - RX_z)^2}) + 32.4 + 20 \cdot log_{10}(f_c) \\ - 9.5 \cdot \log_{10}((d_{BP})^2 + (TX_z - RX_z)^2), \qquad\qquad d > d_{BP} \end{cases} \tag{E.5}$$

where TX_z, RX_z is the height (in m) of the transmitter and receiver, respectively, d is the 2D distance now, and the Breakpoint distance (in m) is given by:

$$d_{BP} = \frac{4 \cdot (TX_z - 1) \cdot (RX_z - 1) \cdot (f_c \cdot 10^9)}{C} \tag{E.6}$$

where C is the speed of light (299792458 m/s) and the f_c is in Hz that time. For more details in respect to the UMi and UMa channel models, the reader can refer to [383] (Table A1-2) and [384] (Note 1 in Table 7.4.1-1).

- Path loss for Sce4a:

  A combination of SCE4 and SCE1.

Figure E.3 illustrates the path loss models for the aforementioned scenarios, where the breakpoint corresponds to the indicator function as defined in the path loss models. Furthermore, **shadowing** has been specified per scenario as: i) SCE1: Log-normal with 5 dB standard deviation, independent and identically distributed (iid) across all links, ii) SCE2: Log-normal with 5 dB standard deviation, iid across all links, iii) SCE3: Log-normal with 5 dB standard deviation, iid across all links, and iv) SCE4: Log-normal with 3 dB standard deviation, iid across all LOS links and Log-normal with 4 dB standard deviation, iid across all NLOS links.

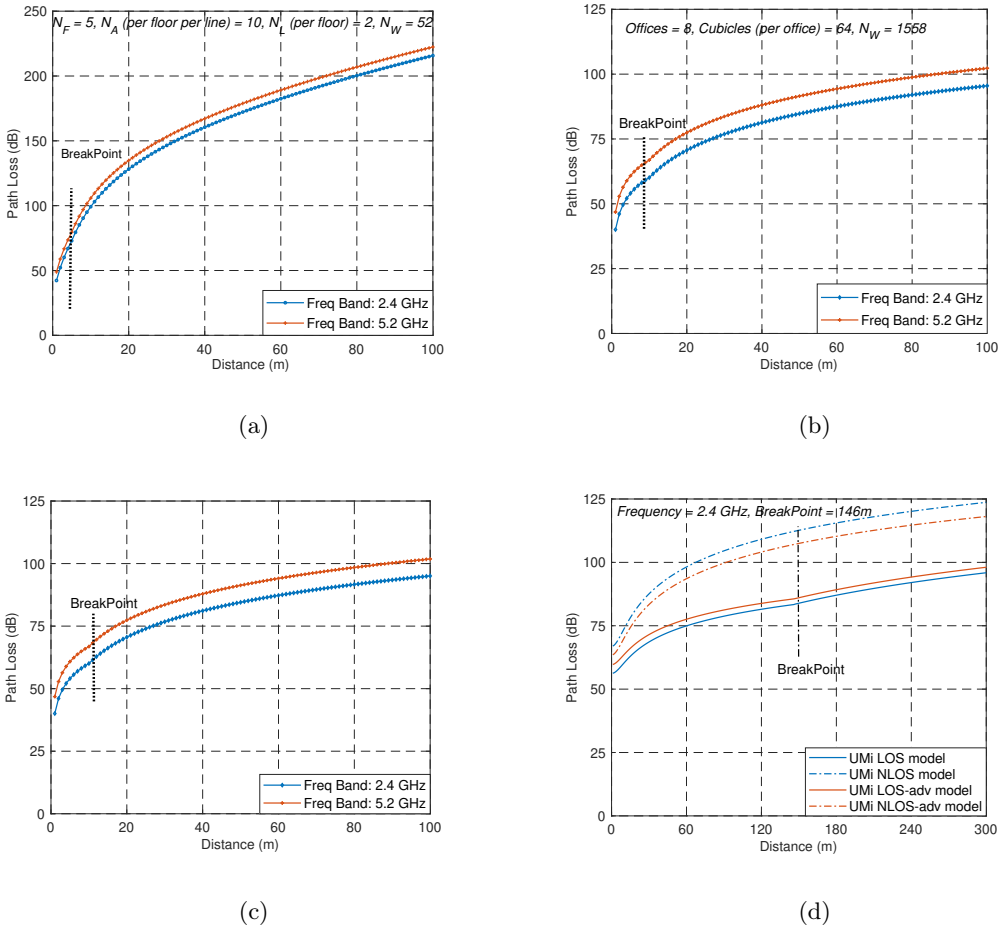

Figure E.3: Path loss models for a) SCE1, b) SCE2, c) SCE3, and d) SCE4.